

Biomedical &  
Life Sciences

Lancaster  
University



---

**Ph.D. Thesis in Biomedical and Life Sciences**

By

**Jyothsna Priyanka Bandi**

**Title**

**Unveiling the Antiviral Potential of chicken  
Poly (ADP-ribose) polymerases Against  
Influenza A Virus**

Under the supervision of

**Prof. Muhammad Munir**

Division of Biomedical and Life Sciences, Lancaster University,  
Lancaster, United Kingdom

**Dr Nikki Copeland**

Division of Biomedical and Life Sciences, Lancaster University,  
Lancaster, United Kingdom

## **Declaration**

**I certify that this thesis, submitted for the degree of [Ph.D. in Biomedical and Life Sciences], is the result of my own work and has not been submitted elsewhere for examination. Any work of other authors cited in this thesis has been acknowledged.**

**Jyothsna Priyanka Bandi**

## **Acknowledgement**

I would like to express my sincere gratitude to my supervisor, Professor Muhammad Munir, for his invaluable guidance, support, and the opportunity to undertake this research. I am also grateful to my secondary supervisor, Dr Nikki Copeland, for his insightful contributions towards my work.

I would like to extend my thanks to Dr Waqas Knokhar for his crucial transcriptomic analyses in Chapter 4. I would also like to acknowledge the contributions of Dr Mohammad Rohaim and Dr Mustafa Atasoy, to Chapter 5. I am indebted to the members of the Molecular Virology lab for their support and collaboration throughout my studies.

Finally, I would like to express my deepest gratitude to my family. To my parents, Mother, Vimala Bandi and Father, Suryanarayana Bandi thank you for your unconditional love, support, and sacrifices. To my sister, Mounika Bandi, thank you for your constant encouragement. To my husband, Peddinti Sai Kiran, thank you for your unwavering love, support, and understanding throughout my Ph.D. journey.

## List of Figures

FIGURE 1. 1 PHYLOGENETIC CLASSIFICATION OF HA AND NA SUBTYPES. A) ILLUSTRATION OF THE EVOLUTIONARY RELATIONSHIPS AMONG THE 16 CLASSICAL HA SUBTYPES, DIVIDED INTO TWO GROUPS AND FOUR CLADES. B) CLASSIFICATION OF 11 NA SUBTYPES, DIVIDED INTO THREE GROUPS. ....	9
FIGURE 1. 2 STRUCTURAL COMPONENTS OF IAV. ILLUSTRATES THE STRUCTURE OF THE INFLUENZA VIRUS AS AN ENVELOPED VIRUS WITH A LIPID BILAYER CONTAINING HA AND NA GLYCOPROTEINS. THE VIRAL GENOME COMPRISES EIGHT SEGMENTS OF SINGLE-STRANDED RNA, EACH ASSOCIATED WITH NUCLEOPROTEIN TO FORM A RIBONUCLEOPROTEIN COMPLEX (VRNP). THE VRNPS ARE BOUND BY THE M1 AND ENCLOSED WITHIN THE LIPID ENVELOPE. THE VRNP COMPLEX CONSISTS OF PA, PB1, AND PB2 SUBUNITS, WHERE A SINGLE-STRANDED RNA SEGMENT IS WRAPPED AROUND A HELICAL ARRAY OF NP SUBUNITS (MOSTAFA ET AL., 2018).....	11
FIGURE 1. 3 MECHANISM OF INVASION OF IAV AND ITS REPLICATION IN THE HOST CELL. IAV INITIATES INFECTION BY BINDING TO SIALIC ACID RECEPTORS ON THE HOST CELL SURFACE THROUGH ITS HA PROTEIN. THIS TRIGGERS CLATHRIN-MEDIATED ENDOCYTOSIS, LEADING TO VIRAL INTERNALISATION. /WITHIN THE ACIDIC ENDOSOME, HA UNDERGOES CONFORMATIONAL CHANGES, FACILITATING MEMBRANE FUSION AND RELEASE OF THE VRNP COMPLEXES INTO THE CYTOPLASM. ALTERNATIVELY, THE M2 ION CHANNEL CONTRIBUTES TO VIRAL UNCOATING. VRNPS ARE TRANSPORTED TO THE NUCLEUS, WHERE VIRAL RNA REPLICATION AND TRANSCRIPTION OCCUR. NEWLY SYNTHESISED VIRAL PROTEINS AND GENOMIC RNA ASSEMBLE AT THE CELL MEMBRANE, FORMING NEW VIRIONS. NA CLEAVES SIALIC ACID RESIDUES ENABLING VIRAL RELEASE (SALOMON & WEBSTER, 2009).....	21
FIGURE 1. 4 MECHANISM OF EVOLUTION OF IAV. A) SHOWS THE ACCUMULATION OF MUTATIONS WITHIN THE GENOME (ANTIGENIC DRIFT). B) SHOWS THE REASSORTMENT OCCURRING WITHIN THE HOST DURING CO-INFECTION (MOSTAFA ET AL., 2018).....	23
FIGURE 1. 5 PREVALENCE OF IAV-HA SUBTYPES IN CHICKEN, DUCK, AND GEESE. OBSERVATIONS INCLUDE THE WIDESPREAD DISTRIBUTION OF THE H9 SUBTYPE ACROSS ALL SPECIES, THE PREDOMINANCE OF THE H6 SUBTYPE IN GEESE, AND THE HIGHER PREVALENCE OF THE H3 SUBTYPE IN DUCKS. THE H4 SUBTYPE IS ALSO FOUND IN ALL THREE SPECIES, WITH THE HIGHEST PREVALENCE IN CHICKENS. NOTABLY, MIXED INFECTIONS WITH MULTIPLE HA SUBTYPES ARE OBSERVED, PARTICULARLY IN DUCKS. ....	26
FIGURE 1. 6 DIVERSE CELLULAR FUNCTIONS OF PARPS. ILLUSTRATES THE NUMEROUS ROLES PARPS IN VARIOUS CELLULAR PATHWAYS, INCLUDING DNA DAMAGE REPAIR, CELL STRUCTURE AND MOTILITY, SPERMATOGENESIS, MEMBRANE AND NUCLEAR ENVELOPE FORMATION, INNATE IMMUNITY, CELL TRANSPORT, CELL STRESS RESPONSE, SPINDLE POLE REGULATION, TRANSCRIPTION REGULATION, AND CHROMATIN STRUCTURE MODULATION, HIGHLIGHTING THE MULTIFACETED IMPORTANCE OF PARPS IN MAINTAINING CELLULAR HOMEOSTASIS AND RESPONDING TO DIVERSE CELLULAR CHALLENGES.....	28
FIGURE 1. 7 MECHANISM OF POLY /MONO (ADP) RIBOSYLATION. A) SHOWS POLY (ADP) RIBOSYLATION WHERE THE PARPS CATALYSE THE TRANSFER OF MULTIPLE ADPR MOIETIES. B) ILLUSTRATES MONO (ADP) RIBOSYLATION, WHERE THE PARPS CATALYSE THE TRANSFER OF A SINGLE ADPR MOIETY. ....	30
FIGURE 3. 1 DOMAIN ORGANIZATION OF CHICKEN PARP PROTEINS. THIS FIGURE ILLUSTRATES THE DIVERSE DOMAIN ORGANISATION OF CHPARP PROTEINS, ANALYSED USING EXPASY-PROSITE AND SMART. PARPS ARE CATEGORISED INTO GROUPS BASED ON THEIR DOMAINS COMPOSITION: DNA-DEPENDENT PARPS WITH ZINC FINGERS AND BRCT DOMAINS FOR DNA DAMAGE RESPONSE; TANKYRASES WITH ANK REPEATS AND SAM DOMAINS FOR TELOMERE MAINTENANCE AND WNT SIGNALLING; MACRO-CONTAINING PARPS WITH MACRO DOMAINS FOR ADP- RIBOSE BINDING INVOLVED IN DNA DAMAGE RESPONSE AND INFLAMMATION; AND CCCH- CONTAINING PARPS WITH CCCH-TYPE ZINC FINGERS AND WWE DOMAINS INVOLVED IN STRESS RESPONSES AND ANTIVIRAL DEFENCE. OTHER PARPS, SUCH AS PARP4, 6, 8, AND 11, EXHIBIT UNIQUE DOMAIN ORGANISATION AND ARE UNCHARACTERIZED. ....	79

FIGURE 3. 2 SYNTENY ANALYSIS OF PARP GENES ACROSS VERTEBRATES. THIS FIGURE ILLUSTRATES THE COMPARATIVE SYNTENY OF PARP GENES ACROSS VARIOUS AVIAN SPECIES (CHICKEN, DUCK, TURKEY) AND MAMMALS (HUMAN, MOUSE). IT HIGHLIGHTS THE OBSERVED CONSERVATION OF GENE ORDER AND PROXIMITY WITHIN AVIAN SPECIES, SPECIFICALLY SHOWING CONSERVED SYNTENY OF PARP4, PARP11, PARP12, AND PARP13 ON CHROMOSOME 1, AND PARP9, PARP14, AND PARP8 ON CHROMOSOMES 7 AND Z, RESPECTIVELY, IN BIRDS. THE FIGURE ALSO EMPHASIZES THE ABSENCE OF SYNTENY BETWEEN AVIAN AND MAMMALIAN SPECIES, AS WELL AS BETWEEN HUMAN AND RODENT LINEAGES, INDICATING SIGNIFICANT GENOMIC REARRANGEMENTS, HIGHLIGHTING THE DYNAMIC NATURE OF GENE FAMILY EVOLUTION ACROSS DIVERSE SPECIES. .... 81

FIGURE 3. 3 PHYLOGENETIC ANALYSIS OF CHICKEN PARP1. DISPLAYS THE PHYLOGENETIC TREE OF THE CHICKEN PARP1 PROTEIN, ILLUSTRATING ITS EVOLUTIONARY RELATIONSHIPS WITH ORTHOLOGOUS PARP1 SEQUENCES FROM DIVERSE VERTEBRATE SPECIES (AVIAN, MAMMALIAN, REPTILIAN, AMPHIBIAN, AND FISH). THE TREE HIGHLIGHTS THE CLUSTERING OF AVIAN PARP1 WITHIN A DISTINCT CLADE, INDICATING ITS EVOLUTIONARY DIVERGENCE FROM OTHER PARP1 ORTHOLOGS. THIS TREE WAS GENERATED IN MEGA 6 USING MAXIMUM LIKELIHOOD METHOD. .... 83

FIGURE 3. 4 PHYLOGENETIC ANALYSIS OF CHICKEN PARP3. DISPLAYS THE PHYLOGENETIC TREE OF THE CHICKEN PARP3 PROTEIN, ILLUSTRATING ITS EVOLUTIONARY RELATIONSHIPS WITH ORTHOLOGOUS PARP3 SEQUENCES FROM DIVERSE VERTEBRATE SPECIES. THE TREE DEMONSTRATES THE FORMATION OF A DISTINCT EVOLUTIONARY GROUPING FOR AVIAN PARP3. THIS TREE WAS GENERATED IN MEGA6 USING MAXIMUM LIKELIHOOD METHOD. .... 84

FIGURE 3. 5 AMINO ACID SEQUENCE HOMOLOGY OF CHICKEN PARP1 WITH HUMAN PARP1. THIS FIGURE ILLUSTRATES THE AMINO ACID SEQUENCE HOMOLOGY BETWEEN CHICKEN PARP1 AND HUMAN PARP1, CALCULATED USING THE SEQUENCE DEMARCATION TOOL (SDT) AND THE CLUSTALW ALGORITHM. THE ANALYSIS REVEALS APPROXIMATELY 75% SEQUENCE IDENTITY, INDICATING SIGNIFICANT CONSERVATION BUT ALSO NOTABLE DIFFERENCES IN PRIMARY STRUCTURE. THE COLOR CODE ALONGSIDE THE FIGURE REPRESENTS THE PERCENTAGE IDENTITY OF THE AMINO ACID SEQUENCE ALIGNMENT. .... 85

FIGURE 3. 6 AMINO ACID SEQUENCE HOMOLOGY OF CHICKEN PARP3 WITH HUMAN PARP3. THIS FIGURE ILLUSTRATES THE AMINO ACID SEQUENCE HOMOLOGY BETWEEN CHICKEN PARP3 AND HUMAN PARP3, CALCULATED USING THE SDT AND THE CLUSTALW ALGORITHM. THE ANALYSIS REVEALS APPROXIMATELY 70% SEQUENCE IDENTITY, INDICATING CONSERVATION BUT ALSO HIGHLIGHTING EVOLUTIONARY DIVERGENCE IN THE PRIMARY STRUCTURE. THE COLOR CODE ALONGSIDE THE FIGURE REPRESENTS THE PERCENTAGE IDENTITY OF THE AMINO ACID SEQUENCE ALIGNMENT..... 86

FIGURE 3. 7 STRUCTURAL ANALYSIS OF CHICKEN PARP1. THIS FIGURE DISPLAYS THE PREDICTED 3D STRUCTURE OF CHPARP1, GENERATED USING A COMBINATION OF *AB INITIO* (I-TASSER) AND DEEP LEARNING-BASED (ALPHAFOLD) METHODS. THE OVERALL PROTEIN STRUCTURE IS DEPICTED IN ORANGE, PROVIDING A COMPREHENSIVE VIEW OF ITS FOLDING PATTERN. THE CATALYTIC DOMAIN, CRUCIAL FOR PARP1'S ENZYMIC ACTIVITY, IS HIGHLIGHTED IN GREEN, EMPHASIZING ITS SPECIFIC STRUCTURAL CONTEXT WITHIN THE PROTEIN. ADDITIONALLY, THE FIGURE PRESENTS A SUPERIMPOSITION OF THE CATALYTIC DOMAINS FROM CHICKEN (GREEN) AND HUMAN (BLUE) PARP1. .... 87

FIGURE 3. 8 MULTIPLE SEQUENCE ALIGNMENT OF CHPARP1 AND CHPARP3 CATALYTIC DOMAINS. (A) MSA OF PARP1, DEMONSTRATING CONSERVED RESIDUES ACROSS HUMAN, MOUSE, CHICKEN, DUCK, AND TURKEY. (B) MSA OF PARP3, HIGHLIGHTING CONSERVED RESIDUES ACROSS THE SAME FIVE SPECIES. THE SEQUENCES WERE ALIGNED USING BIOEDIT SOFTWARE. IDENTICAL AMINO ACID RESIDUES ARE INDICATED BY DOTS. THE CATALYTIC DOMAIN, CRUCIAL FOR ENZYMIC ACTIVITY, IS HIGHLIGHTED WITHIN A RED BOX. THIS COMPARISON REVEALS REGIONS OF HIGH CONSERVATION, SUGGESTING FUNCTIONAL IMPORTANCE, AND HIGHLIGHTS EVOLUTIONARY RELATIONSHIPS BETWEEN THESE PARP FAMILY MEMBERS ACROSS DIVERSE AVIAN AND MAMMALIAN SPECIES..... 88

FIGURE 3. 9 PHYLOGENETIC ANALYSIS OF CHPARP5B ORTHOLOGS DEMONSTRATING AVIAN-SPECIFIC EVOLUTION. A MAXIMUM LIKELIHOOD PHYLOGENETIC TREE, GENERATED USING MEGA6, ILLUSTRATES THE

EVOLUTIONARY RELATIONSHIPS OF CHPARP5B WITH OTHER PARP5B ORTHOLOGS ACROSS DIVERSE SPECIES. THE TREE REVEALS A DISTINCT CLADE FOR AVIAN SPECIES, SUGGESTING A UNIQUE EVOLUTIONARY TRAJECTORY FOR PARP5B WITHIN THE AVIAN LINEAGE. THIS DISTINCT CLUSTERING HIGHLIGHTS POTENTIAL FUNCTIONAL ADAPTATIONS SPECIFIC TO BIRDS. THE SCALE BAR REPRESENTS THE NUMBER OF SUBSTITUTIONS PER SITE, REFLECTING EVOLUTIONARY DISTANCE. .... 90

FIGURE 3. 10 AMINO ACID SEQUENCE HOMOLOGY COMPARISON OF CHPARP5B AND HUMAN PARP5B. A HEATMAP DEPICTING THE AMINO ACID SEQUENCE IDENTITY BETWEEN CHPARP5B AND ITS HUMAN COUNTERPART, GENERATED USING THE CLUSTALW ALGORITHM IN SDT. THE HEATMAP, ACCOMPANIED BY A COLOR-CODED IDENTITY SCALE, DEMONSTRATES APPROXIMATELY 82% SEQUENCE IDENTITY. THIS HIGH DEGREE OF SEQUENCE CONSERVATION SUGGESTS A SIGNIFICANT LEVEL OF STRUCTURAL AND, POTENTIALLY, FUNCTIONAL CONSERVATION DESPITE EVOLUTIONARY DIVERGENCE. THE COLOR-CODING BAR VISUALLY REPRESENTS THE PERCENTAGE OF AMINO ACID IDENTITY, WITH DARKER SHADES INDICATING HIGHER SIMILARITY. .... 91

FIGURE 3. 11 STRUCTURAL COMPARISON AND MULTIPLE SEQUENCE ALIGNMENT OF CHICKEN AND HUMAN PARP5B CATALYTIC DOMAINS. A) THIS PANEL ILLUSTRATES A COMPARATIVE ANALYSIS OF THE CATALYTIC DOMAINS OF CHPARP5B AND ITS HUMAN COUNTERPART. PREDICTED 3D STRUCTURES OF THE FULL-LENGTH PROTEINS ARE DISPLAYED, WITH THE CATALYTIC DOMAINS HIGHLIGHTED IN GREEN AND THE REMAINING PROTEIN IN ORANGE. THE CATALYTIC DOMAINS ARE FURTHER EMPHASIZED BY A BLACK BOX. 3D STRUCTURES WERE PREDICTED USING I-TASSER AND ALPHAFOLD AND VISUALIZED AND EDITED USING PYMOL. A SUPERIMPOSITION OF THE CATALYTIC DOMAINS IS SHOWN, WITH THE CHICKEN CATALYTIC DOMAIN REPRESENTED IN GREEN AND THE HUMAN CATALYTIC DOMAIN IN BLUE. THIS COMPARISON REVEALS THE STRUCTURAL SIMILARITIES AND SUBTLE DIFFERENCES BETWEEN THE CATALYTIC DOMAINS OF THESE ORTHOLOGOUS PROTEINS, PROVIDING INSIGHTS INTO POTENTIAL FUNCTIONAL CONSERVATION AND DIVERGENCE. B) THIS PANEL PRESENTS AN MSA OF THE CATALYTIC DOMAINS OF PARP5B FROM HUMAN, MOUSE, CHICKEN, DUCK, AND TURKEY. THE SEQUENCES WERE ALIGNED USING BIOEDIT SOFTWARE. IDENTICAL AMINO ACID RESIDUES ARE INDICATED BY DOTS. THE CATALYTIC REGIONS ARE HIGHLIGHTED WITHIN A RED BOX. NOTABLY, THE MSA REVEALS A HIGH DEGREE OF CONSERVATION WITHIN THE CATALYTIC DOMAIN, WITH ONLY APPROXIMATELY 10 MUTATIONS OBSERVED ACROSS THE FIVE SPECIES. THIS LIMITED VARIABILITY SUGGESTS STRONG SELECTIVE PRESSURE TO MAINTAIN THE FUNCTIONAL INTEGRITY OF THE CATALYTIC DOMAIN THROUGHOUT EVOLUTION. .... 94

FIGURE 3. 12 PHYLOGENETIC ANALYSIS OF PARP7 ORTHOLOGS REVEALS COMPLEX EVOLUTIONARY HISTORY. THIS FIGURE ILLUSTRATES THE EVOLUTIONARY RELATIONSHIPS OF PARP7 ACROSS VARIOUS VERTEBRATE SPECIES. THE PHYLOGENETIC TREE REVEALS A DISTINCT CLADE FORMED BY AVIAN SPECIES, SUGGESTING A UNIQUE EVOLUTIONARY TRAJECTORY FOR PARP7 WITHIN THE BIRD LINEAGE. HOWEVER, THE EVOLUTIONARY LANDSCAPE OF PARP7 IN REPTILES IS MORE INTRICATE, WITH TWO DISTINCT CLADES OBSERVED, ONE ENCOMPASSING THE CHINESE ALLIGATOR AND THE OTHER THE GREEN SEA TURTLE. NOTABLY, THESE REPTILE CLADES ARE INTERSPERSED WITH CLADES FROM AMPHIBIANS AND FISH, INDICATING A COMPLEX EVOLUTIONARY HISTORY FOR PARP7 IN NON-AVIAN VERTEBRATES. FURTHERMORE, AMPHIBIAN PARP7 ORTHOLOGS ARE ALSO DIVIDED INTO TWO CLADES, ONE INCLUDING WESTERN CLAWED FROGS AND THE OTHER AFRICAN CLAWED FROGS, WHICH ARE POSITIONED WITHIN THE FISH CLADE. THIS INTRICATE PATTERN HIGHLIGHTS THE DYNAMIC AND VARIED EVOLUTIONARY PATHS OF PARP7 ACROSS DIFFERENT VERTEBRATE GROUPS. .... 96

FIGURE 3. 13 PHYLOGENETIC ANALYSIS OF PARP12 ORTHOLOGS DEMONSTRATES COMPLEX AVIAN AND VERTEBRATE RELATIONSHIPS. THIS FIGURE PRESENTS THE EVOLUTIONARY RELATIONSHIPS OF PARP12 ACROSS A RANGE OF VERTEBRATE SPECIES. THE AVIAN LINEAGE FOR PARP12 IS DIVIDED INTO TWO DISTINCT CLADES: ONE COMPRISING THE TURKEY AND ZEBRA FINCH, AND THE OTHER INCLUDING THE CHICKEN, DUCK, AND WESTERN BARN OWL. NOTABLY, THESE AVIAN CLADES ARE SEPARATED BY CLADES FROM REPTILES AND FISH, UNDERSCORING THE COMPLEX EVOLUTIONARY RELATIONSHIPS WITHIN THESE VERTEBRATE GROUPS. THE FISH LINEAGE IS ALSO FURTHER DIVIDED INTO TWO CLADES: ONE CONTAINING NORTHERN PIKE AND ATLANTIC SALMON, AND THE OTHER COMPRISING ZEBRAFISH AND NILE TILAPIA, WITH AMPHIBIANS, AVIANS, AND REPTILES INTERSPERSED BETWEEN THESE FISH CLADES. THIS COMPLEX PATTERN EMPHASIZES THE DIVERSE AND INTRICATE EVOLUTIONARY HISTORY OF PARP12 ACROSS THE VERTEBRATE TREE OF LIFE. .... 97

FIGURE 3. 14 PHYLOGENETIC ANALYSIS OF PARP13 ORTHOLOGS HIGHLIGHTS DISTINCT AVIAN EVOLUTION. THIS FIGURE DEPICTS THE EVOLUTIONARY RELATIONSHIPS OF PARP13 ACROSS VARIOUS VERTEBRATE SPECIES. THE PHYLOGENETIC ANALYSIS OF PARP13 REVEALS A CLEAR SEPARATION BETWEEN THE AVIAN CLADE AND THE OTHER SPECIES INCLUDED IN THE STUDY. THIS DISTINCT CLUSTERING SUGGESTS A MORE SPECIFIC AND POTENTIALLY MORE RECENT EVOLUTIONARY TRAJECTORY FOR PARP13 WITHIN THE BIRD LINEAGE. IT IS IMPORTANT TO NOTE THAT THE AMPHIBIAN SPECIES INCLUDED IN THIS STUDY DID NOT POSSESS A DETECTABLE PARP13 SEQUENCE..... 98

FIGURE 3. 15 SEQUENCE HOMOLOGY ANALYSIS OF CHPARP7. A HEATMAP DEPICTING THE AMINO ACID SEQUENCE IDENTITY BETWEEN CHPARP7 AND ITS HUMAN COUNTERPART. THE HEATMAP, GENERATED USING THE CLUSTALW ALGORITHM IN SDT, REVEALS APPROXIMATELY 72% SEQUENCE IDENTITY, AS INDICATED BY THE COLOR-CODED IDENTITY SCALE. THIS LEVEL OF CONSERVATION SUGGESTS A SIGNIFICANT DEGREE OF STRUCTURAL AND FUNCTIONAL SIMILARITY BETWEEN THE CHICKEN AND HUMAN PARP7 PROTEINS, DESPITE THEIR EVOLUTIONARY DIVERGENCE..... 99

FIGURE 3. 16 SEQUENCE HOMOLOGY ANALYSIS OF PARP12. HEATMAP ILLUSTRATING THE AMINO ACID SEQUENCE IDENTITY BETWEEN CHPARP12 AND HUMAN PARP12. THE ANALYSIS, PERFORMED USING THE CLUSTALW ALGORITHM IN SDT, INDICATES APPROXIMATELY 62% SEQUENCE IDENTITY, AS REFLECTED BY THE COLOR-CODING BAR. THIS LEVEL OF SEQUENCE CONSERVATION SUGGESTS THAT WHILE THERE HAS BEEN EVOLUTIONARY DIVERGENCE, KEY STRUCTURAL AND FUNCTIONAL ELEMENTS OF PARP12 ARE MAINTAINED BETWEEN THESE SPECIES..... 100

FIGURE 3. 17 SEQUENCE HOMOLOGY ANALYSIS OF PARP13. HEATMAP DISPLAYING THE AMINO ACID SEQUENCE IDENTITY BETWEEN CHPARP13 AND ITS HUMAN COUNTERPART. THE SEQUENCE ALIGNMENT, PERFORMED USING THE CLUSTALW ALGORITHM IN SDT, REVEALS APPROXIMATELY 65% SEQUENCE IDENTITY, AS INDICATED BY THE COLOR-CODED IDENTITY SCALE. THIS LEVEL OF CONSERVATION SUGGESTS A MODERATE DEGREE OF STRUCTURAL AND FUNCTIONAL SIMILARITY BETWEEN THE CHICKEN AND HUMAN PARP13 PROTEINS, CONSISTENT WITH THEIR DISTINCT EVOLUTIONARY TRAJECTORY WITHIN THE AVIAN LINEAGE. 101

FIGURE 3. 18 MULTIPLE SEQUENCE ALIGNMENT OF PARP7, PARP12 & PARP13 CATALYTIC DOMAINS. A) THE CATALYTIC DOMAIN OF CHPARP7 EXHIBITS A HIGH DEGREE OF CONSERVATION COMPARED TO ITS HUMAN COUNTERPART, WITH ONLY A SMALL NUMBER OF POINT MUTATIONS OBSERVED. B) THE CATALYTIC DOMAIN OF CHPARP12 SHOWS THE SECOND-HIGHEST LEVEL OF CONSERVATION, WITH APPROXIMATELY TWO-THIRDS OF ITS STRUCTURE CONSERVED RELATIVE TO THE HUMAN PROTEIN. C) THE CATALYTIC DOMAIN OF CHPARP13 DEMONSTRATES A LOWER DEGREE OF CONSERVATION COMPARED TO THE OTHER TWO CHICKEN PARPS ANALYSED. MSAS WERE GENERATED FOR PARP7, PARP12, AND PARP13 PROTEINS FROM CHICKEN, TURKEY, DUCK, HUMAN, AND MOUSE. THE ALIGNMENTS WERE PERFORMED USING BIOEDIT SOFTWARE. IDENTICAL AMINO ACID RESIDUES ACROSS THE ALIGNED SEQUENCES ARE INDICATED BY DOTS. THE CATALYTIC DOMAINS OF EACH PROTEIN ARE HIGHLIGHTED WITHIN RED BOXES..... 103

FIGURE 3. 19 STRUCTURAL COMPARISON OF CHICKEN AND HUMAN CCCH-CONTAINING PARPS. THIS FIGURE PRESENTS A COMPARISON OF THE CATALYTIC DOMAINS OF CHPARP7, CHPARP12, AND CHPARP13 WITH THEIR HUMAN COUNTERPARTS. PREDICTED 3D STRUCTURES OF THE FULL-LENGTH PROTEINS ARE DISPLAYED, WITH THE CATALYTIC DOMAINS HIGHLIGHTED IN GREEN AND THE REMAINING PROTEIN IN ORANGE. THE CATALYTIC DOMAINS ARE FURTHER EMPHASIZED BY A BLACK BOX. 3D STRUCTURES WERE PREDICTED USING I-TASSER AND ALPHAFOLD AND VISUALIZED AND EDITED USING PYMOL. A SUPERIMPOSITION OF THE CATALYTIC DOMAINS IS SHOWN, WITH THE CHICKEN CATALYTIC DOMAIN REPRESENTED IN GREEN AND THE HUMAN CATALYTIC DOMAIN IN BLUE. THIS COMPARISON REVEALS THE STRUCTURAL SIMILARITIES AND SUBTLE DIFFERENCES BETWEEN THE CATALYTIC DOMAINS OF THESE ORTHOLOGOUS PROTEINS. .... 104

FIGURE 3. 20 PHYLOGENETIC ANALYSIS OF PARP9. THIS FIGURE ILLUSTRATES THE EVOLUTIONARY RELATIONSHIPS OF PARP9 ACROSS VARIOUS VERTEBRATE SPECIES, INCLUDING MAMMALS, AMPHIBIANS, REPTILES, AND FISH, WITH A SPECIFIC FOCUS ON THE AVIAN LINEAGE. THE PHYLOGENETIC TREE REVEALS A DISTINCT CLADE FORMED BY AVIAN SPECIES, SUGGESTING A UNIQUE EVOLUTIONARY TRAJECTORY FOR PARP9

WITHIN THE BIRD LINEAGE. THE TREE WAS CONSTRUCTED USING MAXIMUM LIKELIHOOD METHOD IN MEGA6. ....	106
FIGURE 3. 21 PHYLOGENETIC ANALYSIS OF PARP14. THIS FIGURE PRESENTS THE EVOLUTIONARY RELATIONSHIPS OF PARP14 ACROSS A RANGE OF VERTEBRATE SPECIES. THE AVIAN LINEAGE FOR PARP14 IS DIVIDED INTO THREE CLADES: ONE COMPRISING THE TURKEY, WESTERN BARN OWL AND ZEBRA FINCH, AND THE OTHER INCLUDING THE CHICKEN, AND THE LAST ONE COMPRISING DUCK. NOTABLY, THESE AVIAN CLADES ARE SEPARATED BY CLADES FROM REPTILES, AMPHIBIANS AND FISH, UNDERSCORING THE COMPLEX EVOLUTIONARY RELATIONSHIPS WITHIN THESE VERTEBRATE GROUPS. THE REPTILE LINEAGE IS ALSO FURTHER DIVIDED INTO TWO CLADES: ONE CONTAINING GREEN SEA TURTLE, AND THE OTHER COMPRISING SCHLEGEL'S JAPANESE GECKO, WITH AVIANS INTERSPERSED BETWEEN THEM. THIS COMPLEX PATTERN EMPHASIZES THE DIVERSE AND INTRICATE EVOLUTIONARY HISTORY OF PARP14 ACROSS THE VERTEBRATE TREE OF LIFE. ....	107
FIGURE 3. 22 AMINO ACID SEQUENCE HOMOLOGY OF CHICKEN AND HUMAN PARP9. HEATMAP DISPLAYING THE AMINO ACID SEQUENCE IDENTITY BETWEEN CHPARP9 AND ITS HUMAN COUNTERPART. THE SEQUENCE ALIGNMENT, PERFORMED USING THE CLUSTALW ALGORITHM IN SDT, REVEALS APPROXIMATELY 60% SEQUENCE IDENTITY, AS INDICATED BY THE COLOR-CODED IDENTITY SCALE. THIS LEVEL OF CONSERVATION SUGGESTS A MODERATE DEGREE OF STRUCTURAL AND FUNCTIONAL SIMILARITY BETWEEN THE CHICKEN AND HUMAN PARP9 PROTEINS, CONSISTENT WITH THEIR DISTINCT EVOLUTIONARY TRAJECTORY WITHIN THE AVIAN LINEAGE. ....	108
FIGURE 3. 23 AMINO ACID SEQUENCE HOMOLOGY OF CHICKEN AND HUMAN PARP14. HEATMAP DISPLAYING THE AMINO ACID SEQUENCE IDENTITY BETWEEN CHPARP14 AND ITS HUMAN COUNTERPART. THE SEQUENCE ALIGNMENT, PERFORMED USING THE CLUSTALW ALGORITHM IN SDT, REVEALS APPROXIMATELY 50% SEQUENCE IDENTITY, AS INDICATED BY THE COLOR-CODED IDENTITY SCALE. THIS LEVEL OF CONSERVATION SUGGESTS A LOW DEGREE OF STRUCTURAL AND FUNCTIONAL SIMILARITY BETWEEN THE CHICKEN AND HUMAN PARP14 PROTEINS, CONSISTENT WITH THEIR DISTINCT EVOLUTIONARY TRAJECTORY WITHIN THE AVIAN LINEAGE. ....	109
FIGURE 3. 24 MULTIPLE SEQUENCE ALIGNMENT OF PARP9 AND PARP14 CATALYTIC DOMAINS. A) THE CATALYTIC DOMAIN OF CHPARP9 EXHIBITS MODERATE DEGREE OF CONSERVATION COMPARED TO ITS HUMAN COUNTERPART. B) THE CATALYTIC DOMAIN OF CHPARP14 SHOWS THE LOWEST LEVEL OF CONSERVATION, WITH ONLY HALF OF ITS STRUCTURE CONSERVED RELATIVE TO THE HUMAN PROTEIN. MSAS WERE GENERATED FOR PARP9, PARP14 PROTEINS FROM CHICKEN, TURKEY, DUCK, HUMAN, AND MOUSE. THE ALIGNMENTS WERE PERFORMED USING BIOEDIT SOFTWARE. IDENTICAL AMINO ACID RESIDUES ACROSS THE ALIGNED SEQUENCES ARE INDICATED BY DOTS. THE CATALYTIC DOMAINS OF EACH PROTEIN ARE HIGHLIGHTED WITHIN RED BOXES. ....	110
FIGURE 3. 25 STRUCTURAL COMPARISON OF PARP9 AND PARP14 CATALYTIC DOMAINS. THIS PANEL ILLUSTRATES A COMPARATIVE ANALYSIS OF THE CATALYTIC DOMAINS OF CHPARP9 AND PARP14 AND THEIR HUMAN COUNTERPARTS. PREDICTED 3D STRUCTURES OF THE FULL-LENGTH PROTEINS ARE DISPLAYED, WITH THE CATALYTIC DOMAINS HIGHLIGHTED IN GREEN AND THE REMAINING PROTEIN IN ORANGE. THE CATALYTIC DOMAINS ARE FURTHER EMPHASIZED BY A BLACK BOX. 3D STRUCTURES WERE PREDICTED USING I-TASSER AND ALPHAFOLD AND VISUALIZED AND EDITED USING PYMOL. A SUPERIMPOSITION OF THE CATALYTIC DOMAINS IS SHOWN, WITH THE CHICKEN CATALYTIC DOMAIN REPRESENTED IN GREEN AND THE HUMAN CATALYTIC DOMAIN IN BLUE. ....	111
FIGURE 3. 26 PHYLOGENETIC AND SEQUENCE ANALYSIS OF PARP4. THIS FIGURE ILLUSTRATES THE EVOLUTIONARY RELATIONSHIPS OF PARP4 ACROSS VARIOUS VERTEBRATE SPECIES, INCLUDING MAMMALS, AMPHIBIANS, REPTILES, AND FISH, WITH A SPECIFIC FOCUS ON THE AVIAN LINEAGE. THE PHYLOGENETIC TREE REVEALS A DISTINCT CLADE FORMED BY AVIAN SPECIES, SUGGESTING A UNIQUE EVOLUTIONARY TRAJECTORY FOR PARP4 WITHIN THE BIRD LINEAGE. THE TREE WAS CONSTRUCTED USING MAXIMUM LIKELIHOOD METHOD IN MEGA6. ....	112

FIGURE 3. 27 SEQUENCE HOMOLOGY OF PARP4. HEATMAP DISPLAYING THE AMINO ACID SEQUENCE IDENTITY BETWEEN CHPARP4 AND ITS HUMAN COUNTERPART. THE SEQUENCE ALIGNMENT, PERFORMED USING THE CLUSTALW ALGORITHM IN SDT, REVEALS APPROXIMATELY 62% SEQUENCE IDENTITY, AS INDICATED BY THE COLOR-CODED IDENTITY SCALE. THIS LEVEL OF CONSERVATION SUGGESTS A MODERATE DEGREE OF STRUCTURAL AND FUNCTIONAL SIMILARITY BETWEEN THE CHICKEN AND HUMAN PARP4 PROTEINS..... 113

FIGURE 3. 4 MULTIPLE SEQUENCE ALIGNMENT OF CHPARP4 CATALYTIC DOMAIN. THE CATALYTIC DOMAIN OF CHPARP4 EXHIBITS A HIGH DEGREE OF CONSERVATION WITH ITS HUMAN COUNTERPART, WITH ONLY A SMALL NUMBER OF POINT MUTATIONS OBSERVED. MSA WAS GENERATED FOR CHICKEN, TURKEY, DUCK, HUMAN, AND MOUSE. THE ALIGNMENTS WERE PERFORMED USING BIOEDIT SOFTWARE. IDENTICAL AMINO ACID RESIDUES ACROSS THE ALIGNED SEQUENCES ARE INDICATED BY DOTS. THE CATALYTIC DOMAINS OF EACH PROTEIN ARE HIGHLIGHTED WITHIN RED BOXES. .... 114

FIGURE 3. 29 STRUCTURAL COMPARISON OF PARP4 CATALYTIC DOMAIN. THIS PANEL ILLUSTRATES A COMPARATIVE ANALYSIS OF THE CATALYTIC DOMAINS OF CHPARP4 AND ITS HUMAN COUNTERPART. PREDICTED 3D STRUCTURE OF THE FULL-LENGTH PROTEIN IS DISPLAYED, WITH THE CATALYTIC DOMAIN HIGHLIGHTED IN GREEN AND THE REMAINING PROTEIN IN ORANGE. THE CATALYTIC DOMAIN IS FURTHER EMPHASIZED BY A BLACK BOX. 3D STRUCTURE WAS PREDICTED USING I-TASSER AND ALPHAFOLD AND VISUALIZED AND EDITED USING PYMOL. A SUPERIMPOSITION OF THE CATALYTIC DOMAINS IS SHOWN, WITH THE CHICKEN CATALYTIC DOMAIN REPRESENTED IN GREEN AND THE HUMAN CATALYTIC DOMAIN IN BLUE. THIS COMPARISON REVEALS THE STRUCTURAL SIMILARITIES AND SUBTLE DIFFERENCES BETWEEN THE CATALYTIC DOMAINS OF THESE ORTHOLOGOUS PROTEINS..... 115

FIGURE 3. 30 PHYLOGENETIC AND SEQUENCE ANALYSIS OF PARP6. THIS FIGURE ILLUSTRATES THE EVOLUTIONARY RELATIONSHIPS OF PARP6 ACROSS VARIOUS VERTEBRATE SPECIES, INCLUDING MAMMALS, AMPHIBIANS, REPTILES, AND FISH, WITH A SPECIFIC FOCUS ON THE AVIAN LINEAGE. THE PHYLOGENETIC TREE REVEALS A DISTINCT CLADE FORMED BY AVIAN SPECIES, SUGGESTING A UNIQUE EVOLUTIONARY TRAJECTORY FOR PARP6 WITHIN THE BIRD LINEAGE. THE TREE WAS CONSTRUCTED USING MAXIMUM LIKELIHOOD METHOD IN MEGA6. .... 117

FIGURE 3. 31 SEQUENCE HOMOLOGY OF PARP6. HEATMAP DISPLAYING THE AMINO ACID SEQUENCE IDENTITY BETWEEN CHPARP6 AND ITS HUMAN COUNTERPART. THE SEQUENCE ALIGNMENT, PERFORMED USING THE CLUSTALW ALGORITHM IN SDT, REVEALS APPROXIMATELY 82% SEQUENCE IDENTITY, AS INDICATED BY THE COLOR-CODED IDENTITY SCALE. THIS LEVEL OF CONSERVATION SUGGESTS A HIGH DEGREE OF STRUCTURAL AND FUNCTIONAL SIMILARITY BETWEEN THE CHICKEN AND HUMAN PARP6 PROTEINS, CONSISTENT WITH THEIR DISTINCT EVOLUTIONARY TRAJECTORY WITHIN THE AVIAN LINEAGE. .... 118

FIGURE 3. 32 MULTIPLE SEQUENCE ALIGNMENT OF PARP6 CATALYTIC DOMAIN. THE CATALYTIC DOMAIN OF CHPARP6 EXHIBITS A VERY HIGH DEGREE OF CONSERVATION WHEN COMPARED TO ITS HUMAN COUNTERPART, WITH A FEW NUMBERS OF POINT MUTATIONS OBSERVED. THE ALIGNMENT WAS GENERATED FOR CHICKEN, TURKEY, DUCK, HUMAN, AND MOUSE. THE ALIGNMENT WAS PERFORMED USING BIOEDIT SOFTWARE. IDENTICAL AMINO ACID RESIDUES ACROSS THE ALIGNED SEQUENCES ARE INDICATED BY DOTS. THE CATALYTIC DOMAINS OF EACH PROTEIN ARE HIGHLIGHTED WITHIN RED BOXES..... 119

FIGURE 3. 33 STRUCTURAL COMPARISON OF PARP6 CATALYTIC DOMAIN. THIS PANEL ILLUSTRATES A COMPARATIVE ANALYSIS OF THE CATALYTIC DOMAINS OF CHPARP6 AND ITS HUMAN COUNTERPART. PREDICTED 3D STRUCTURE OF THE FULL-LENGTH PROTEIN IS DISPLAYED, WITH THE CATALYTIC DOMAIN HIGHLIGHTED IN GREEN AND THE REMAINING PROTEIN IN ORANGE. THE CATALYTIC DOMAIN IS FURTHER EMPHASIZED BY A BLACK BOX. 3D STRUCTURE WAS PREDICTED USING I-TASSER AND ALPHAFOLD AND VISUALIZED AND EDITED USING PYMOL. A SUPERIMPOSITION OF THE CATALYTIC DOMAINS IS SHOWN, WITH THE CHICKEN CATALYTIC DOMAIN REPRESENTED IN GREEN AND THE HUMAN CATALYTIC DOMAIN IN BLUE. THIS COMPARISON REVEALS THE STRUCTURAL SIMILARITIES AND SUBTLE DIFFERENCES BETWEEN THE CATALYTIC DOMAINS OF THESE ORTHOLOGOUS PROTEINS..... 120

FIGURE 3. 34 PHYLOGENETIC AND SEQUENCE ANALYSIS OF PARP8. THIS FIGURE ILLUSTRATES THE EVOLUTIONARY RELATIONSHIPS OF PARP8 ACROSS VARIOUS VERTEBRATE SPECIES, INCLUDING MAMMALS, AMPHIBIANS,

REPTILES, AND FISH, WITH A SPECIFIC FOCUS ON THE AVIAN LINEAGE. THE PHYLOGENETIC TREE REVEALS A DISTINCT CLADE FORMED BY AVIAN SPECIES, SUGGESTING A UNIQUE EVOLUTIONARY TRAJECTORY FOR PARP8 WITHIN THE BIRD LINEAGE. THE TREE WAS CONSTRUCTED USING MAXIMUM LIKELIHOOD METHOD IN MEGA6. .... 122

FIGURE 3. 35 AMINO ACID SEQUENCE HOMOLOGY OF PARP8. HEATMAP DISPLAYING THE AMINO ACID SEQUENCE IDENTITY BETWEEN CHPARP8 AND ITS HUMAN COUNTERPART. THE SEQUENCE ALIGNMENT, PERFORMED USING THE CLUSTALW ALGORITHM IN SDT, REVEALS APPROXIMATELY 85% SEQUENCE IDENTITY, AS INDICATED BY THE COLOR-CODED IDENTITY SCALE. THIS LEVEL OF CONSERVATION SUGGESTS A MODERATE DEGREE OF STRUCTURAL AND FUNCTIONAL SIMILARITY BETWEEN THE CHICKEN AND HUMAN PARP8 PROTEINS, CONSISTENT WITH THEIR DISTINCT EVOLUTIONARY TRAJECTORY WITHIN THE AVIAN LINEAGE. 123

FIGURE 3. 36 MULTIPLE SEQUENCE ALIGNMENT OF PARP8 CATALYTIC DOMAIN. THE CATALYTIC DOMAIN OF CHPARP8 EXHIBITS A VERY HIGH DEGREE OF CONSERVATION WHEN COMPARED TO ITS HUMAN COUNTERPART, WITH LESS THAN TEN-POINT MUTATIONS OBSERVED. THE ALIGNMENT WAS GENERATED FOR CHICKEN, TURKEY, DUCK, HUMAN, AND MOUSE WAS PERFORMED USING BIOEDIT SOFTWARE. IDENTICAL AMINO ACID RESIDUES ACROSS THE ALIGNED SEQUENCES ARE INDICATED BY DOTS. THE CATALYTIC DOMAINS ARE HIGHLIGHTED WITHIN RED BOXES. .... 124

FIGURE 3. 37 STRUCTURAL COMPARISON OF PARP8 CATALYTIC DOMAIN. THIS PANEL ILLUSTRATES A COMPARATIVE ANALYSIS OF THE CATALYTIC DOMAINS OF CHPARP8 AND ITS HUMAN COUNTERPART. PREDICTED 3D STRUCTURE OF THE FULL-LENGTH PROTEIN IS DISPLAYED, WITH THE CATALYTIC DOMAIN HIGHLIGHTED IN GREEN AND THE REMAINING PROTEIN IN ORANGE. THE CATALYTIC DOMAIN IS FURTHER EMPHASIZED BY A BLACK BOX. 3D STRUCTURE WAS PREDICTED USING I-TASSER AND ALPHAFOLD AND VISUALIZED AND EDITED USING PYMOL. A SUPERIMPOSITION OF THE CATALYTIC DOMAINS IS SHOWN, WITH THE CHICKEN CATALYTIC DOMAIN REPRESENTED IN GREEN AND THE HUMAN CATALYTIC DOMAIN IN BLUE. THIS COMPARISON REVEALS THE STRUCTURAL SIMILARITIES AND SUBTLE DIFFERENCES BETWEEN THE CATALYTIC DOMAINS OF THESE ORTHOLOGOUS PROTEINS. .... 125

FIGURE 3. 38 PHYLOGENETIC ANALYSIS OF PARP11. THIS FIGURE ILLUSTRATES THE EVOLUTIONARY RELATIONSHIPS OF PARP11 ACROSS VARIOUS VERTEBRATE SPECIES, INCLUDING MAMMALS, AMPHIBIANS, REPTILES, AND FISH. THE PHYLOGENETIC TREE REVEALS A DISTINCT CLADE FORMED BY AVIAN SPECIES, SUGGESTING A UNIQUE EVOLUTIONARY TRAJECTORY FOR PARP11 WITHIN THE BIRD LINEAGE. THE TREE WAS CONSTRUCTED USING MAXIMUM LIKELIHOOD METHOD IN MEGA6. .... 127

FIGURE 3. 39 SEQUENCE HOMOLOGY OF PARP11. HEATMAP DISPLAYING THE AMINO ACID SEQUENCE IDENTITY BETWEEN CHPARP11 AND ITS HUMAN COUNTERPART. THE SEQUENCE ALIGNMENT, PERFORMED USING THE CLUSTALW ALGORITHM IN SDT, REVEALS APPROXIMATELY 77% SEQUENCE IDENTITY, AS INDICATED BY THE COLOR-CODED IDENTITY SCALE. THIS LEVEL OF CONSERVATION SUGGESTS A HIGH DEGREE OF STRUCTURAL AND FUNCTIONAL SIMILARITY BETWEEN THE CHICKEN AND HUMAN PARP11 PROTEINS. .... 128

FIGURE 3. 40 MULTIPLE SEQUENCE ALIGNMENT OF PARP11 CATALYTIC DOMAIN. THE CATALYTIC DOMAIN OF CHPARP11 EXHIBITS A HIGH DEGREE OF CONSERVATION COMPARED TO ITS HUMAN COUNTERPART, WITH ONLY A SMALL NUMBER OF POINT MUTATIONS OBSERVED. MSA WAS GENERATED FROM CHICKEN, TURKEY, DUCK, HUMAN, AND MOUSE. THE ALIGNMENTS WERE PERFORMED USING BIOEDIT SOFTWARE. IDENTICAL AMINO ACID RESIDUES ACROSS THE ALIGNED SEQUENCES ARE INDICATED BY DOTS. THE CATALYTIC DOMAINS OF EACH PROTEIN ARE HIGHLIGHTED WITHIN RED BOXES. .... 129

FIGURE 3. 41 STRUCTURAL COMPARISON OF PARP11 CATALYTIC DOMAIN. THIS PANEL ILLUSTRATES A COMPARATIVE ANALYSIS OF THE CATALYTIC DOMAINS OF CHPARP11 AND ITS HUMAN COUNTERPART. PREDICTED 3D STRUCTURE OF THE FULL-LENGTH PROTEIN IS DISPLAYED, WITH THE CATALYTIC DOMAIN HIGHLIGHTED IN GREEN AND THE REMAINING PROTEIN IN ORANGE. THE CATALYTIC DOMAIN IS FURTHER EMPHASIZED BY A BLACK BOX. 3D STRUCTURE WAS PREDICTED USING I-TASSER AND ALPHAFOLD AND VISUALIZED AND EDITED USING PYMOL. A SUPERIMPOSITION OF THE CATALYTIC DOMAINS IS SHOWN, WITH THE CHICKEN CATALYTIC DOMAIN REPRESENTED IN GREEN AND THE HUMAN CATALYTIC DOMAIN IN BLUE. THIS COMPARISON REVEALS THE STRUCTURAL SIMILARITIES AND SUBTLE DIFFERENCES BETWEEN THE

FIGURE 4. 1 OVERVIEW OF THE EXPERIMENTAL DESIGN USED FOR TRANSCRIPTOMIC STUDY. THE EXPERIMENTAL APPROACH INVOLVED INFECTING A POPULATION OF CEF CELLS WITH THE IAV STRAIN AT A SPECIFIED MULTIPLICITY OF INFECTION (MOI) TO ENSURE CONSISTENT VIRAL EXPOSURE ACROSS REPLICATES. MOCK-INFECTED CELLS WERE MAINTAINED IN PARALLEL AS A CONTROL GROUP. THE EXTRACTED RNA FROM BOTH BIOLOGICAL CONDITIONS UNDERWENT LIBRARY PREPARATION AND HIGH-THROUGHPUT RNA SEQUENCING TO GENERATE TRANSCRIPTOMIC PROFILES FOR EACH CONDITION..... 139

FIGURE 4. 2 DISPERSION BOX PLOT OF RNA-SEQ DATA. THIS FIGURE DISPLAYS THE DISPERSION BOX PLOT GENERATED USING DESEQ2, DEMONSTRATING THE VARIATION IN RNA-SEQ DATA FROM CEF CELLS. DISPERSION MEASURES THE VARIABILITY OF GENE EXPRESSION ACROSS BIOLOGICAL REPLICATES. A HIGH DISPERSION INDICATES SIGNIFICANT VARIABILITY, WHILE A LOW DISPERSION SUGGESTS STABLE GENE EXPRESSION. THE BOX PLOT PROVIDES AN OVERVIEW OF THE DISTRIBUTION OF DISPERSION VALUES ACROSS THE DATASET, HIGHLIGHTING THE OVERALL LEVEL OF VARIABILITY IN GENE EXPRESSION BETWEEN REPLICATES. .... 142

FIGURE 4. 3 GENE-WISE DISPERSION ESTIMATION PLOT. THIS FIGURE PRESENTS THE GENE-WISE DISPERSION ESTIMATION PLOT, ILLUSTRATING THE RELATIONSHIP BETWEEN MEAN GENE EXPRESSION LEVELS AND DISPERSION. EACH BLACK DOT REPRESENTS THE INITIAL DISPERSION ESTIMATE FOR A GENE, CALCULATED USING MAXIMUM LIKELIHOOD ESTIMATION. THE BLUE LINE REPRESENTS THE FITTED CURVE, INDICATING THE EXPECTED DISPERSION VALUE FOR GENES WITH A GIVEN EXPRESSION LEVEL. THIS PLOT DEMONSTRATES THE DIVERSE LEVELS OF VARIABILITY ACROSS INDIVIDUAL GENES AND THE OVERALL DISTRIBUTION OF ACCEPTABLE DISPERSION ESTIMATES. THE FINAL DISPERSION ESTIMATES ARE SHRUNK TOWARDS THE FITTED CURVE TO MINIMIZE THE RISK OF FALSE POSITIVES IN SUBSEQUENT DIFFERENTIAL EXPRESSION ANALYSIS. .... 142

FIGURE 4. 4 DENSITY PLOT OF TRANSFORMED RNA-SEQ DATA. THIS FIGURE DEPICTS THE DENSITY PLOT OF TRANSFORMED RNA-SEQ DATA FROM CEF CELLS, COMPARING MOCK AND IAV-INFECTED SAMPLES. THE PLOT ILLUSTRATES THE NORMALIZED LIKELIHOODS OF THE BIOLOGICAL SAMPLES. A WIDER AND LESS SHARP LIKELIHOOD CURVE (RED LINE) FOR THE IAV-TREATED SAMPLE INDICATES A HIGHER DISPERSION OF GENE EXPRESSION COMPARED TO THE UNTREATED SAMPLE. THIS REFLECTS THE INCREASED VARIABILITY IN GENE EXPRESSION OBSERVED IN INFECTED CELLS..... 143

FIGURE 4. 5 PRINCIPAL COMPONENT ANALYSIS OF RNA-SEQ DATA FROM IAV-TREATED AND MOCK CEF CELLS. (A & B) PCA SCATTER PLOT: THIS FIGURE DISPLAYS THE RESULTS OF PCA PERFORMED ON RNA-SEQ DATA FROM TRIPPLICATE BIOLOGICAL REPLICATES OF MOCK AND IAV-TREATED CEF CELLS. THE PLOT ILLUSTRATES THE RELATIONSHIP BETWEEN SAMPLES BASED ON THEIR GENE EXPRESSION LEVELS. PC1 AND PC2 REPRESENT THE DIRECTIONS OF MAXIMUM VARIANCE IN THE DATA. PC1 ACCOUNTS FOR 95.6% OF THE VARIANCE, DISTINGUISHING BETWEEN MOCK AND IAV-TREATED SAMPLES. PC2 ACCOUNTS FOR 4.3% OF THE VARIANCE, SHOWING VARIANCE WITHIN THE IAV TREATED SAMPLES. THE CLOSE CLUSTERING OF BIOLOGICAL REPLICATES WITHIN EACH TREATMENT GROUP INDICATES HIGH REPRODUCIBILITY. THE SEPARATION OF MOCK AND IAV-TREATED SAMPLES DEMONSTRATES DISTINCT GENE EXPRESSION PROFILES. (C) SCREE PLOT: THE SCREE PLOT SHOWS THE PERCENTAGE OF VARIANCE EXPLAINED BY EACH PRINCIPAL COMPONENT. THIS PLOT AIDS IN DETERMINING THE OPTIMAL NUMBER OF PRINCIPAL COMPONENTS TO REPRESENT THE DATA, CONFIRMING THAT THE MAJORITY OF VARIANCE IS CAPTURED BY THE FIRST TWO PRINCIPAL COMPONENTS. THIS VALIDATES THE USE OF PC1 AND PC2 TO VISUALIZE THE DATA IN THE SCATTER PLOT. PC3 ACCOUNTED FOR 1.9% OF THE VARIANCE. .... 145

FIGURE 4. 6 DIFFERENTIAL GENE EXPRESSION ANALYSIS OF IAV-INFECTED CEF CELLS. THIS FIGURE SUMMARIZES THE DIFFERENTIAL GENE EXPRESSION ANALYSIS COMPARING IAV-INFECTED CEF CELLS TO MOCK. THE ANALYSIS QUANTIFIED GENE EXPRESSION CHANGES USING RNA-SEQ DATA TO IDENTIFY DEGS. A-B) THE RNA-SEQ ANALYSIS INITIALLY IDENTIFIED 9672 GENES. AFTER APPLYING AN INITIAL FILTERING STEP, 3785 DEGS WERE OBTAINED. THE DISTRIBUTION OF THESE DEGS IS SHOWN, WITH 1603 UPREGULATED AND 2182 DOWNREGULATED IN IAV-INFECTED CELLS. THE X-AXIS INDICATES THE DIRECTION OF GENE EXPRESSION

CHANGE (UPREGULATION OR DOWNREGULATION), AND THE Y-AXIS REPRESENTS THE CORRESPONDING NUMBER OF GENES. C) FOLLOWING FINAL FILTERING FOR STATISTICAL SIGNIFICANCE, 2243 DEGS WERE IDENTIFIED AS HAVING SIGNIFICANTLY DIFFERENT EXPRESSION LEVELS. OF THESE, 910 GENES WERE UPREGULATED, AND 1333 GENES WERE DOWNREGULATED IN IAV-INFECTED CEF CELLS COMPARED TO MOCK-TREATED CELLS. THIS FIGURE REPRESENTS THE FINAL COUNT OF STATISTICALLY SIGNIFICANT DEGS USED FOR FURTHER ANALYSIS. .... 146

FIGURE 4. 7 COMPARISON OF TOP 100 DEGS IN MOCK AND IAV-TREATED CEF CELLS. THE HEATMAP VISUALISATION OF THE TOP 100 DEGS IN CEF CELLS FOLLOWING H9N2 INFECTION. RED INDICATES UPREGULATED GENES, WHILE GREEN INDICATES DOWNREGULATED GENES, RELATIVE TO MOCK CONTROLS. NOTABLY, GENES INVOLVED IN ANTIVIRAL DEFENCE, SUCH AS MX2, OAS1, AND IRF7, ARE SIGNIFICANTLY UPREGULATED, SUGGESTING AN ACTIVATED HOST IMMUNE RESPONSE. CONVERSELY, DOWNREGULATION OF GENES INVOLVED IN CELLULAR PROCESSES LIKE CELL ADHESION AND EXTRACELLULAR MATRIX FORMATION MAY REFLECT A DISRUPTION OF CELLULAR FUNCTIONS DURING VIRAL INFECTION. .... 148

FIGURE 4. 8 COMPARISON OF DIFFERENTIALLY EXPRESSED PARP GENES IN MOCK AND IAV-TREATED CEF CELLS. A) NORMALIZED HISTOGRAM DEPICTING THE DIFFERENTIAL EXPRESSION OF PARP GENES IN IAV-INFECTED CEF CELLS COMPARED TO MOCK CONTROLS. NOTABLE UPREGULATION IS OBSERVED FOR PARP14, PARP12, AND PARP10, FOLLOWED BY PARP9. CONVERSELY, SLIGHT DOWNREGULATION IS EVIDENT FOR PARP1, PARP3, AND PARP4, WHILE PARP2 EXPRESSION REMAINS LARGELY UNCHANGED. B) HEATMAP VISUALISATION OF THE TOP TWO THOUSAND DEGS IN IAV-INFECTED CEF CELLS. THE X-AXIS REPRESENTS THE GENE NAME, AND THE Y-AXIS REPRESENTS THE TYPE OF TREATMENT ADMINISTERED. NOTABLY, ALL FIVE DIFFERENTIALLY EXPRESSED PARP GENES (PARP1, PAR3, PARP4, PARP10, PARP14) EXHIBIT INCREASED VARIABILITY IN EXPRESSION LEVELS IN THE INFECTED CELLS, WITH PARP14 DEMONSTRATING THE HIGHEST LEVEL OF VARIABILITY. .... 150

FIGURE 4. 9 THE VOLCANO PLOT OF DIFFERENTIALLY EXPRESSED GENES IN IAV-TREATED CEF CELLS. A) THIS VOLCANO PLOT DISPLAYS THE DIFFERENTIAL EXPRESSION OF PARP GENES IN IAV-INFECTED CEF CELLS COMPARED TO MOCK-TREATED CELLS. THE Y-AXIS REPRESENTS THE NEGATIVE BASE-10 LOGARITHM OF THE ADJUSTED P-VALUE ( $-\log_{10}(P\text{-VALUE})$ ), INDICATING STATISTICAL SIGNIFICANCE. THE X-AXIS REPRESENTS THE BASE-2 LOGARITHM OF THE FOLD CHANGE ( $\log_2(\text{FOLD CHANGE})$ ), INDICATING THE MAGNITUDE OF GENE EXPRESSION CHANGE. RED DATA POINTS SIGNIFY UPREGULATED PARP GENES. PARP14 IS THE MOST SIGNIFICANTLY UPREGULATED GENE, FOLLOWED BY PARP12, PARP10, PARP9, AND PARP11, SUGGESTING THEIR POTENTIAL ROLES IN THE CELLULAR RESPONSE TO IAV INFECTION. B) THIS VOLCANO PLOT SHOWS THE GLOBAL DIFFERENTIAL GENE EXPRESSION BETWEEN IAV-INFECTED AND MOCK-TREATED CEF CELLS. THE AXES ARE THE SAME AS IN (A). RED DATA POINTS INDICATE UPREGULATED GENES, AND BLUE DATA POINTS INDICATE DOWNREGULATED GENES. UPREGULATED GENES INCLUDE IL6, DHX58, IL8L2, AND GSDME, ASSOCIATED WITH IMMUNE RESPONSE, INFLAMMATION, AND CELL DEATH. DOWNREGULATED GENES INCLUDE ACTG2, TIMP3, ACTA2, COL1A2, PTN, AND ALDH1A1, INVOLVED IN CELL MOTILITY, EXTRACELLULAR MATRIX REMODELLING, AND CELLULAR DIFFERENTIATION. THIS PLOT PROVIDES A COMPREHENSIVE OVERVIEW OF THE GENE EXPRESSION CHANGES INDUCED BY IAV INFECTION. .... 152

FIGURE 4. 10 THE LOLLIPOP CHART FOR CELLS INFECTED WITH IAV PROVIDES A COMPELLING VISUAL REPRESENTATION OF THE VARIOUS BIOLOGICAL PATHWAYS AT PLAY. IT HIGHLIGHTS THE CELLS EFFORTS TO COMBAT THE VIRAL INFECTION. EACH LOLLIPOP REPRESENTS A SIGNIFICANTLY ENRICHED BIOLOGICAL PATHWAY, WITH THE HORIZONTAL POSITION INDICATING THE FOLD ENRICHMENT. THE SIZE OF THE DOT CORRESPONDS TO THE NUMBER OF GENES WITHIN THAT PATHWAY, AND THE COLOR INTENSITY REFLECTS THE STATISTICAL SIGNIFICANCE, REPRESENTED BY  $-\log_{10}(\text{FDR})$ . THE NAD<sup>+</sup> ADP-RIBOSYLTRANSFERASE ACTIVITY PATHWAY SHOWS THE HIGHEST FOLD ENRICHMENT (~14), AND HIGHEST STATISTICAL SIGNIFICANCE ( $-\log_{10}(\text{FDR}) = 6$ ), DESPITE HAVING FEWER GENES, STRONGLY IMPLICATING PARP PROTEINS IN THE CELLULAR RESPONSE TO IAV INFECTION. THE CHART ALSO HIGHLIGHTS OTHER ACTIVATED PATHWAYS SUCH AS RESPONSE TO EXTERNAL STIMULUS, RESPONSE TO OTHER ORGANISM, IMMUNE SYSTEM DEVELOPMENT, AND VARIOUS IMMUNE AND INFLAMMATORY RESPONSE CATEGORIES, ILLUSTRATING THE COMPREHENSIVE AND INTERCONNECTED NATURE OF THE HOST CELL'S DEFENSE MECHANISMS AGAINST VIRAL INFECTION. THIS ANALYSIS PROVIDES INSIGHTS INTO THE KEY BIOLOGICAL PROCESSES MODULATED DURING IAV INFECTION IN CEF CELLS, POTENTIALLY INFORMING THE

FIGURE 4. 11 VALIDATION OF PARP EXPRESSION BY RT-QPCR. THE ANALYSIS REVEALED THAT SEVERAL PARP FAMILY MEMBERS, INCLUDING PARP3, 5, 4, 7, 8, AND 11, EXHIBITED MINIMAL OR NEGLIGIBLE CHANGES IN EXPRESSION LEVELS ( $\Delta\Delta CT < 0.5$ ) FOLLOWING H9N2 INFECTION IN THE CONTEXT OF TRANSIENT OVEREXPRESSION. PARP1, 6, 9, AND 12 SHOWED A MODEST UPREGULATION WITH SLIGHTLY HIGHER  $\Delta\Delta CT$  VALUES. NOTABLY, PARP14 DEMONSTRATED THE MOST NOTICEABLE UPREGULATION, WITH A  $\Delta\Delta CT$  VALUE OF 1.6, STRONGLY SUPPORTING THE FINDINGS FROM THE TRANSCRIPTOMIC ANALYSIS AND HIGHLIGHTING A POTENTIAL CRUCIAL ROLE FOR PARP14 IN THE HOST RESPONSE TO H9N2 INFECTION. THE  $2^{-\Delta\Delta CT}$  METHOD WAS USED TO CALCULATE RELATIVE GENE EXPRESSION LEVELS, WHICH WERE THEN NORMALISED TO GAPDH. THE DATA REPRESENTS THE MEAN  $\pm$  SEM OF THREE INDEPENDENT EXPERIMENTS. .... 156

FIGURE 4.12 CELLULAR LOCALISATION OF CHPARPS IN DF1 CELLS DEPICTS THE SUBCELLULAR LOCALIZATION OF VARIOUS CHPARPS IN DF1 CELLS. PARP1 WAS OBSERVED EXCLUSIVELY WITHIN THE NUCLEUS, SUGGESTING A FUNCTIONAL ROLE IN NUCLEAR PROCESSES SUCH AS DNA REPAIR AND GENE REGULATION. IN CONTRAST, PARP3 EXHIBITED A DUAL LOCALIZATION, PRESENT IN BOTH THE NUCLEUS AND CYTOPLASM, IMPLYING A MORE VERSATILE ROLE POTENTIALLY INVOLVING SHUTTLING BETWEEN THESE COMPARTMENTS. PARP5, 6, 7, 8, 9, 12, 13, AND 14 ALL DEMONSTRATED CYTOPLASMIC LOCALIZATION, INDICATING THEIR INVOLVEMENT IN CYTOPLASMIC FUNCTIONS SUCH AS SIGNALING OR PROTEIN TRAFFICKING. .... 157

FIGURE 5. 1 ANTIVIRAL EFFICACY OF CHPARP PROTEINS. THIS BAR GRAPH COMPARES THE ANTIVIRAL ACTIVITY OF VARIOUS CHPARP PROTEINS AGAINST IAV H9N2. THE FORMATION OF PLAQUE-FORMING UNITS (PFUS) WAS MEASURED TO ASSESS THE ANTIVIRAL EFFICACY. STATISTICAL ANALYSIS REVEALED THAT CHPARP1, 7, 8, 9, 11, 12, 13, AND 14 EXHIBITED SIGNIFICANT ANTIVIRAL ACTIVITY, WHILE CHPARP3 DEMONSTRATED THE LOWEST SIGNIFICANCE, COUPLED WITH INCREASED PFU COUNTS COMPARED TO THE CONTROL, SUGGESTING POTENTIAL IMPAIRMENT OF THE ANTIVIRAL RESPONSE. PROTEINS 4 AND 5 WERE FOUND TO BE NON-SIGNIFICANT. THE REMAINING PROTEINS, WITH THE EXCEPTION OF CHPARP6, EFFECTIVELY RESTRICTED VIRAL REPLICATION AND SPREAD, AS EVIDENCED BY REDUCED PFU COUNTS. .... 168

FIGURE 5. 2 STRUCTURAL PREDICTION OF CHPARP14. A) DOMAIN ORGANISATION OF CHPARP14. B) PREDICTED 3D STRUCTURE OF THE CHPARP14. .... 173

FIGURE 5. 3 STRUCTURE BASIS FOR PRIMER DESIGNING. DESIGN OF PRIMERS BASED ON THE DOMAIN STRUCTURE FOR CLONING CHPARP14 INTO EGFP-FLAG-C1-KU70 MAMMALIAN EXPRESSION VECTOR. .... 175

FIGURE 5. 4 MAP OF EGFP-FLAG-C1-KU 70 MAMMALIAN EXPRESSION VECTOR (ADDGENE). THE PLASMID CONTAINS THE ENHANCED GREEN FLUORESCENT PROTEIN (EGFP) GENE FUSED IN-FRAME WITH A FLAG-TAGGED KU70 GENE. KEY FEATURES OF THE PLASMID ARE INDICATED, INCLUDING THE CMV PROMOTER, EGFP CODING SEQUENCE, FLAG TAG, KU70 CODING SEQUENCE, AND THE SELECTION MARKER. .... 176

FIGURE 5. 5 LABELLING OF CHPARP14 CONSTRUCTS CELLULAR LOCALISATION. DF1 CELLS WERE TRANSFECTED WITH PLASMIDS ENCODING DIFFERENT CHPARP14 CONSTRUCTS: FULL-LENGTH (FL), CHP14 $\Delta$ N, CHP14 $\Delta$ MAC, CHP14 $\Delta$ MACD, CHP14 $\Delta$ CWC, CHP14 $\Delta$ WC, AND CAT. AFTER 24 HOURS, CELLS WERE FIXED AND STAINED WITH AN ANTIBODY AGAINST FLAG, FOLLOWED BY A SECONDARY ANTIBODY. NUCLEI WERE STAINED WITH DAPI. SCALE BAR: 5  $\mu$ M. .... 179

FIGURE 5. 6 CONFIRMING THE EXPRESSION OF CHPARP14 CONSTRUCTS IN THE PROTEIN EXTRACT. DF1 CELLS WERE TRANSFECTED WITH PLASMIDS ENCODING DIFFERENT CHPARP14 CONSTRUCTS: FULL-LENGTH (FL), CHP14 $\Delta$ N, CHP14 $\Delta$ MAC, CHP14 $\Delta$ MACD, CHP14 $\Delta$ CWC, CHP14 $\Delta$ WC, AND CHP14 $\Delta$ CAT. WHOLE-CELL LYSATES WERE SUBJECTED TO SDS-PAGE AND WESTERN BLOT ANALYSIS USING AN ANTIBODY AGAINST FLAG. .... 180

FIGURE 5. 7 RT-QPCR ANALYSIS OF VIRAL REPLICATION IN CELLS TREATED WITH VARIOUS PROTEIN CONSTRUCTS. VIRAL RNA LEVELS WERE MEASURED IN CELLS TREATED WITH FULL-LENGTH PROTEIN, TRUNCATED

CONSTRUCTS, OR A CONTROL GROUP (VIRUS ONLY). RELATIVE VIRAL REPLICATION FOLD CHANGE WAS CALCULATED COMPARED TO THE CONTROL GROUP.....	181
FIGURE 5. 8 PLAQUE ASSAY TO DETERMINE THE ANTIVIRAL EFFICACY OF CHPARP14 AND ITS CONSTRUCTS AGAINST IAV IN DF1 CELLS. ALL THE CONSTRUCTS SHOW A REDUCTION IN PLAQUE FORMATION, ALTHOUGH NOT ALL OF THEM BEING STATISTICALLY SIGNIFICANT IMPLIES THE ANTIVIRAL NATURE OF THE PROTEIN. PLAQUES WERE COUNTED AT $10^{-3}$ DILUTION AND THE SIGNIFICANCE BETWEEN GROUPS WAS ASSESSED USING ONE-WAY ANOVA WITH GRAPHPAD PRISM 10 SOFTWARE.....	183
FIGURE 5. 9 DOMAIN STRUCTURE FRAMEWORK FOR THE DESIGN OF HUPARP14 CONSTRUCT CLONING INTO EGFP-FLAG-C1-KU70 MAMMALIAN EXPRESSION VECTOR. ....	185
FIGURE 5. 10 CELLULAR LOCALISATION OF HUPARP14 CONSTRUCTS IN HEK CELLS. IMMUNOFLUORESCENCE IMAGES SHOWING THE LOCALIZATION OF HUPARP14 CONSTRUCTS. FULL-LENGTH HUPARP14 WAS NUCLEAR. MACRODOMAIN-CONTAINING CONSTRUCTS (HUPARP14 $\Delta$ MAC, HUPARP14 $\Delta$ C) AND HUPARP14 $\Delta$ CW WERE CYTOPLASMIC. HUPARP14 $\Delta$ WC WAS BOTH CYTOPLASMIC AND NUCLEAR. HUPARP14 $\Delta$ MACD AND HUPARP14 $\Delta$ CAT WERE NOT DETECTED. MACRODOMAINS AND D/WWE/CAT DOMAINS DICTATE CYTOPLASMIC LOCALIZATION; WWE/CAT ALONE ALLOWS DUAL LOCALIZATION. ....	186
FIGURE 5. 11 CONFIRMING THE EXPRESSION OF HUPARP14 CONSTRUCTS IN THE PROTEIN EXTRACT. HEK CELLS WERE TRANSFECTED WITH FULL-LENGTH HUPARP14, HUPARP14 $\Delta$ MAC, HUPARP14 $\Delta$ MACD, HUPARP14 $\Delta$ C, HUPARP14 $\Delta$ CWC, HUPARP14 $\Delta$ WC, AND HUPARP14 $\Delta$ CAT. ANTI-FLAG ANTIBODIES WERE USED TO ANALYSE WHOLE-CELL LYSATES VIA SDS-PAGE AND WESTERN BLOT.....	187
FIGURE 5. 12 STATISTICAL ANALYSIS OF PLAQUE ASSAY FOR HUPARP14 CONSTRUCTS IN HEK CELLS. PLAQUES WERE COUNTED AT $10^{-1}$ DILUTION AND THE SIGNIFICANCE BETWEEN GROUPS WAS ASSESSED USING ONE-WAY ANOVA WITH GRAPHPAD PRISM 10 SOFTWARE. ....	189

## List of tables

TABLE 1. 1 PRIMARY FUNCTIONS OF IAV PROTEINS .....	19
TABLE 1. 2 ANTIVIRAL/PROVIRAL PROPERTIES OF THE PARPS.....	41
TABLE 1. 3 PARP INHIBITORS. ....	43
TABLE 2. 1 LIST OF CHPARP14 CLONED INTO EGFP-FLAG-C1-KU 70 MAMMALIAN EXPRESSION VECTOR.....	54
TABLE 2. 2 LIST OF PRIMERS USED FOR CLONING (PRIMERS WERE ORDERED FROM THERMO-SCIENTIFIC).....	55
TABLE 2. 3 PRIMERS FOR CHPARP RT-QPCR .....	65
TABLE 2. 4 LIST OF PRIMARY ANTIBODIES.....	67
TABLE 2. 5 LIST OF SECONDARY ANTIBODIES .....	67
TABLE 2. 6 BUFFERS AND REAGENTS .....	68
TABLE 4. 1 PRIMERS USED FOR RT-QPCR VALIDATION OF PARP EXPRESSION.....	155
TABLE 5. 1 LOCALISATION AND ANTIVIRAL/PROVIRAL NATURE OF CHPARPS.....	171
TABLE 5. 2 PRIMERS USED FOR CLONING CHPARP14 CONSTRUCTS.....	177
TABLE 5. 3 ANTIVIRAL EFFICACY OF CHPARP14 AND HUPARP14 CONSTRUCTS.....	192

# Contents

Declaration.....	i
Acknowledgement .....	ii
List of Figures.....	iii
List of tables .....	xiv
Abstract.....	1
<b>Chapter 1: General Information .....</b>	<b>3</b>
1.1: Influenza viruses .....	4
1.2: History of Influenza Viruses.....	5
1.3: Classification and Nomenclature of Influenza Viruses .....	6
1.3.1: Sub-Classification of Influenza A virus .....	7
1.4: Structure of Influenza A Virus .....	10
1.4.1: Influenza A virus Genome and its Proteins.....	11
1.4.1.1: Basic Polymerase2 (PB2)- Segment 1.....	12
1.4.1.2: Basic Polymerase1 (PB1)- Segment 2.....	13
1.4.1.3: Acidic Polymerase Protein (PA)- Segment 3.....	13
1.4.1.4: Hemagglutinin (HA)- Segment 4 .....	14
1.4.1.5: Nucleoprotein (NP)- Segment 5.....	15
1.4.1.6: Neuraminidase (NA)- Segment 6 .....	15
1.4.1.7: Matrix Protein1 (M1)- Segment 7.....	16
1.4.1.8: Matrix Protein2 (M2)- Segment 7.....	16
1.4.1.9: Non-Structural Protein1 (NS1)- Segment 8.....	17
1.4.1.10: Non-Structural Protein2 (NS2/NEP)- Segment 8 .....	18
1.5: IAV invasion and the antiviral response of the host cell.....	19
1.6: Evolution of IAV .....	21
1.7: Viral Pathogenicity .....	23
1.8: Zoonotic Potential of IAV .....	24
1.8.1: Human .....	24
1.8.2: Birds.....	25
1.9: Poly (ADP-ribose) polymerases (PARPs) .....	26
1.9.1: Classification of PARPs .....	28
1.9.2: PARP1.....	30
1.9.3: PARP3.....	31
1.9.4: PARP4.....	32
1.9.5: PARP5.....	33

1.9.6: PARP6.....	33
1.9.7: PARP7.....	34
1.9.8: PARP8.....	35
1.9.9: PARP9.....	36
1.9.10: PARP11.....	37
1.9.11: PARP12.....	37
1.9.12: PARP13.....	38
1.9.13: PARP14.....	39
1.9.14: PARP Inhibitors .....	42
<b>Chapter 2: Materials and Methods .....</b>	<b>46</b>
2.1: Mammalian Cell Culture .....	47
2.1.1: Growing Mammalian Cells.....	47
2.1.2: Passaging mammalian cells .....	47
2.1.3: Freezing Mammalian Cells.....	48
2.1.4: Transient Transfection .....	49
2.2: E. coli.....	50
2.2.1: Bacterial Transformation .....	50
2.2.2: Plasmid DNA Preparation from <i>E. coli</i> .....	51
2.2.3: Plasmid DNA isolation from <i>E. coli</i> (Qiagen) .....	51
2.2.4: Quantifying DNA concentration .....	52
2.2.5: Isopropanol Precipitation .....	52
2.3: Cloning and PCR .....	54
2.3.1: Chicken PARP14 Constructs.....	54
2.3.2: Primer design.....	55
2.3.3: PCR amplification of chPARP14 constructs .....	55
2.3.4: Q5-HF PCR Reaction Mixture .....	56
2.3.5: Q5-High-fidelity PCR reaction thermocycling conditions.....	56
2.3.6: Restriction Digestion .....	57
2.3.7: Agarose Gel Electrophoresis for DNA Fragment Analysis.....	57
2.3.8: DNA Gel Extraction .....	58
2.3.9: Ligation.....	59
2.3.10: Colony PCR.....	59
2.3.11: DNA Sequencing for Confirmation .....	61
2.4: Immunofluorescence Assay.....	61
2.5: SDS-PAGE .....	62
2.5.1: Western Blotting .....	62

2.6: Viral Quantification .....	63
2.6.1: Virus Propagation .....	63
2.6.2: Plaque Assay .....	64
2.6.3: RT-qPCR .....	65
2.6.4: RT-qPCR Reaction Mixture .....	66
2.6.5: RT-qPCR Thermocycling Conditions .....	66
2.7: Antibodies .....	67
2.8: Buffers and Reagents .....	68
2.9: Bioinformatic Analysis .....	69
2.9.1: Sequence Data Mining .....	69
2.9.2: Multiple Sequence Alignment (MSA) .....	69
2.9.3: Phylogenetic Analysis .....	69
2.9.4: Pairwise Identity Matrix .....	70
2.9.5: Protein Domain Prediction .....	70
2.9.6: Syntenic Analysis .....	70
2.9.7: 3D Protein Prediction .....	71
2.9.8: Statistical Analysis .....	71
2.9.9: Heatmap Visualization .....	71
2.9.10: Volcano Plots .....	71
2.9.11: Principal Component Analysis (PCA) .....	72
2.9.12: Scree Plot .....	72
2.9.13: Lollipop Chart .....	73
<b>Chapter 3: Bioinformatic Analysis of chPARPs .....</b>	<b>74</b>
3.1: Abstract .....	75
3.2: Introduction .....	75
3.3: Results .....	77
3.3.1: Domain organisation of PARP genes .....	77
3.3.2: Variation in synteny among PARP genes .....	80
3.3.3: Evolutionary variations in chicken DNA-dependent PARPs .....	81
3.3.4: Evolutionary Variations in Tankyrases .....	89
3.3.5: Evolutionary Variations in CCCH containing PARPs .....	94
3.3.6: Evolutionary Variations in Macro PARPs .....	105
3.3.7: Evolutionary Variations in chPARP4 .....	111
3.3.8: Evolutionary Variations in chPARP6 .....	116
3.3.9: Evolutionary Variations in chPARP8 .....	121
3.3.10: Evolutionary Variations in chPARP11 .....	126

3.4: Chapter Discussion .....	131
3.5: Future Directions: .....	134
<b>Chapter 4: Influenza Virus Transcriptionally Regulates PARP Genes in Chicken Primary Fibroblasts</b> .....	135
4.1: Abstract .....	136
4.2: Introduction .....	137
4.2.1: Chicken as Influenza Virus Reservoirs .....	137
4.2.2: Influenza-induced transcriptomics in chicken .....	138
4.3: Results.....	140
4.3.1: Pre-processing of RNA-seq data.....	140
4.3.2: IAV-induced Differential Gene Expression Analysis. ....	145
4.3.3: IAV-induced Differential Gene Expression Analysis of Top 100 DEGs.....	147
4.3.4: IAV-induced Differential Gene Expression Analysis of PARP genes.....	148
4.3.5: Volcano Plot Analysis Reveals Differential Expression of PARP Genes and Global Gene Changes in IAV-infected CEF Cells .....	150
4.3.6: PARP-Related Pathways Dominate the Cellular Response to IAV infection .....	153
4.3.7: Confirmation of the Transcriptomics with conventional RT-PCR .....	154
4.3.8: Cellular Localisation of Chicken PARPs.....	156
4.4: Discussion .....	158
4.5: Conclusion .....	160
<b>Chapter 5: PARP14 Protein of chicken and human Display Antiviral Effects Against Influenza A viruses</b> .....	162
5.1: Abstract .....	163
5.2: Introduction .....	163
5.2.1: Impact of PARP14 on Viral Replication and Host Responses .....	164
5.2.2: Implications for Antiviral Therapies .....	165
5.3: Results.....	167
5.3.1: Determining the Antiviral Efficacy of Several chPARP Proteins.....	167
5.3.2: Summary of chPARPs Characteristics .....	169
5.3.3: Rationale for Mechanistic Investigation of chPARP14.....	171
5.3.4: The Importance of Cloning Gene Fragments to Understand Antiviral Responses.....	174
5.3.5: Cloning of chPARP14 Constructs into pEGFP-C1-FLAG-ku70 Expression Vector .....	175
5.3.6: Cloning of chPARP14 Constructs .....	177
5.3.7: Cellular Localisation of chPARP14 Constructs in DF1 .....	177
5.3.8: Expression of chPARP14 using Western Blot.....	179
5.3.9: RT-qPCR Analysis for Quantification of Viral Gene Expression in DF1 cells treated with chPARP14 constructs. ....	180

5.3.10: Plaque Assay Analysis to determine the Antiviral Efficacy of chPARP14 constructs in DF1 cells.....	182
5.3.11: Cellular Localisation of huPARP14 Constructs .....	183
5.3.12: Western Blot Confirmation of huPARP14 constructs in the HEK cell protein extract.	186
5.3.13: Plaque Assay Analysis to determine the Antiviral Efficacy of huPARP14 constructs in HEK cells.....	188
5.4: Discussion .....	190
5.5: Limitations and Future Directions .....	193
5.6: Conclusion .....	194
<b>Chapter 6: Discussion</b> .....	195
<b>Chapter 7: Conclusions</b> .....	199
<b>Chapter 8: Future Directions</b> .....	200
<b>Chapter 9: References</b> .....	201

## Abstract

The Influenza A Virus (IAV) continues to pose a significant global health risk due to its capacity to trigger seasonal epidemics and occasional pandemics. Although vaccines and antiviral medications are available, the emergence of drug-resistant strains necessitates the development of novel therapeutic approaches. Poly (ADP-ribose) polymerases (PARPs) are a family of enzymes that participate in diverse cellular processes, such as DNA repair and immune response. Recent research has emphasized the potential of targeting PARPs as a novel antiviral strategy. This study aims to investigate the antiviral properties of the chicken PARP (chPARP) against IAV infection.

To identify potential antiviral PARP candidates, we employed a bioinformatic approach to analyse the PARP family in chickens, which is a susceptible host for IAV infection. We focused on chPARP due to its unique structural features and potential role in antiviral immunity. To further investigate the antiviral mechanism of chPARP, we performed transcriptomic analysis to identify differentially expressed genes in IAV-infected cells treated with chPARPs. Our findings provides a comprehensive understanding of the role of PARP proteins in IAV infection. Bioinformatic analysis of chicken PARP genes revealed diverse domain organizations, evolutionary divergence, and potential antiviral roles. RNA-seq analysis of IAV-infected cells identified over 3,700 differentially expressed genes, including significant upregulation of several PARP family members, particularly PARP14. Functional studies on chPARP14 demonstrated its antiviral activity, with some truncated forms exhibiting reduced viral replication. Notably, full-length chPARP14 and chPARP14 $\Delta$ CWC exhibited the most significant antiviral effects. While human PARP14

homologues showed varying antiviral activity, with some even exhibiting proviral effects, certain constructs, such as huPARP14 $\Delta$ MACD, displayed potent antiviral activity. These findings highlight the potential of targeting PARPs, particularly chPARP14, for developing novel antiviral strategies. However, further research with increased sample sizes and employing alternative approaches, such as chemical inhibition, RNA interference, and gene editing, is crucial to fully elucidate the role of PARPs in antiviral defence. This work has significant implications for our understanding of viral pathogenesis and the development of novel antiviral strategies. The identification of chPARP14 as a key player in antiviral defence, coupled with the observation that specific domains within the protein contribute to its antiviral activity, suggests novel therapeutic targets for combating IAV and potentially other viral infections. Furthermore, the study highlights the importance of considering species-specific variations in antiviral responses, as observed in the differing antiviral activities of chicken and human PARP14 homologues. These findings lay the groundwork for future investigations into the specific mechanisms of PARP14-mediated antiviral activity and the development of strategies to modulate its activity for therapeutic purposes.

# **Chapter 1: General Information**

## **1.1: Influenza viruses**

Influenza viruses are a class of highly contagious pathogens that can cause widespread illness and even severe pandemics. These microscopic viral agents are members of the Orthomyxoviridae family, which includes viruses such as Isavirus, Thogotovirus, and Quaranjavirus, and they come in a variety of strains, including the well-known A, B, C, and D (Mostafa et al., 2018). Influenza viruses are distinguished by their rapid mutation and evolution, which allows them to evade the human immune system and infect new hosts. The viruses primarily infect the respiratory system, invading the nose, throat, and lungs before hijacking host cells to replicate and spread. Influenza infections are characterised by a variety of symptoms, such as fever, body aches, fatigue, and coughing, which can last for days or even weeks. While most cases are minor, influenza can result in serious complications such as pneumonia, especially in vulnerable populations such as the elderly or those with underlying health conditions (Javanian et al., 2021).

IAV is a highly contagious respiratory pathogen and remains one of the leading causes of seasonal illness globally, infecting an estimated 3-5 million people annually (Kuriakose & Kanneganti, 2017; Tate & Mansell, 2018). The impact of IAV is staggering, with the World Health Organization estimating that deaths associated with influenza infection could be as high as 290-650 thousand per year, disproportionately affecting vulnerable populations like the young, elderly, immunocompromised, and those with underlying lung or heart conditions (Allen et al., 2009; Laghlali et al., 2020).

The seasonality of influenza outbreaks is well-documented, with the northern and southern hemispheres typically experiencing peaks in the winter months, while equatorial regions may see sporadic outbreaks year-round. The virus is primarily

transmitted through the air via infected individuals coughing or sneezing, as well as through contact with contaminated bodily fluids like saliva, nasal secretions, faeces, and even blood from infected animals. In humans, the hallmark symptoms of IAV infection include fever, severe muscle aches, debilitating headaches, persistent coughing, sore throat, and overall weakness and fatigue that can last for weeks (Shao et al., 2017). The rapid mutation rate of IAV also allows it to evade immune defences, necessitating annual vaccine updates to protect vulnerable populations (Neumann et al., 2009). As a highly adaptable pathogen, IAV remains one of the most pressing global health challenges, requiring constant surveillance, research, and preparedness to mitigate the devastating impact of seasonal outbreaks and potential pandemics.

## **1.2: History of Influenza Viruses**

Influenza viruses have a long and significant history, causing widespread illness and devastation around the world for centuries. The earliest recorded influenza-like illnesses date back to antiquity, with possible references to flu-like symptoms found in texts as early as the 5th century BCE in China and the 10th century CE in the Middle East (Taubenberger & Morens, 2010). However, the first well-documented influenza pandemic is thought to be the Russian Flu outbreak of 1889-1890, which is estimated to have infected roughly 40% of the world's population at the time and killed over 1 million people (Berche, 2022). Since then, numerous major influenza pandemics have swept across the globe, including the 1918 Spanish Flu pandemic, which was one of the deadliest outbreaks in human history, killing an estimated 50-100 million people worldwide. Other notable flu pandemics include the Asian Flu of 1957-1958, the Hong Kong Flu of 1968-1969, and the most recent Swine Flu pandemic in 2009-2010 (Taubenberger & Morens,

2010). In addition to these major global events, influenza viruses continue to cause seasonal epidemics on a yearly basis, with the World Health Organisation estimating that seasonal flu causes approximately 3-5 million cases of severe illness and 290,000 to 650,000 deaths globally (Kuriakose & Kanneganti, 2017; Laghlali et al., 2020; Tate & Mansell, 2018). Because of influenza viruses' ability to rapidly mutate and spread, as well as the difficulty of developing effective universal vaccines, they will most likely remain a persistent public health threat for the foreseeable future, necessitating ongoing global surveillance, research, and preparedness efforts.

### **1.3: Classification and Nomenclature of Influenza Viruses**

The classification and nomenclature of influenza viruses are complex and intricate topics that reflect the virulent pathogens' dynamic and ever-changing nature. Influenza viruses are part of the Orthomyxoviridae family, which is further divided into four types: Influenza A, Influenza B, Influenza C, and Influenza D (Kuriakose & Kanneganti, 2017; Mostafa et al., 2018). This taxonomy is based on significant differences in the antigenic properties of the nucleoprotein and matrix protein found within the viral structure. Influenza B and Influenza C, for instance, are known to typically cause milder infections in humans compared to other strains. Influenza D, on the other hand, is specifically adapted to infect cattle, and its ability to efficiently infect and spread between humans remains largely unknown (Mostafa et al., 2018).

Influenza A is the most prominent and well-known member of the influenza virus family. These viruses cause the majority of seasonal flu outbreaks as well as the most devastating pandemics in history. Influenza A viruses are further classified into distinct

subtypes based on the expression patterns of two critical surface proteins, hemagglutinin (HA) and neuraminidase (NA) (Ong et al., 2017).

### **1.3.1: Sub-Classification of Influenza A virus**

The influenza virus is a complex and fascinating organism, with a unique structure and genetic makeup that allows it to infect a wide range of hosts. At the heart of this virus are two key glycoproteins - HA and the NA. To date, 19 HA subtypes (H1-H19) and 11 NA subtypes (N1-N11) have been identified in influenza A viruses isolated from a variety of host species, including humans, birds, swine, and other mammals (Fereidouni et al., 2023; Ong et al., 2017). The numerous combinations of HA and NA subtypes result in a vast diversity of IAV strains that can infect and circulate within various host populations. The HA and NA proteins on IAV play an important role in determining which host species they can bind to and infect. With 19 known HA subtypes and 11 known NA subtypes, the potential for novel HA-NA pairings is enormous, resulting in the emergence of a diverse range of IAV strains capable of crossing the species barrier. The HA is a trimeric glycoprotein, composed of three identical monomers, each containing an intact HA0 single polypeptide chain as well as the HA1 and HA2 regions. This intricate structure enables the HA to bind to and fuse with the host cell's membrane, facilitating viral entry. In contrast, the NA is a tetramer, made up of four identical polypeptide chains. This tetrameric structure equips the NA with the ability to cleave the sialic acid residues that tether the newly formed viral particles to the host cell, allowing the virus to be released and spread to infect other cells.

While there is a remarkable genetic diversity within the influenza virus, with 19 known HA subtypes (H1 through H19) and 11 NA subtypes (N1 through N11), only a select few have been observed to cause human epidemics. Specifically, just 3 HA subtypes (H1, H2, and H3) and 2 NA subtypes (N1 and N2) have been responsible for the majority of influenza outbreaks in humans, resulting in combinations such as H1N1, H2N2, and H3N2. This selective tropism is a testament to the intricate evolutionary adaptations that enable certain influenza strains to effectively infect and transmit between human hosts.

The classification of the HA subtypes further highlights the complexity of this viral protein. As depicted in Figure 1.1, the 16 classical HA subtypes are divided into two distinct groups, with Group 1 containing the H1 (H1, H2, H5, H6, H11, H13, and H16), and H9 (H8, H9, and H12) clades, and Group 2 encompassing the H3 (H3, H4, and H14) and H7 (H7, H10, and H15) clades. Conventional influenza A virus (IAV) subtypes (H1-H16) bind to sialic acid (Sia) receptors, which are sugar molecules found on the surface of host cells. The specific type of Sia receptor determines which species an IAV can infect. Avian IAVs typically bind to  $\alpha$ 2,3-linked Sia receptors, while human IAVs prefer  $\alpha$ 2,6-linked Sia receptors (Carroll & Paulson, 1985; Matrosovich et al., 1997; Weis et al., 1988). Unique IAV subtypes H17 and H18 don't bind to Sia receptors. Instead, they use a different mechanism to enter cells, binding to major histocompatibility complex class II (MHC II) molecules found on the surface of various species, including humans, pigs, chickens, and bats (Karakus et al., 2019; Sun et al., 2013; Zhu et al., 2013). The newly characterised H19 subtype, like H17 and H18, is another HA subtype that binds to MHC II molecules instead of Sia receptors (Karakus et al., 2024). This phylogenetic organisation reflects the gradual diversification of the HA protein over time, as the IAV has adapted to infect a wide range of avian and mammalian hosts. Similarly, the NA subtypes can be classified into

three distinct groups, with Group 1 containing N1, N4, N5, and N8, Group 2 comprising N2, N3, N6, N7, and N9, and Group 3 consisting of the NA subtypes found in influenza B viruses. The recent discovery of the N10 and N11 subtypes in bats further underscores the remarkable evolutionary potential of this versatile virus (Shao et al., 2017).

The intricate structures and genetic diversity of the HA and NA glycoproteins demonstrate the influenza virus's remarkable adaptability and ability to exploit a variety of host species. While only a few subtypes have successfully crossed the species barrier to cause human epidemics, the ongoing evolution and emergence of novel influenza strains remains a significant public health challenge, necessitating close monitoring and the development of effective prevention and treatment strategies (Shao et al., 2017; Taubenberger & Kash, 2010).

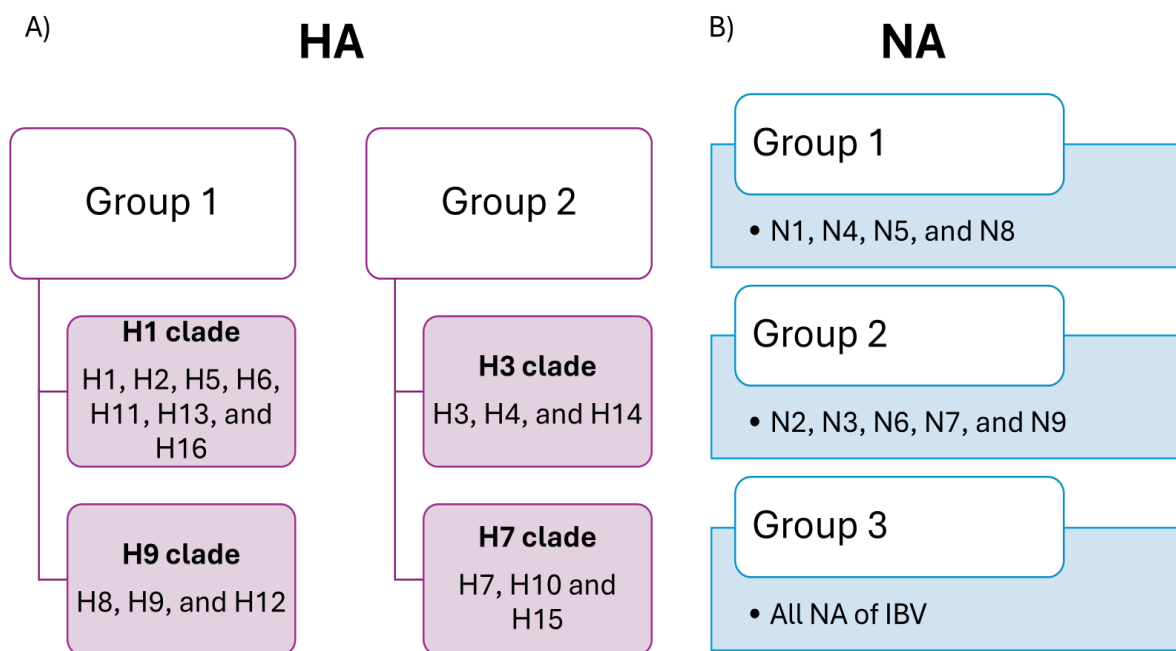


**Figure 1. 1 Phylogenetic Classification of HA and NA subtypes.** A) Illustration of the evolutionary relationships among the 16 classical HA subtypes, divided into two groups and four clades. B) Classification of 11 NA subtypes, divided into three groups.

## **1.4: Structure of Influenza A Virus**

IAV is a complex and intricate pathogen, displaying a unique and highly organized structure that allows it to effectively infect and replicate within host cell. At the core of this virus is its genome, a single-stranded, negative-sense RNA molecule that encodes the essential proteins necessary for its survival and propagation. Surrounding this genetic material is a protective capsid, a roughly spherical shell composed of multiple copies of viral nucleoprotein. This capsid is further enveloped by a lipid membrane derived from the host cell, which incorporates two key viral glycoproteins - hemagglutinin and neuraminidase. These proteins play a critical role in the virus' ability to bind to and enter host cells, as well as facilitate its release and transmission to new hosts. Protruding from the viral envelope, these glycoproteins form a distinctive spike-like pattern, a hallmark of IAV's morphology. Underneath the envelope, the viral RNA is associated with various other proteins, including the RNA-dependent RNA polymerase complex that is essential for viral replication. This intricate assembly of genetic material, structural components, and functional proteins allows influenza A to hijack the machinery of infected cells, commandeering their resources to rapidly produce new viral particles and spread the infection. It is this sophisticated and highly adapted structure that makes influenza A such a formidable and persistent threat to public health (Kawaoka & Neumann, 2012).

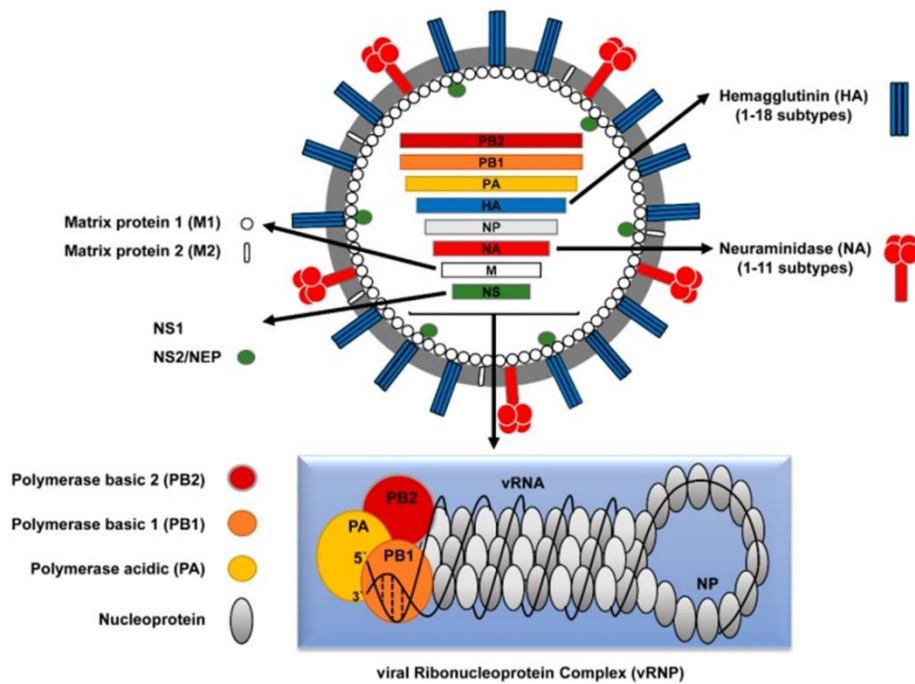


**Figure 1. 2 Structural Components of IAV.** Illustrates the structure of the influenza virus as an enveloped virus with a lipid bilayer containing HA and NA glycoproteins. The viral genome comprises eight segments of single-stranded RNA, each associated with nucleoprotein to form a ribonucleoprotein complex (vRNP). The vRNPs are bound by the M1 and enclosed within the lipid envelope. The vRNP complex consists of PA, PB1, and PB2 subunits, where a single-stranded RNA segment is wrapped around a helical array of NP subunits (Mostafa et al., 2018).

### 1.4.1: Influenza A virus Genome and its Proteins

IAV's genome is remarkably complex, encoding eleven distinct proteins, each of which is critical to the virus's structure and functionality. At the heart of this genome is a segmented, eight-segmented single-stranded RNA molecule that contains the genetic instructions for assembling the various viral components (Kuriakose & Kanneganti, 2017; Ong et al., 2017). The HA protein forms spike-like structures on the virus's surface mediating binding and entry into host cells. The NA protein, another surface protein, then facilitates the release of newly formed viral particles from infected cells. The viral RNA is encapsulated by the nucleoprotein (NP), which also assists in the replication and

transcription of the viral genome inside the host cell. Three viral polymerase proteins - the PB1, PB2, and PA proteins - work in concert to replicate the viral RNA and produce the necessary messenger RNA for protein synthesis. The matrix protein (M1) forms the structural framework of the virus, while the M2 protein acts as an ion channel, regulating the acidity within the virion. Finally, the non-structural proteins NS1 and NS2 play crucial regulatory roles, with NS1 helping the virus evade the host's immune defences and NS2 facilitating the export of viral ribonucleoproteins from the nucleus (Kawaguchi et al., 2005; Kerviel et al., 2013; Mostafa et al., 2018). Together, this remarkable eight-protein arsenal equips the influenza A virus with the versatility and adaptability to infect a wide range of host species and pose an ongoing public health challenge.

#### **1.4.1.1: Basic Polymerase2 (PB2)- Segment 1**

PB2 protein is an essential component of the IAV genome, playing an important role in viral replication. PB2 is one of three subunits that comprise the viral RNA-dependent RNA polymerase complex, and it is in charge of initiating transcription and replication of the viral genome (Long & Fodor, 2016). This highly conserved protein has a cap-binding domain that enables it to recognise and bind to the 5' cap structure of cellular mRNA, which it then uses as a primer to start viral mRNA synthesis (Nilsson et al., 2017; Szeto et al., 2020). PB2 also has a nuclear localisation signal, which allows it to enter the host cell nucleus and replicate the viral genome. Mutations in the PB2 gene, particularly at key amino acid positions such as 627 and 701, can significantly impact the host range, virulence, and adaptation of IAV strains, enabling them to more efficiently infect and replicate within different host species (Nilsson et al., 2017).

#### **1.4.1.2: Basic Polymerase1 (PB1)- Segment 2**

PB1 protein is a crucial component of the IAV genome, playing a vital role in the virus's ability to replicate and proliferate. As one of the three subunits that make up the viral RNA-dependent RNA polymerase complex, PB1 is responsible for catalysing the synthesis of new viral RNA strands, a process that is essential for the virus to produce copies of itself and spread to infect more host cells (Y. Li et al., 2023). The PB1 subunit, containing the active site for enzymatic activity, utilizes the viral genome as a template to construct complementary RNA strands, enabling the influenza virus to rapidly hijack the host cell's machinery and churn out large quantities of new viral particles (Y. Li et al., 2023). Beyond its core polymerase duties, the PB1 protein also interacts with the other polymerase subunits, PB2 and PA, to form the complete RNA replication complex, where the precise coordination and cooperation between these three subunits is necessary for the virus to transcribe its segmented genome efficiently and accurately (Biswas & Nayak, 1996; Y. Li et al., 2023). Overall, the basic polymerase 1 subunit is an indispensable element of the IAV, serving as a lynchpin for the virus's ability to proliferate and spread to new host cells.

#### **1.4.1.3: Acidic Polymerase Protein (PA)- Segment 3**

PA protein is an essential component of the IAV genome that aids the virus's ability to replicate and infect host cells. This protein, one of three subunits that comprise the viral RNA-dependent RNA polymerase complex, is in charge of initiating viral transcription and replication by binding to the viral RNA genome and catalysing the synthesis of new viral

RNA strands, whereas the PA subunit contains an endonuclease domain that allows it to cleave the 5' caps from host cell mRNA, which are then used to prime viral mRNA transcription (Chauhan & Gordon, 2022; Massari et al., 2016). This "cap-snatching" mechanism is essential for the virus to hijack the host's cellular machinery and produce the viral proteins needed for assembly of new virions. Additionally, the PA subunit has been shown to interact with numerous host factors, modulating their activity to create a more favourable environment for viral replication. Mutations in the PA gene can alter the enzyme's structure and function, affecting viral fitness, host range, and susceptibility to antiviral drugs (Chauhan & Gordon, 2022).

#### **1.4.1.4: Hemagglutinin (HA)- Segment 4**

IAV's envelope contains HA, a critical surface protein that aids the virus's ability to infect and replicate within the host cell. This mushroom-shaped glycoprotein protrudes from the viral surface and acts as the primary attachment mechanism, binding to sialic acid receptors on the target cell membrane (Shao et al., 2017). The HA protein is made up of two subunits, HA1 and HA2, which work together to promote viral entry. The HA1 subunit contains the receptor-binding domain, which allows the virus to attach to the host cell, whereas the HA2 subunit facilitates the fusion of the viral and cellular membranes, allowing the viral genome to enter the cytoplasm (DuBois et al., 2011; Sriwilaijaroen & Suzuki, 2012). Remarkably, the HA protein exhibits high genetic variability, with numerous subtypes identified based on antigenic differences (Galloway et al., 2013).

#### **1.4.1.5: Nucleoprotein (NP)- Segment 5**

NP is a critical component of the IAV that plays a vital role in the virus's life cycle and replication. As one of the viral ribonucleoproteins (vRNPs), the NP associates with the viral genomic RNA segments, forming a helical structure that allows the viral genetic material to be efficiently packaged within the viral particle (Chauhan & Gordon, 2022). The NP protein is characterized by its ability to bind single-stranded RNA, a property that enables it to encapsulate the viral genome and protect it from cellular nucleases (Turrell et al., 2013). NP is also essential for the nuclear import of the viral genetic material, as it contains nuclear localization signals that direct the vRNPs to the host cell's nucleus - the site of viral transcription and replication (Chauhan & Gordon, 2022).

#### **1.4.1.6: Neuraminidase (NA)- Segment 6**

NA, a key enzyme found in IAVs, is essential for viral replication and infection. This surface glycoprotein serves as a molecular key, allowing the virus to break free from the host cell and infect other cells (Cohen et al., 2013). NA specifically cleaves the sialic acid receptors that the virus used to gain entry, allowing the newly formed viral particles to detach and be released, which is essential for the virus to spread throughout the body and continue its infectious cycle (Matrosovich et al., 2004; McAuley et al., 2019). Neuraminidase also helps the virus penetrate the mucus lining of the respiratory tract, an important first step in establishing an infection. Without this crucial enzyme, the virus would essentially become trapped, unable to escape the initial host cell (Cohen et al., 2013).

#### **1.4.1.7: Matrix Protein1 (M1)- Segment 7**

M1 is a crucial structural component of the IAV that plays a vital role in the virus's assembly and budding processes. This small but mighty protein serves as the scaffold that holds the virus particles together, providing the framework upon which the viral envelope and other key components are built (Baudin et al., 2001). M1 is composed of a series of alpha helices that intertwine to form a compact, globular structure, giving it the ability to multimerize and self-assemble into a lattice-like matrix underneath the viral lipid membrane, which provides the mechanical support and organization needed to package the viral genome and other essential viral proteins into a cohesive virion (Selzer et al., 2020). Beyond its structural duties, M1 also acts as a regulatory hub, interacting with various viral and host factors to orchestrate the complex choreography of the IAV replication cycle. For instance, M1 protein binds to the viral ribonucleoprotein (RNP) complexes, aiding in their transport to the nucleus of the host cell (Bui et al., 1996). Furthermore, M1 plays a key role in the virus budding process itself, driving the membrane curvature and scission that releases the mature virion from the host cell (Chauhan & Gordon, 2022).

#### **1.4.1.8: Matrix Protein2 (M2)- Segment 7**

M2 is a tetrameric proton-selective ion channel that is embedded in the viral envelope and is responsible for several essential functions that allow the virus to effectively infect and replicate within host cells (Chauhan & Gordon, 2022).

Firstly, M2 is instrumental in the process of viral uncoating, where the virus sheds its outer layers to release the genetic material into the host cell. As the virus particle is taken up

into the endosome, the acidic environment triggers M2 to open its ion channel, allowing protons to flow into the viral core. This acidification causes the viral ribonucleoprotein complexes to dissociate, enabling the viral genome to be imported into the host cell nucleus and hijack the cellular machinery for viral replication (Cady et al., 2009). However, M2's functional repertoire extends beyond viral entry. During the assembly and budding stages of the viral life cycle, M2 helps to create the highly curved neck region of the nascent viral particle, facilitating the pinching off of the virus from the host cell membrane (Rossman et al., 2010). M2 protein plays a crucial role in the trans-Golgi network (TGN) membrane. It prevents premature conformational changes in newly synthesized hemagglutinin (HA) proteins during their transport to the cell surface by maintaining the pH of the TGN at a level that is compatible with the proper folding and assembly of HA. (Schnell & Chou, 2008).

#### **1.4.1.9: Non-Structural Protein1 (NS1)- Segment 8**

NS1 is an essential component of the IAV, playing a variety of roles in the virus's life cycle and ability to evade the host's immune defences. As a non-structural protein, NS1 is not incorporated into the viral particle but rather acts as an accessory protein, significantly increasing the virus's replication and propagation within the infected host cells. One of the primary functions of NS1 is to act as an antagonist to the host's innate immune response, particularly the type I interferon (IFN) system. NS1 achieves this by binding to and inhibiting key cellular factors involved in IFN induction pathways, thereby crippling the host's first line of defence against the invading virus (Hao et al., 2020).

In addition to dampening the innate immune response, NS1 also plays a critical role in regulating viral gene expression and the processing of viral RNAs. It can bind to and stabilize viral mRNAs, enhancing their translation into viral proteins, while also blocking the maturation of cellular mRNAs that would compete for the host cell's protein synthesis machinery (Hao et al., 2020; Nogales et al., 2018).

#### **1.4.1.10: Non-Structural Protein2 (NS2/NEP)- Segment 8**

NS2, also known as the nuclear export protein (NEP), is an essential component of the IAV that regulates the viral life cycle. This small yet multifunctional protein facilitates the export of viral ribonucleoprotein (vRNP) complexes from the nucleus to the cytoplasm, which is an important step in viral replication. The NS2 protein accomplishes this by interacting with the viral matrix protein M1, which serves as an adaptor, allowing the vRNP to bind to the cellular nuclear export machinery and be transported outside the nucleus. This nuclear export function is required to complete the IAV life cycle because the vRNP complexes must be exported from the nucleus before being packaged into new viral particles (Hao et al., 2020). Furthermore, the NS2 protein has been discovered to be involved in other aspects of the viral life cycle, such as regulating the activity of the viral polymerase complex and modulating the host cell's antiviral response. Through these various functions, the NS2 protein emerges as a critical player in the complex and intricate process of IAV replication (Hao et al., 2020).

**Table 1. 1 Primary Functions of IAV Proteins**

Genome segment	Viral Protein	Primary Functions	References
1	PB2	(i) Recognises and binds to the 5'cap structure of cellular mRNA and initiates viral mRNA synthesis.	(Szeto, Hsia et al. 2020)
2	PB1	(i) Catalyses the synthesis of new viral RNA strands.	(Li, Arcos et al. 2023)
3	PA	(i) Cleaves the 5' caps from the host cell mRNA and helps in transcription of viral mRNA.	(Chauhan and Gordon 2022)
4	HA	(i) Helps the virus to attach to the host cell and, also facilitates the fusion of viral and cellular membranes.	(Shao, Li et al. 2017)
5	NP	(i) Interacts with the cap-binding domain of PB2 and initiates replication. (ii) Helps in packaging the genetic material within the viral particle.	(Chauhan and Gordon 2022)
6	NA	(i) Cleaves the sialic acid receptors and facilitates the release of viral particles. (ii) Helps the virus to penetrate the mucus lining of the respiratory tract.	(Matrosovich, Matrosovich et al. 2004, Cohen, Zhang et al. 2013)
7	M1	(i) Provides the framework to hold the viral particle together.	(Baudin, Petit et al. 2001)
	M2	(i) Facilitates the acidification of viral ribonucleoprotein resulting in their dissociation. (ii) Facilitates the successful membrane scission of nascent viral particle from the host cell membrane.	(Cady, Luo et al. 2009, Rossman, Jing et al. 2010)
8	NS1	(i) Suppresses the production and signaling of IFNs. (ii) Regulates the viral gene expression and the processing of viral RNAs.	(Hao, Wang et al. 2020)
	NEP/NS 2	(i) Facilitates the export of viral ribonucleoprotein complexes from the nucleus to the cytoplasm.	(Hao, Wang et al. 2020)

### 1.5: IAV invasion and the antiviral response of the host cell

IAV initiates infection by binding to specific receptors on the host cell surface. As shown in Figure 1.3, the HA protein recognizes and binds to sialic acid residues on the host cell's glycoproteins or glycolipids, triggering virus internalization into the cell through a process called clathrin-mediated endocytosis (Shao et al., 2017; Urbaniak & Markowska-Daniel, 2014). This involves the formation of a clathrin-coated vesicle that engulfs the virus-receptor complex and transports it into the cell. Inside the acidic environment of the endosome, the HA protein undergoes conformational changes, leading to the fusion of the viral and endosomal membranes, which allows the viral genome, in the form of viral ribonucleoprotein (vRNP) complexes, to be released into the host cell cytoplasm (Bouvier & Palese, 2008; Urbaniak & Markowska-Daniel, 2014). Alternatively, the M2 ion channel on the viral surface, can also facilitate viral uncoating, where the low pH triggers M2 ion

channel activation and HA conformational change, thus releasing the vRNPs into the cytoplasm (Bouvier & Palese, 2008; Dou et al., 2018). Once in the cytoplasm, viral ribonucleoprotein complexes (vRNPs) are transported to the nucleus. Here, viral RNA replication and transcription take place. The viral RNA-dependent RNA polymerase (RdRP) synthesizes new viral RNA strands. These strands are then exported back to the cytoplasm for translation into viral proteins. Newly synthesized viral proteins and genomic RNA assemble at the cell membrane, forming new virions. The NA protein cleaves sialic acid residues on the host cell surface, enabling the newly formed virions to be released and infect other cells (Dou et al., 2018).

The host immune system detects viral infections through pattern recognition receptors (PRRs), which recognize viral components like viral RNA and proteins. This triggers the production of interferons and pro-inflammatory cytokines, activating immune cells and inducing antiviral responses (Kuriakose & Kanneganti, 2017; Laghlali et al., 2020). However, IAV has developed strategies to evade the host immune response, including inhibiting interferon signaling and degrading host cell proteins. This allows the virus to replicate efficiently and spread within the host (Shao et al., 2017).

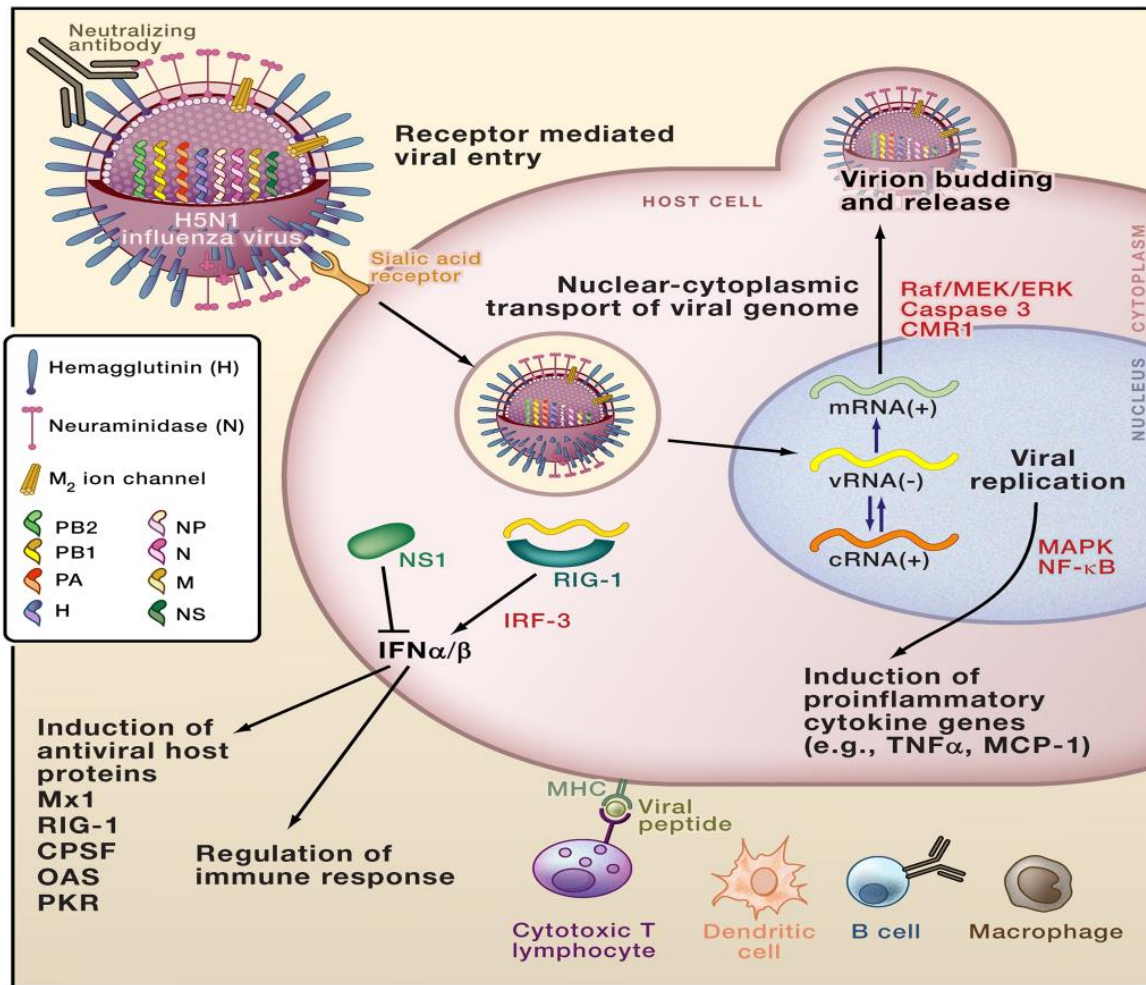


**Figure 1. 3 Mechanism of invasion of IAV and its replication in the host cell.** IAV initiates infection by binding to sialic acid receptors on the host cell surface through its HA protein. This triggers clathrin-mediated endocytosis, leading to viral internalisation. Within the acidic endosome, HA undergoes conformational changes, facilitating membrane fusion and release of the vRNP complexes into the cytoplasm. Alternatively, the M2 ion channel contributes to viral uncoating. vRNPs are transported to the nucleus, where viral RNA replication and transcription occur. Newly synthesised viral proteins and genomic RNA assemble at the cell membrane, forming new virions. NA cleaves sialic acid residues enabling viral release (Salomon & Webster, 2009)

## 1.6: Evolution of IAV

IAV evolves rapidly due to two primary mechanisms: one is Antigenic Drift, where point mutations accumulate in the viral genome, primarily driven by the error-prone nature of

viral RNA polymerase. This gradual genetic change allows the virus to evade the host's immune response. The second one is Antigenic Shift, where genetic reassortment occurs when two different IAV strains infect the same host cell (Figure 1.4) (Mostafa et al., 2018; Urbaniak & Markowska-Daniel, 2014). Genetic reassortment is a key driver of IAV evolution. When a cell is infected with multiple IAV strains, their eight individual RNA segments can mix and match during replication, creating novel viral progeny. This process is facilitated by the independent functioning of vRNP complexes. This genetic shuffling can lead to the emergence of entirely new viral subtypes with the potential to cause pandemics (Urbaniak & Markowska-Daniel, 2014).

The diversity of host species, Pigs, in particular, play a significant role in IAV reassortment due to their ability to be infected by both avian and human influenza viruses. Their respiratory tracts possess receptors for both types of viruses, making them ideal mixing vessels for genetic exchange, resulting in the development of new viral strains. Historically, all major influenza pandemics, except for the 1918 Spanish Flu, For instance: 1957 Asian Flu, a reassortant virus with avian-origin genes for PB1, HA, and NA. 1968 Hong Kong Flu, a reassortant virus with avian-origin genes for HA and PB1. 2009 Swine Flu, a reassortant virus with genes derived from avian, human, and swine influenza viruses have been caused by reassortant viruses (Chen et al., 2008; Urbaniak & Markowska-Daniel, 2014; Ye et al., 2010).

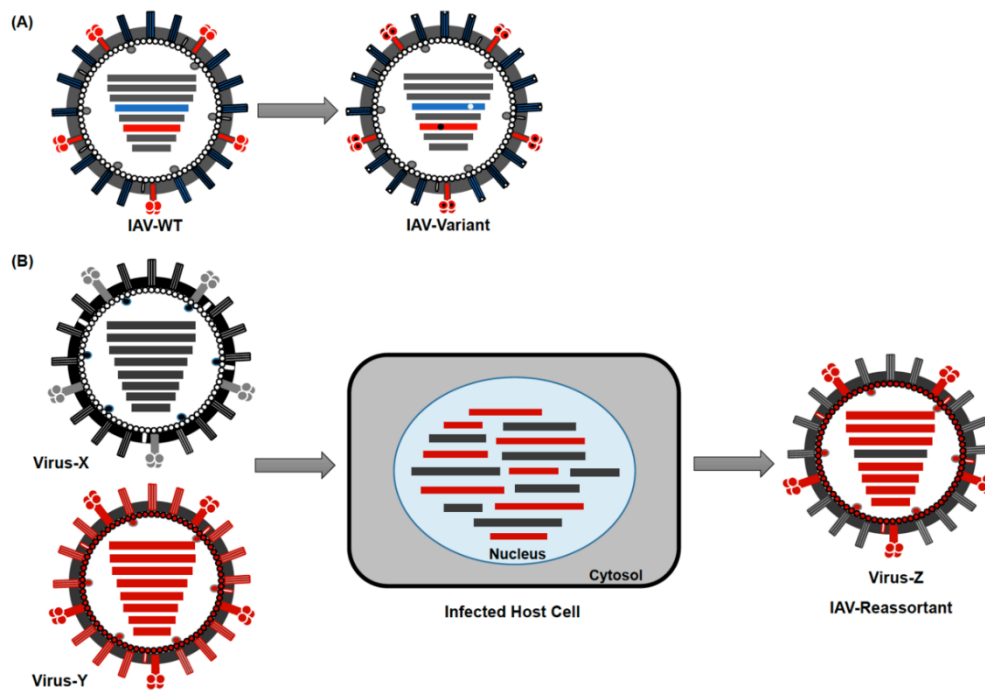


**Figure 1. 4 Mechanism of Evolution of IAV.** A) Shows the accumulation of mutations within the genome (Antigenic Drift). B) Shows the reassortment occurring within the host during co-infection (Mostafa et al., 2018)

## 1.7: Viral Pathogenicity

Avian influenza viruses (AIVs) can infect a diverse array of bird species, from domesticated poultry such as chickens and turkeys to wild birds like ducks and geese. Based on their pathogenicity, these viruses are categorized into two primary types: (i) Low Pathogenic Avian Influenza (LPAI), which usually results in mild, often asymptomatic, respiratory infections in birds. While commonly found in wild birds and able to circulate in poultry populations without causing significant disease outbreaks, LPAI viruses can mutate into highly pathogenic forms under specific conditions. (ii) Highly Pathogenic Avian Influenza (HPAI) are highly contagious and can cause severe illness with high mortality rates in poultry (Luo et al., 2017; Sid et al., 2017). While human infections are relatively uncommon, they can occur. The H5 and H7 subtypes are particularly

associated with highly pathogenic strains (Alexander, 2000; Sid et al., 2017). The presence of a multi-basic cleavage site in the HA protein allows HPAI viruses to be activated by a broader range of proteases, enabling systemic infection. In contrast, LPAI viruses typically have a monobasic cleavage site, restricting their ability to spread beyond the respiratory tract (Sid et al., 2017). While most human infections with avian influenza have been associated with direct contact with infected poultry or contaminated environments, there have been instances of human-to-human transmission, particularly with the H5N1 virus. The emergence of novel strains, such as H7N9 and H10N8, highlights the ongoing threat of avian influenza to public health (Kalthoff et al., 2010; Luo et al., 2017).

## **1.8: Zoonotic Potential of IAV**

### **1.8.1: Human**

The most common forms are influenza types A, B, and C, which can all infect and spread among the human population. Of particular concern are the circulating subtypes of the influenza A virus (IAV), such as the well-known H1N1 and H3N2 strains, which are typically responsible for causing the seasonal influenza epidemics that occur annually (Mostafa et al., 2018). These seasonal outbreaks can be severe, leading to significant morbidity, hospitalizations, and even deaths in vulnerable populations. However, the threat posed by influenza viruses extends beyond just these seasonal epidemics, as certain IAV subtypes, including the likes of H5N1, H7N9, and H10N8, have demonstrated the ability to cross the species barrier from their natural avian reservoirs and infect

humans as well. These zoonotic infections, while sporadic, can be extremely dangerous, often resulting in severe illness and fatalities in the afflicted individuals (Mostafa et al., 2018). The recent emergence of the H10N8 virus, first identified in humans in China in 2013 after initially being detected in quails in Italy decades earlier, highlights the ongoing evolution and adaptability of these influenza strains. Genetic analysis has revealed that the H10N8 strain involved in human cases is a reassortant virus, with the H10 gene segment likely originating from the H9N2 avian influenza virus and the remaining internal genes derived from other wild bird influenza viruses (Qi et al., 2014).

### **1.8.2: Birds**

The effectiveness of influenza virus infection is influenced by the interaction between viral proteins, particularly HA, and host cell receptors. These receptors are sialic acid molecules found on the surface of cells. The type of sialic acid present in host cells can determine the susceptibility of a species to a particular influenza virus. Human influenza viruses typically bind to 2,6-linked sialic acids, while avian influenza viruses typically bind to 2,3-linked sialic acids. However, the distribution of sialic acid types can vary among different bird species (Kida et al., 1980; Takahashi et al., 2001). This variation can influence the susceptibility of different bird species to human influenza viruses and the severity of disease. Different poultry species can be affected differently by various influenza virus subtypes. For example, turkeys are highly susceptible to both low-pathogenic and highly pathogenic avian influenza viruses, while chickens can be infected by a wide range of influenza virus subtypes. Ducks often serve as natural reservoirs for influenza viruses and can transmit the virus to other bird species, including poultry.

Figure 1.5 illustrates the prevalence of different HA subtypes in chickens, ducks, and geese, highlighting the complex epidemiology of avian influenza, with the H9 subtype being widely distributed across chickens, ducks, and geese, while the H6 subtype is most prevalent in geese, the H3 subtype is more common in ducks, and the H4 subtype is found in all three species, with the highest prevalence in chickens. Additionally, mixed infections, where multiple subtypes infect the same bird, are relatively common, particularly in ducks, highlighting the potential for the emergence of novel strains through reassortment (Luo et al., 2017).

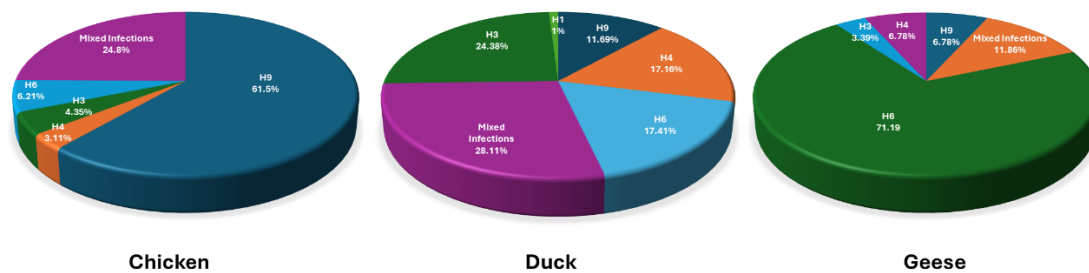


**Figure 1. 5 Prevalence of IAV-HA subtypes in chicken, duck, and geese.** Observations include the widespread distribution of the H9 subtype across all species, the predominance of the H6 subtype in geese, and the higher prevalence of the H3 subtype in ducks. The H4 subtype is also found in all three species, with the highest prevalence in chickens. Notably, mixed infections with multiple HA subtypes are observed, particularly in ducks.

### 1.9: Poly (ADP-ribose) polymerases (PARPs)

The history of PARPs dates back to the 1960s when Severo Ochoa and his team discovered the first PARP enzyme (W. Lee Kraus, 2015). They identified an enzyme capable of synthesizing poly (ADP-ribose) (PAR) from nicotinamide adenine dinucleotide (NAD<sup>+</sup>). PARP homologs have been identified in a wide range of organisms, including animals, plants, fungi, bacteria, and viruses, suggesting that the functions of this enzyme

class are likely conserved across diverse taxa. PARPs are a critical family of 17 enzymes that play a vital role in regulating a diverse array of fundamental cellular processes and stress responses. These versatile enzymes, also known as Diphtheria toxin-like ADP-ribosyl transferases (ARTDs), modify target proteins by attaching chains of ADP-ribose units using the essential cofactor NAD<sup>+</sup> as their substrate (Hoch & Polo, 2019; van Beek et al., 2021).

Through this enzymatic activity, PARPs are able to orchestrate complex cellular functions, including DNA repair, gene transcription, chromatin remodelling, cell death, cellular signalling, and the antiviral response (D'Amours et al., 1999; Schuller & Ahel, 2022; Wei & Yu, 2016). They play a critical role in DNA repair, particularly in response to DNA damage caused by ionizing radiation and oxidative stress. PARPs regulate gene transcription by modifying histones and other transcription factors, and they can alter chromatin structure, affecting gene expression and DNA replication. Additionally, PARPs are involved in both apoptotic and necrotic cell death pathways, and they can modulate cellular signalling pathways by modifying key signalling proteins. Furthermore, PARPs play a role in the innate immune response to viral infections, contributing to antiviral defence mechanisms (Hoch & Polo, 2019; Zhu et al., 2021).

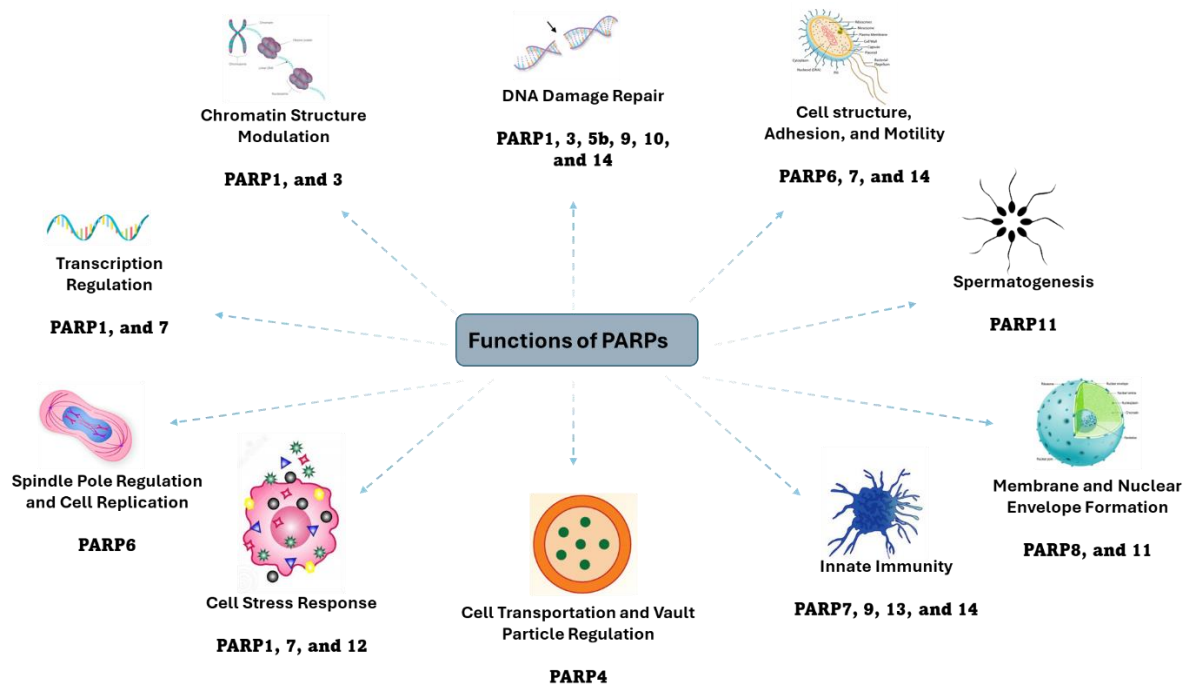


**Figure 1. 6 Diverse Cellular Functions of PARPs.** Illustrates the numerous roles PARPs in various cellular pathways, including DNA damage repair, cell structure and motility, spermatogenesis, membrane and nuclear envelope formation, innate immunity, cell transport, cell stress response, spindle pole regulation, transcription regulation, and chromatin structure modulation, highlighting the multifaceted importance of PARPs in maintaining cellular homeostasis and responding to diverse cellular challenges.

### 1.9.1: Classification of PARPs

The PARP family is further divided into distinct subgroups based on their structural and functional characteristics. The DNA-dependent PARPs, which include PARP1, PARP2, and PARP3, are intimately involved in sensing and responding to DNA damage. In contrast, the tankyrases PARPs, comprising PARP5a and PARP5b, play pivotal roles in telomere maintenance and Wnt signaling. Meanwhile, the macrodomain-containing PARPs, such as PARP9, PARP14, and PARP15, have been implicated in the regulation of the interferon-mediated antiviral response, while the CCCH zinc finger-containing PARPs, including PARP7, PARP12, and PARP13, also contribute to antiviral defence mechanisms. The remaining PARPs, including PARP4 and

PARP16, possess unique or as-yet uncharacterized domains, underscoring the remarkable diversity within this enzyme family (McLachlan et al., 2016; Zhu et al., 2021).

PARPs are also categorized into three primary types based on their catalytic activities (Figure 1.7): (i) Poly (ADP-ribose) Polymerases: These PARPs, including PARP1, PARP2, PARP3, PARP4, and PARP5, catalyse the addition of multiple ADP-ribose units to target proteins, forming long, branched chains of poly (ADP-ribose) (PAR). This process, known as poly (ADP-ribosyl) ation (PARylation), is essential for DNA repair, chromatin remodelling, and gene transcription. PARylation can result in the formation of both linear and branched chains of PAR. (ii) Mono(ADP-ribose) Polymerases (MARTs): This group of PARPs, encompassing PARP6, PARP7, PARP8, PARP9, PARP11, PARP12, and PARP14, catalyse the addition of a single ADP-ribose unit to target proteins, a process known as mono-ADP-ribosylation (MARylation). MARylation is involved in various cellular processes, including signal transduction and cell death. (iii) Catalytically Inactive PARP: PARP13 lack the necessary NAD<sup>+</sup> binding residues and is therefore considered catalytically inactive, but retain the auto modification and catalytic domains, indicating their involvement in distinct cellular processes (Sousa et al., 2012; Steffen et al., 2013; Tang et al., 2018; Welsby et al., 2014; Zhu et al., 2021).

The catalytic domain of PARP enzymes is highly conserved across different family members. This domain contains a critical sequence of amino acids that is essential for its catalytic activity. The H-Y-E motif is a highly conserved sequence within the catalytic domain of PARP enzymes. This motif plays a crucial role in binding to NAD<sup>+</sup>, the essential substrate for ADP-ribose transfer. The histidine residue within this motif is particularly important for the catalytic mechanism (Gibson & Kraus, 2012; Gupte et al., 2017). While the H-Y-E motif is vital for the catalytic activity of PARPs, MARTs often exhibit variations in

this motif. The glutamate residue in the H-Y-E motif is frequently replaced by other amino acids, such as leucine, isoleucine, or tyrosine (H-Y-I/L/Y) (Vyas et al., 2014). This modification significantly impacts the catalytic properties of MARTs. The specific amino acid substitution in the H-Y-E motif can influence the catalytic efficiency and substrate specificity of MARTs. For example, the presence of a hydrophobic amino acid, like leucine or isoleucine, may alter the local environment of the active site, affecting the binding of NAD<sup>+</sup> and the subsequent transfer of ADP-ribose (Vyas et al., 2014).

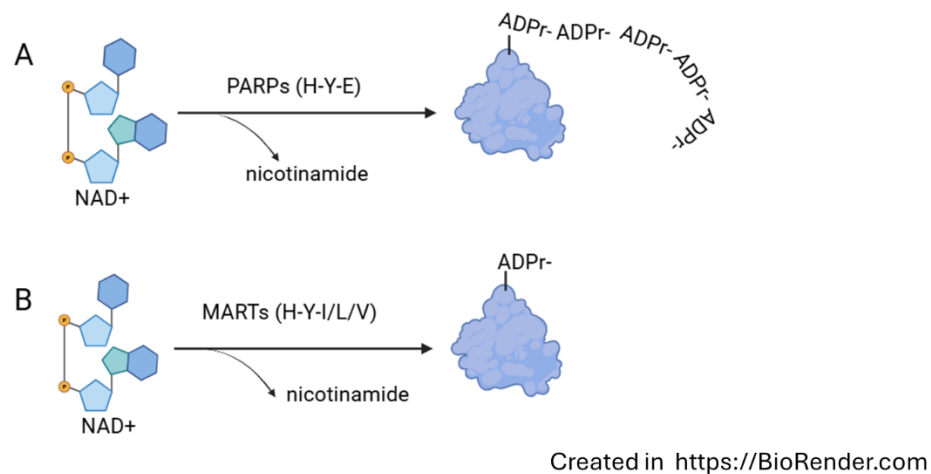


**Figure 1. 7 Mechanism of Poly /Mono (ADP) ribosylation.** A) Shows poly (ADP) ribosylation where the PARPs catalyse the transfer of multiple ADPr moieties. B) illustrates mono (ADP) ribosylation, where the PARPs catalyse the transfer of a single ADPr moiety.

### 1.9.2: PARP1

PARP1, or Poly(ADP-ribose) Polymerase 1, is a crucial enzyme involved in various cellular processes, primarily DNA repair and cellular proliferation (Kumar et al., 2022). It is a multi-domain protein with several functional regions. Its most important domain is the catalytic PARP domain, which is responsible for synthesizing PAR chains, which is a

polymer of ADP-ribose units that are attached to target proteins, primarily histones and PARP1 itself (Feldes & Alvares, 2024).

When DNA strands become broken or otherwise compromised, PARP1 rapidly binds to the damaged sites, catalysing the addition of long, branching chains of ADP-ribose polymers onto itself and other target proteins. This enzymatic activity recruits and coordinates the various repair pathways the cell can utilise, from base excision repair to homologous recombination, ensuring that genetic integrity is restored. During mild DNA damage it PARylates the H1 and H2B histones, which facilitates access to the DNA damage site and relaxes the chromatin structure. Upon activation, it synthesizes PAR chains, which serve as a platform for the recruitment of base excision repair (BER) and single strand break repair (SSBR) components, such as DNA ligase and XRCC1 (Spiegel et al., 2021). PAR chains can modify proteins involved in various cellular processes, including apoptosis, inflammation, and gene expression (Kumar et al., 2022). Dysregulation of PARP1 activity has been implicated in several human diseases such as Alzheimer's and Parkinson's disease (Mao & Zhang, 2022). Overactivation of PARP1 can lead to excessive PAR synthesis, which can deplete cellular NAD<sup>+</sup> levels and cause cell death (Hurtado-Bages et al., 2020).

### **1.9.3: PARP3**

Poly (ADP-ribose) Polymerase 3 (PARP3) is a crucial enzyme found within the cells of the human body that plays a vital role in various cellular processes, particularly in the response to DNA damage. As a member of the PARP family of enzymes, PARP3 is responsible for catalysing the addition of PAR chains onto target proteins, which serves

as a signal to recruit other proteins involved in DNA repair pathways (Rose et al., 2020). Beyond its role in DNA repair, PARP3 has also been implicated in other cellular functions, such as the regulation of chromatin structure and the modulation of gene expression. By attaching PAR to histones and other chromatin-associated proteins, PARP3 can influence the accessibility of genetic material, thereby affecting transcriptional programs within the cell (Grundy et al., 2016). This multifaceted involvement in both DNA repair and chromatin dynamics highlights the versatility and significance of PARP3 in maintaining genomic integrity and cellular homeostasis. Interestingly, the dysregulation or malfunction of PARP3 has been linked to the development of various disease states. PARP3 has been implicated in neurodegenerative diseases such as Alzheimer's disease and Parkinson's disease. In these diseases, PARP3 may contribute to neuronal cell death by inducing DNA damage and oxidative stress. PARP3 has also been linked to cardiovascular disease, particularly heart failure. In heart failure, PARP3 may contribute to cardiac dysfunction by inducing cell death and inflammation. In these pathological conditions, the impairment of PARP3's enzymatic activity or its disruption of normal cellular processes can contribute to genomic instability, uncontrolled cell proliferation, and the emergence of cancerous phenotypes (Beck et al., 2019).

#### **1.9.4: PARP4**

PARP4, or vPARP is a unique member of the PARP family, distinct from other subfamilies. It is a 193-kDa catalytically active mono-[ADP-ribosyl] transferase found within vault complexes, large ribonucleoprotein particles (Daugherty et al., 2014; Kickhoefer et al., 1999). While primarily associated with vaults, vPARP has also been observed in the

nucleus and mitotic spindle, suggesting diverse cellular roles (Kickhoefer et al., 1999; Liu et al., 2004; Richard et al., 2021). Interestingly, the localization of vPARP to vault particles coincides with the production of PAR chains. Lower levels of vPARP have been linked to poorer prognoses, suggesting a potential role in cancer inhibition. Although direct evidence linking vPARP to DNA repair is lacking, its possession of a BRCT domain, common to many DNA repair proteins like PARP1, raises the possibility of involvement in DNA repair and carcinogenesis (Richard et al., 2021).

#### **1.9.5: PARP5**

PARP5b, also known as Tankyrase-2 (TNKS2), is a versatile enzyme within the PARP family. It plays a crucial role in various cellular processes by modifying target proteins with ADP-ribose units, a process known as PARylation, which allow it to influence a wide range of cellular functions, including DNA damage repair, telomere maintenance, and mitosis (Ke, Wang, et al., 2019). Initially identified as a TNKL-related protein associated with the Golgi apparatus, TNKS2 has been found to localize to the perinuclear region. Overexpression of TNKS2 has been linked to necrotic cell death, a type of cell death that can be inhibited by 3-aminobenzamide (Virag & Szabo, 2002).

#### **1.9.6: PARP6**

PARP6, is a protein with a distinct structure that sets it apart from other PARP subfamilies. This unique architecture suggests a specialized role in cellular processes. While PARP6 does not currently fit neatly into any existing PARP subfamilies, its unique properties and functions are proving to be quite fascinating and impactful (Richard et al., 2021).

One of the key functions of PARP6 is its role as a tumour suppressor. By negatively impacting cellular proliferation, PARP6 helps to prevent uncontrolled cell growth (Tuncel et al., 2012; Vermehren-Schmaedick et al., 2021). Overexpression of PARP6 has been shown to inhibit the progression of the S-phase of the cell cycle, further supporting its role in suppressing cellular proliferation. Interestingly, the catalytic domain of PARP6 appears to be necessary for it to carry out these anti-proliferative functions, as mutations that lack this domain have no impact on the cells (Vermehren-Schmaedick et al., 2021). PARP6 has been implicated in the regulation of colorectal cancer. Patients with high levels of PARP6 in their tumours tend to have a better prognosis. This suggests that PARP6 may play a protective role against colorectal cancer progression (Ke, Wang, et al., 2019; Tuncel et al., 2012). However, PARP6's impact on cancer extends beyond just colorectal tumours - recent studies have revealed that in breast cancer cells, PARP6 plays a crucial part in preserving centrosome integrity. It does so by directly modifying the protein Checkpoint Kinase 1 (Chk1) through MARylation, which then regulates Chk1's activity. When PARP6 activity is inhibited, Chk1 becomes more frequently phosphorylated, leading to impairment of mitotic signaling (Ke, Wang, et al., 2019; Richard et al., 2021).

#### **1.9.7: PARP7**

PARP7, also known as 2,3,7,8-tetrachlorodibenzo-p-dioxin (TCDD)-inducible poly (ADP-ribose) polymerase (or TiPARP, ARTD14), is a member of the CCCH-Zn finger PARP subfamily. Unique among its family members, PARP7 adds mono-ADP-ribose (MAR) modifications to its target proteins (Ke, Wang, et al., 2019; Richard et al., 2021). Its zinc

finger domain exhibits a strong affinity for RNA, suggesting a potential role in transcriptional regulation (Richard et al., 2021).

Beyond its enzymatic activities, PARP7 has emerged as an important player in several key signaling pathways. Most notably, it has been found to act as a negative regulator of the aryl hydrocarbon receptor (AHR) signaling cascade. AHR is a well-known mediator of toxic responses triggered by environmental contaminants like TCDD, and it also regulates critical processes such as immune function, inflammation, and cancer progression. By reining in AHR signaling, PARP7 appears to exert a protective effect against the detrimental consequences of AHR activation (MacPherson et al., 2013).

Interestingly, PARP7 has also been identified as a positive regulator of other important transcriptional regulators, including liver X receptors (LXRs), type I interferons (IFN-Is), and hypoxia-inducible factor 1 (HIF-1 $\alpha$ ). This diverse array of regulatory functions suggests that PARP7 plays a pivotal role in modulating innate immunity and cellular responses to various environmental and physiological stressors (Richard et al., 2021).

#### **1.9.8: PARP8**

PARP8, or Poly (ADP-ribose) Polymerase 8, plays a crucial role in various cellular processes. PARP8 is primarily a nuclear envelope protein, but it relocates to centrosomes and spindle poles during mitosis (Vyas et al., 2013). Depletion of PARP8 leads to mitotic and nuclear abnormalities and reduced cell viability, although the underlying mechanisms remain unclear. While the specific biological pathways regulated by PARP8 are still unknown, structural and functional studies indicate that it possesses PARylation activity, although its target substrates have yet to be identified (Richard et al., 2021).

### **1.9.9: PARP9**

PARP9, originally known as B-aggressive lymphoma 1 gene (BAL1), was first identified as a risk factor for large diffuse B-cell lymphomas (Yang et al., 2017). Initially, it was believed to be catalytically inactive due to its inability to undergo auto-ADP-ribosylation. However, subsequent research has revealed that PARP9 possesses mono-ADP-ribosylation (MAR) activity (Tang et al., 2018).

One of the most intriguing discoveries about PARP9 is its involvement in the innate immune response to viral infections. PARP9 has been identified as a non-canonical sensor for viral double-stranded RNA (dsRNA), a hallmark of viral infection. Upon recognizing viral dsRNA, PARP9 activates the PI3K/AKT3 signaling pathway, leading to the production of type I interferons (IFN-I) (Xing et al., 2021; Zhang et al., 2015). PARP9 has also been implicated in the regulation of gene expression. It can interact with transcription factors and histone proteins, influencing the accessibility of DNA to transcriptional machinery. Additionally, PARP9 can modify target proteins through MARYlation, which can alter their activity and function (Zhang et al., 2015). PARP9 exhibits complex interactions with other PARP family members, particularly PARP14. While PARP14 is a well-known MAR enzyme with antiviral properties, PARP9 has been found to antagonize the pro-inflammatory effects of PARP14. PARP9 can inhibit PARP14-induced MARYlation of STAT1, a key transcription factor involved in the interferon response, thereby modulating the immune response (Iwata et al., 2016; Morone & Grimaldi, 2024).

### **1.9.10: PARP11**

PARP11 is a multifaceted protein that is essential for a variety of cellular processes in the nucleus. One of PARP11's key functions is to localise at nuclear envelope, where it interacts with the nucleoporin protein NUP153 and contributes to the stability of the nuclear envelope while also participating in the dynamic remodelling of the nucleus during the critical process of spermatogenesis (Meyer-Ficca et al., 2015; Richard et al., 2021).

Beyond its structural roles, PARP11 has also emerged as an important regulator of cellular signalling pathways, particularly the interferon (IFN) response. Researchers have discovered that PARP11 can inhibit IFN signalling by ADP-ribosylating the E3 ubiquitin ligase-transducin repeat-containing protein ( $\beta$ -TrCP), leading to the ubiquitination and subsequent degradation of the interferon receptor (IFNAR) (Du et al., 2023; Guo et al., 2019). This mechanism of action effectively dampens the cell's antiviral response, as evidenced by the finding that silencing PARP11 or treating cells with the pan-PARP inhibitor rucaparib can inhibit the replication of viruses such as vesicular stomatitis virus (VSV) and herpes simplex virus 1 (HSV-1) (Du et al., 2023; Guo et al., 2019). Interestingly, while rucaparib is primarily known to target PARP1 and PARP2, in this context, it appears to preferentially inhibit PARP11, highlighting the potential for PARP11-specific inhibitors as a therapeutic strategy against certain viral infections (Guo et al., 2019).

### **1.9.11: PARP12**

PARP12 is a catalytically active member of the PARP family, characterized by its zinc finger CCCH domain. This unique domain enables PARP12 to recognize specific target

proteins and MARylation reactions (Shao et al., 2018). PARP12 primarily localizes to the Golgi apparatus, where it is thought to play a role in maintaining Golgi structure and function under normal conditions (Ke, Zhang, et al., 2019). However, in response to cellular stress, such as oxidative stress, PARP12 undergoes dramatic re-localisation to stress granules. PARP12 translocation to stress granules is thought to be a protective mechanism that inhibits protein translation under stress (Welsby et al., 2014). Emerging evidence suggests that PARP12 may have tumor-suppressant properties. Low levels of PARP12 expression have been associated with increased tumorigenesis suggesting its role in suppressing tumour growth and progression (Shao et al., 2018). PARP12 also interacts with TRIF, a key adaptor protein involved in Toll-like receptor signalling and hence enhances NF- $\kappa$ B signalling and subsequent production of pro-inflammatory cytokines such as IL-8 (Kerr et al., 2023).

#### **1.9.12: PARP13**

PARP13, also known as the zinc-finger antiviral protein (ZAP), was the first member of the PARP family to be identified and studied as having potent antiviral capabilities. This versatile protein functions as a viral sensor, able to recognize and bind to a wide variety of viruses, including those from the Filoviridae, Alphaviridae, and Retroviridae families (Zhu & Zheng, 2021). Its antiviral activity is facilitated through direct binding to the viral RNA, which then recruits the cellular exosome complex to degrade the target viral RNA sequences. PARP13 has two distinct splice variants - the short form (ZAPS) and the long form (ZAPL). While ZAPL acts as the primary antiviral effector, ZAPS plays a more nuanced role as a feedback regulator, targeting host type I interferon (IFN-I) mRNAs in

response to the inflammatory signaling triggered by IFN. Intriguingly, recent studies in cell models infected with viruses like Sindbis, Japanese encephalitis, Newcastle disease, and Influenza A have revealed that ZAP can actually enhance the antiviral innate immune response associated with the RIG-I signaling pathway (Hayakawa et al., 2011). The E3 ubiquitin ligase TRIM25, which is responsible for the polyubiquitination and activation of RIG-I, was found to catalyze both K48- and K63-linked polyubiquitination of ZAP during Sindbis virus infection in 293T cells. While this ubiquitination of ZAP did not appear to be essential for its antiviral function, the interaction with TRIM25 could significantly potentiate ZAP's broad-spectrum antiviral activity (Goncalves-Carneiro et al., 2021). However, the extent to which ZAP's antiviral effects are dependent on or synergistic with the RIG-I signaling axis remains an open and intriguing question for further investigation.

#### **1.9.13: PARP14**

Initially identified as BAL2 (B-cell aggressive lymphoma 2), PARP14 has since been implicated in a variety of cellular processes, including immune regulation, gene expression, and mRNA stability (Qin et al., 2019). One of the key functions of PARP14 is its involvement in the regulation of the immune response, particularly in response to viral infections. It is an interferon-stimulated gene (ISG), and can be activated by various stimuli, including viral RNA and DNA, leading to the production of type I interferons (IFNs). PARP14 has been shown to inhibit IFN- $\gamma$  and STAT1 signalling, where it negatively regulates the IFN- $\gamma$  signalling pathway by inhibiting STAT1 activation (Iwata et al., 2016). PARP14 can also positively regulate the IL-4 signalling pathway by promoting STAT6 activation (Shreevrat Goenka et al., 2007).

PARP14 has also been implicated in the regulation of mRNA stability. It forms a complex with tristetraprolin (TTP), a well-known mRNA-destabilizing factor. This complex binds to the 3'UTR of target mRNAs, such as tissue factor mRNA, promoting its degradation (Iqbal et al., 2014).

**Table 1. 2 Antiviral/Proviral Properties of the PARPs.** \*HIV-1-human immunodeficiency virus; KSHV-Kaposi's sarcoma associated herpesvirus; PRRSV-porcine reproductive and respiratory syndrome virus; RSV-respiratory syncytial virus; MHV-mouse hepatitis virus; VSV-vesicular stomatitis virus; EMCV-encephalomyocarditis virus; MLV-murine leukaemia virus; NDV-Newcastle disease virus; SARS-CoV-2-severe acute respiratory syndrome coronavirus2; MPS-myeloproliferative sarcoma virus, EBV-Epstein-Barr virus; and Niv-nipah virus.

PARP	ARTD name	Other Names	MW (kDa)	Catalytic Activity	Virus Targeted	Proviral/Antiviral	References
PARP1	ARTD1		~113	PAR	HIV-1* MLV* MPSV* EBV* KSHV* PRRSV*	Both Both Pro Anti Anti Pro	(Daugherty, Young et al. 2014, Kuny and Sullivan 2016, Fehr, Singh et al. 2020, Li, Shi et al. 2021, Richard, Burgess et al. 2021, Parthasarathy, Saenjamsai et al. 2024, Kar, Chatrin et al. 2024)
PARP3	ARTD3		~60	PAR			
PARP4	ARTD4	Vault PARP	~37	PAR			
PARP5b	ARTD6	TAnkyrase2	~126	PAR			
PARP6	ARTD17		~71	MAR			
PARP7	ARTD14	TIPARP	~76	MAR	IAV* SINV* RV* MHV*	Pro Anti Anti Pro	
PARP8	ARTD16		~95	MAR			
PARP9	ARTD9	BAL1	~96	Inactive			
PARP11	ARTD11		~39	MAR	VSV* HIV-1* ZIKA*	Pro Pro Anti	
PARP12	ARTD12	ZC3HDC1	~79	MAR	VEEV* SINV* EMCV* VSV* CHIKV* ZIKA*	Anti Anti Anti Anti Anti Anti	
PARP13	ARTD13	ZC3HAV1	~101	Inactive	HIV-1* SINV* NDV* EBOV* IAV* JEV*	Anti Anti Anti Anti Anti Anti	
PARP14	ARTD8	BAL2	~202	MAR	MHV* SARS-CoV-2* HSV-1* VSV* EBOV* NiV*	Anti Anti Anti Pro Pro Pro	

#### **1.9.14: PARP Inhibitors**

Poly (ADP-ribose) polymerase (PARP) inhibitors (PARPi) represent a significant advancement in cancer treatment. These drugs target PARP enzymes, essential for DNA repair, by blocking their interaction with NAD<sup>+</sup>. This strategy is particularly effective against tumours with defects in homologous recombination (HR) repair, a crucial DNA repair pathway. Normal cells possess robust HR repair mechanisms, rendering them relatively insensitive to PARPi (Sharif-Askari et al., 2018; Wu et al., 2023). Conversely, tumours with mutations in essential HR genes, such as BRCA1 and BRCA2, rely highly on alternative DNA repair pathways, including those involving PARP. By inhibiting PARP, these tumours are unable to efficiently repair DNA damage, leading to cell death (Rose et al., 2020; Sharif-Askari et al., 2018). Compared to traditional broad-spectrum chemotherapies or radiation, these targeted PARPi therapies demonstrate greater specificity and reduced off-target toxicities.

While PARP1 is considered the primary target, some PARPi also inhibit the activity of other PARP family members like PARP2 and PARP3 due to the structural similarities in their NAD<sup>+</sup> binding domains. Several PARP inhibitors, including Olaparib, rucaparib, and niraparib, have already been approved for the treatment of BRCA-mutated breast, ovarian, pancreatic, and prostate cancers (Rose et al., 2020; Sharif-Askari et al., 2018; Wu et al., 2023). However, emerging evidence suggests these agents may have even wider applications, potentially benefiting tumours harbouring deficiencies in other DNA damage response pathways beyond just HR status. In contrast to the limited potency and nonspecific effects of early PARP inhibitors like nicotinamide and 3-aminobenzamide, the latest generation of PARPi have been designed with improved pharmacological properties to enhance their clinical utility (Chen, 2011; W. H. Li et al., 2023). Overall, the

development of PARP inhibitors represents a significant advancement in precision oncology, offering a more targeted and effective approach to treating a variety of difficult-to-treat cancers.

**Table 1. 3 PARP Inhibitors.** \*FDA: Food and Drug Administration and EMA: The European Medicines Agency.

Inhibitor	Approving Organization	Indication	Target	References
Olaparib	FDA* and EMA*  FDA  EMA	Advanced ovarian carcinoma; Reoccurring ovarian, fallopian and primary peritoneal carcinoma.  First-line treatment of advanced ovarian, fallopian and primary peritoneal carcinoma in combination with Bevacizumab; Metastatic castration-resistant prostate cancer.  Fallopian and primary peritoneal carcinoma.	PARP1, and 3	(Sharif-Askari, Amrein et al. 2018, Rose, Burgess et al. 2020, Wu, Xu et al. 2023)
Rucaparib	FDA and EMA  FDA	Advanced ovarian carcinomas, following multiple chemotherapy treatments; Reoccurring ovarian, fallopian and primary peritoneal carcinoma.  Metastatic castration-resistant prostate cancer.	PARP1	(Sisay and Edessa 2017, Dal Molin, Westin et al. 2018, Rose, Burgess et al. 2020)
Niraparib	FDA and EMA	Reoccurring ovarian, fallopian and primary peritoneal carcinoma; Advanced ovarian carcinomas and primary peritoneal carcinoma.	PARP1	(Sisay and Edessa 2017, Dal Molin, Westin et al. 2018, Wu, Xu et al. 2023)
Talazoparib	FDA and EMA	Advanced or metastatic HER2-negative breast cancer	PARP1	(Hoy 2018, Exman, Barroso-Sousa et al. 2019)
ME0328		Breast cancer	PARP3	(Sharif-Askari, Amrein et al. 2018)
Fuzuloparib		Platinum-sensitive recurrent ovarian cancer, fallopian tube cancer, or primary peritoneal cancer in patients with germline BRCA mutation who have received second-line or higher-dose chemotherapy.	PARP1	(Lee 2021)
AZ0108		Breast cancer	PARP6	(Johannes, Almeida et al. 2015, Wang, Grosskurth et al. 2019)
AEP07			PARP4	(Kirby, Person et al. 2021)
ITK7			PARP11	(Kirby, Kojic et al. 2018)
RBN012759			PARP14	(Schenkel, Molina et al. 2021)

PARPs are essential enzymes involved in various cellular processes, including DNA repair, gene expression, and cell death. Their role in DNA repair and cell signaling makes them particularly important in the context of viral infections like influenza A virus (IAV). By studying PARPs, we can gain a deeper understanding of how IAV infection impacts cellular processes and how to potentially target these pathways for therapeutic intervention. PARPs are crucial for DNA repair, especially in response to IAV-induced DNA damage, preventing cellular dysfunction and death. They also influence the immune response by regulating the production of inflammatory cytokines and chemokines. Additionally, PARPs can regulate cell death pathways, which can be detrimental during viral infections. Some viruses, including IAV, can manipulate PARP activity to promote their replication or evade the host immune response. Understanding the specific mechanisms by which PARPs influence IAV infection, such as their involvement in DNA repair, immune response modulation, and viral replication, is crucial for developing novel antiviral therapies. By targeting PARP activity, we may be able to develop new strategies to combat IAV infections and other viral diseases.

The aim of this study is to investigate the role of PARPs in the chicken antiviral response to IAV infection. Using bioinformatic analysis, transcriptomic profiling, subcellular localisation studies, and plaque assay results, we will screen and prioritise chPARP proteins with potential antiviral activity. This multifaceted research will begin with a detailed evolutionary and structural analysis of the chPARP protein family to better understand its evolutionary history and functional diversity. Subsequently, the study will delve into the intricate interplay between chPARPs and IAV infection by analysing global gene expression changes in chicken embryonic fibroblasts (CEF) cells upon viral infection, focusing on the expression patterns of chPARP genes, identifying those with

potential antiviral efficacy. Further by examining their subcellular localisation, antiviral efficacy and the functional contributions of their distinct domains, we aim to assess the antiviral potential of the selected chPARP, investigate the species-specific aspects of chPARP14 antiviral function. This study will help to advance our understanding of avian antiviral immunity and potentially help in the development of new strategies to improve chicken health and disease resistance.

# **Chapter 2: Materials and Methods**

## **2.1: Mammalian Cell Culture**

### **2.1.1: Growing Mammalian Cells**

The cells were carefully grown and passaged in a laminar flow hood, which provided a sterile, controlled environment to prevent any contamination. The specific cell lines used were, DF1 cells (ATCC), HEK293T cells (ATCC), and MDCK cells (ATCC). All the cells were both cultured in Gibco Dulbecco's modified eagle medium (DMEM) supplemented with GlutaMAX, 10% fetal bovine serum (FBS) from Gibco, and 1% penicillin-streptomycin also from Gibco. This media formulation provided the cells with the necessary nutrients, growth factors, and antibiotics to thrive. Maintaining the cells at the ideal temperature of 37°C and 5% carbon dioxide concentration, a Panasonic CO<sub>2</sub> incubator provided the optimal environmental conditions for the cells to proliferate.

### **2.1.2: Passaging mammalian cells**

The process involves regularly transferring cells from one culture vessel to another, typically every 2-3 days, in order to prevent the cells from becoming overcrowded and to ensure they have sufficient nutrients and space to continue growing and dividing.

To passage the cells, the spent culture medium, which contains waste products and depleted nutrients, was removed via gentle aspiration. The cells were then gently washed with a phosphate-buffered saline (PBS) solution to remove any remaining traces of the old medium. Next, the cells were treated with a dissociation reagent such as trypsin (Gibco), or trypsin-versene (Gibco), which enzymatically cleaves the proteins that anchor the cells to the culture vessel's surface. Once the cells are no longer adhering to the flask,

an equal volume of fresh growth medium is added to neutralize the trypsin activity, as the presence of serum proteins in the medium inhibits the enzyme. The cell was then centrifuged at 1000rpm for 5 minutes, separating them from the dissociation solution. The cell pellet was resuspended in a small volume of fresh, pre-warmed growth medium and were generally passaged at a 1:3 ratio. This dilution helps to maintain the cells in a healthy, actively dividing state.

### **2.1.3: Freezing Mammalian Cells**

The cells were first grown to approximately 50% density in T75 flasks, a standard tissue culture vessel used to maintain and propagate adherent cell lines. Once the desired cell density was reached, the cells were gently washed with 5mL of phosphate-buffered saline (PBS), a physiologically balanced salt solution that helps maintain the cells' osmotic environment. Next, the cells were dissociated with trypsin, as described in the materials and methods section 2.1.2. The cell suspension was centrifuged at 1,000 revolutions per minute (rpm) for 5 minutes. After carefully aspirating the supernatant, the remaining cell pellet was resuspended in 500 microliters ( $\mu\text{L}$ ) of a specialized freezing medium. This freezing medium contained 250  $\mu\text{L}$  of the cryoprotective agent dimethyl sulfoxide (DMSO) (Sigma), and 250  $\mu\text{L}$  of the standard cell growth medium DMEM. DMSO helps protect the cells from damage during the freezing process. The cell suspension was then carefully aliquoted into 1mL cryogenic storage vials. To ensure a controlled, gradual freezing process, the cryotubes were placed into a specialized Mr. Frosty™ freezing container, which provides a consistent cooling rate of approximately 1°C per minute

when placed in a -80°C freezer. After being frozen overnight, the cryotubes were transferred to long-term storage in liquid nitrogen for long term storage.

#### **2.1.4: Transient Transfection**

To introduce a desired plasmid DNA into the cells, cells were first seeded and cultured to approximately 80% confluency, the optimal density for efficient transfection. Subsequently, the plasmid DNA was prepared for delivery by diluting it in 100 µl of Opti-MEM (Thermo Scientific), a reduced-serum media that enhances DNA uptake. The plasmid DNA amount was determined individually for each experiment based on factors such as cell type and the desired level of gene expression. Concurrently, the transfection reagent (Viafect from Promega) was also diluted in Opti-MEM in a separate tube. A 1:2.5 ratio of plasmid DNA to transfection reagent was commonly used, which helps form complexes that can efficiently enter the cells. After allowing the plasmid and transfection reagent to incubate separately for 5 minutes, they were combined, mixed thoroughly, and then left to incubate for 30 minutes at room temperature. This allows the complexes to fully assemble before being added to the cells. The existing cell culture media was then removed, and fresh growth medium was added to provide optimal conditions for the cells. Finally, the transfection mixture was carefully added dropwise to the wells, and the plates are gently rocked to ensure even distribution of the reagents. The transfected cells were then incubated in a 37°C, 5% CO<sub>2</sub> incubator for 24 hours to allow for sufficient protein expression. Subsequently, the transfection media was replaced with fresh growth medium to maintain cell viability and proceed with downstream experimental procedures.

## 2.2: E. coli

### 2.2.1: Bacterial Transformation

In this process of bacterial transformation plasmid DNA was carefully combined with a specialized strain of competent *Escherichia coli* cells, in order to facilitate the uptake and incorporation of the foreign genetic material.

The plasmid was added in a minute 1  $\mu$ L quantity and gently mixed with the 30  $\mu$ L aliquot of competent DH5 $\alpha$  cells (Thermo-Scientific) on ice. This initial incubation period of half an hour allowed the plasmid to make contact with the bacterial cells and begin the process of adsorption to the cell surface.

Following this delicate incubation, the transformation mixture was then subjected to a brief heat shock treatment at 42 degrees Celsius on a heat block for 30 seconds. This thermal stress causes the bacterial cell membranes to become temporarily permeable, facilitating the uptake of the plasmid DNA into the cytoplasm of the DH5 $\alpha$  cells. Immediately after this heat shock, the samples were quickly transferred back to the ice for 1 minute, allowing the cell membranes to rapidly reseal and stabilize. The transformed bacterial cells were then allowed to recover in 250 microliters of nutrient-rich LB broth media (Thermo-Scientific), incubated at the optimal growth temperature of 37 degrees Celsius with gentle agitation for 1 hour. This recovery period provided the cells the opportunity to express the new genetic information encoded on the plasmid, preparing them for selection on antibiotic-containing agar plates. Finally, aliquots of the transformed cell suspension, approximately 80 microliters, were carefully spread onto LB agar plates (Thermo-Scientific) supplemented with either ampicillin (100 $\mu$ g/ml) or kanamycin (50 $\mu$ g/ml), antibiotics to which the plasmid confers resistance. These

selective plates were then incubated overnight at 37 degrees Celsius, allowing the transformed bacterial cells harbouring the plasmid to proliferate and form discrete colonies on selective media.

### **2.2.2: Plasmid DNA Preparation from *E. coli***

*E. coli* cells were prepared from glycerol stocks or freshly transformed cultures, as described in section 2.2.1 of the protocol. These bacterial cells were then supplemented with the appropriate antibiotic, using a ratio of 4µL of antibiotic per 1µL of LB broth to ensure the cells maintained the desired plasmid. Next, 9ml of the bacterial culture supplemented with antibiotics were grown overnight at 37 degrees Celsius in LB growth medium, allowing the cells to proliferate and reach a high density. Finally, plasmid DNA from the harvested bacterial cells was harvested using the protocol outlined in the QIAprep Spin Miniprep Kit provided by Qiagen.

### **2.2.3: Plasmid DNA isolation from *E. coli* (Qiagen)**

The overnight culture from section 2.2.2 was transferred to a microcentrifuge tube and was centrifuged at 6800 x g for 3 minutes at room temperature. The supernatant was discarded, and the bacterial pellet was resuspended in 250 µL Buffer P1 was transferred to a microcentrifuge tube and were vortexing gently to ensure that no cell clumps were left. After that, 250 µL Buffer P2 was added, and the cells were mixed gently by inverting the tube 10-12 times until solution turns completely blue. No vortex was involved at this step. The solution was incubated at room temperature for 5 minutes. 350 µL Buffer P3

was then added to the solution and was mixed immediately by inverting the tube 10-12 times until the solution turns colourless. Cells were centrifuged for 10 minutes, and the supernatant was transferred to the QIAprep spin column and was centrifuged for 1 minute. The flow-through was discarded and 500 µl of buffer PB was added to the spin column and was centrifuged for 1 minute. The flow-through was discarded and the 750 µl of buffer PE was added to the spin column and was centrifuged for 1 minute. After that empty spin column was centrifuged for 1 minute to remove residual wash buffer. The spin column was transferred to a clean 1.4 mL microcentrifuge tube. 60 µL of buffer EB (10 mM Tris-Cl, pH 8.5) was added to the column, and the tube was incubated for 1 minute. Finally, the tube was centrifuged at maximum speed for 1 minute to elute the DNA.

#### **2.2.4: Quantifying DNA concentration**

DNA concentration was measured using a NanoDrop 2000c spectrophotometer (Thermo Scientific) according to manufacturer's instructions.

#### **2.2.5: Isopropanol Precipitation**

Isopropanol precipitation is a common technique for concentrating DNA after miniprep or gel extraction. This method takes advantage of DNA's reduced solubility in isopropanol, which causes DNA molecules to precipitate out of solution and form a pellet. This concentrated DNA pellet can then be collected and resuspended in a smaller amount of buffer to increase its overall concentration.

First, 100mL of room temperature isopropanol was added directly to the DNA-containing sample and thoroughly mixed to ensure even distribution. The samples were then

incubated at 4°C for 3 hours, allowing the isopropanol to interact with and aggregate the DNA over an extended period. After this incubation, the samples were centrifuged at 15,000 x g for 30 minutes at 4°C. This powerful spinning causes the precipitated DNA to be pulled out of the solution and form a small pellet at the bottom of the tube. The clear supernatant liquid was then carefully decanted off, leaving just the concentrated DNA pellet behind. To further purify the DNA, the pellet was rinsed with 500nL of room temperature 70% ethanol solution and centrifuged for 20 minutes at 15,000 x g at 4°C. This additional washing step helps remove any remaining contaminants or salts.

The ethanol supernatant was removed, and the DNA pellet was air-dried for 20 minutes to evaporate off the last traces of ethanol. Once fully dry, the purified DNA was dissolved 20ml of elution buffer solution. The concentration of the final DNA solution was measured using a Nanodrop spectrophotometer as described in the previous section.

## 2.3: Cloning and PCR

### 2.3.1: Chicken PARP14 Constructs

The following chicken PARP14 constructs were designed and cloned into EGFP-Flag-C1-ku70 mammalian expression vector (a gift from Dr Gabriella Grundy, North West Cancer Research Fellow, University of Liverpool).

**Table 2. 1** List of chPARP14 cloned into EGFP-Flag-C1-ku 70 mammalian expression vector.

S.No	Constructs	Amino Acids	Domains
1	chPARP14wt	1-1823	Full-length chPARP14
2	chPARP14 $\Delta$ N	1-795	RRM domains of chPARP14
3	chPARP14 $\Delta$ MAC	796-1455	Macrodomains of chPARP14
4	chPARP14 $\Delta$ MACD	796-1540	Macrodomains and the D domain of chPARP14
5	chPARP14 $\Delta$ C	796-1823	Macrodomains, D-domain, WWE-domain and the catalytic domain of chPARP14
6	chPARP14 $\Delta$ CWC	1456-1823	D-domain, WWE-domain and the catalytic domain of chPARP14
7	chPARP14 $\Delta$ WC	1541-1823	WWE-domain and the catalytic domain of chPARP14
8	chPARP14 $\Delta$ CAT	1674-1823	Catalytic domain of chPARP14

### 2.3.2: Primer design

**Table 2. 2 List of primers used for cloning** (primers were ordered from Thermo-Scientific)

<b>Primer</b>	<b>Sequence</b>
pGFP-chPARP14 Wt-F	AAGCTCGAGATGGCCGGACCTAGGCCTGGCAG
pGFP-chPARP14 Wt-R	CTTGGATCCCTAGCGTCTAAAGGTTATCAGGTA CT CAGGGTAC
pGFP-chPARP14 N-R	CTTGGATCCCTACTTATCCACGTTCTTACTCTTTTGCTGCTC
pGFP-chPARP14 MAC-F	AAGCTCGAGGTGGAACGTAAACTGTATTACAAGTTGAC
pGFP-chPARP14 MAC-R	CTTGGATCCCTAGTCGACATTCTTCTGGCTCTCGCCACAAATC
pGFP-chPARP14 MACD-R	CTTGGATCCCTATTCTGAGCAGCTTTCTTCTTCTGGATCATCTTCTG
pGFP-chPARP14 CWC-F	AAGCTCGAGGCCACGGAGTCTGGATAATTGACGTGATC
pGFP-chPARP14 WC-F	AAGCTCGAGGAGCAGAACAAGCTGAACTGATATATAAACTGG
pGFP-chPARP14 CAT-F	AAGCTCGAGCAGAACCCATTCTGTGGCAGTCCTATCAG

### 2.3.3: PCR amplification of chPARP14 constructs

Specific target regions within the chPARP14 gene were amplified from the full-length chPARP14 gene using Q5 High-Fidelity DNA polymerase, following the manufacturer's protocol.

### 2.3.4: Q5-HF PCR Reaction Mixture

Reaction Mixture	Volume
Q5 Amplification Buffer (10X)	10 $\mu$ l
GC enhancer	10 $\mu$ l
dNTPs mixture (10mM)	1 $\mu$ l
F-primer	2.5 $\mu$ l
R-primer	2.5 $\mu$ l
Q5 DNA Polymerase	0.5 $\mu$ l
Template DNA (200ng)	2 $\mu$ l
Nuclease free water	Up to 50 $\mu$ l
Total	50 $\mu$ l

PCR reactions were assembled on ice, mixed by pipetting, centrifuged, and transferred to a PTC-200 Thermal Cycler (Marshall Scientific) for PCR amplification.

### 2.3.5: Q5-High-fidelity PCR reaction thermocycling conditions

Step	Temperature	Time	Cycles
Initial Denaturation	98°C	30 seconds	1 cycle
Denaturation	98°C	10 seconds	40 cycles
Annealing	55°C	30 seconds	
Extension	72°C	30 seconds	
Final Extension	72°C	5 minutes	1 cycle
Final hold	10°C	Indefinite period	

### 2.3.6: Restriction Digestion

Restriction enzymes were sourced from New England Biolabs and used in 25  $\mu$ L reaction volumes. Digestions were carried out according to the manufacturer's recommended conditions, including temperature, duration, and deactivation protocols. Following PCR amplification, samples were immediately placed on ice to prevent non-specific DNA degradation.

Reaction Mixture	Volume
DNA	2 $\mu$ g
10X Cutsmart Buffer	2 $\mu$ l
XhoI	1 $\mu$ l
Bam HI	1 $\mu$ l
Nuclease free water	Up to 25 $\mu$ l
Total	25 $\mu$ l

### 2.3.7: Agarose Gel Electrophoresis for DNA Fragment Analysis

Restriction digest products were analysed by 1% agarose gel electrophoresis to confirm the presence of expected DNA fragments. DNA samples were mixed with 6X DNA loading dye (NEB) in a 1:5 ratio. Agarose gels were prepared by dissolving 0.5g of ultrapure agarose (Thermo Scientific) in 50 mL of TAE buffer (Thermo Scientific) and melting in a microwave. 0.01% (v/v) GelRed nucleic acid stain (Thermo Scientific) was added to the cooled agarose solution. The mixture was poured into a gel tray and solidified, with a comb inserted to form sample wells. DNA samples and a 1 kb DNA ladder (GeneRuler, Thermo Scientific) were loaded into the wells. Electrophoresis was performed in TAE buffer at 100V for 60 minutes, or until the dye front reached the end of the gel. DNA bands

were visualized using a Bio-Rad GelDoc EZ Imager or a Bio-Rad GelDoc UVP Dual-intensity Transilluminator.

### **2.3.8: DNA Gel Extraction**

Specific DNA fragments of the desired molecular weight were excised from the agarose gel using a sterile razor blade. DNA extraction was performed following the manufacturer's instructions for the GeneJET Gel Extraction Kit. The gel slice was placed in a pre-weighed 1.4 mL microcentrifuge tube and incubated with binding buffer at 50-60°C for 10 minutes to dissolve the agarose. Isopropanol was added to the dissolved gel solution, and the mixture was transferred to a GeneJET purification column. The column was centrifuged to bind the DNA, followed by two wash steps to remove contaminants. Finally, the purified DNA was eluted in 20 µL of elution buffer. The recovered DNA was quantified and stored at -20°C for future use or directly used in subsequent subcloning experiments.

### 2.3.9: Ligation

Ligation of linearized PCR products, and annealed oligonucleotides was performed following the manufacturer's protocol for T4 DNA ligase.

Ligation Mixture	Volume
Purified linearized plasmid	50ng
Purified DNA insert	50ng
T4 DNA ligase reaction buffer (10X)	2 $\mu$ l
T4 DNA ligase enzyme	1 $\mu$ l
Nuclease free water	Up to 20 $\mu$ l
Total	20 $\mu$ l

The reaction mixture was gently mixed before incubating at room temperature for 2 hours or overnight at 4°C. The ligation mixture (1-20  $\mu$ L) was used to transform chemically competent E. coli cells, as described in Section. To identify positive transformants, a suitable number of colonies were selected and screened using colony PCR.

### 2.3.10: Colony PCR

Individual bacterial colonies were transferred to microcentrifuge tubes and centrifuged at 5,000 rpm for 5 minutes to pellet the cells. The supernatant was gently removed. To lyse and release genomic DNA, the cell pellet was resuspended in 100  $\mu$ L of sterile water and incubated at 100°C for 10 minutes. The lysate was then centrifuged at 10,000 rpm for 5 minutes to remove any remaining cell debris. The supernatant containing genomic DNA was transferred to a fresh microcentrifuge tube.

Target genes were amplified by PCR using gene-specific primers. The PCR reaction mixture was prepared using a PCR master mix that included the following components:

<b>Reaction Mixture</b>	<b>Volume</b>
DreamTaq Green PCR Master Mix (2X)	12.5µl
Forward Primer	1µl
Reverse Primer	1µl
Template DNA	1µl
Nuclease free water	Up to 25µl
<b>Total</b>	<b>25µl</b>

The reaction mixture was added to each sample, and the tubes were briefly centrifuged to collect the liquid at the bottom. PCR amplification was carried out in a thermal cycler using the following cycling conditions:

<b>Step</b>	<b>Temperature</b>	<b>Time</b>	<b>Cycles</b>
Initial Denaturation	98°C	30 seconds	1 cycle
Denaturation	98°C	10 seconds	40 cycles
Annealing	55°C	30 seconds	
Extension	72°C	30 seconds	
Final Extension	72°C	5 minutes	1 cycle
Final hold	10°C	Indefinite period	

The number of cycles and the annealing temperature were optimised for each primer pair.

### **2.3.11: DNA Sequencing for Confirmation**

Following PCR amplification and selection of potential positive colonies, DNA sequencing was employed for further identification. Twenty microliter aliquots were prepared in 0.2 mL PCR tubes, containing: Plasmid DNA (100 ng/ $\mu$ L) for suspected positive clones, or purified PCR product (2  $\mu$ L at 10 ng/ $\mu$ L), and target-specific primers (5.2 pmol). These samples were then sent to Source Bioscience Ltd. (Cambridge, UK) for sequencing.

Sequence contigs generated from the sequencing run were edited and assembled using BioEdit software (version 7.2.5, Ibis Biosciences, CA, USA), and were subsequently analysed using a combination of bioinformatics tools: NCBI BLAST (Basic Local Alignment Search Tool), Ensembl, and SnapGene.

### **2.4: Immunofluorescence Assay**

Cells were cultured on Nunc™ Thermanox™ coverslips in 24-well plates (Thermo Scientific). After washing with PBS, cells were fixed with 4% paraformaldehyde in PBS (Thermo Scientific) for 1 hour, permeabilized with 0.1% Triton X-100 (Thermo Scientific) for 10 minutes, and blocked with 0.5% BSA (Sigma-Aldrich) for 1 hour. Primary antibodies were applied for 1.5 hours, followed by three washes with PBS. Secondary antibodies were incubated for 1.5 hours, and cells were washed again with PBS. Finally, cells were

stained with DAPI (Thermo Scientific) for 15-30 minutes, mounted with Vectashield, and imaged using a Zeiss LSM 880 confocal microscope.

## **2.5: SDS-PAGE**

Gels were prepared using a Bio-Rad Mini-PROTEAN tetra handset system. Separating gels were cast with 30% acrylamide/bis (Bio-Rad), 1.5 M Tris-HCl (pH 8.8), 10% sodium dodecyl sulphate (SDS), and 10% ammonium persulphate (APS) (Sigma). Tetramethyl ethylenediamine (TEMED) was added as a catalyst, and isopropanol was used to remove bubbles. After the separating gel set, a stacking gel containing 30% acrylamide/bis, 0.5 M Tris-HCl (pH 6.8), 10% SDS, and 10% APS was added, and a comb was inserted.

Samples were loaded onto 10% separating gels with 5% stacking gels and run in a Mini-PROTEAN Tetra Cell Tank at 80V for 30 minutes, followed by 100V until the dye front reached the bottom of the gel.

### **2.5.1: Western Blotting**

For western blot analysis, the proteins were first separated using SDS-PAGE and then transferred to a PVDF membrane (Thermo Scientific) using a semi-dry trans-blot turbo transfer system (Bio-Rad). Four pieces of filter paper and one piece of PVDF membrane were prepared for each gel (9cm x 7cm per gel). The filter paper was soaked in transfer buffer (containing SDS running buffer, methanol (Sigma-Aldrich), and distilled water with pH adjusted to 8.3) for 2 minutes, while the PVDF membrane was soaked in methanol for

5 minutes. The transfer stack was then assembled by layering the filter paper, PVDF membrane, SDS-PAGE gel, and another piece of filter paper, with air bubbles removed using a roller. The proteins were transferred to the membrane for 10 minutes at 1.3A and 25V. The membrane was then blocked with 5% skim milk in PBST ((PBS+0.5% Tween) +5% skim milk) for 1 hour, incubated with primary antibody overnight at 4°C, washed, and incubated with HRP-conjugated secondary antibody for 2 hours. Following the incubation of the secondary antibody, the membranes underwent three PBST washes. After that, the blots were developed for three minutes with agitation using Pierce enhanced chemiluminescence (ECL) Western Blotting Substrate (Thermo Scientific) at a 1:1 ratio. The western blots were imaged using either the Bio-Rad ChemiDoc MP imaging system or the iBright750 imaging system (Thermo-Scientific). The developing times varied depending on the specific antibodies and samples used.

## **2.6: Viral Quantification**

### **2.6.1: Virus Propagation**

DF1 and HEK cells were grown to 70-90% confluence in appropriate media. After removing the growth media, cells were washed twice with sterile PBS. Virus inoculum was added at an MOI 1.0 to infection media containing 1x DMEM, 1x Antibiotic-Antimycotic solution, 0.2% BSA, and 50 mM HEPES buffer. To improve viral entry in MDCK cells, 2 µg/ml of TPCK-treated trypsin was added to the infection media. To ensure uniform virus distribution, cells were incubated at 37°C for 2 hours, with gentle tilting. Unbound virus was removed from cells by washing them with PBS. For antiviral assays,

cells were incubated at 37°C for 24 hours. For virus propagation, cells were incubated at 37°C for 3-4 days, or until cytopathic effects (CPE) were observed. Virus-containing supernatant was harvested by centrifugation at 3000 rpm for 10-15 minutes and stored at -80°C.

### **2.6.2: Plaque Assay**

MDCK cells were prepared in 6-well plates, one plate for each supernatant. The cells were grown to 100% confluence. A 10-fold serial dilution of each supernatant was prepared using DMEM without serum or antibodies. The spent media was removed from the MDCK cells, and 500 µl of diluted virus suspension from each tube was added to the corresponding well. Control cells were maintained with DMEM only. The plates were incubated at 37°C for 2 hours with gentle rotation every 20 minutes.

An overlay media was prepared by mixing 1.6% agar with 25 ml of culture media and 9 µl of TPCK. The viral dilutions were removed from the wells, and 1.5 ml of overlay media was added to each well. The plates were allowed to solidify and then incubated at 37°C for three days. After three days, the plates were fixed with paraformaldehyde for an hour. The agar was removed, and the plates were stained with crystal violet to visualize the plaques.

### 2.6.3: RT-qPCR

Primer pairs were designed to amplify 100-250 base pair fragments of the target genes and were synthesized by Invitrogen. Real-time quantitative reverse transcription PCR (RT-qPCR) was used to profile the expression levels of chPARPs in DF1 cells. Additionally, RT-qPCR was employed to quantify the fold-change in the expression of IAV (H9N2) in chPARP14 construct-transfected cells compared to mock-transfected cells, using the SuperScript III Platinum SYBR Green One-Step RT-qPCR Kit. To profile gene expression in IAV-treated DF1 cells, total RNA is extracted from treated and untreated cells using a suitable RNA extraction kit. To quantify viral RNA in transfected cells, RNA was extracted from the cells using TRIzol Reagent, treated with DNase I to remove DNA contamination, and reverse transcribed into cDNA. Quantitative PCR (qPCR) was used to amplify and quantify the target viral gene. A standard curve was generated to accurately determine the viral load, and the results were normalized to a housekeeping gene.

**Table 2. 3** Primers for chPARP RT-qPCR

PARP	5'-F-Primer-3'	5'-R-Primer-3'
PARP1	AGCTAAACTGCAAGAGCGGT	CCCCACAAATAGAAGCGGT
PARP3	ACACCCTGATCGAAGTGCCAG	GTGGTCTCATCCAAGGCACA
PARP4	AGGGCCATGCTGTCATCCAGAGAG	CTGTTTTCCAGCTGAGCAACCCCC
PARP5b	AGTTGTCAATCTCCTCCTGCGGCA	GTTCCGGATGGTTGTTTCAGCACC
PARP6	GGACGATGACTCCGATGGGGACAA	CGCTGTAGATCTCCTTCACGGCCT
PARP7	TGTCCCAGCTCCAGCTCCAACACTAC	CCAGGTAACGAAGCGGACCTCCTT
PARP8	ACCGTGGCTTCTTGTGCAGACTA	TCACAAACGGTGGGCCTCAGCATA
PARP9	TATCAAGTCCGTGGCTATCCGGC	TGGATCTCCTTGAGGCAGCTTGCC
PARP11	TGCTGCTGTATATGGAAAAGGGACC	CTGGTTTGTGCAAATGAGGCTGCA
PARP12	AGCCTCCTCTGTGACCAAACCACC	GCTTACAGTGGCAGCTGCTCGATC
PARP13	CACCTCATGGGCAGGTGCAGTCTG	TGGAGAAGCAGATTTCGCAGCTCA
PARP14	GCGCAAGAAGCTGCTGCTCTACTT	TCTCAAGGACCTGCTGCTTCAGGT

#### 2.6.4: RT-qPCR Reaction Mixture

Reaction Mixture	Volume
Platinum Mix	0.4 $\mu$ l
2X Reaction Mix	12.5
Forward Primer	0.4 $\mu$ l
Reverse Primer	0.4 $\mu$ l
Template RNA	<10 $\mu$ l
Nuclease free water	Up to 25 $\mu$ l
Total	25 $\mu$ l

#### 2.6.5: RT-qPCR Thermocycling Conditions

Step	Temperature	Time	Cycles
Reverse Transcriptase	50°C	15 minutes	1 cycle
Initial denaturation	95°C	5 minutes	1 cycle
Denaturation	95°C	10 seconds	40 cycles
Annealing-Extension	60°C	30 seconds	
Final hold	4°C	Indefinite period	

## 2.7: Antibodies

**Table 2. 4** List of Primary Antibodies

Primary Antibody	Animal Raised In	Concentration	Supplier	Application
Monoclonal Anti-FLAG	Rabbit	1:1000	Sigma - Aldrich	WB
Monoclonal Anti- $\alpha$ tubulin	Mouse	1:1000	Abcam	WB
Monoclonal Anti-FLAG	Rabbit	1:1000	Sigma - Aldrich	1FA
Monoclonal Anti-FLAG	Mouse	1:1000	Abcam	IFA

**Table 2. 5** List of Secondary Antibodies

Secondary Antibody	Animal Raised In	Concentration	Supplier	Application
Polyclonal Anti-Rabbit IgG (HRP)	Rabbit	1:2000	Abcan	WB
Polyclonal Anti-Mouse IgG (HRP)	Mouse	1:2000	Abcam	WB
Alexafluor 488 Anti-Rabbit	Goat	1:2000	Thermo-Fisher	1FA
Alexafluor 568 Anti-Mouse	Goat	1:2000	Thermo-Fisher	IFA

## 2.8: Buffers and Reagents

**Table 2. 6** Buffers and Reagents

Reagent	Make-up
PBS	80g NaCl, 2g KCl, 14.4g Na <sub>2</sub> HPO <sub>4</sub> ·2H <sub>2</sub> O, 2.4g KH <sub>2</sub> PO <sub>4</sub> , ddH <sub>2</sub> O up to 1l
4% Paraformaldehyde	40g paraformaldehyde, 1l ddH <sub>2</sub> O
Triton X-100 stock (1%)	2.5ml Triton X-100, 250ml ddH <sub>2</sub> O
BSA 1% stock	1g BSA, 100ml PBS
TAE (10X)	48.4g Tris base, 11.4ml glacial acetic acid, 3.7g EDTA , ddH <sub>2</sub> O up to 1l
NP40	25ml HEPES, 1ml EDTA, 20ml NaCl, 50ml glycerol, 5ml NP40, make up to 500ml with ddH <sub>2</sub> O, protease inhibitor tablet
1.5M Tris-HCl pH 8.8	90.75g Tris base + up to 500ml ddH <sub>2</sub> O
0.5 M Tris-HCl pH 6.8	30,35g Tris base + up to 500ml ddH <sub>2</sub> O
10% APS	5g ammonium persulphate + upto 50ml with ddH <sub>2</sub> O
SDS Running Buffer (10X)	30g Tris base, 114g glycine (adjust pH to 8.3), make up to 1l with ddH <sub>2</sub> O, 1-% SDS
Blocking solution	5ml PBST, 0.5g skim milk
PBST	100ml 10X PBS, 900ml ddH <sub>2</sub> O, 1ml Tween20
10X transfer Buffer	30.3g Tris base, 144g glycine + up to 1l ddH <sub>2</sub> O
LB broth	20g LB Broth, ddH <sub>2</sub> O up to 1l
2X Overlay Media	142 ml sterile bottled water, 50 ml MEM, 15ml sodium bicarbonate solution (7.5%), 5ml glutamax, 5ml antibiotic, 5ml non-essential amino acids, 13ml HEPES (1M), 20ml FCS (heat inactivated)
0.2% Crystal Violet Solution	0.2g crystal violet powder, 80ml ddH <sub>2</sub> O, 20 ml methanol

## **2.9: Bioinformatic Analysis**

### **2.9.1: Sequence Data Mining**

We directly compared the nucleotide sequences of selected bat immune genes with those from other representative species. To achieve this, we retrieved coding sequences in FASTA format for each gene of interest from the National Center for Biotechnology Information (NCBI) database ([www.ncbi.nlm.nih.gov](http://www.ncbi.nlm.nih.gov)).

### **2.9.2: Multiple Sequence Alignment (MSA)**

To directly compare amino acid sequences and identify mutations, MSA analysis was used with BioEdit software. The FASTA sequences for each gene were aligned using the ClustalW algorithm with a neighbor-joining bootstrap value of 1000.

### **2.9.3: Phylogenetic Analysis**

Evolutionary analysis was performed to estimate the divergence time between genes from different species. Aligned sequences from BioEdit were saved in FASTA format and imported into MEGA6. Phylogenetic trees were constructed using the Maximum-likelihood method with a bootstrap value of 1000.

#### **2.9.4: Pairwise Identity Matrix**

Aligned amino acid sequences in FASTA format were imported into the Sequence Demarcation Tool (SDT) software to calculate pairwise identity scores. SDT aligns each unique pair of sequences and calculates pairwise identity scores, represented by a color-coded matrix. The MUSCLE algorithm was used to generate these scores, which are calculated as  $1-(M/N)$ , where M is the number of mismatches and N is the total number of aligned positions without gaps.

#### **2.9.5: Protein Domain Prediction**

To identify conserved domains within the immune genes, we utilized the SMART and Prosite ExPasy tools. The FASTA sequences retrieved from the NCBI database for analysis. The tool then predicted and displayed the locations of conserved domains within each gene sequence, along with the specific amino acid intervals they occupy.

#### **2.9.6: Syntenic Analysis**

To understand the context and location of selected immune genes across different species, we employed the NCBI gene function database ([www.ncbi.nlm.nih.gov](http://www.ncbi.nlm.nih.gov)). The database provided information on genomic regions, transcripts, and gene products. This allowed us to determine chromosomal location, where each gene resides, enabling comparison between species.

### **2.9.7: 3D Protein Prediction**

Nucleotide sequences for immune genes were submitted to the I-TASSER and AlphaFold online servers for protein structure prediction. The predicted structures were then visualized and analysed using PyMOL software (Schrodinger 2015).

### **2.9.8: Statistical Analysis**

To compare multiple groups multiple groups within a single factor, a one-way analysis of variance (ANOVA) was employed in GraphPad software.

### **2.9.9: Heatmap Visualization**

Heatmaps are used to visualise normalised gene expression. They are good for expressing the expression levels of many genes simultaneously across samples. They provide an overview of global expression patterns as well as gene and sample clustering based on expression level similarities. However, they are less specific regarding the statistical significance (p-value). Although the colour intensity indicates the extent of change, it does not immediately display p-values.

### **2.9.10: Volcano Plots**

Volcano plots are a powerful visualisation technique for RNA-seq data interpretation, particularly for illustrating the outcomes of differential gene expression. They offer a rapid and straightforward technique to determine which genes have experienced the most

substantial changes in expression between two situations. They clearly demonstrate the relationship between the degree of expression difference (fold change) and the p-value. They excel at highlighting genes with both huge expression changes and high statistical significance, making it simple to identify the most important differentially expressed genes (DEGs).

### **2.9.11: Principal Component Analysis (PCA)**

PCA is a statistical approach used largely to reduce dimensionality. It converts a dataset with many variables into a smaller set of principle components (PCs), that retain most of the original data's volatility. It facilitates data visualisation, allowing for the detection of patterns, clusters, and outliers. It aims to maximise the variance recorded by the PCs. PCs are orthogonal, which means they reflect different directions in the data and the higher variance suggests that the component has more information.

### **2.9.12: Scree Plot**

A scree plot is used in PCA to find the best number of optimal components to keep. It visibly displays the eigenvalues for each principal component in descending order. The methodology consists of graphing the PC number on the x-axis and the matching eigenvalue on the y-axis. Typically, the figure shows a rapid decrease in eigenvalues for the first few components, followed by a flattening or "elbow" when the remaining eigenvalues level out. PCs to the left of this point are considered significant, accounting for the majority of the data variance. Observing the scree plot can help you make an

informed decision about how many PCs to include in the analysis while balancing dimensionality reduction and information retention. This method allows for the removal of components that largely represent noise or slight variations, resulting in a more compact and interpretable representation of data.

### **2.9.13: Lollipop Chart**

To gain insights into the biological pathways significantly altered during IAV infection in Chicken Embryo Fibroblast (CEF) cells, we performed a pathway enrichment analysis on the differentially expressed genes (DEGs) identified through our RNA-sequencing analysis, visualizing the results using lollipop charts for clarity. This analysis was conducted using ShinyGO 0.76, calculating statistical measures for each identified pathway including the number of genes, fold enrichment, and  $-\log_{10}$  False Discovery Rate (FDR). The fold enrichment indicates the degree to which pathway-associated genes are overrepresented in our DEG list, suggesting a stronger link between the pathway and the infection, while the  $-\log_{10}(\text{FDR})$  reflects the statistical significance, with higher values indicating greater confidence in the enrichment. The lollipop chart visually represents these findings, with the head size proportional to the pathway gene count, the color indicating  $-\log_{10}(\text{FDR})$ , and the position on the x-axis representing fold enrichment.

# **Chapter 3: Bioinformatic Analysis of chPARPs**

### **3.1: Abstract**

This chapter provides a comprehensive bioinformatic analysis of the chicken Poly (ADP-ribose) Polymerase (PARP) gene family. We investigated the evolutionary relationships, domain organisation, and functional variations in chicken PARPs using phylogenetic analysis, multiple sequence alignments, and structural comparisons. Our findings reveal distinct evolutionary clades for avian PARPs, emphasising their specific adaptations within this lineage. In addition, we discovered conserved structural features, particularly in the catalytic domains, implying shared functional roles. This study sheds light on the evolutionary history and functional diversity of chicken PARPs, paving the way for future research into their potential roles in a variety of biological processes such as DNA repair, inflammation, and antiviral responses.

### **3.2: Introduction**

PARPs are an intriguing family of proteins that play a crucial role in several biological pathways. PARPs use NAD<sup>+</sup> as a substrate and catalyse the transfer of ADP-ribose polymers to target proteins, a reversible post-translational modification that has a significant impact on protein function, localisation, and interactions (Alemasova & Lavrik, 2019). Given the central role of PARPs in DNA repair, genomic stability, cell signalling, cell death, and innate immunity pathways (Duan, 2024; Zhu et al., 2021), a thorough understanding of this protein family is critical for progressing our understanding of fundamental biology and identifying potential therapeutic targets.

In this context, the bioinformatic analysis of a group of 12 PARP proteins is an especially interesting topic of study. We decided to investigate the 12 PARP proteins' structural features, evolutionary relationships, and functional domains using computational tools and databases. As our understanding of the PARP family grows through such diverse bioinformatic analyses, we will gain invaluable insights into the mechanisms underlying cellular homeostasis, disease pathogenesis, and potential therapeutic interventions.

The study aims to

- (i) To Investigate the Evolutionary Conservation of PARP Gene Organization in Chicken: This aims to establish the degree to which the genomic arrangement and chromosomal locations of PARP genes are conserved between chicken and other species, particularly humans.
- (ii) To Determine the Sequence Similarity of Chicken PARP Proteins to Their Human Homologs: This aim focuses on quantifying the level of amino acid sequence identity between the identified chicken PARP proteins and their corresponding human PARP counterparts.
- (iii) To Analyze the Conservation of Catalytic Domains in Chicken PARP Proteins Compared to Humans: This aim specifically targets the functional core of the PARP proteins – the catalytic domain.

The overarching goal of this chapter is to provide a comparative genomic and proteomic analysis of PARP proteins between chicken and humans. Achieving this will contribute to a better understanding of the evolutionary conservation, structural similarities, and potential functional relevance of these proteins across different

vertebrate species. This will also lay the groundwork for further functional studies in the chicken model system.

### **3.3: Results**

#### **3.3.1: Domain organisation of PARP genes**

The domain organization of chicken PARPs is highly complex and diverse, with several distinct groups emerging based on their structural features. The PARPs can be broadly categorized into four main types: DNA-dependent PARPs, Tankyrases, Macro-containing PARPs, and CCCH (cysteine<sup>3</sup>Histidine) -containing PARPs (Vyas et al., 2013; Zhu et al., 2021). Understanding the importance of this domain organization is crucial, as it relates to the diverse functional roles these proteins play within the cell.

The DNA-dependent PARPs, such as PARP1 and PARP3, possess a catalytic domain at the C-terminus, as do the rest of the PARPs, but they also contain additional domains that are important for their functions. PARP1, for instance, has two zinc finger (Znf) domains and a BRCA1 C Terminus (BRCT) domain, which allow it to bind to and be activated by DNA strand breaks, playing a key role in the cellular DNA damage response. PARP3, on the other hand, shares the Tryptophan-Glycine-Arginine (WGR) domain with PARP1, but lacks the zinc finger and BRCT domains, suggesting it may have a more specialized function within the DNA repair machinery. The Tankyrases, represented by PARP5b, have a unique domain structure, featuring Ankyrin (ANK) repeats and a Sterile alpha motif (SAM) domain. These domains are critical for their roles in telomere maintenance and Wnt signalling pathways, highlighting the importance of domain organization in determining the specific cellular functions of PARPs. The CCCH-

containing PARPs, including PARP7, PARP12, and PARP13, possess a single or double zinc finger domain, as well as a Tryptophan-Tryptophan-Glutamate (WWE) domain, which is thought to mediate protein-protein interactions. These PARPs are implicated in various cellular processes, such as stress response and antiviral defence, underscoring how the domain architecture can shape the diverse biological roles of these proteins. Finally, the Macro-containing PARPs, represented by PARP9 and PARP14, have a unique domain structure featuring one or more Macro domains, which are known to bind to ADP-ribose and play a role in the cellular response to DNA damage and inflammation. PARP14 also contains a WWE domain, further expanding its functional repertoire.

However, there are several other PARP proteins that remain largely unclassified. These include PARP4, PARP6, PARP8, and PARP11 (Zhu et al., 2021). PARP4, also known as vault PARP, is unique among this group in that it possesses a catalytic domain at its N-terminal end. It also contains several additional domains not found in its more studied counterparts, including a BRCT domain, a Viral Interferon trigger (VIT) domain, and a von Willebrand factor A (VWFA) domain. The BRCT domain is commonly associated with DNA damage response proteins, while the VIT and VWFA domains suggest PARP4 may play a role in protein-protein interactions and intracellular transport processes. In contrast, PARP6 and PARP8 are the only members of the PARP family that lack any additional domains beyond the core catalytic region, making their precise cellular functions more elusive. Finally, PARP11 contains a WWE domain in addition to its catalytic core, hinting at potential regulatory roles in ubiquitin-related pathways, though the exact nature of PARP11 activities remains an open area of investigation. Overall, these lesser-known PARP proteins represent an intriguing frontier in understanding the diverse cellular functions and mechanisms of this important enzyme family (Figure 3.1). The remarkable

variation in the length and domain composition of chicken PARPs, exemplified by the shortest PARP11 (343 amino acids) and the longest PARP14 (1823 amino acids), underscores the evolutionary adaptability and functional versatility of this enzyme family. By understanding the intricate domain organization of these PARPs, we can gain valuable insights into their specialized roles in various cellular processes, from DNA repair and telomere maintenance to stress response and immune signalling to antiviral responses.

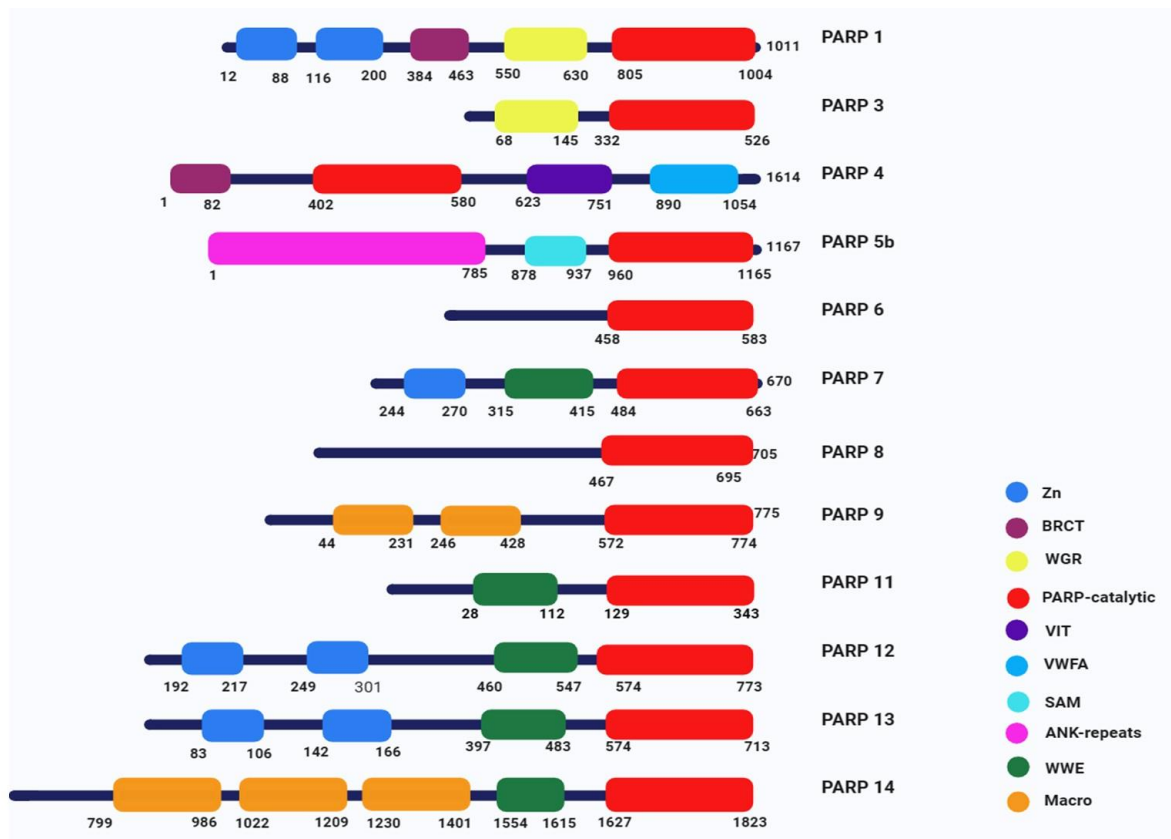


**Figure 3.1 Domain Organization of Chicken PARP Proteins.** This figure illustrates the diverse domain organisation of chPARP proteins, analysed using ExPASy-PROSITE and SMART. PARPs are categorised into groups based on their domains composition: DNA-dependent PARPs with zinc fingers and BRCT domains for DNA damage response; Tankyrases with ANK repeats and SAM domains for telomere maintenance and Wnt signalling; Macro-containing PARPs with Macro domains for ADP- ribose binding involved in DNA damage response and inflammation; and CCCH- containing PARPs with CCCH-type zinc fingers and WWE domains involved in stress responses and antiviral defence. Other PARPs, such as PARP4, 6, 8, and 11, exhibit unique domain organisation and are uncharacterized.

### **3.3.2: Variation in synteny among PARP genes**

The study of synteny, the conservation of gene order and proximity between different species, is fascinating, particularly when examining the PARP gene family. When comparing the PARP genes across various avian and mammalian species, some intriguing patterns emerge. In chickens, for instance, the PARP genes were found to be present on both autosomal and sex chromosomes, whereas in mammals PARP genes were located solely on autosomal chromosomes. This distinction emphasises the evolutionary divergence of the two major vertebrate lineages. Interestingly, while the PARP genes showed clear synteny, or conserved gene order, across different avian species such as chicken, duck, and turkey, no such synteny was found between chickens and humans. Similarly, humans and mice also display a complete lack of PARP gene synteny. This suggests that the PARP gene family has undergone significant rearrangements and reorganization during the evolutionary separation of avian and mammalian species, which is estimated to have occurred approximately 300 million years ago. Specific PARP genes, such as PARP4, PARP11, PARP12, and PARP13, were found to exhibit conserved synteny on chromosome 1 in birds, while PARP9, PARP14, and PARP8 showed synteny on chromosomes 7 and Z, respectively (Figure 3.2). The loss of this syntenic relationship between avian and mammalian species, as well as between humans and rodents, provides valuable insights into the complex genomic alterations that have shaped the PARP gene family over evolutionary timescales.

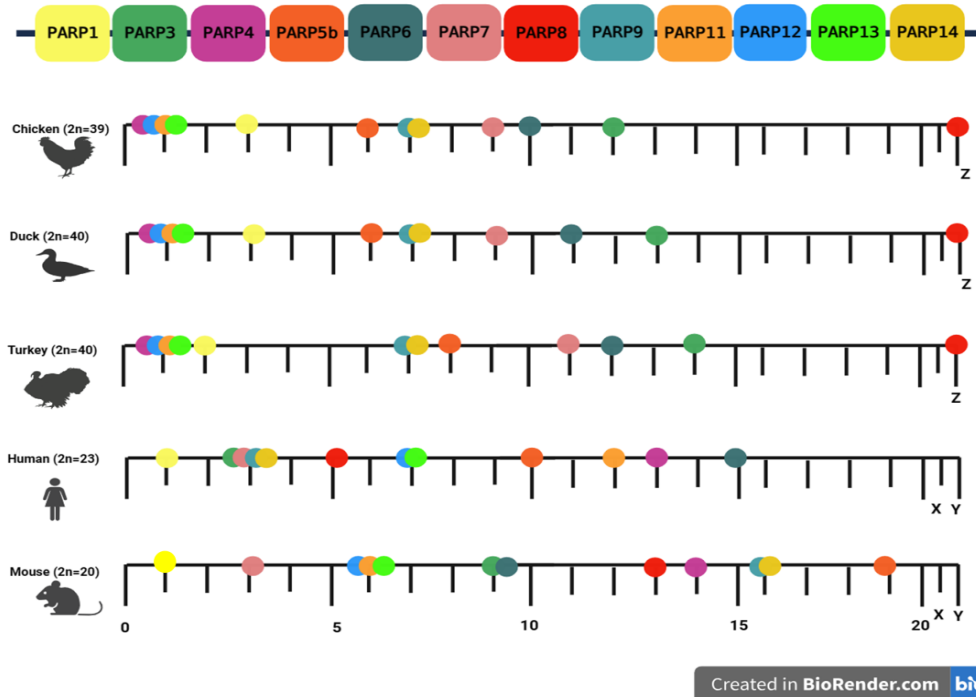


**Figure 3. 2 Synteny Analysis of PARP Genes Across Vertebrates.** This figure illustrates the comparative synteny of PARP genes across various avian species (chicken, duck, turkey) and mammals (human, mouse). It highlights the observed conservation of gene order and proximity within avian species, specifically showing conserved synteny of PARP4, PARP11, PARP12, and PARP13 on chromosome 1, and PARP9, PARP14, and PARP8 on chromosomes 7 and Z, respectively, in birds. The figure also emphasizes the absence of synteny between avian and mammalian species, as well as between human and rodent lineages, indicating significant genomic rearrangements, highlighting the dynamic nature of gene family evolution across diverse species.

### 3.3.3: Evolutionary variations in chicken DNA-dependent PARPs

The evolutionary history of the PARP enzymes in *Gallus gallus* (chickens) was thoroughly investigated through a comparative genomic analysis. We examined the genotypic variation of multiple orthologs, or gene variants, representing various orders of life, including avian, mammals, reptiles, amphibians, and fish. The phylograms, constructed for the chicken PARP1 and PARP3 proteins revealed that they clustered together in a distinct clade, or evolutionary branch, separate from the other PARP orthologs analysed (Figure 3.3 & Figure 3.4).

Interestingly, the amino acid sequence homology, between the chicken PARP1 and PARP3 proteins and their human equivalents was found to be slightly different, at around 75% and 70% respectively (Figure 3.5 & Figure 3.6). This indicates that while these PARP enzymes are evolutionarily conserved across species, there are notable differences in their primary structures.

### chPARP1

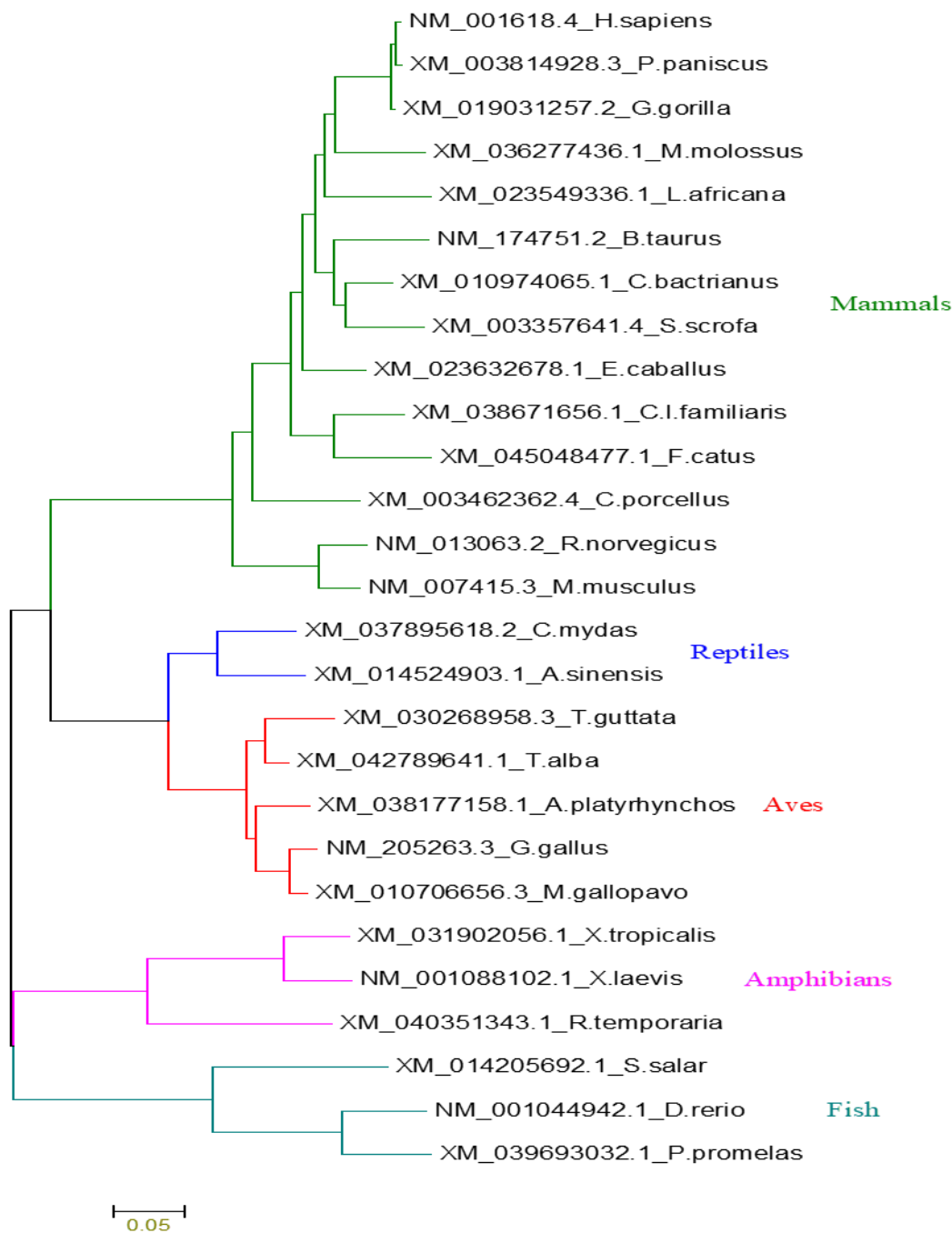


**Figure 3. 3 Phylogenetic Analysis of Chicken PARP1.** Displays the phylogenetic tree of the chicken PARP1 protein, illustrating its evolutionary relationships with orthologous PARP1 sequences from diverse vertebrate species (avian, mammalian, reptilian, amphibian, and fish). The tree highlights the clustering of avian PARP1 within a distinct clade, indicating its evolutionary divergence from other PARP1 orthologs. This tree was generated in MEGA 6 using maximum likelihood method.

### chPARP3

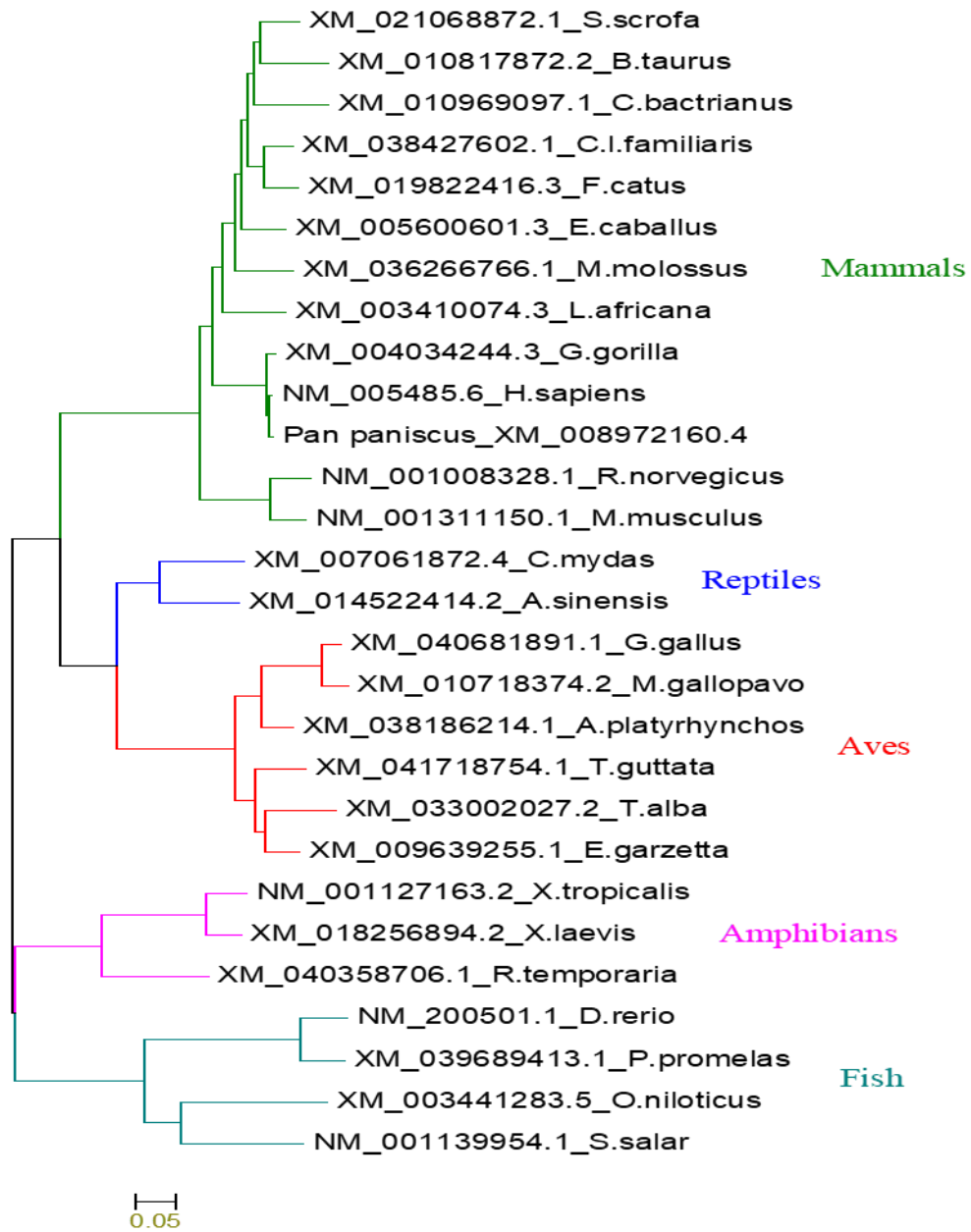


**Figure 3. 4 Phylogenetic Analysis of Chicken PARP3.** Displays the phylogenetic tree of the chicken PARP3 protein, illustrating its evolutionary relationships with orthologous PARP3 sequences from diverse vertebrate species. The tree demonstrates the formation of a distinct evolutionary grouping for avian PARP3. This tree was generated in MEGA6 using maximum likelihood method.

### chPARP1

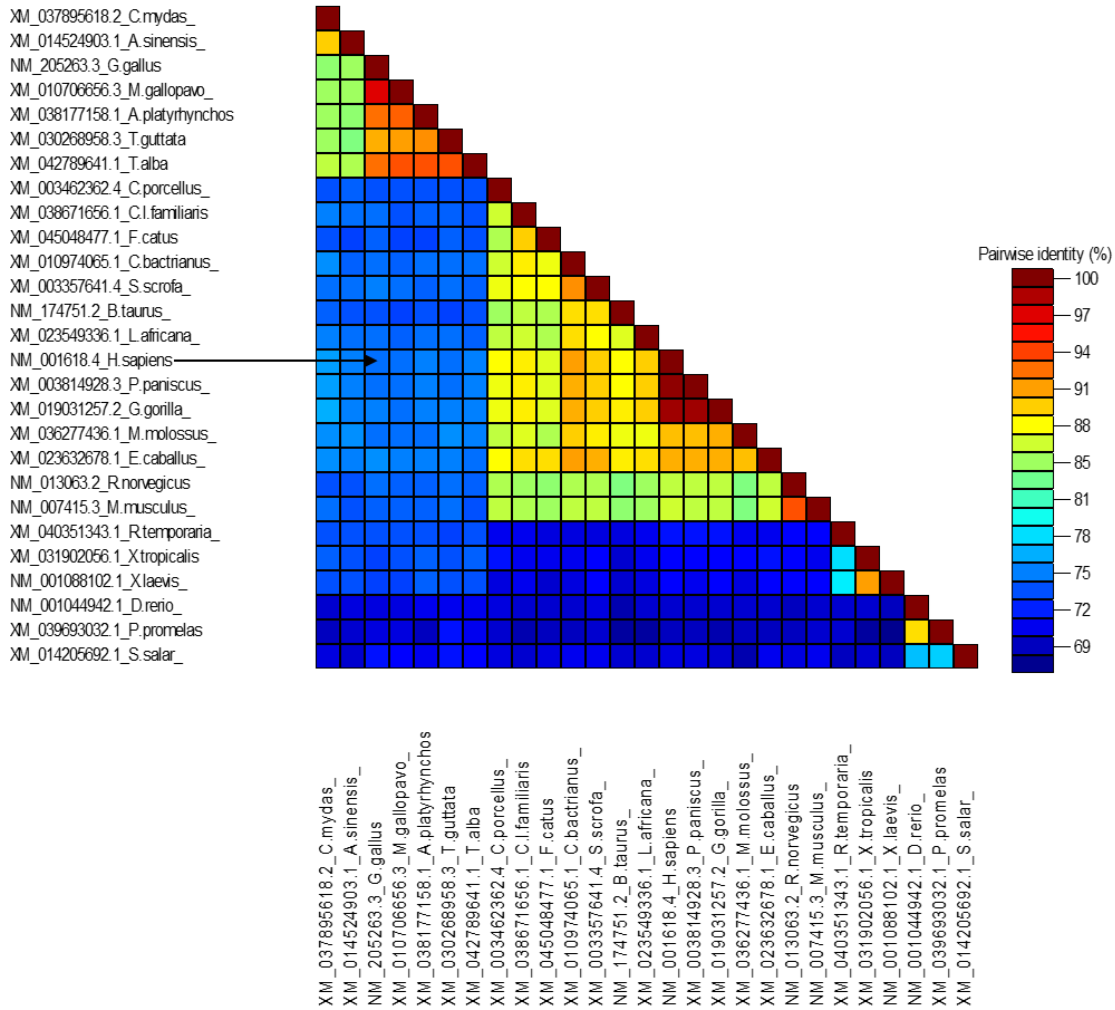


**Figure 3. 5 Amino Acid Sequence Homology of Chicken PARP1 with Human PARP1.** This figure illustrates the amino acid sequence homology between chicken PARP1 and human PARP1, calculated using the Sequence Demarcation Tool (SDT) and the ClustalW algorithm. The analysis reveals approximately 75% sequence identity, indicating significant conservation but also notable differences in primary structure. The color code alongside the figure represents the percentage identity of the amino acid sequence alignment.

### chPARP3

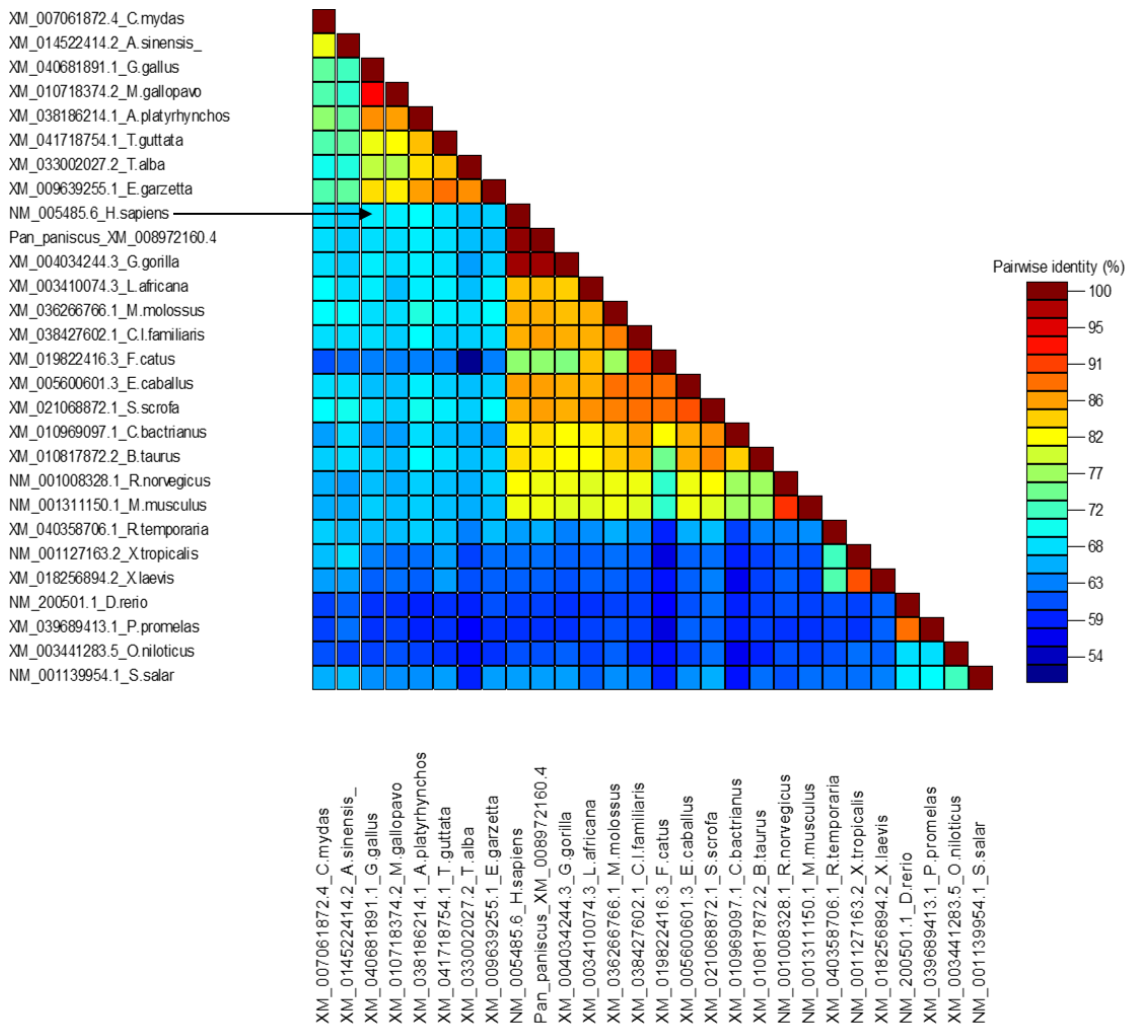


**Figure 3. 6 Amino Acid Sequence Homology of Chicken PARP3 with Human PARP3.** This figure illustrates the amino acid sequence homology between chicken PARP3 and human PARP3, calculated using the SDT and the ClustalW algorithm. The analysis reveals approximately 70% sequence identity, indicating conservation but also highlighting evolutionary divergence in the primary structure. The color code alongside the figure represents the percentage identity of the amino acid sequence alignment.

Further analysis of the predicted three-dimensional (3D) structures of the chicken PARP proteins, including the superimposition of their catalytic domains with their human orthologs (Figure 3.6), and the multiple sequence alignment (MSA) data provided additional insights into the structural variations that have arisen during evolution (Figure 3.7 & Figure 3.8). This revealed that the chicken PARP1 catalytic domain exhibits multiple

point mutations compared to humans, while the chicken PARP3 catalytic domain displays an even more substantial number of amino acid substitutions. These structural differences likely contribute to functional variations in the activities and roles of the PARP enzymes across different vertebrate species.

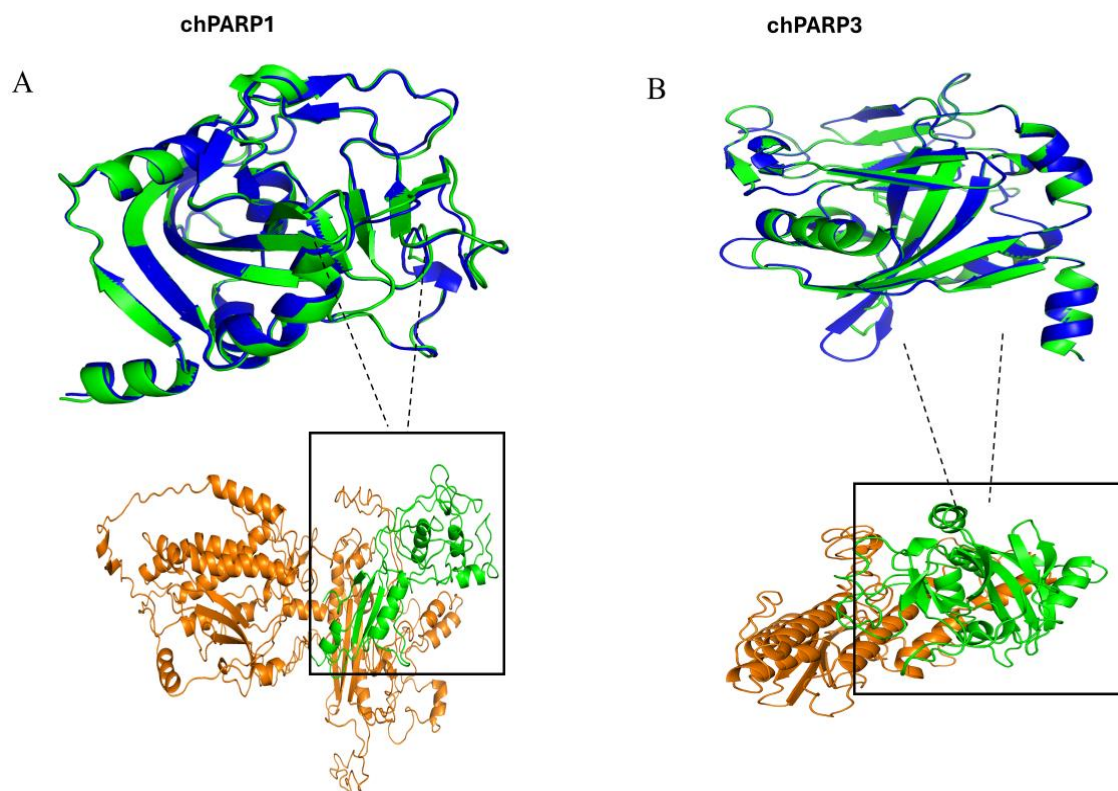
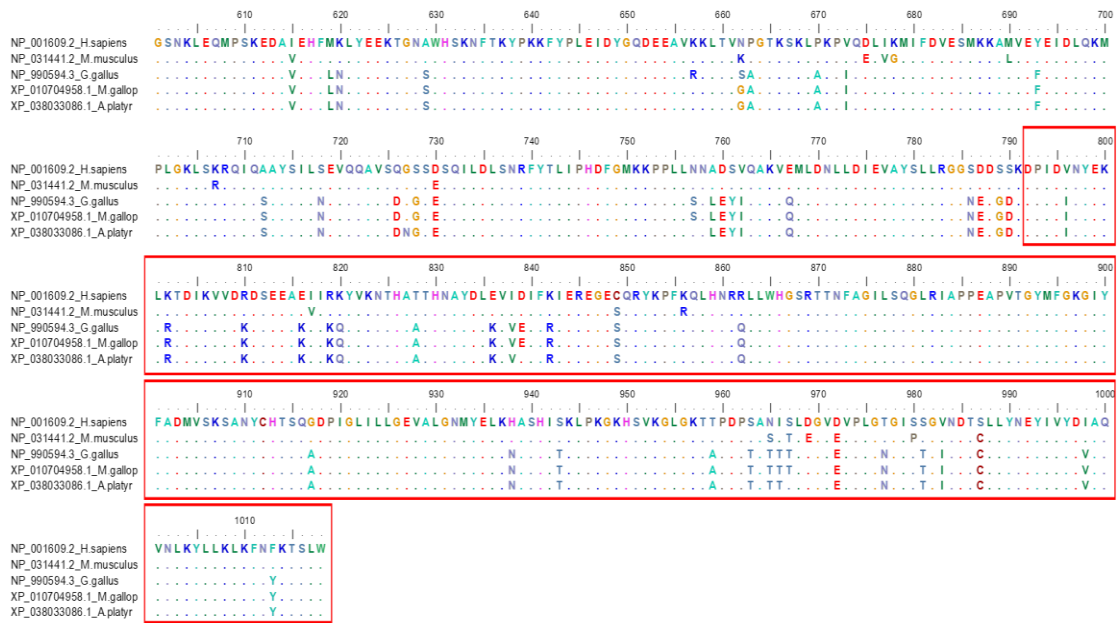


**Figure 3. 7 Structural Analysis of Chicken PARP1.** This figure displays the predicted 3D structure of chPARP1, generated using a combination of *ab initio* (I-TASSER) and deep learning-based (AlphaFold) methods. The overall protein structure is depicted in orange, providing a comprehensive view of its folding pattern. The catalytic domain, crucial for PARP1's enzymatic activity, is highlighted in green, emphasizing its specific structural context within the protein. Additionally, the figure presents a superimposition of the catalytic domains from chicken (green) and human (blue) PARP1.

A

### chPARP1



B

### chPARP3

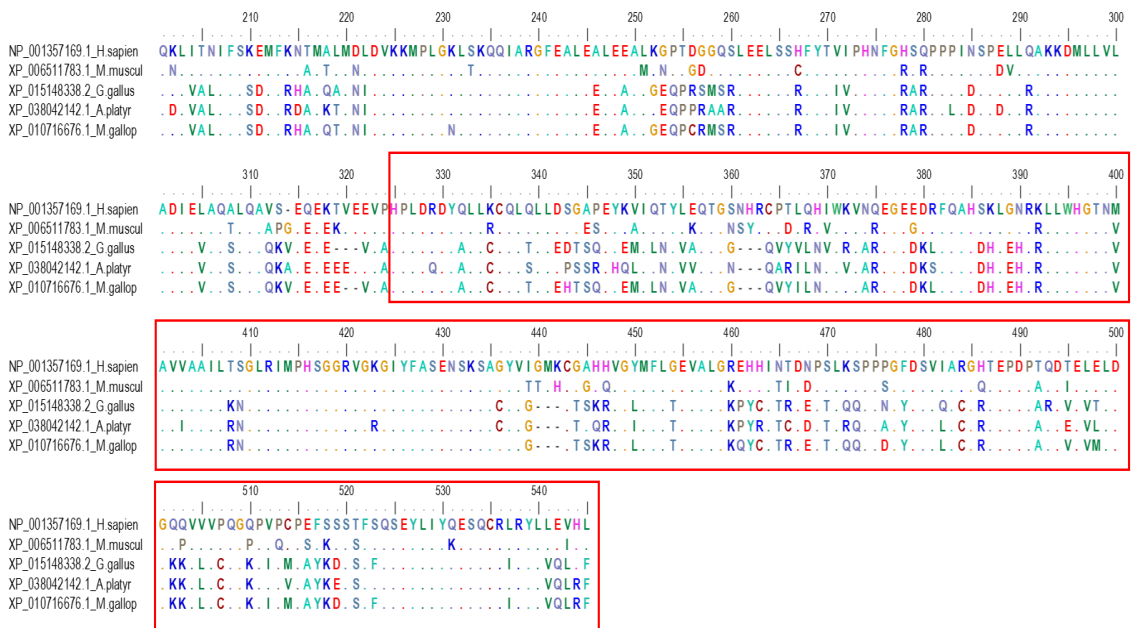


**Figure 3. 8 Multiple Sequence Alignment of chPARP1 and chPARP3 Catalytic Domains.** (A) MSA of PARP1, demonstrating conserved residues across human, mouse, chicken, duck, and turkey. (B) MSA of PARP3, highlighting conserved residues across the same five species. The sequences were aligned using BioEdit software. Identical amino acid residues are indicated by dots. The catalytic domain, crucial for enzymatic activity, is highlighted within a red box. This comparison reveals regions of high conservation, suggesting functional importance, and highlights evolutionary relationships between these PARP family members across diverse avian and mammalian species.

### **3.3.4: Evolutionary Variations in Tankyrases**

The phylogenetic trees, constructed for the chicken PARP5b protein revealed that this particular protein in birds is clustered together in a distinct evolutionary branch, which was separate from the other PARP orthologs that were analysed in the study. This indicates that the avian PARP5b has diverged significantly from the other PARP family orthologs throughout evolutionary history, likely developing unique structural and functional characteristics that set it apart from its counterparts (Figure 3.9).

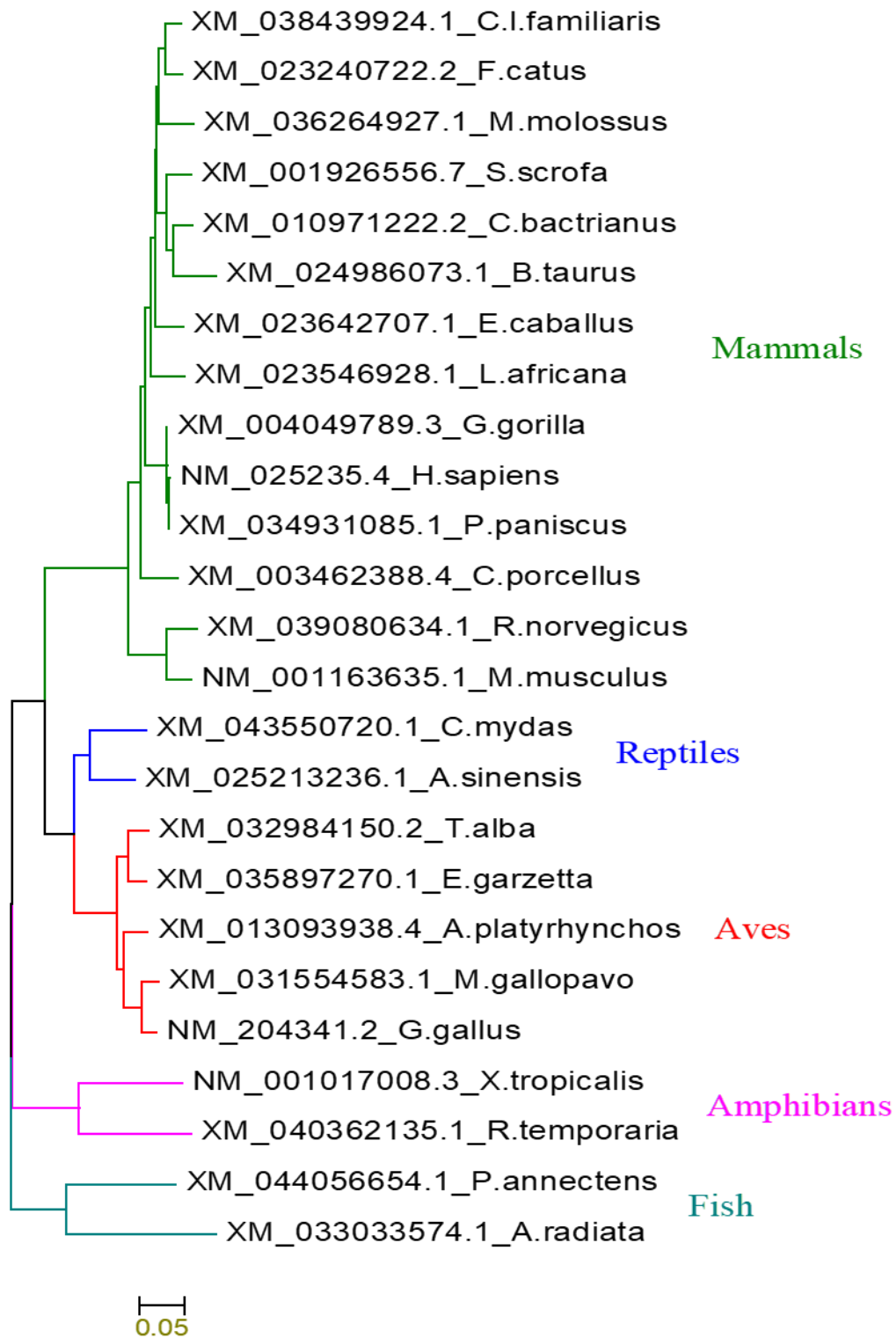


**Figure 3. 9 Phylogenetic Analysis of chPARP5b Orthologs Demonstrating Avian-Specific Evolution.** A maximum likelihood phylogenetic tree, generated using MEGA6, illustrates the evolutionary relationships of chPARP5b with other PARP5b orthologs across diverse species. The tree reveals a distinct clade for avian species, suggesting a unique evolutionary trajectory for PARP5b within the avian lineage. This distinct clustering highlights potential functional adaptations specific to birds. The scale bar represents the number of substitutions per site, reflecting evolutionary distance.

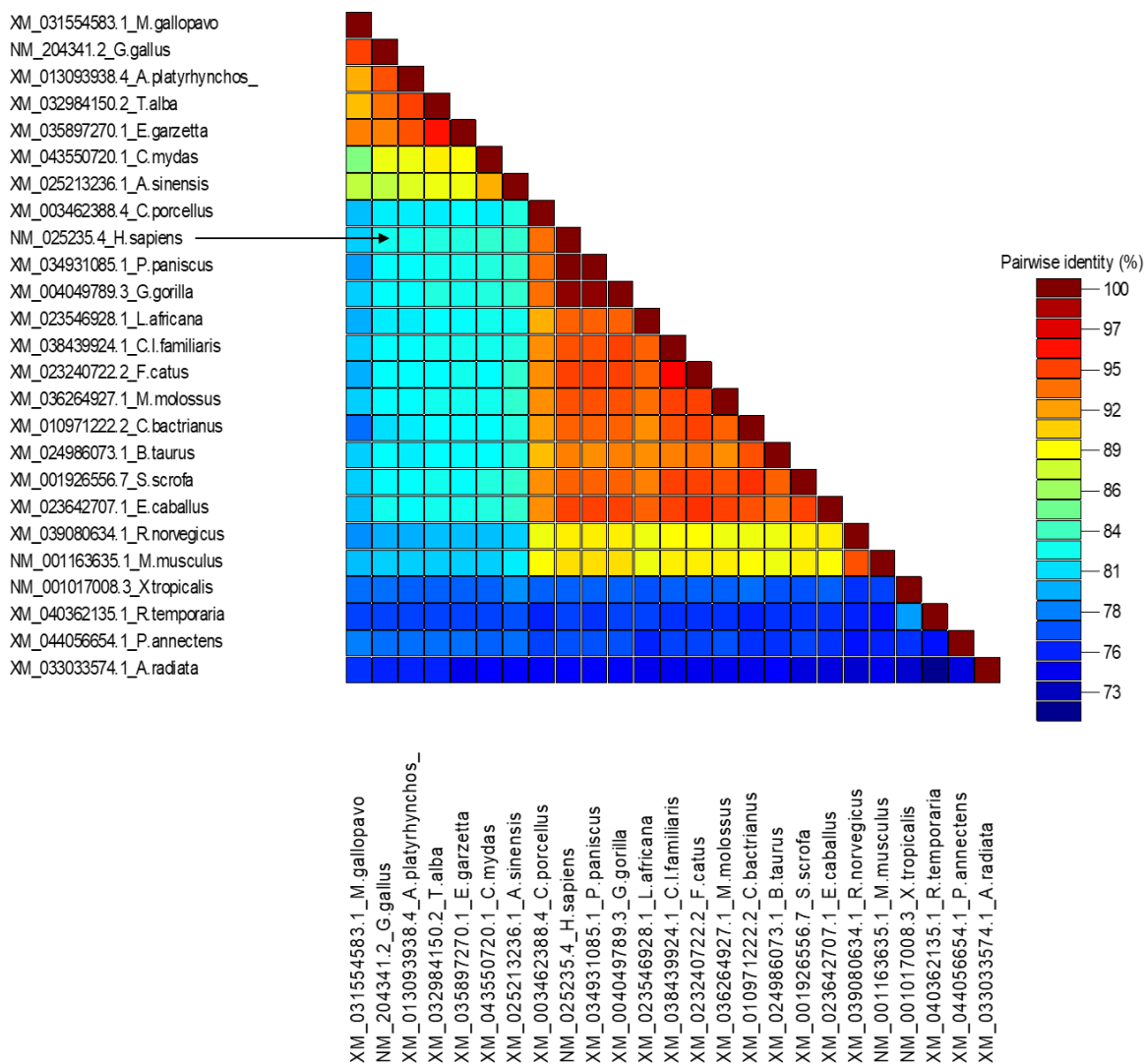


**Figure 3. 10 Amino Acid Sequence Homology Comparison of chPARP5b and Human PARP5b.** A heatmap depicting the amino acid sequence identity between chPARP5b and its human counterpart, generated using the ClustalW algorithm in SDT. The heatmap, accompanied by a color-coded identity scale, demonstrates approximately 82% sequence identity. This high degree of sequence conservation suggests a significant level of structural and, potentially, functional conservation despite evolutionary divergence. The color-coding bar visually represents the percentage of amino acid identity, with darker shades indicating higher similarity.

Further analysis delved into the amino acid sequence homology, or similarity, between the chPARP5b and its human equivalents, and found a high degree of conservation - around 82% sequence identity. This suggests that despite their evolutionary divergence, the chicken and human versions of this enzyme have retained a substantial amount of

structural and functional similarity, implying conserved roles and mechanisms of action across species (Figure 3.10). To gain deeper insight, we also examined the multiple sequence alignment of the catalytic domains and predicted three-dimensional structures of the chPARP5b, including superimposing its catalytic domain onto the structure of the human counterpart (Figure 3.11A). This structural comparison showed that the catalytic domain of the chicken enzyme is highly conserved relative to the human version, with only a small number of point mutations differentiating the two (Figure 3.11B). The high degree of structural conservation in this critical functional region further underscores the evolutionary relatedness and functional similarities between the chicken and human PARP5b proteins, even as the overall sequences have diverged to a moderate degree. Taken together, these phylogenetic, sequence, and structural analyses paint a picture of a chicken enzyme that, while distinct from other PARP family members, has maintained a close evolutionary and functional relationship with its human counterpart.



**Figure 3. 11 Structural Comparison and Multiple Sequence Alignment of Chicken and Human PARP5b Catalytic Domains.** A) This panel illustrates a comparative analysis of the catalytic domains of chPARP5b and its human counterpart. Predicted 3D structures of the full-length proteins are displayed, with the catalytic domains highlighted in green and the remaining protein in orange. The catalytic domains are further emphasized by a black box. 3D structures were predicted using i-Tasser and AlphaFold and visualized and edited using PyMOL. A superimposition of the catalytic domains is shown, with the chicken catalytic domain represented in green and the human catalytic domain in blue. This comparison reveals the structural similarities and subtle differences between the catalytic domains of these orthologous proteins, providing insights into potential functional conservation and divergence. B) This panel presents an MSA of the catalytic domains of PARP5b from human, mouse, chicken, duck, and turkey. The sequences were aligned using BioEdit software. Identical amino acid residues are indicated by dots. The catalytic regions are highlighted within a red box. Notably, the MSA reveals a high degree of conservation within the catalytic domain, with only approximately 10 mutations observed across the five species. This limited variability suggests strong selective pressure to maintain the functional integrity of the catalytic domain throughout evolution.

### 3.3.5: Evolutionary Variations in CCCH containing PARPs

The evolutionary variations in CCCH-containing PARPs provide interesting insights into the phylogenetic relationships between different species. The phylogeny of PARP7, for example, shows a distinct clade formed by avians, implying that this protein evolved uniquely within the bird lineage (Figure 3.12). However, when looking at PARP7 in reptiles, the picture becomes more complicated with two distinct clades - one containing the chinese alligator and the other the green sea turtle. Interestingly, these reptile clades coexist with amphibian and fish clades. PARP7 Amphibians are also divided into two clades, one containing western clawed frogs and the other African clawed frogs that are interspersed with the fish clade indicating a more complex evolutionary history for PARP7 in non-avian vertebrates. When analysing the phylogeny of PARP12, a similar pattern emerges, with avians again divided into two distinct clades: one containing the Turkey and Zebra finch, and the other containing the Chicken, Duck, and Western barn owl. Notably, these avian clades are separated by reptile and fish clades, emphasising the complexity of these vertebrate groups' evolutionary relationships. The fish lineage is also

divided into two clades: Northern pike and Atlantic salmon, and Zebrafish and Nile tilapia, with amphibians, avians, and reptiles in between (Figure 3.13). The phylogeny of PARP13, on the other hand, shows a clear separation between the avian clade and the other species, implying a more distinct evolutionary trajectory for this enzyme within the bird lineage. The amphibians included in this study did not have the PARP13 sequence (Figure 3.14). This pattern emphasises the complex and dynamic nature of CCCH-containing PARP evolution, in which different enzymes can show varying degrees of divergence and specialisation across the vertebrate tree of life.

## chPARP7

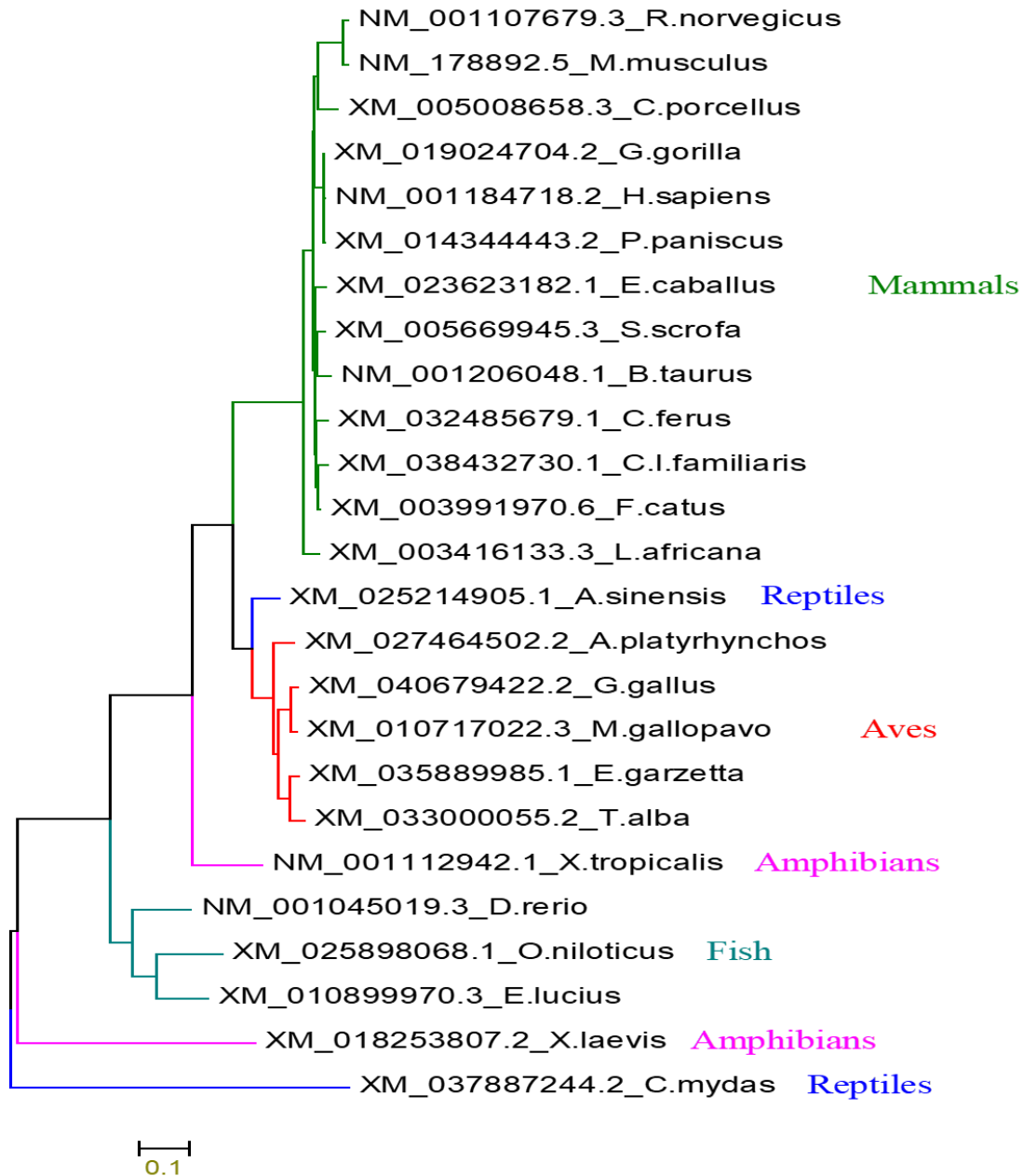


**Figure 3. 12 Phylogenetic Analysis of PARP7 Orthologs Reveals Complex Evolutionary History.** This figure illustrates the evolutionary relationships of PARP7 across various vertebrate species. The phylogenetic tree reveals a distinct clade formed by avian species, suggesting a unique evolutionary trajectory for PARP7 within the bird lineage. However, the evolutionary landscape of PARP7 in reptiles is more intricate, with two distinct clades observed, one encompassing the Chinese alligator and the other the green sea turtle. Notably, these reptile clades are interspersed with clades from amphibians and fish, indicating a complex evolutionary history for PARP7 in non-avian vertebrates. Furthermore, amphibian PARP7 orthologs are also divided into two clades, one including western clawed frogs and the other African clawed frogs, which are positioned within the fish clade. This intricate pattern highlights the dynamic and varied evolutionary paths of PARP7 across different vertebrate groups.

## chPARP12

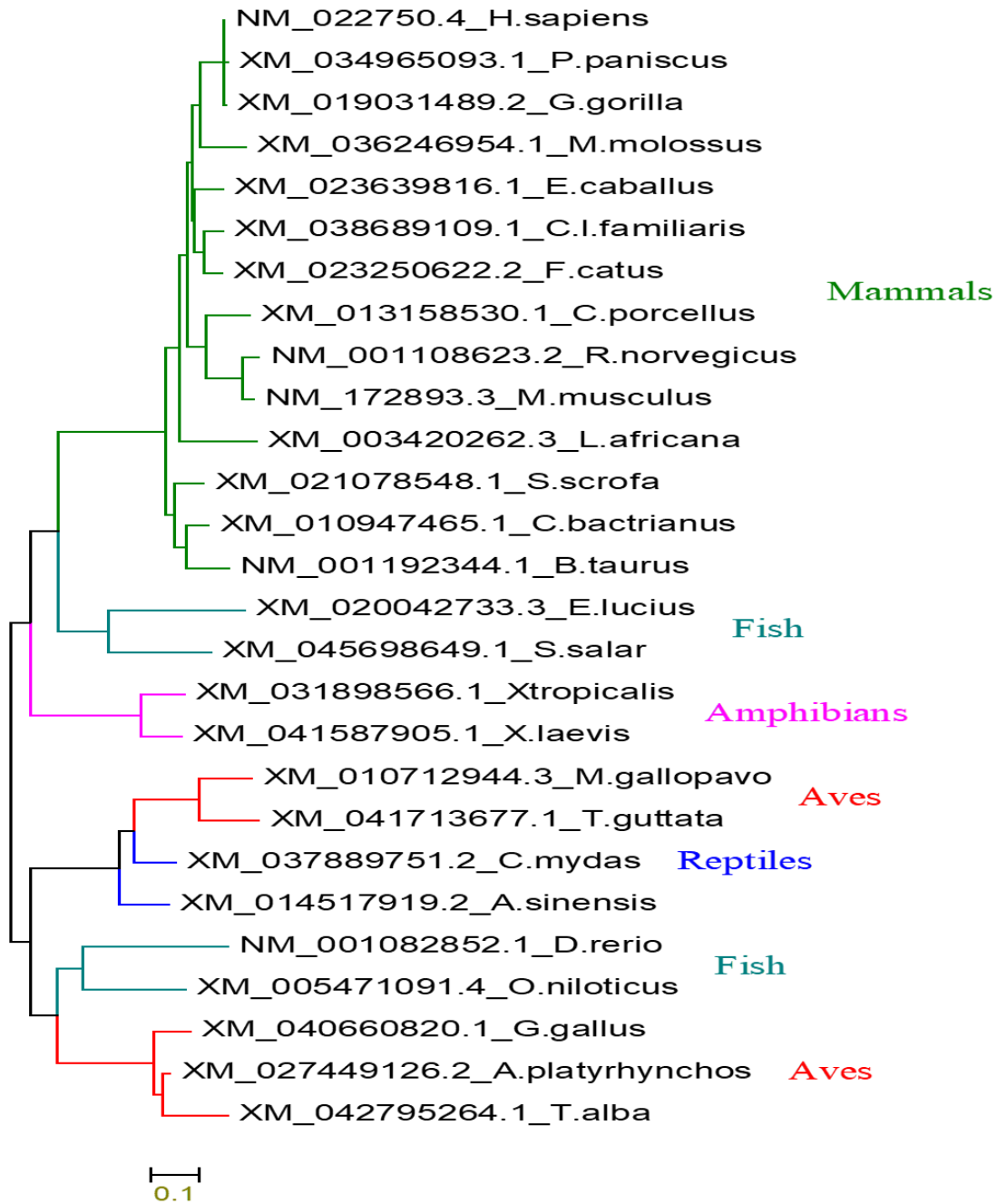


**Figure 3. 13 Phylogenetic Analysis of PARP12 Orthologs Demonstrates Complex Avian and Vertebrate Relationships.** This figure presents the evolutionary relationships of PARP12 across a range of vertebrate species. The avian lineage for PARP12 is divided into two distinct clades: one comprising the Turkey and Zebra finch, and the other including the Chicken, Duck, and Western barn owl. Notably, these avian clades are separated by clades from reptiles and fish, underscoring the complex evolutionary relationships within these vertebrate groups. The fish lineage is also further divided into two clades: one containing Northern pike and Atlantic salmon, and the other comprising Zebrafish and Nile tilapia, with amphibians, avians, and reptiles interspersed between these fish clades. This complex pattern emphasizes the diverse and intricate evolutionary history of PARP12 across the vertebrate tree of life.

## chPARP13

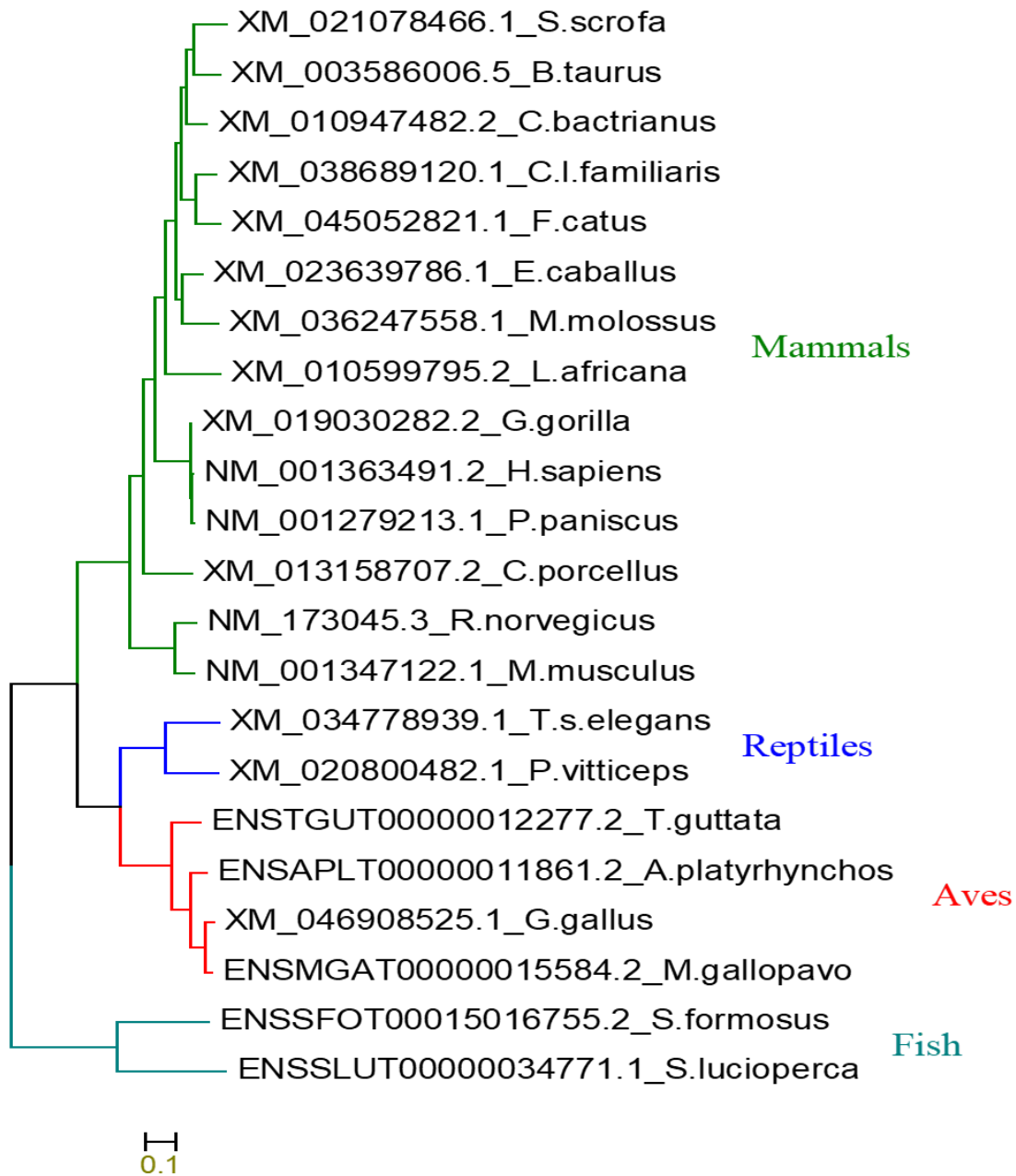


**Figure 3. 14 Phylogenetic Analysis of PARP13 Orthologs Highlights Distinct Avian Evolution.** This figure depicts the evolutionary relationships of PARP13 across various vertebrate species. The phylogenetic analysis of PARP13 reveals a clear separation between the avian clade and the other species included in the study. This distinct clustering suggests a more specific and potentially more recent evolutionary trajectory for PARP13 within the bird lineage. It is important to note that the amphibian species included in this study did not possess a detectable PARP13 sequence.

Further, the amino acid sequence homology of the chicken and human versions of PARP7, PARP12, and PARP13 was investigated. chPARP7 has approximately 72% sequence identity with its human counterpart, whereas chPARP12 and chPARP13 have approximately 62% and 65% sequence identity with their human counterparts, respectively (Figure 3.15, 3.16 & 3.17).

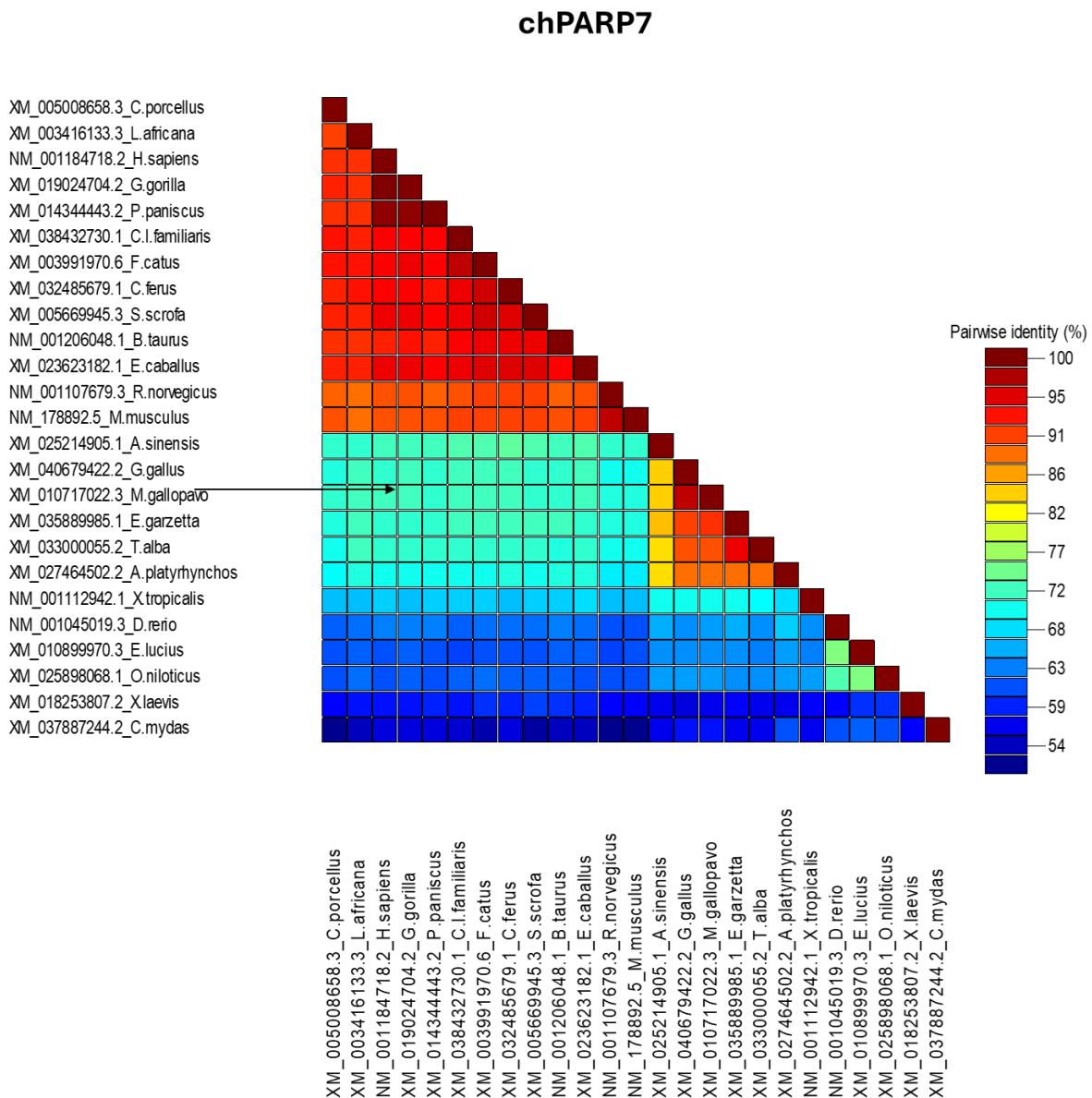


**Figure 3. 15 Sequence Homology Analysis of chPARP7.** A heatmap depicting the amino acid sequence identity between chPARP7 and its human counterpart. The heatmap, generated using the ClustalW algorithm in SDT, reveals approximately 72% sequence identity, as indicated by the color-coded identity scale. This level of conservation suggests a significant degree of structural and functional similarity between the chicken and human PARP7 proteins, despite their evolutionary divergence.

## chPARP12

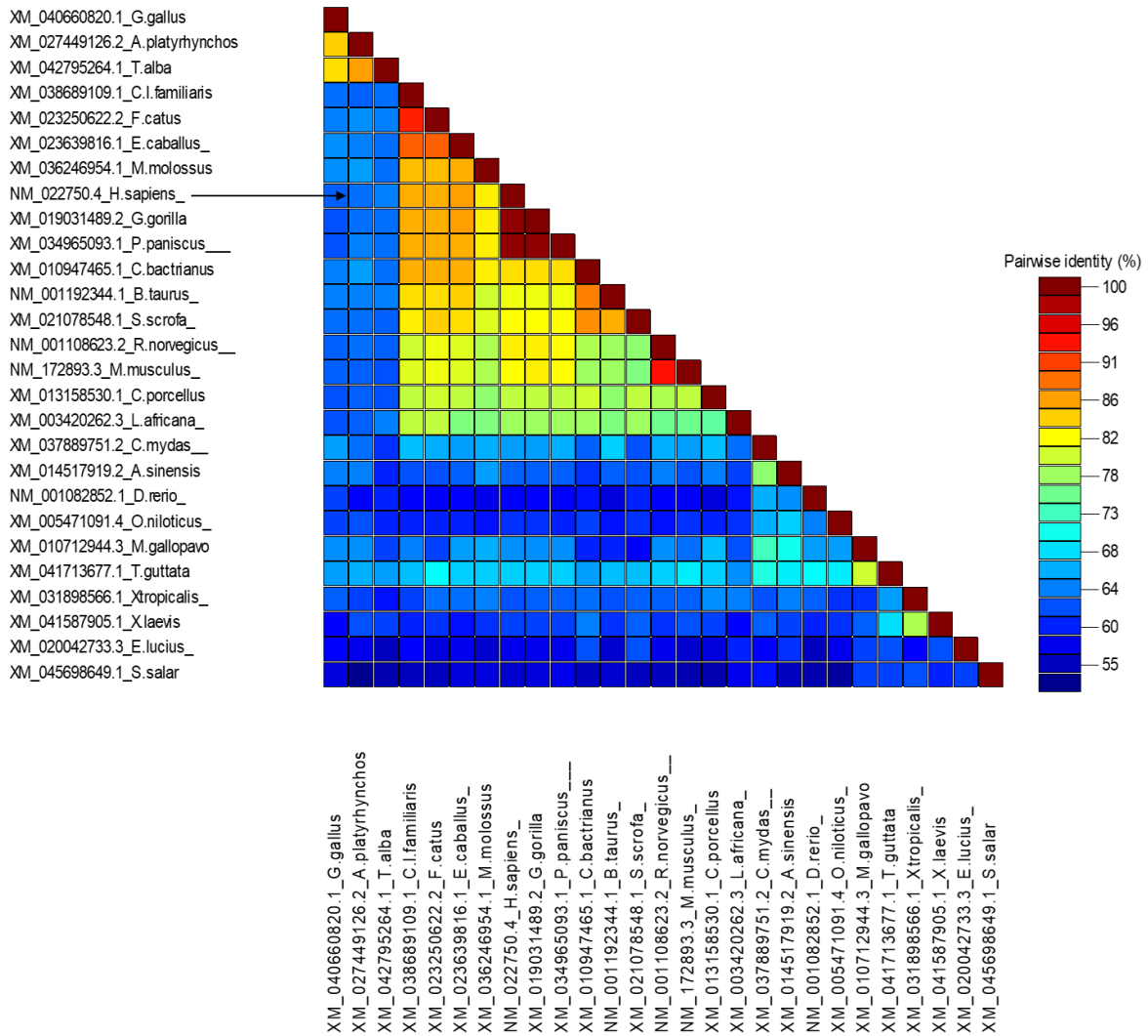


**Figure 3. 16 Sequence Homology Analysis of PARP12.** Heatmap illustrating the amino acid sequence identity between chPARP12 and human PARP12. The analysis, performed using the ClustalW algorithm in SDT, indicates approximately 62% sequence identity, as reflected by the color-coding bar. This level of sequence conservation suggests that while there has been evolutionary divergence, key structural and functional elements of PARP12 are maintained between these species.

### chPARP13

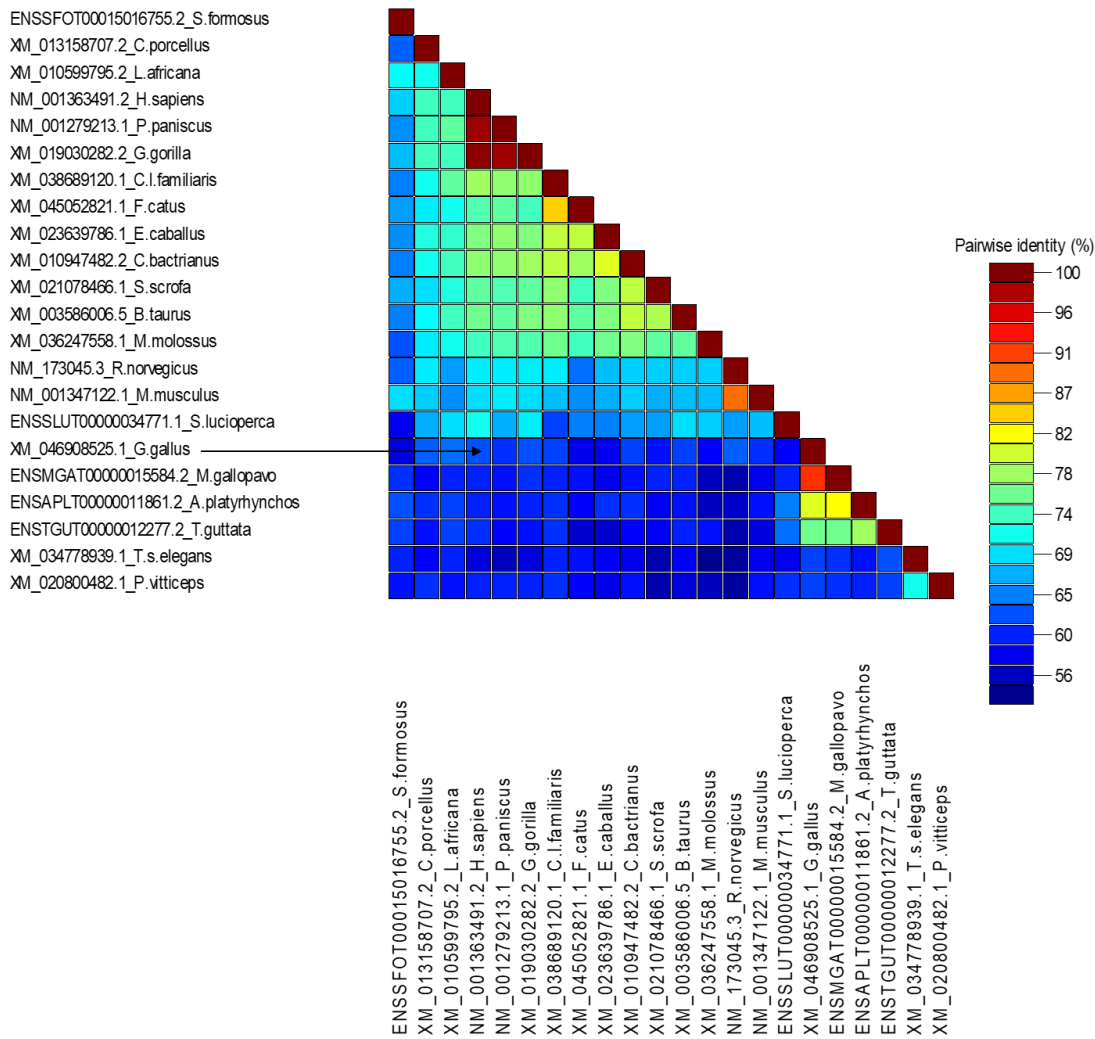


**Figure 3. 17 Sequence Homology Analysis of PARP13.** Heatmap displaying the amino acid sequence identity between chPARP13 and its human counterpart. The sequence alignment, performed using the ClustalW algorithm in SDT, reveals approximately 65% sequence identity, as indicated by the color-coded identity scale. This level of conservation suggests a moderate degree of structural and functional similarity between the chicken and human PARP13 proteins, consistent with their distinct evolutionary trajectory within the avian lineage.

Multiple sequence alignments were conducted for PARP7, PARP12, and PARP13 in chicken, turkey, duck, human and mouse (Figure 3.18). These analyses revealed that among the CCCH-containing PARPs, the catalytic domain of chPARP7 is highly conserved relative to the human version, with only a small number of point mutations differentiating the two. chPARP12 has the second highest conservation of the catalytic domain, with two-thirds of its structure conserved compared to the human protein. In contrast, the catalytic domain of chPARP13 is not as well conserved as the other two chicken PARPs. Additionally, structural comparisons were performed, including superimposing the catalytic domains of the chPARPs onto the structures of their human counterparts (Figure 3.19). These structural findings corroborated the sequence alignments, further highlighting the high degree of conservation in the catalytic domains of chPARP7 and chPARP12 compared to their human counterparts, while chPARP13 exhibited a lower level of sequence conservation.

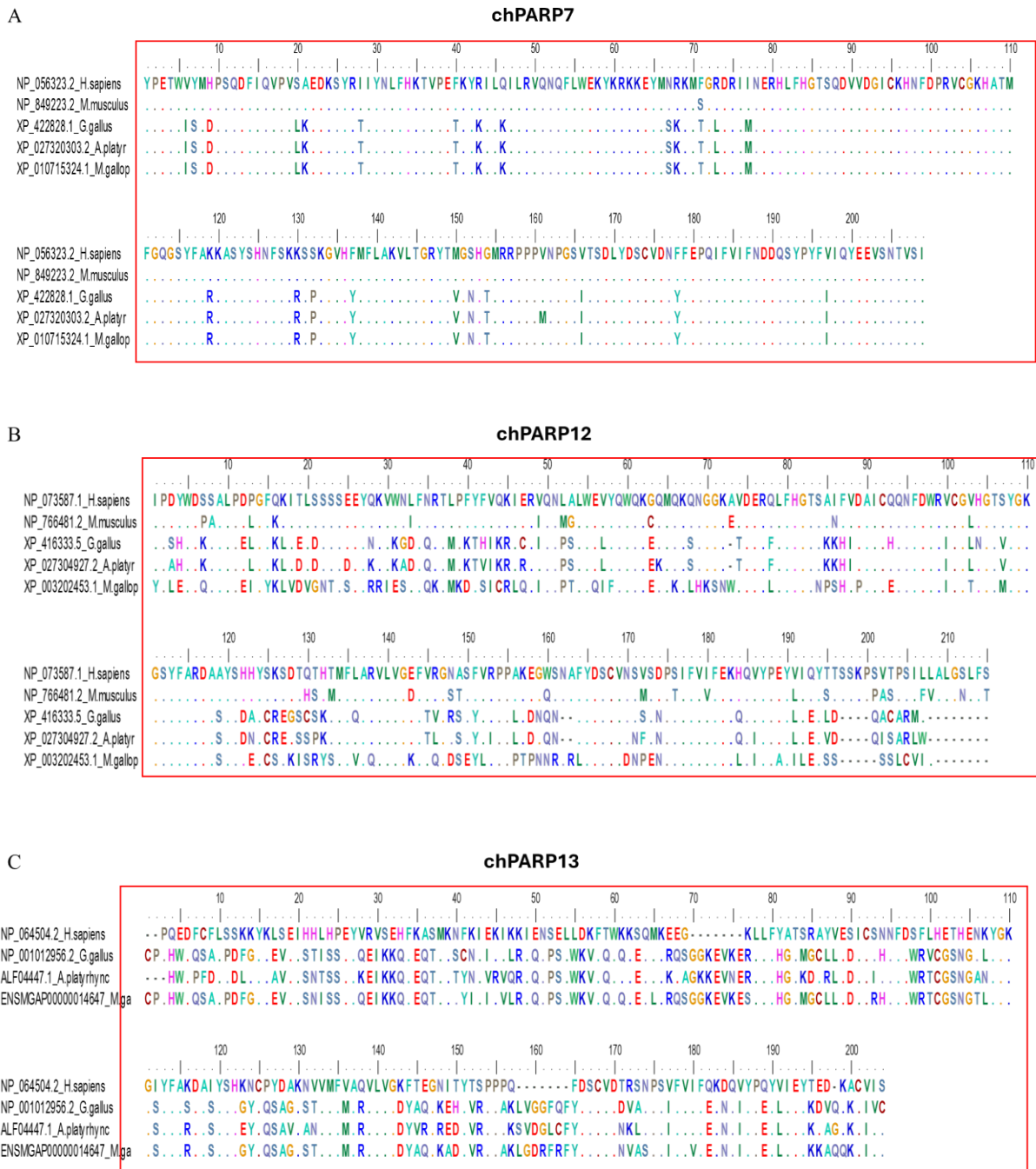


**Figure 3. 18 Multiple Sequence Alignment of PARP7, PARP12 & PARP13 Catalytic Domains.** A) The catalytic domain of chPARP7 exhibits a high degree of conservation compared to its human counterpart, with only a small number of point mutations observed. B) The catalytic domain of chPARP12 shows the second-highest level of conservation, with approximately two-thirds of its structure conserved relative to the human protein. C) The catalytic domain of chPARP13 demonstrates a lower degree of conservation compared to the other two chicken PARPs analysed. MSAs were generated for PARP7, PARP12, and PARP13 proteins from chicken, turkey, duck, human, and mouse. The alignments were performed using BioEdit software. Identical amino acid residues across the aligned sequences are indicated by dots. The catalytic domains of each protein are highlighted within red boxes.

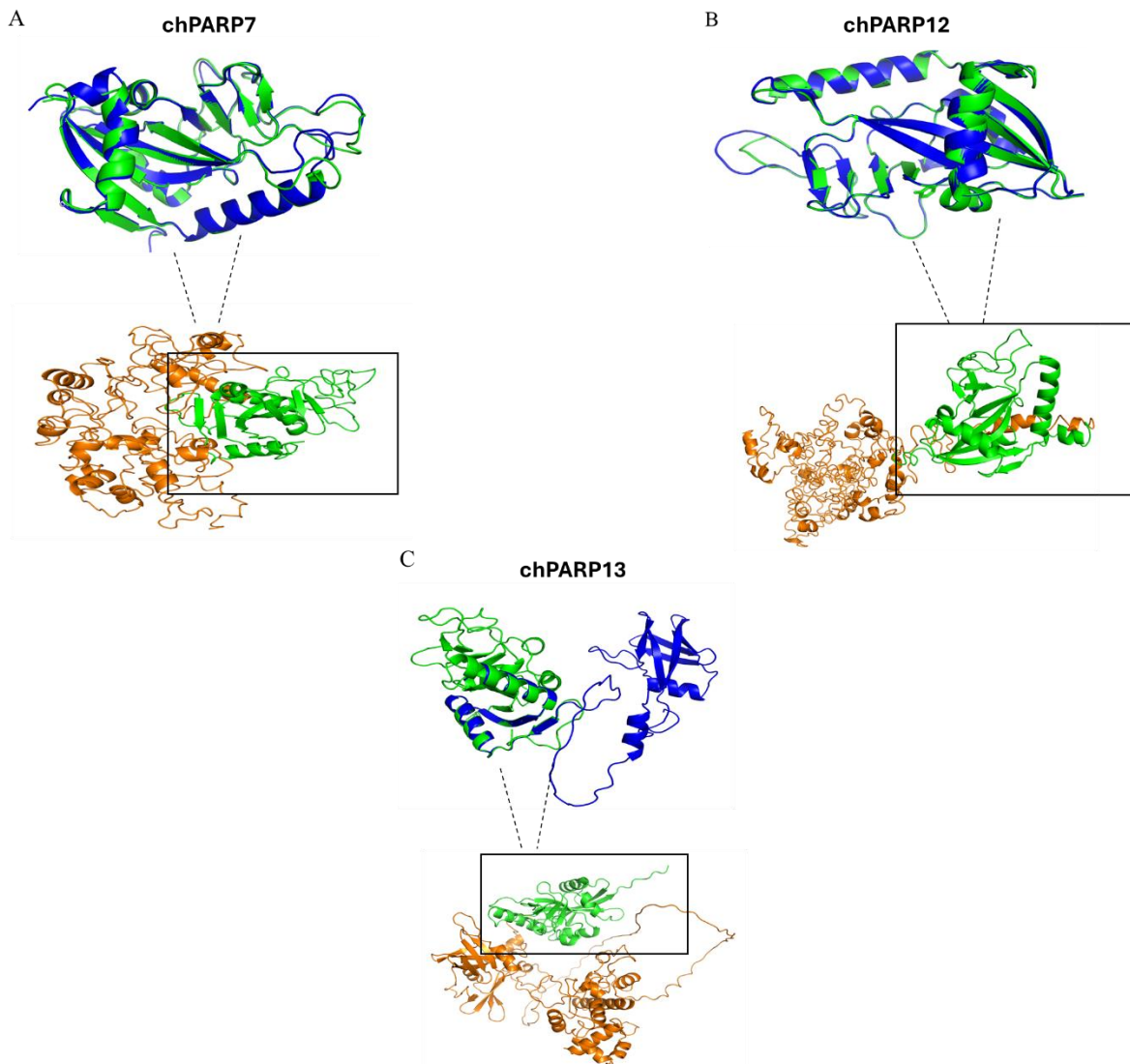


**Figure 3. 19 Structural Comparison of Chicken and Human CCCH-Containing PARPs.** This figure presents a comparison of the catalytic domains of chPARP7, chPARP12, and chPARP13 with their human counterparts. Predicted 3D structures of the full-length proteins are displayed, with the catalytic domains highlighted in green and the remaining protein in orange. The catalytic domains are further emphasized by a black box. 3D structures were predicted using i-Tasser and AlphaFold and visualized and edited using PyMOL. A superimposition of the catalytic domains is shown, with the chicken catalytic domain represented in green and the human catalytic domain in blue. This comparison reveals the structural similarities and subtle differences between the catalytic domains of these orthologous proteins.

### **3.3.6: Evolutionary Variations in Macro PARPs**

The phylogenetic tree analysis reveals distinct evolutionary relationships for the PARP9 and PARP14 proteins across different vertebrate groups. The avian PARP9 protein forms a distinct clade when comparing its sequence to mammals, amphibians, reptiles, and fish (Figure 3.20). In contrast, the avian PARP14 protein shows a more complex pattern, forming three separate clades - one with chicken, another with zebra finch, turkey, and western barn owl, and a third clade interspersed with amphibians, fish, and reptiles (Figure 3.21). The reptile lineage also exhibits two distinct PARP14 clades, one with Schlegel's Japanese gecko and another with the green sea turtle, interspersed with avian species like turkey, zebra finch and western barn owl.

## chPARP9

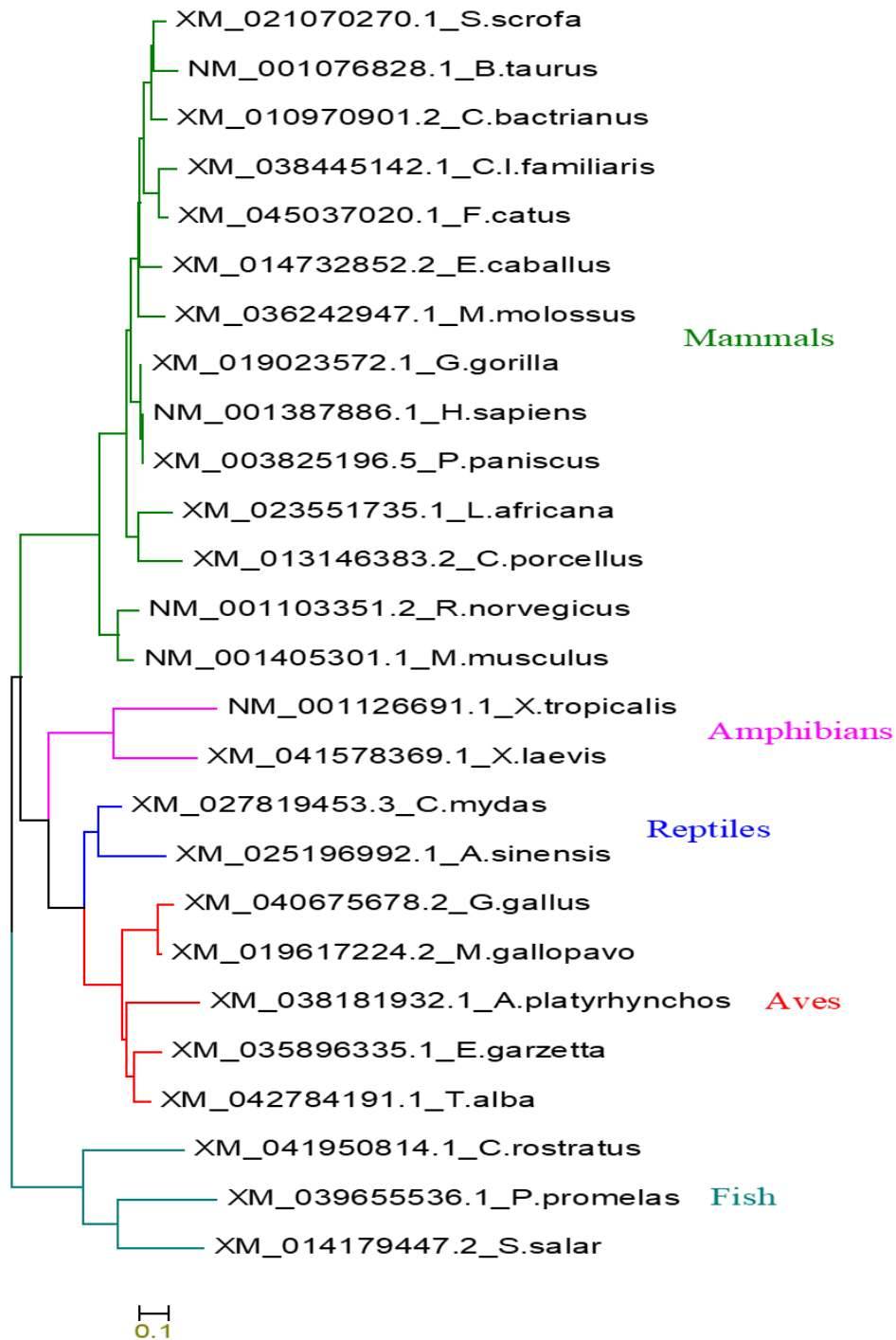


**Figure 3. 20 Phylogenetic Analysis of PARP9.** This figure illustrates the evolutionary relationships of PARP9 across various vertebrate species, including mammals, amphibians, reptiles, and fish, with a specific focus on the avian lineage. The phylogenetic tree reveals a distinct clade formed by avian species, suggesting a unique evolutionary trajectory for PARP9 within the bird lineage. The tree was constructed using maximum likelihood method in MEGA6.

## chPARP14

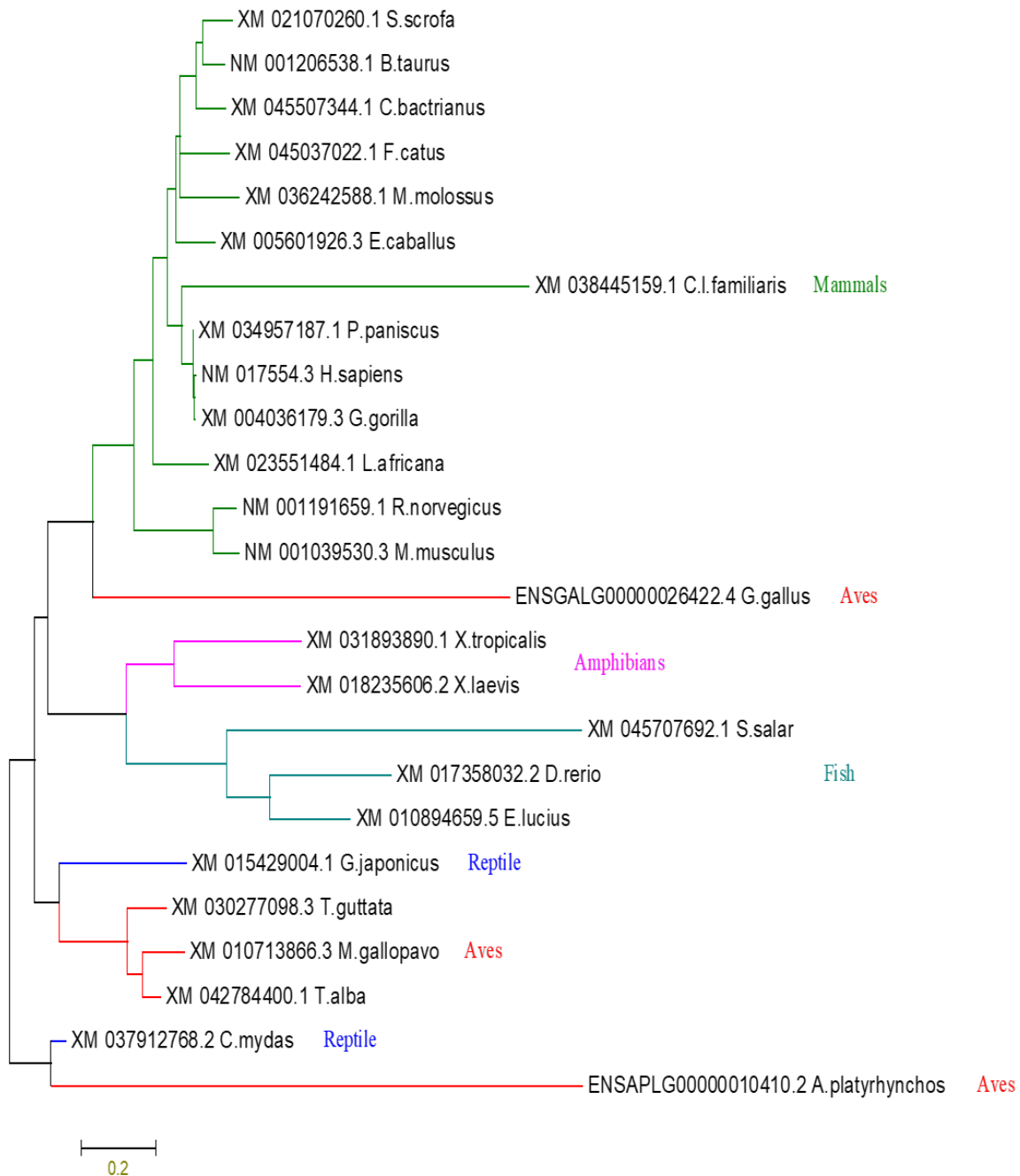


**Figure 3. 21 Phylogenetic Analysis of PARP14.** This figure presents the evolutionary relationships of PARP14 across a range of vertebrate species. The avian lineage for PARP14 is divided into three clades: one comprising the turkey, western barn owl and zebra finch, and the other including the chicken, and the last one comprising duck. Notably, these avian clades are separated by clades from reptiles, amphibians and fish, underscoring the complex evolutionary relationships within these vertebrate groups. The reptile lineage is also further divided into two clades: one containing green sea turtle, and the other comprising schlegel's japanese gecko, with avians interspersed between them. This complex pattern emphasizes the diverse and intricate evolutionary history of PARP14 across the vertebrate tree of life.

Sequence analysis indicates that PARP9 shares approximately 60% amino acid identity with its human counterpart (Figure 3.22), while PARP14 shows around 50% identity (Figure 3.23).

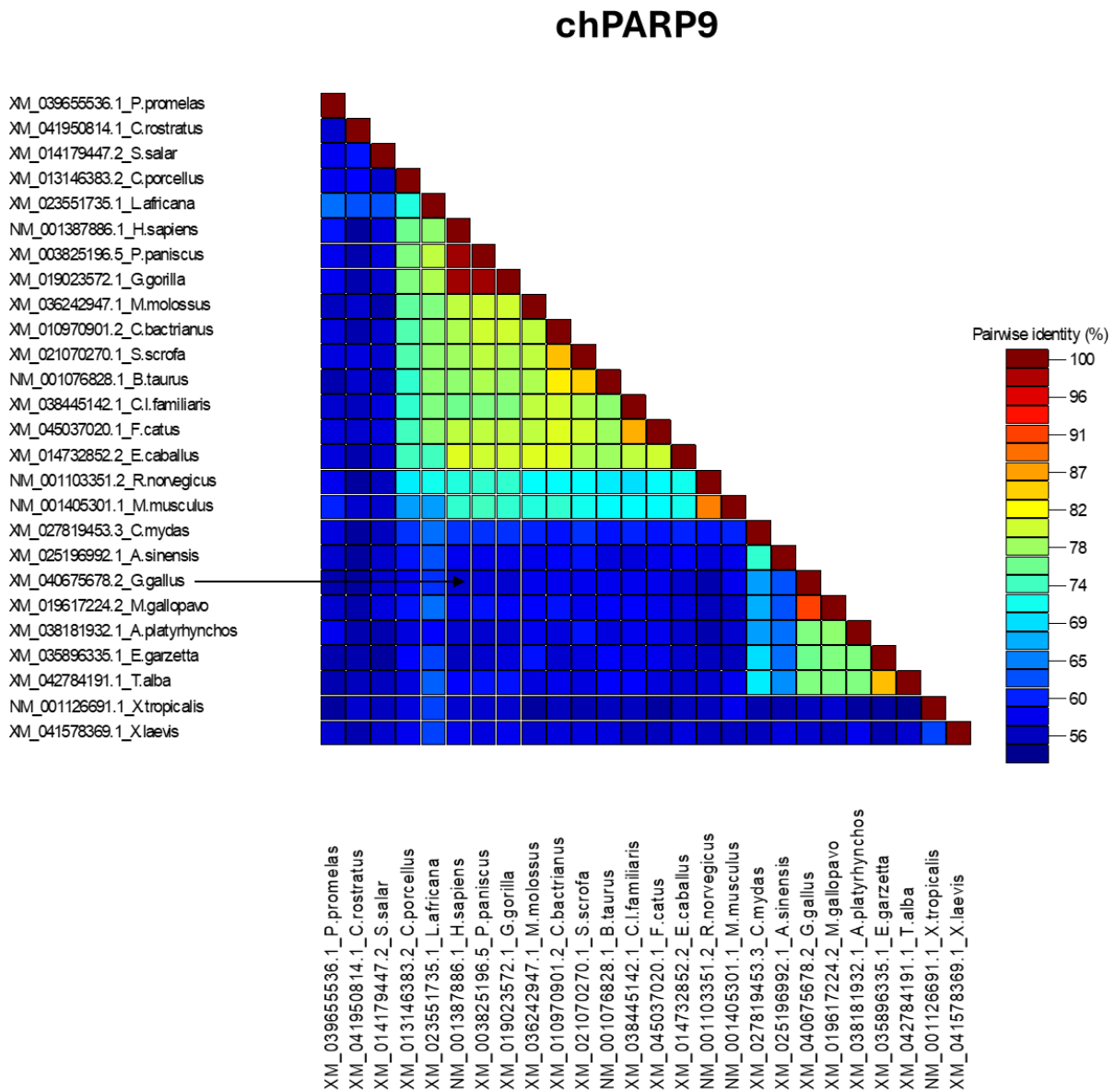


**Figure 3. 22 Amino Acid Sequence Homology of Chicken and Human PARP9.** Heatmap displaying the amino acid sequence identity between chPARP9 and its human counterpart. The sequence alignment, performed using the ClustalW algorithm in SDT, reveals approximately 60% sequence identity, as indicated by the color-coded identity scale. This level of conservation suggests a moderate degree of structural and

functional similarity between the chicken and human PARP9 proteins, consistent with their distinct evolutionary trajectory within the avian lineage.

## chPARP14

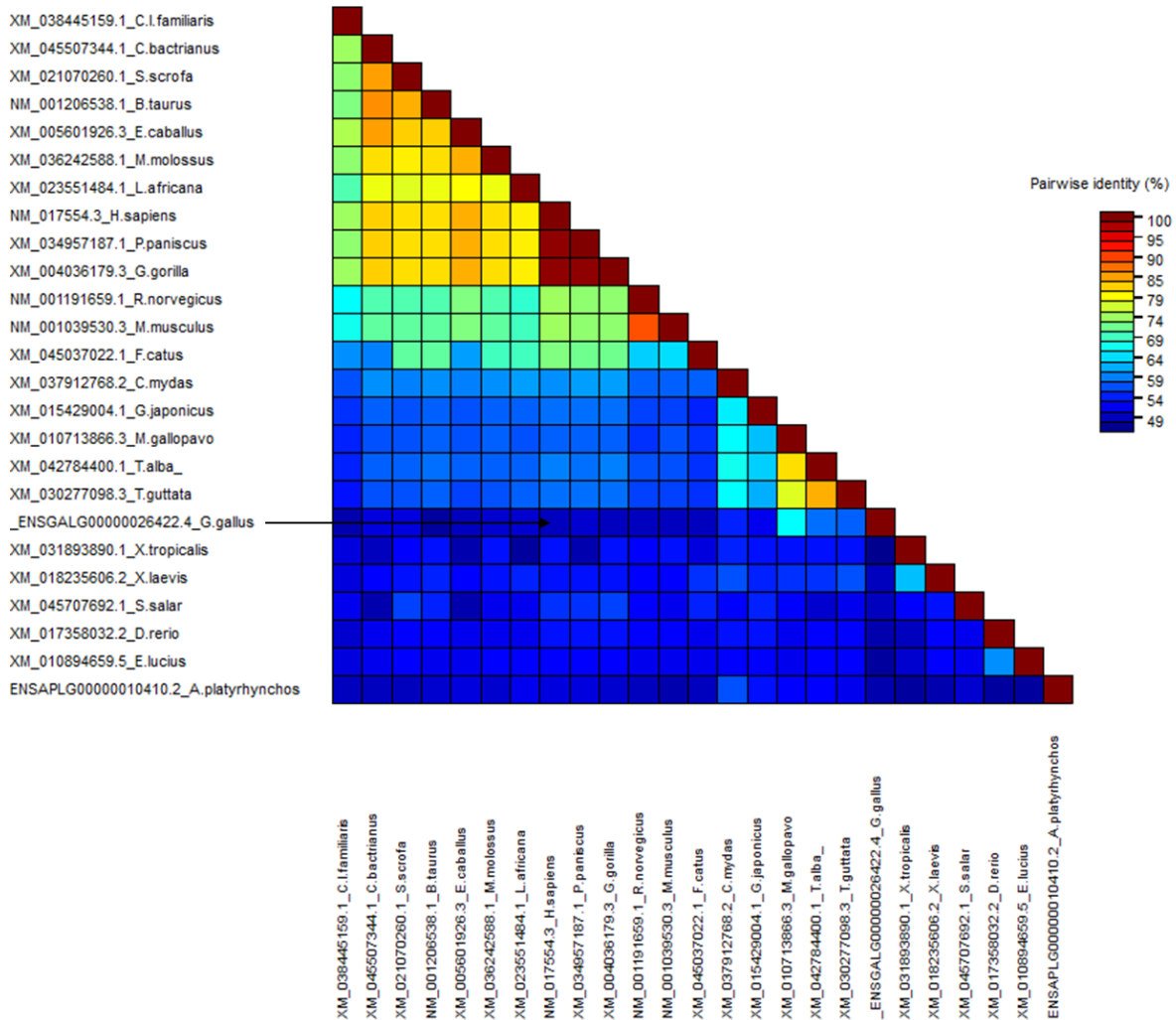


**Figure 3. 23 Amino Acid Sequence Homology of Chicken and Human PARP14.** Heatmap displaying the amino acid sequence identity between chPARP14 and its human counterpart. The sequence alignment, performed using the ClustalW algorithm in SDT, reveals approximately 50% sequence identity, as indicated by the color-coded identity scale. This level of conservation suggests a low degree of structural and functional similarity between the chicken and human PARP14 proteins, consistent with their distinct evolutionary trajectory within the avian lineage.

Further, multiple sequence alignment and 3D structural comparisons of the catalytic domains reveal that nearly half of this region is conserved between the vertebrate and human versions of these two PARP proteins (Figure 3.24 & Figure 3.25).

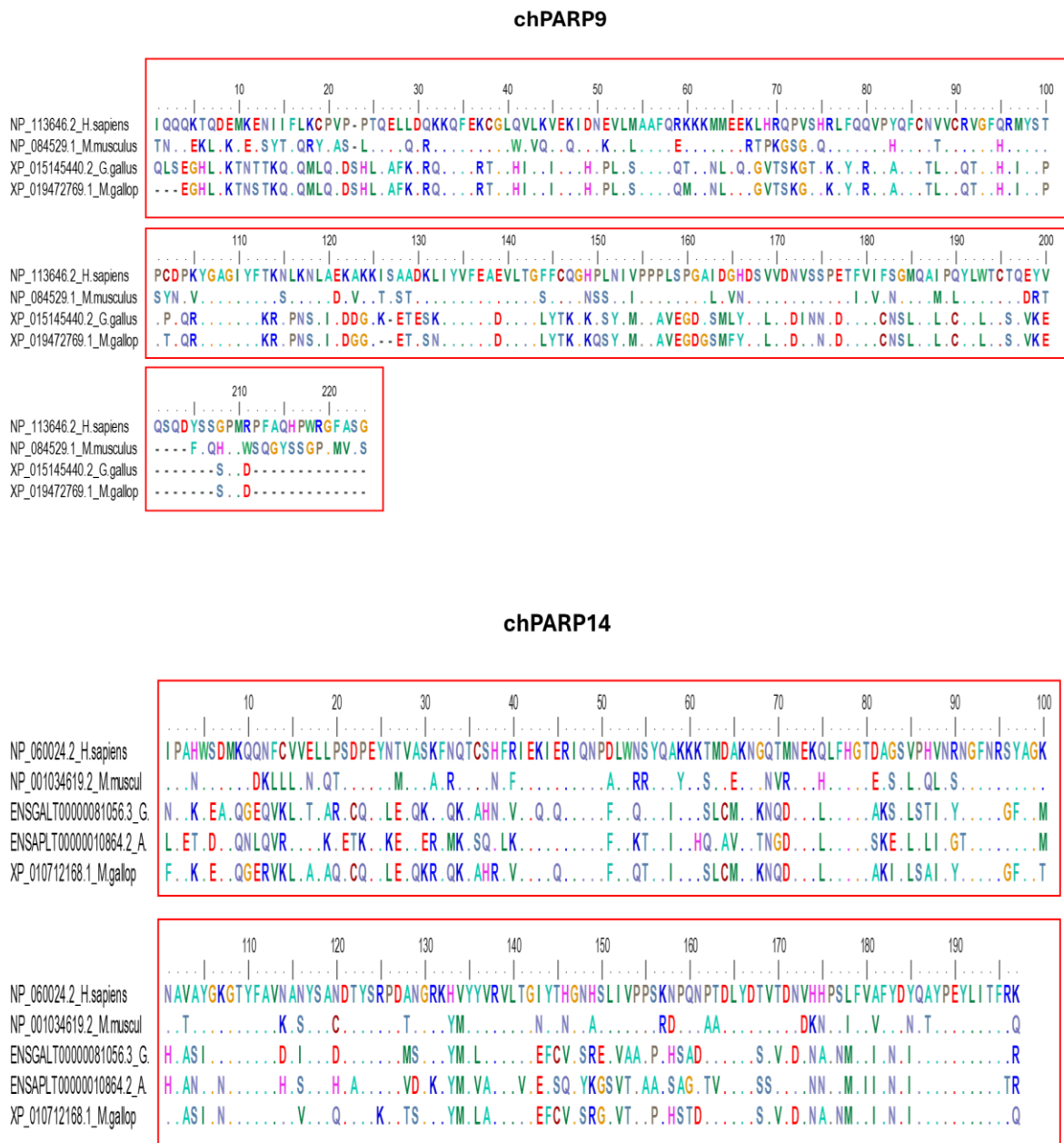


**Figure 3. 24 Multiple Sequence Alignment of PARP9 and PARP14 Catalytic Domains.** A) The catalytic domain of chPARP9 exhibits moderate degree of conservation compared to its human counterpart. B) The catalytic domain of chPARP14 shows the lowest level of conservation, with only half of its structure conserved relative to the human protein. MSAs were generated for PARP9, PARP14 proteins from chicken, turkey, duck, human, and mouse. The alignments were performed using BioEdit software. Identical amino acid residues across the aligned sequences are indicated by dots. The catalytic domains of each protein are highlighted within red boxes.

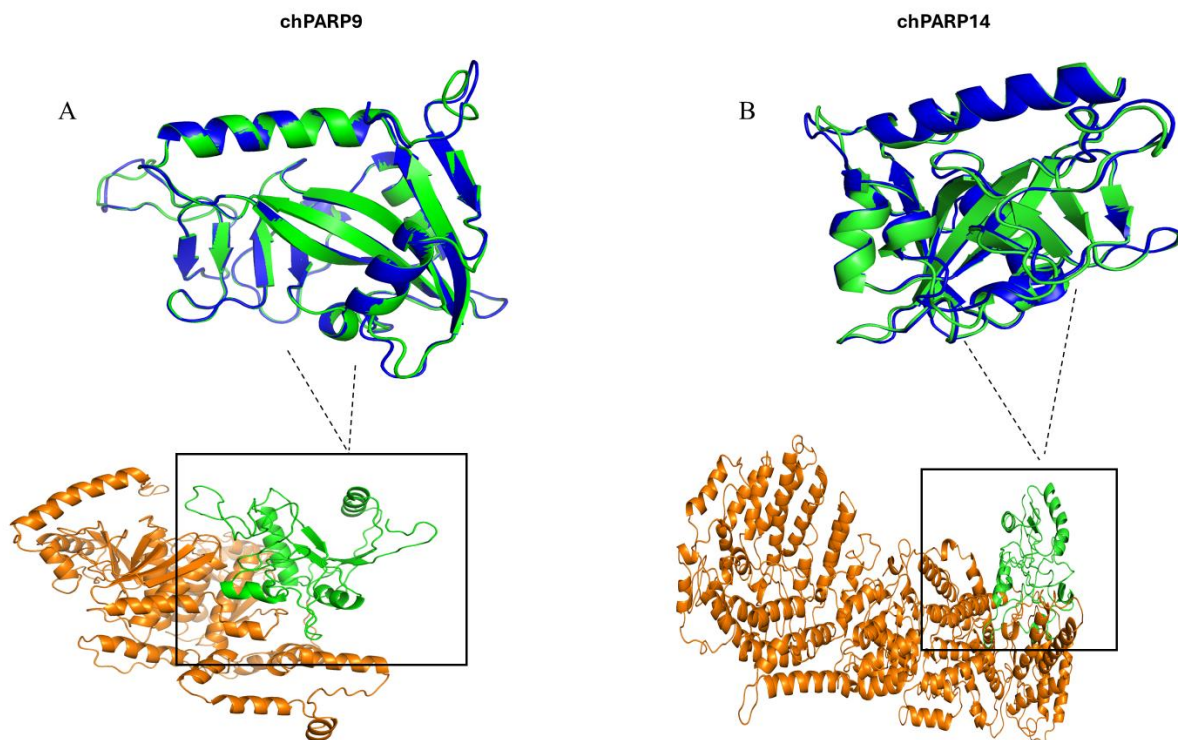


**Figure 3.25 Structural Comparison of PARP9 and PARP14 Catalytic Domains.** This panel illustrates a comparative analysis of the catalytic domains of chPARP9 and PARP14 and their human counterparts. Predicted 3D structures of the full-length proteins are displayed, with the catalytic domains highlighted in green and the remaining protein in orange. The catalytic domains are further emphasized by a black box. 3D structures were predicted using i-Tasser and AlphaFold and visualized and edited using PyMOL. A superimposition of the catalytic domains is shown, with the chicken catalytic domain represented in green and the human catalytic domain in blue.

### 3.3.7: Evolutionary Variations in chPARP4

The phylogenetic analysis of chPARP4, a vault protein in the PARP family, shows a distinct clade formation for the avian species (Figure 3.26). When the amino acid sequences were compared with several other species, chPARP4 exhibited around 62% identity with its human counterpart (Figure 3.27). Further, a multiple sequence alignment of the catalytic domain was performed with counterparts from four other species, including duck, turkey,

human, and mouse (Figure 3.28). Additionally, an alignment of the chicken and human catalytic domains was performed (Figure 3.29). The multiple sequence alignment, coupled with the predicted 3D structure of the catalytic domain, reveals that more than half (nearly two-thirds) of the chPARP4 catalytic domain is conserved in chickens compared to the human counterpart.

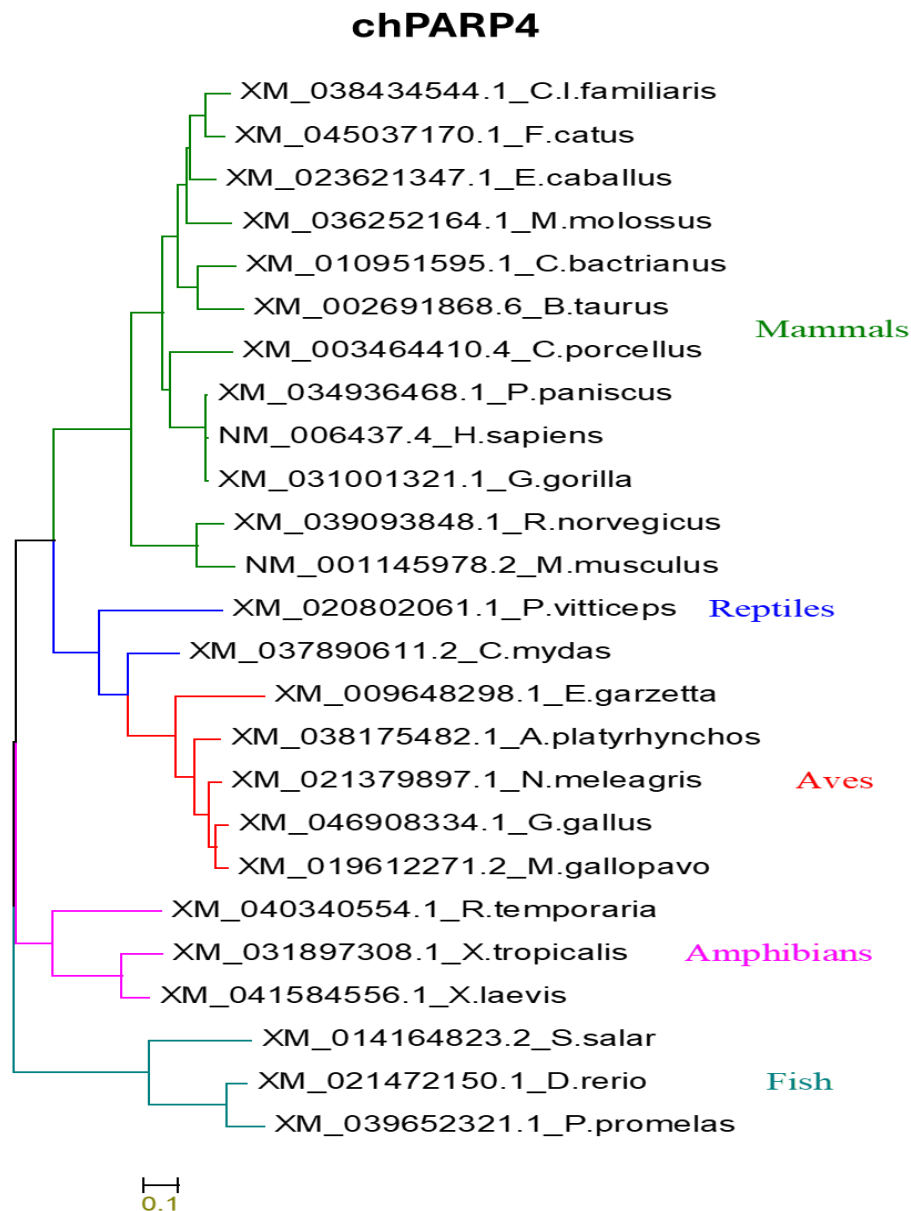


**Figure 3. 26 Phylogenetic and Sequence Analysis of PARP4.** This figure illustrates the evolutionary relationships of PARP4 across various vertebrate species, including mammals, amphibians, reptiles, and fish, with a specific focus on the avian lineage. The phylogenetic tree reveals a distinct clade formed by avian species, suggesting a unique evolutionary trajectory for PARP4 within the bird lineage. The tree was constructed using maximum likelihood method in MEGA6.

### chPARP4

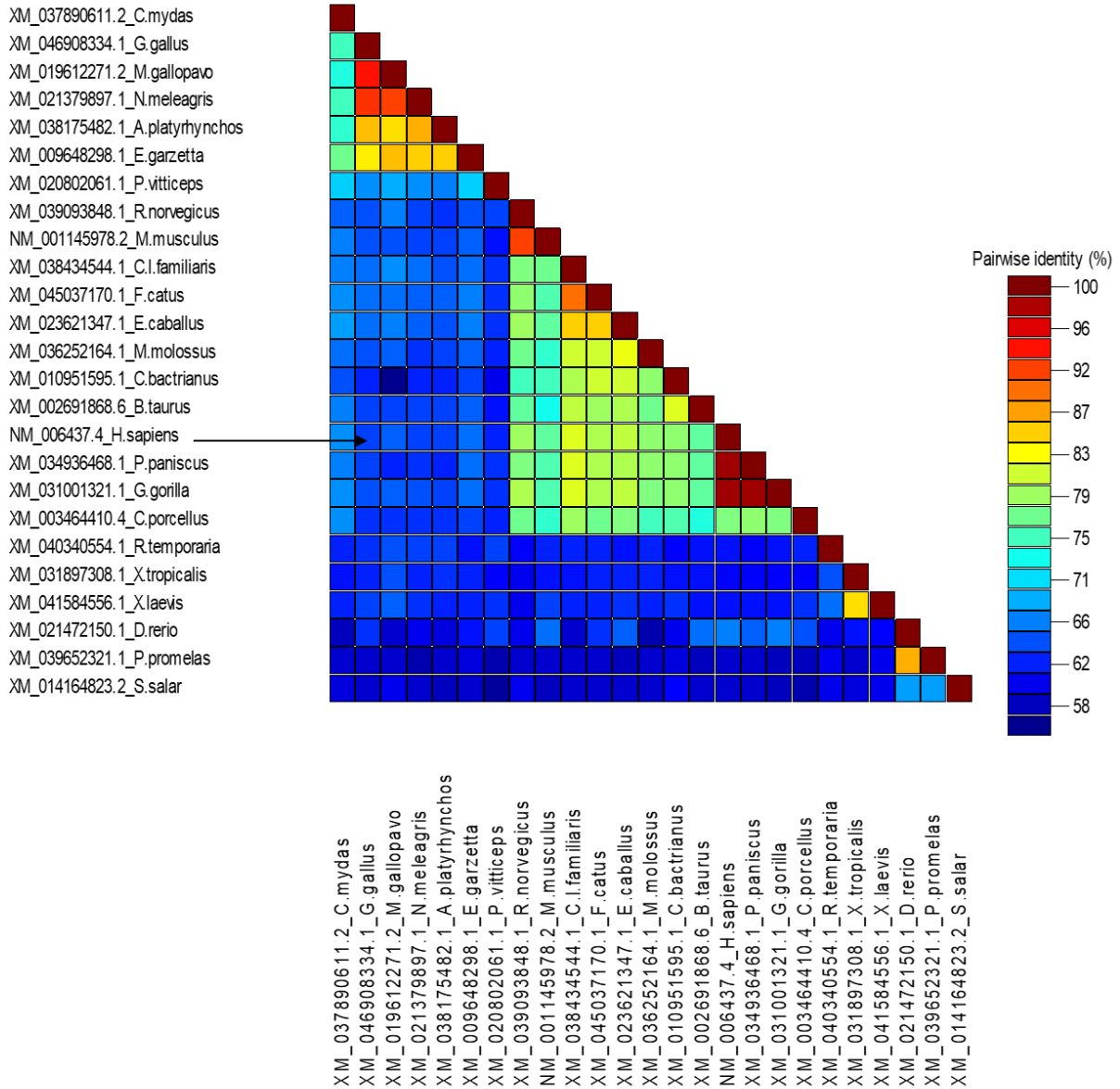


**Figure 3. 27 Sequence Homology of PARP4.** Heatmap displaying the amino acid sequence identity between chPARP4 and its human counterpart. The sequence alignment, performed using the ClustalW algorithm in SDT, reveals approximately 62% sequence identity, as indicated by the color-coded identity scale. This level of conservation suggests a moderate degree of structural and functional similarity between the chicken and human PARP4 proteins.

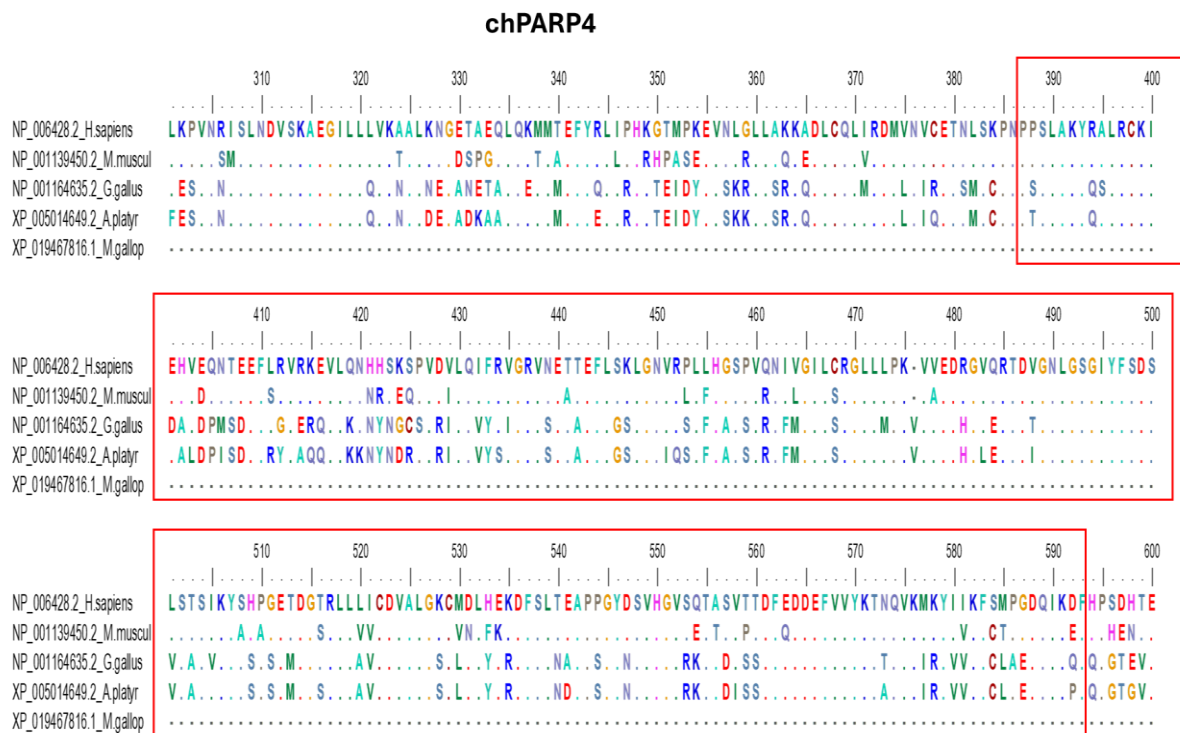


**Figure 3. 4 Multiple Sequence Alignment of chPARP4 Catalytic Domain.** The catalytic domain of chPARP4 exhibits a high degree of conservation with its human counterpart, with only a small number of point mutations observed. MSA was generated for chicken, turkey, duck, human, and mouse. The alignments were performed using BioEdit software. Identical amino acid residues across the aligned sequences are indicated by dots. The catalytic domains of each protein are highlighted within red boxes.

## chPARP4

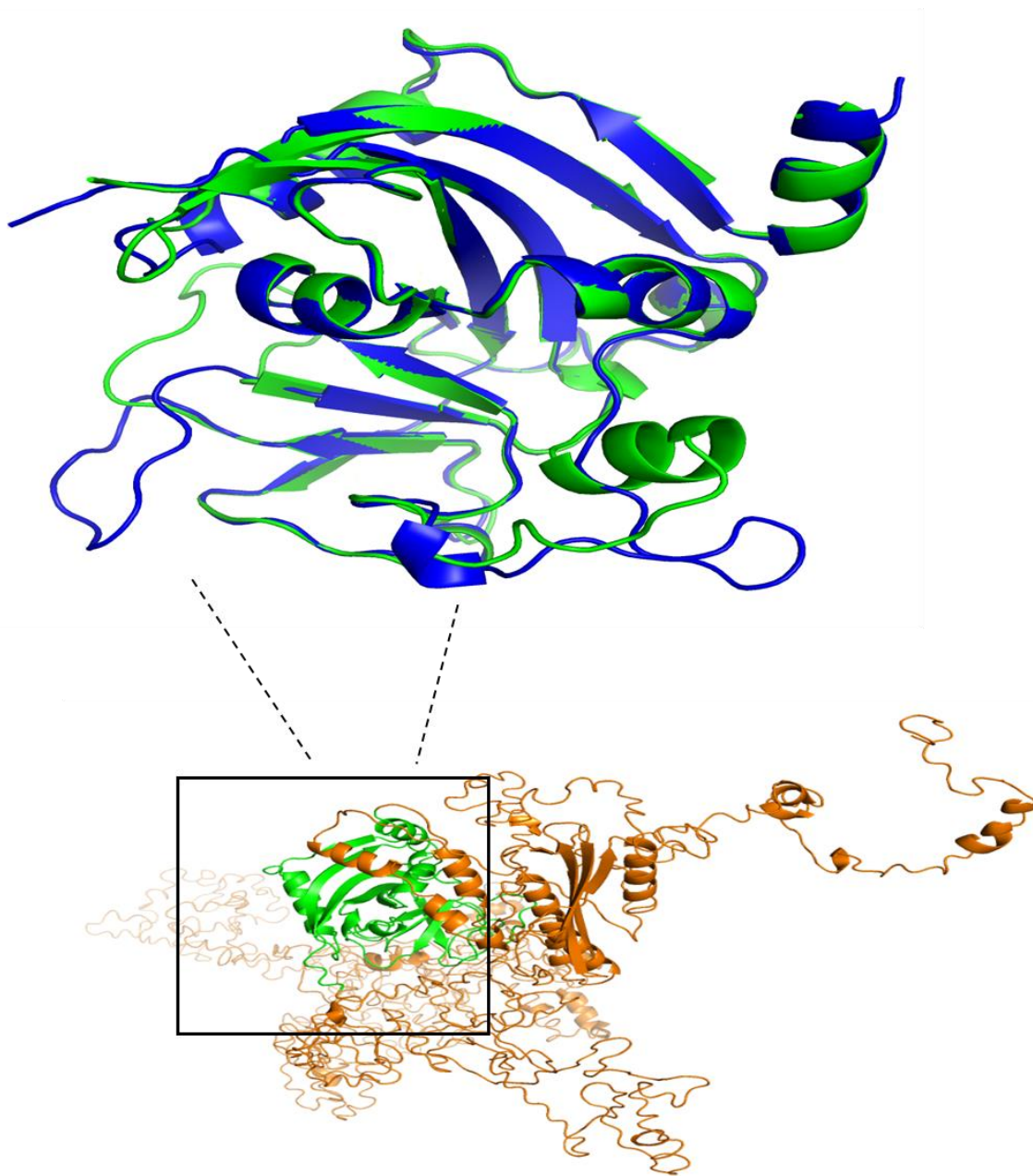


**Figure 3. 29 Structural Comparison of PARP4 Catalytic Domain.** This panel illustrates a comparative analysis of the catalytic domains of chPARP4 and its human counterpart. Predicted 3D structure of the full-length protein is displayed, with the catalytic domain highlighted in green and the remaining protein in orange. The catalytic domain is further emphasized by a black box. 3D structure was predicted using i-Tasser and AlphaFold and visualized and edited using PyMOL. A superimposition of the catalytic domains is shown, with the chicken catalytic domain represented in green and the human catalytic domain in blue. This comparison reveals the structural similarities and subtle differences between the catalytic domains of these orthologous proteins.

### **3.3.8: Evolutionary Variations in chPARP6**

The phylogenetic analysis of the chPARP6 protein provides fascinating insights into its evolutionary history and relationship to its counterparts in other species. The data clearly shows that the avian version of chPARP6 forms a distinct clade, separate from its mammalian equivalents (Figure 3.30). This indicates that the avian chPARP6 has diverged and developed unique characteristics compared to the human and other mammalian versions of the enzyme. Digging deeper into the molecular details, the amino acid sequence analysis reveals that chPARP6 shares around 82% identity with its human counterpart (Figure 3.31).

## chPARP6

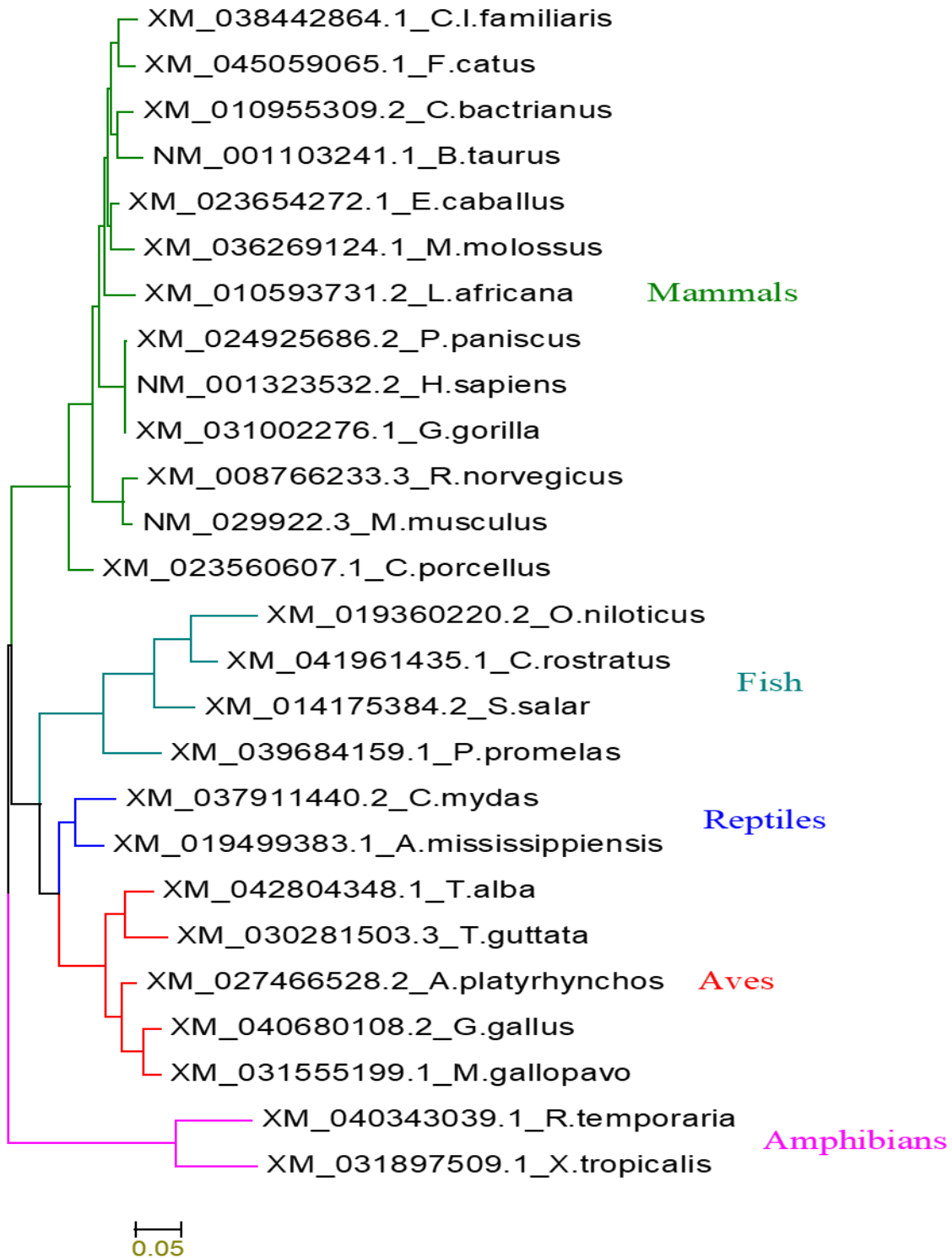


**Figure 3. 30 Phylogenetic and Sequence Analysis of PARP6.** This figure illustrates the evolutionary relationships of PARP6 across various vertebrate species, including mammals, amphibians, reptiles, and fish, with a specific focus on the avian lineage. The phylogenetic tree reveals a distinct clade formed by avian species, suggesting a unique evolutionary trajectory for PARP6 within the bird lineage. The tree was constructed using maximum likelihood method in MEGA6.

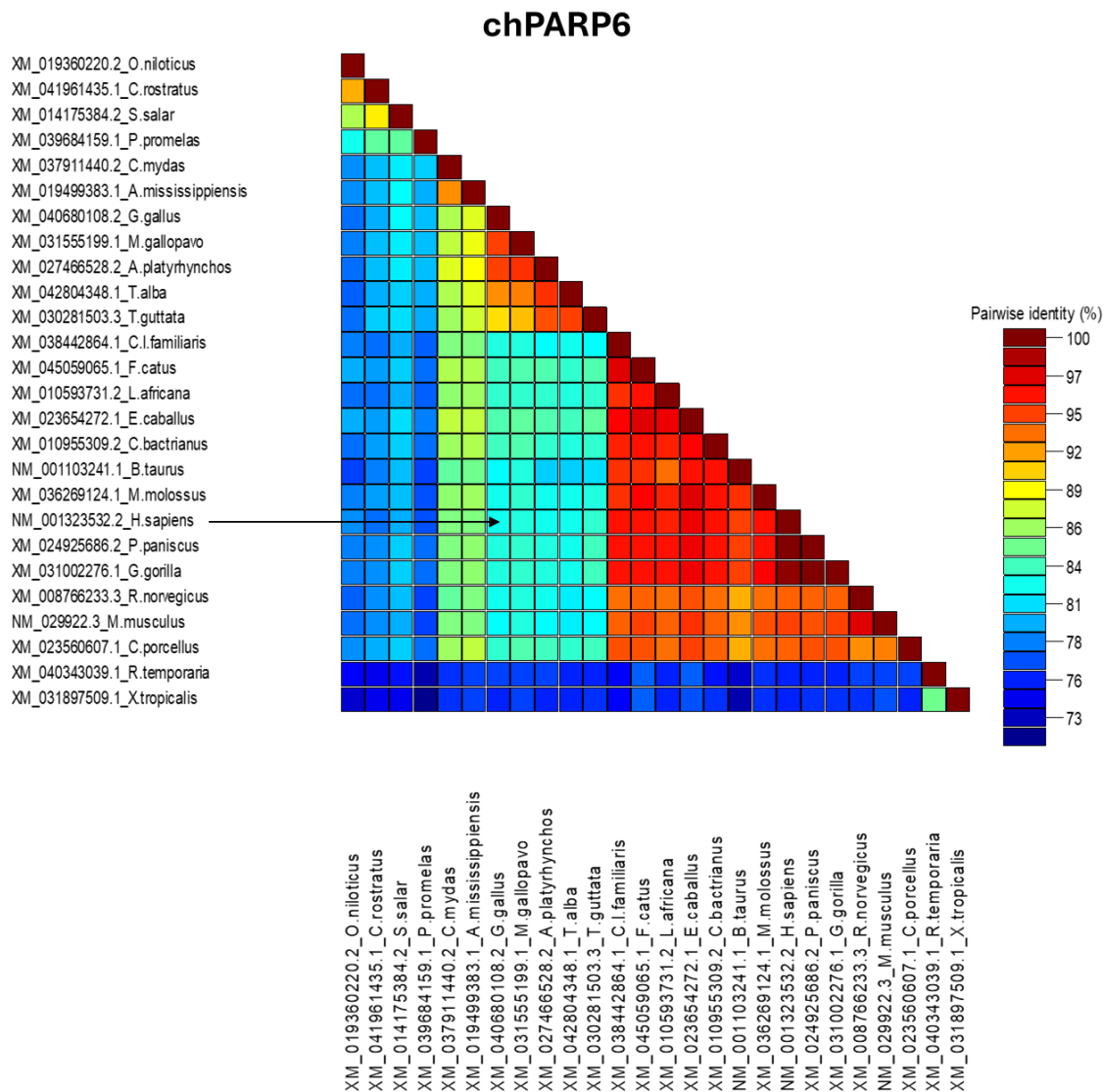


**Figure 3. 31 Sequence Homology of PARP6.** Heatmap displaying the amino acid sequence identity between chPARP6 and its human counterpart. The sequence alignment, performed using the ClustalW algorithm in SDT, reveals approximately 82% sequence identity, as indicated by the color-coded identity scale. This level of conservation suggests a high degree of structural and functional similarity between the chicken and human PARP6 proteins, consistent with their distinct evolutionary trajectory within the avian lineage.

While there is a high degree of similarity, the 18% difference in amino acid composition points to significant structural and functional variations between the avian and human enzymes. Furthermore, the multiple sequence alignment of the catalytic domains across species, including duck, turkey, human and mouse, coupled with the superimposition of the human and chicken catalytic domains, demonstrates that this crucial functional

region is remarkably conserved (Figure 3.32 & 3.33). Despite the evolutionary distance between birds and mammals, the catalytic domain has maintained its core structure and function, with only a few point mutations differentiating the avian and mammalian versions. This high degree of conservation underscores the essential role this enzyme plays in cellular processes that are fundamental across vertebrate species. Overall, the phylogenetic and structural analyses of chPARP6 provide a fascinating window into the intricate evolutionary relationships and functional adaptations of this important protein.

### chPARP6

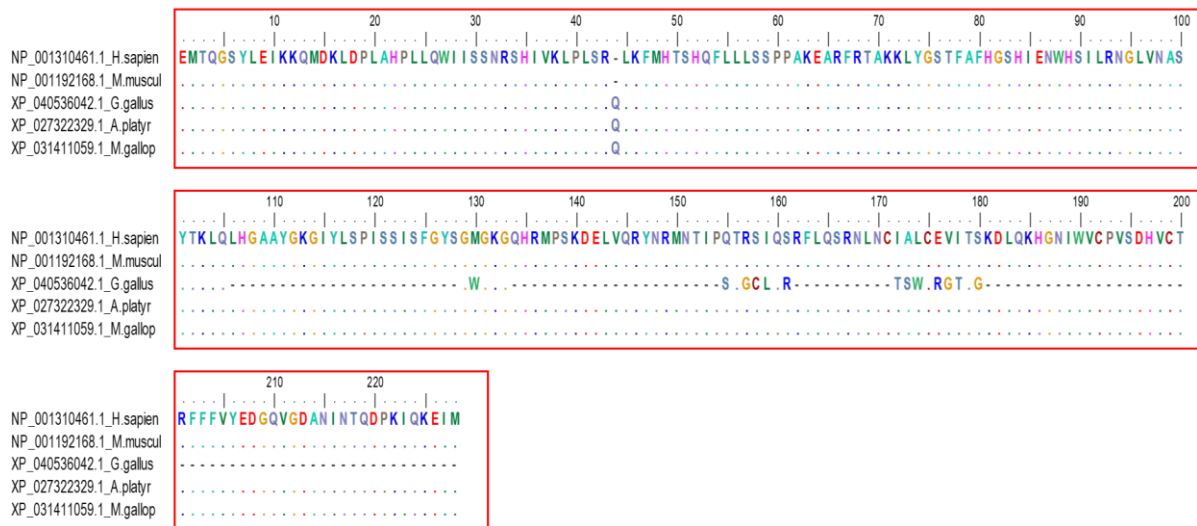


**Figure 3. 32 Multiple Sequence Alignment of PARP6 Catalytic domain.** The catalytic domain of chPARP6 exhibits a very high degree of conservation when compared to its human counterpart, with a few numbers of point mutations observed. The alignment was generated for chicken, turkey, duck, human, and mouse. The alignment was performed using BioEdit software. Identical amino acid residues across the aligned sequences are indicated by dots. The catalytic domains of each protein are highlighted within red boxes.

## chPARP6

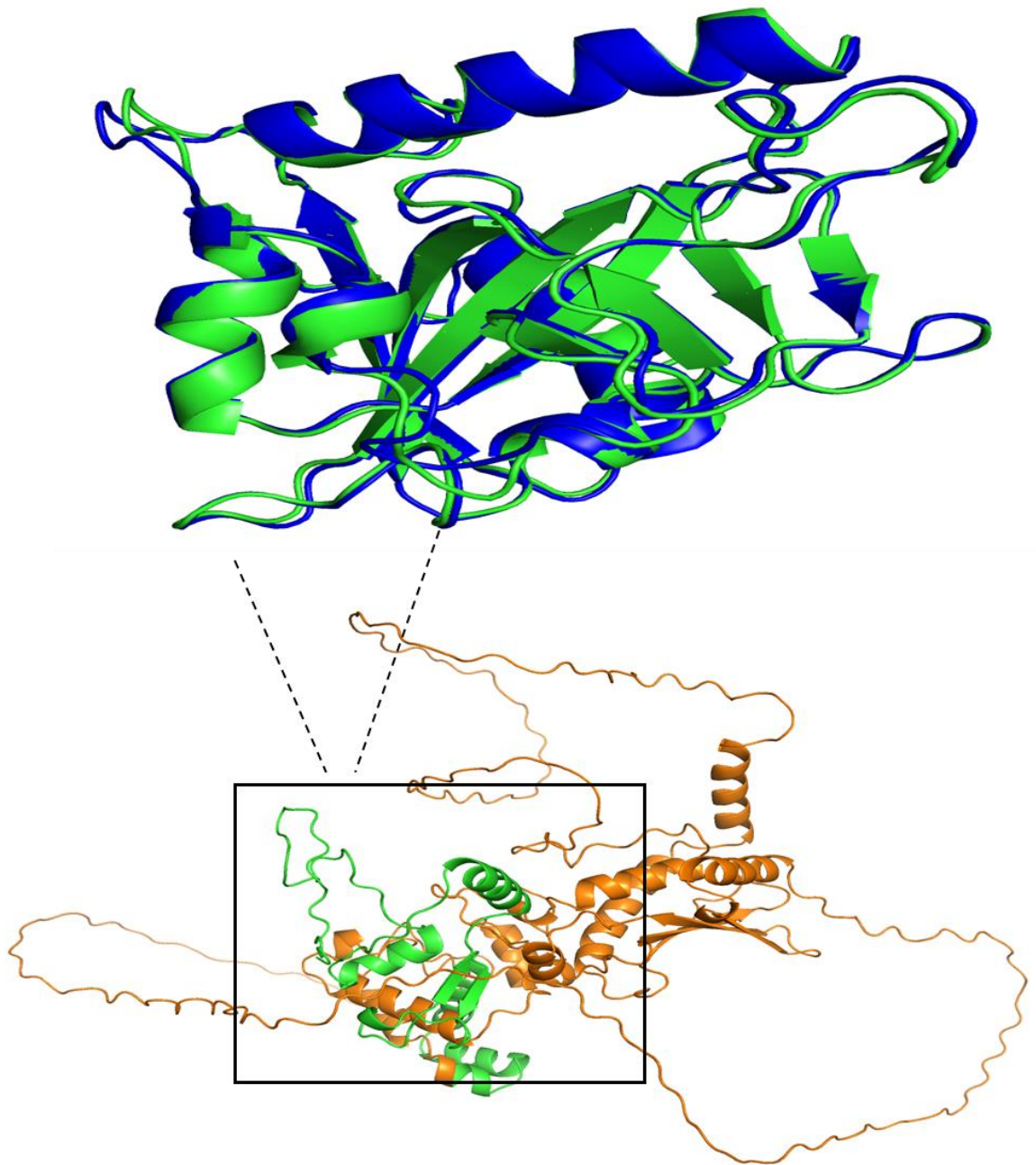


**Figure 3. 33 Structural Comparison of PARP6 Catalytic domain.** This panel illustrates a comparative analysis of the catalytic domains of chPARP6 and its human counterpart. Predicted 3D structure of the full-length protein is displayed, with the catalytic domain highlighted in green and the remaining protein in orange. The catalytic domain is further emphasized by a black box. 3D structure was predicted using i-Tasser and AlphaFold and visualized and edited using PyMOL. A superimposition of the catalytic domains is shown, with the chicken catalytic domain represented in green and the human catalytic domain in blue. This comparison reveals the structural similarities and subtle differences between the catalytic domains of these orthologous proteins.

### **3.3.9: Evolutionary Variations in chPARP8**

The phylogenetic analysis of the chPARP8 gene provides fascinating insights into the evolutionary relationships between avians and other vertebrate species. By examining the genetic sequences and structural features of this protein, we were able to determine that birds, form a distinct clade when compared to mammals, amphibians, reptiles, and fish (Figure 3.34). This means that the avian lineage has diverged significantly from these other vertebrate groups over the course of evolution. Further analysis delving into the amino acid sequence of the chPARP8 protein reveals an approximately 85% identity between the avian and human versions of this protein (Figure 3.35). This high degree of sequence similarity suggests that the core functions and structures of chPARP8 have been strongly conserved, likely due to the critical biological roles this protein plays in cellular processes. When examining the catalytic domains of the avian and human chPARP8 proteins through sequence alignments and 3D structural comparisons, we found that these regions are remarkably conserved, again indicating the evolutionary pressures to maintain the essential functions of this enzyme across distant vertebrate lineages (Figure 3.36 & 3.37). Overall, this phylogenetic and structural analysis of chPARP8 provides compelling evidence for the unique evolutionary path of birds, while also highlighting the fundamental similarities in core cellular machinery shared between avians and mammals like humans.

## chPARP8

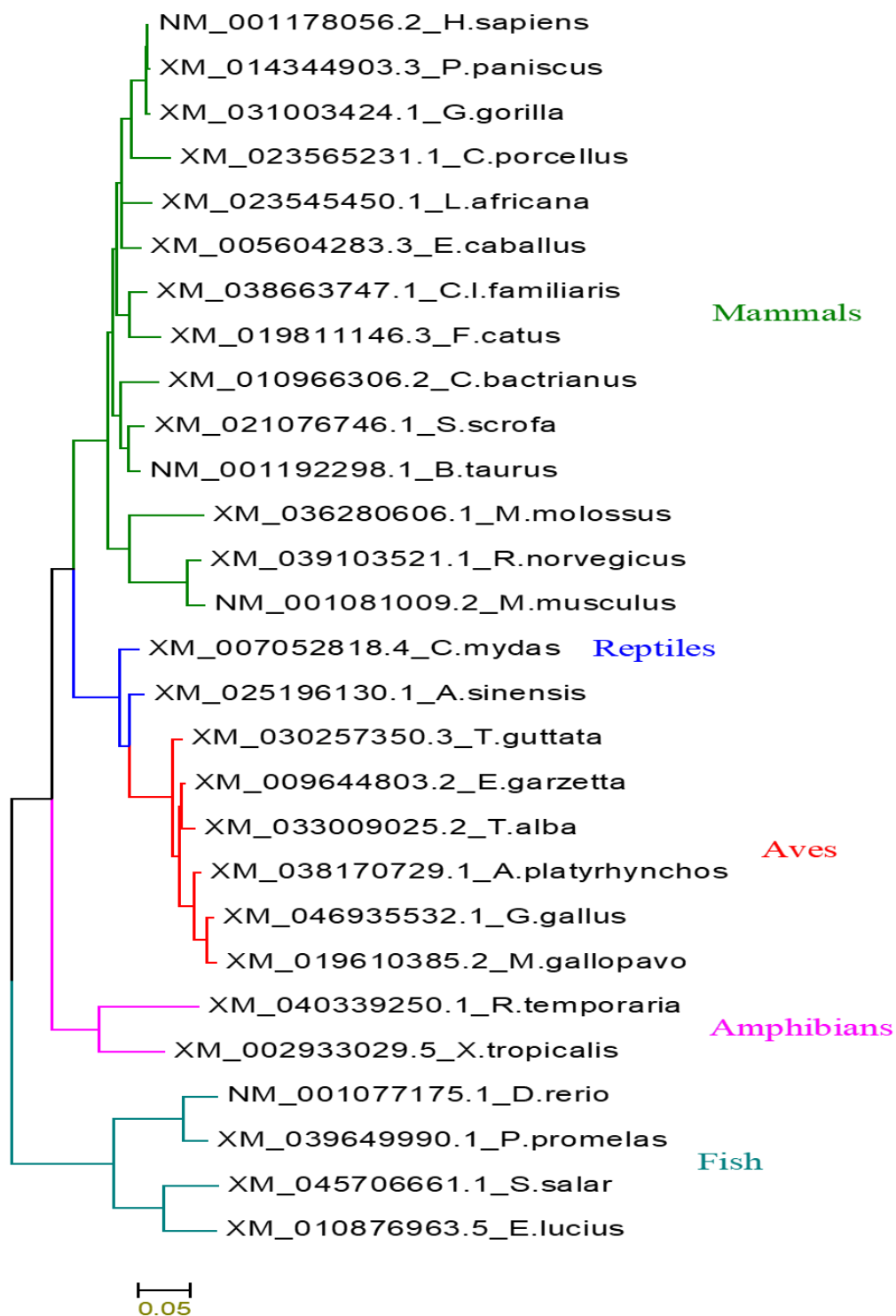


**Figure 3. 34 Phylogenetic and Sequence Analysis of PARP8.** This figure illustrates the evolutionary relationships of PARP8 across various vertebrate species, including mammals, amphibians, reptiles, and fish, with a specific focus on the avian lineage. The phylogenetic tree reveals a distinct clade formed by avian species, suggesting a unique evolutionary trajectory for PARP8 within the bird lineage. The tree was constructed using maximum likelihood method in MEGA6.

## chPARP8

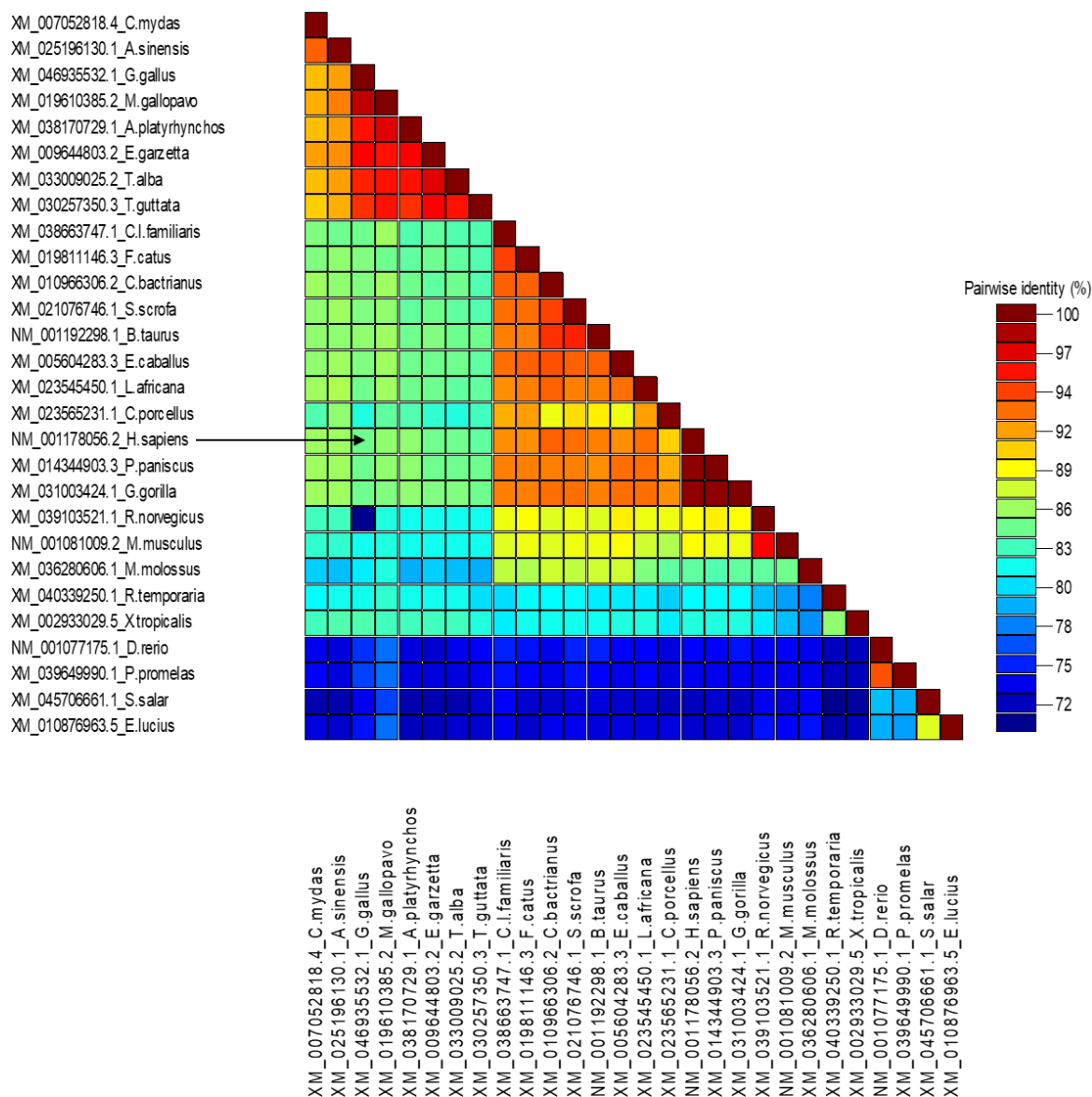


**Figure 3. 35 Amino Acid Sequence Homology of PARP8.** Heatmap displaying the amino acid sequence identity between chPARP8 and its human counterpart. The sequence alignment, performed using the ClustalW algorithm in SDT, reveals approximately 85% sequence identity, as indicated by the color-coded identity scale. This level of conservation suggests a moderate degree of structural and functional similarity between the chicken and human PARP8 proteins, consistent with their distinct evolutionary trajectory within the avian lineage.

### chPARP8

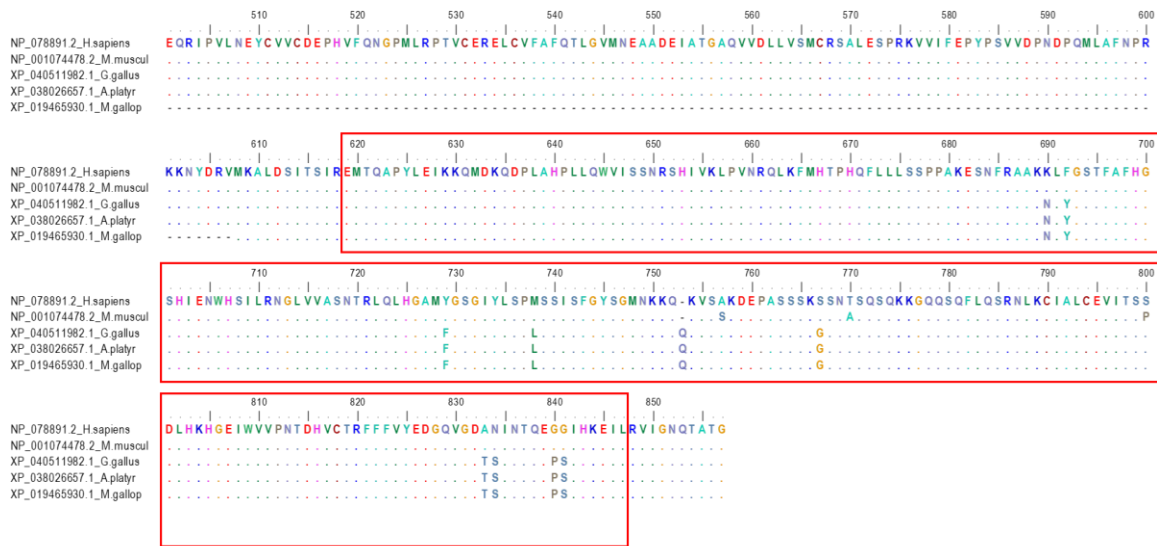


**Figure 3. 36 Multiple Sequence Alignment of PARP8 Catalytic Domain.** The catalytic domain of chPARP8 exhibits a very high degree of conservation when compared to its human counterpart, with less than ten-point mutations observed. The alignment was generated for chicken, turkey, duck, human, and mouse was performed using BioEdit software. Identical amino acid residues across the aligned sequences are indicated by dots. The catalytic domains are highlighted within red boxes.

## chPARP8

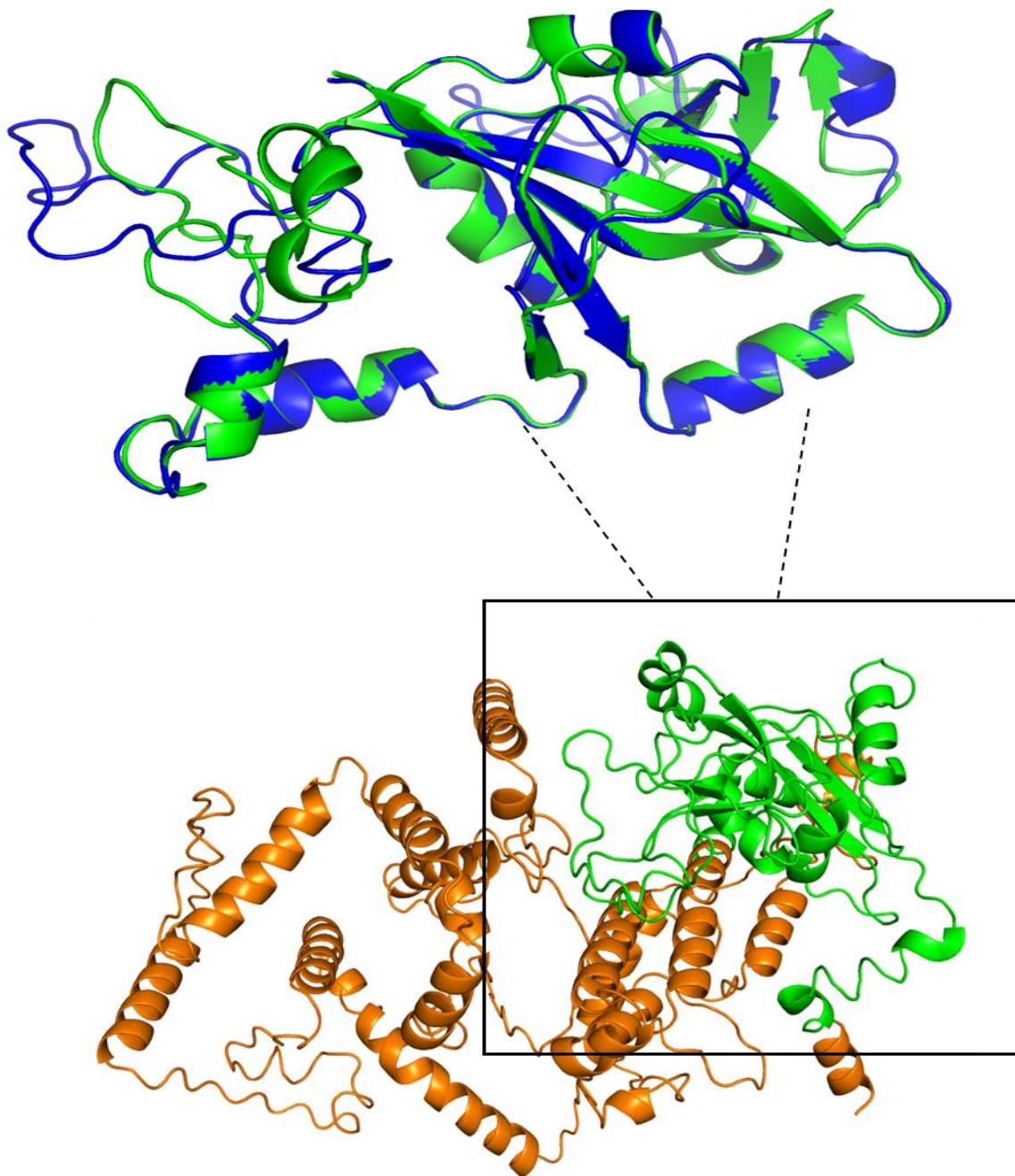


**Figure 3. 37 Structural Comparison of PARP8 Catalytic Domain.** This panel illustrates a comparative analysis of the catalytic domains of chPARP8 and its human counterpart. Predicted 3D structure of the full-length protein is displayed, with the catalytic domain highlighted in green and the remaining protein in orange. The catalytic domain is further emphasized by a black box. 3D structure was predicted using i-Tasser and AlphaFold and visualized and edited using PyMOL. A superimposition of the catalytic domains is shown, with the chicken catalytic domain represented in green and the human catalytic domain in blue. This comparison reveals the structural similarities and subtle differences between the catalytic domains of these orthologous proteins.

### **3.3.10: Evolutionary Variations in chPARP11**

The phylogenetic analysis of the chPARP11 gene reveals fascinating insights into the evolutionary relationships of this important protein across different species. The data shows that the avian PARP11 forms a distinct clade, separate from its human counterpart. This indicates that the PARP11 gene has diverged significantly between birds and humans over the course of millions of years of evolution, likely adapting to fulfil specialized functions within each lineage (Figure 3.38). Interestingly, the avian and human PARP11 proteins still share around 77% sequence similarity, suggesting a core set of conserved structural and functional elements (Figure 3.39). Further investigation through sequence alignment and 3D structural comparisons of the catalytic domain bolsters this notion, revealing that this critical region remains well-conserved despite the overall divergence (Figure 3.40 & 3.41). While a handful of point mutations can be detected, the catalytic domain appears to have maintained its essential architecture and properties across these distant vertebrate groups. This high degree of conservation underscores the vital role PARP11 plays in fundamental cellular processes, which have been preserved through the course of evolution.

## chPARP11

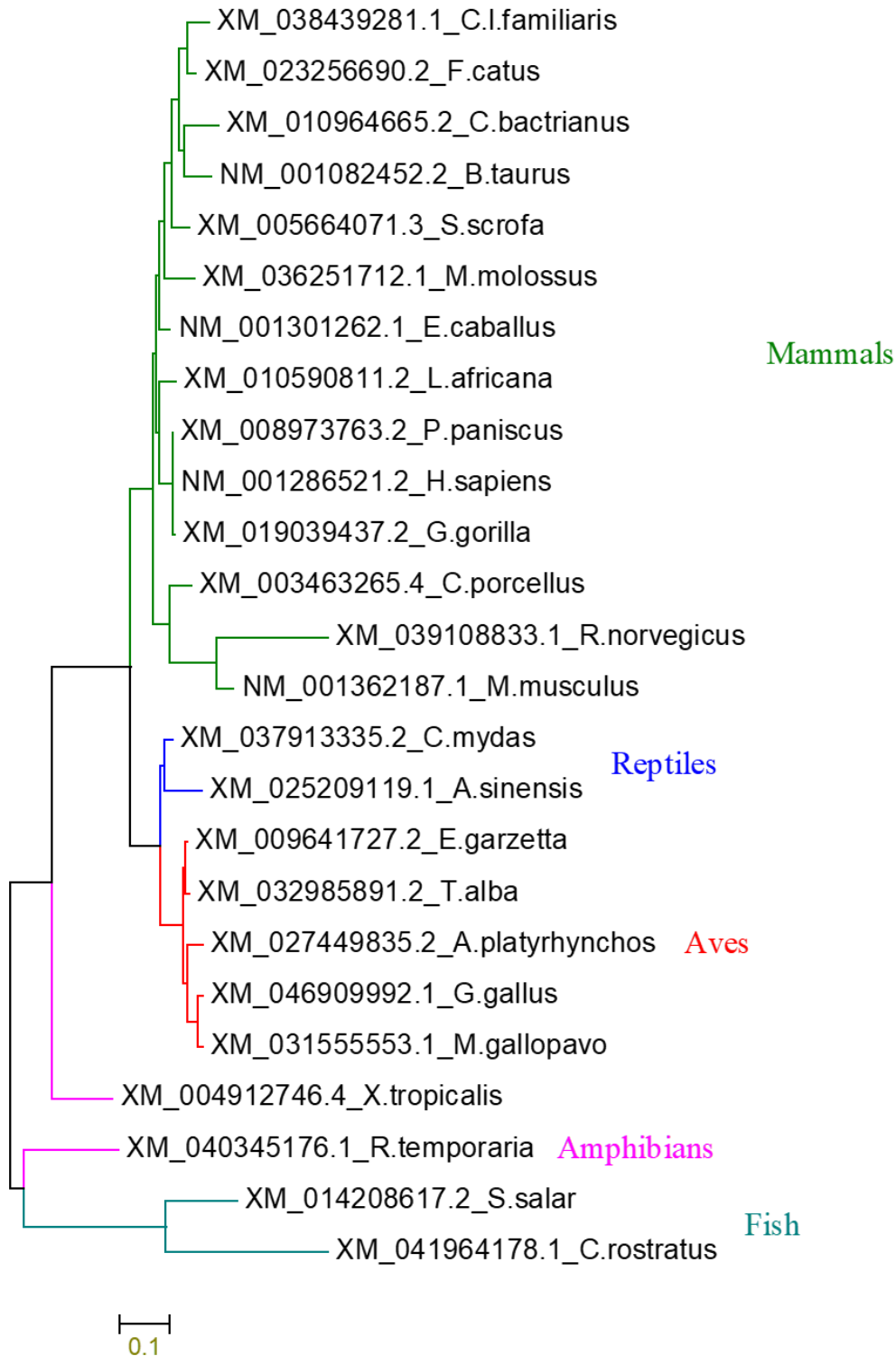


**Figure 3. 38 Phylogenetic Analysis of PARP11.** This figure illustrates the evolutionary relationships of PARP11 across various vertebrate species, including mammals, amphibians, reptiles, and fish. The phylogenetic tree reveals a distinct clade formed by avian species, suggesting a unique evolutionary trajectory for PARP11 within the bird lineage. The tree was constructed using maximum likelihood method in MEGA6.

## chPARP11

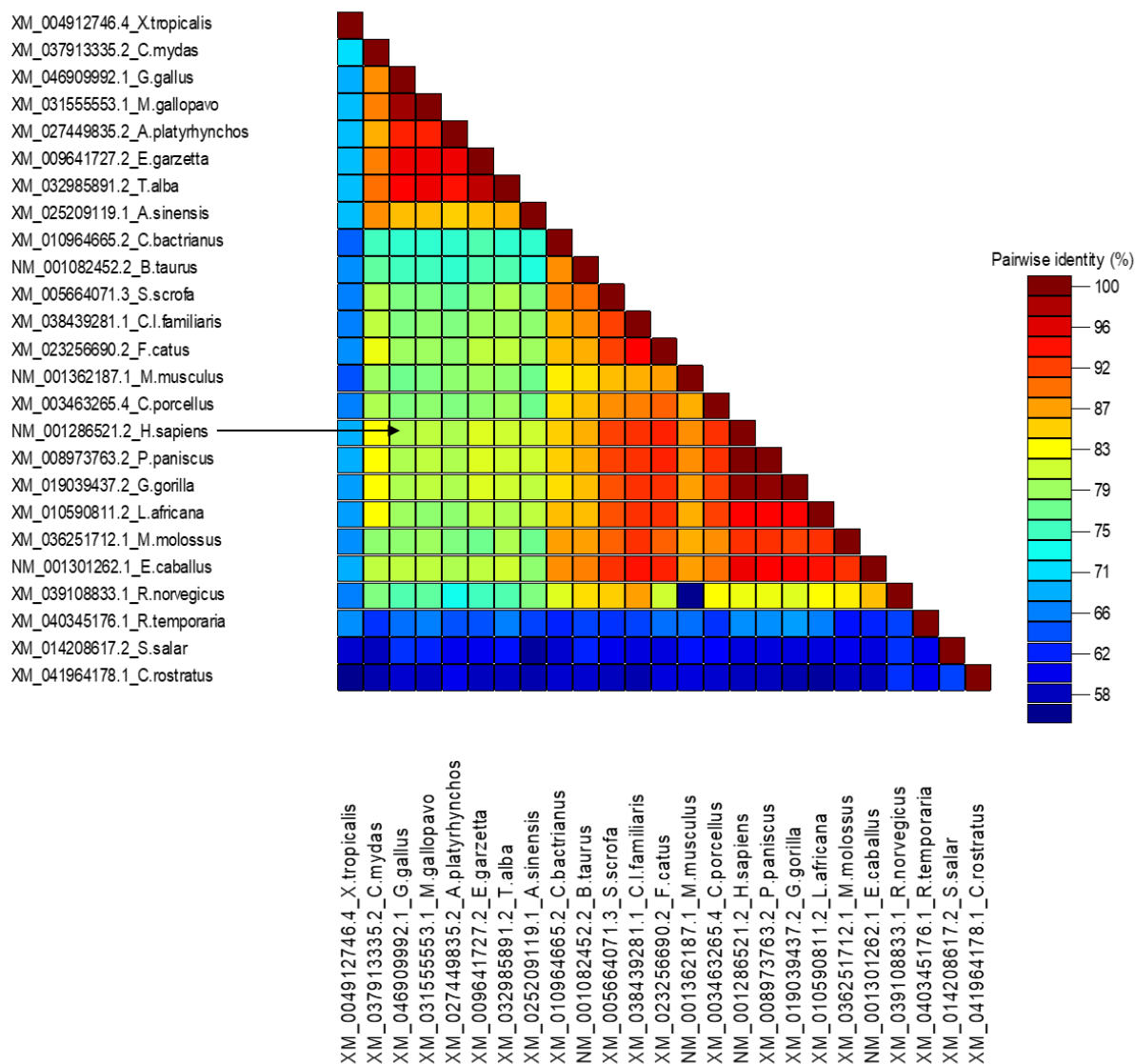


**Figure 3. 39 Sequence Homology of PARP11.** Heatmap displaying the amino acid sequence identity between chPARP11 and its human counterpart. The sequence alignment, performed using the ClustalW algorithm in SDT, reveals approximately 77% sequence identity, as indicated by the color-coded identity scale. This level of conservation suggests a high degree of structural and functional similarity between the chicken and human PARP11 proteins.

### chPARP11

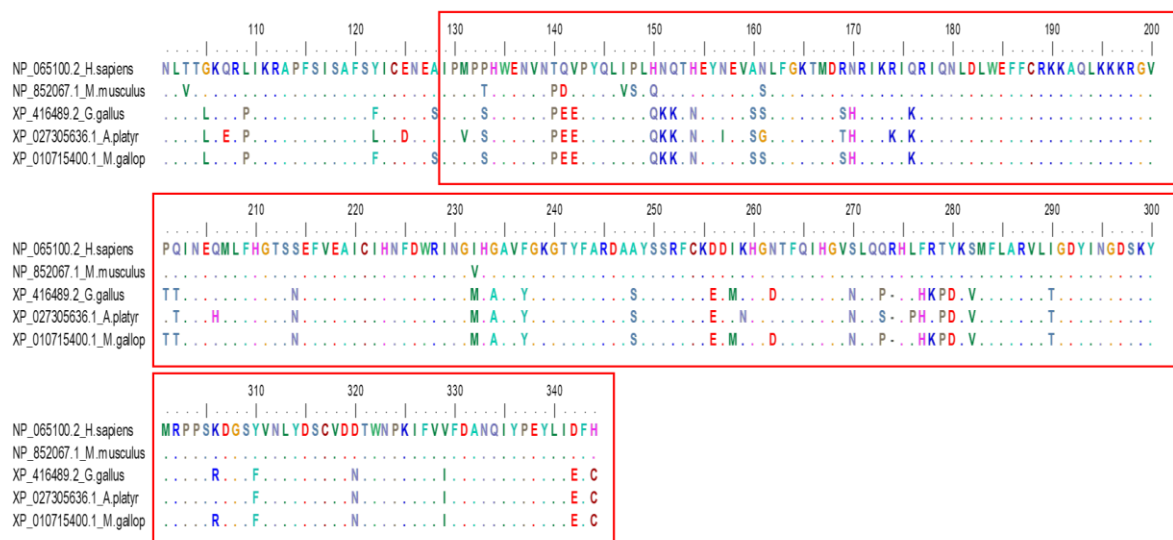


**Figure 3. 40 Multiple Sequence Alignment of PARP11 Catalytic Domain.** The catalytic domain of chPARP11 exhibits a high degree of conservation compared to its human counterpart, with only a small number of point mutations observed. MSA was generated from chicken, turkey, duck, human, and mouse. The alignments were performed using BioEdit software. Identical amino acid residues across the aligned sequences are indicated by dots. The catalytic domains of each protein are highlighted within red boxes.

### chPARP11

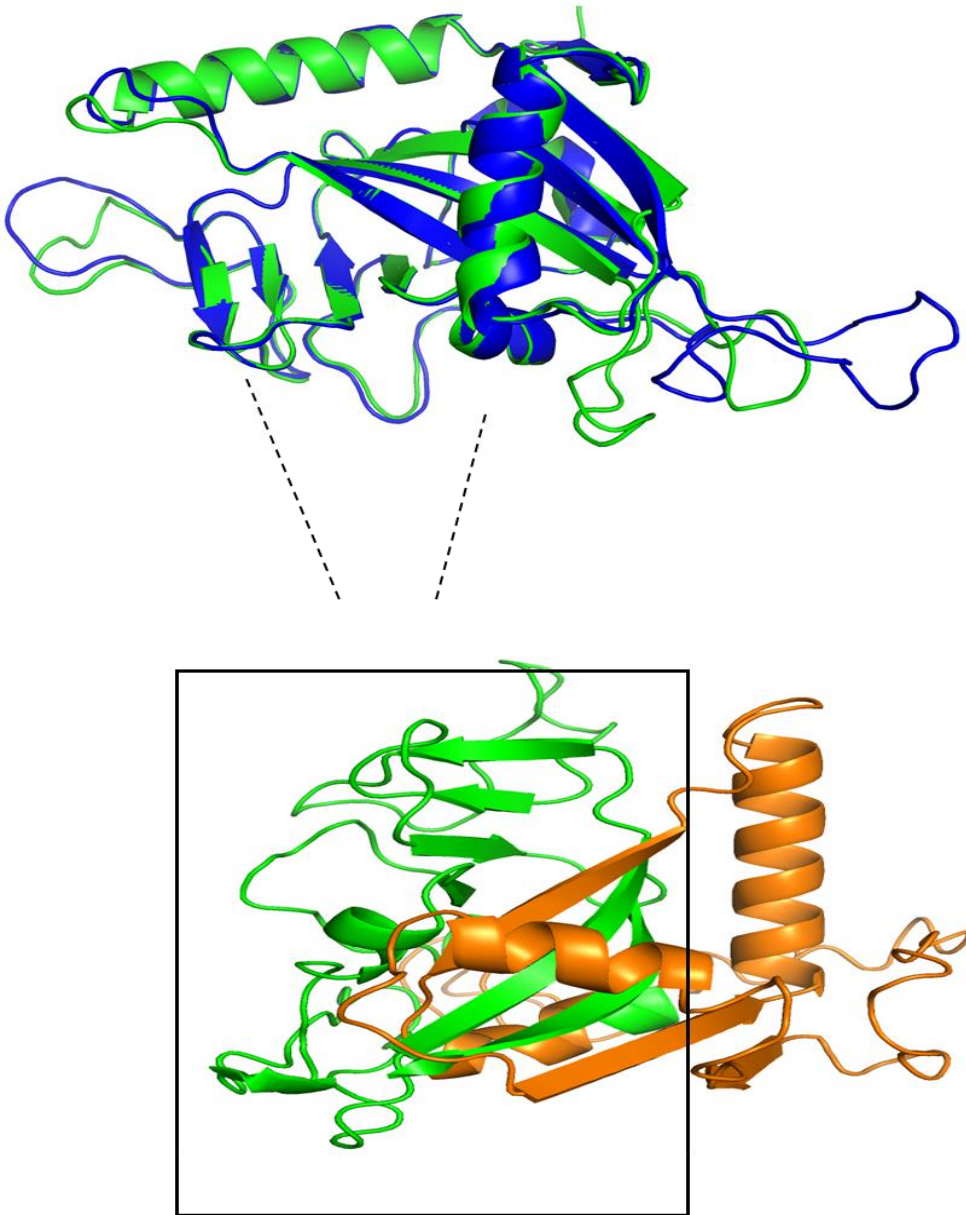


**Figure 3. 41 Structural Comparison of PARP11 Catalytic Domain.** This panel illustrates a comparative analysis of the catalytic domains of chPARP11 and its human counterpart. Predicted 3D structure of the full-length protein is displayed, with the catalytic domain highlighted in green and the remaining protein in orange. The catalytic domain is further emphasized by a black box. 3D structure was predicted using i-Tasser and AlphaFold and visualized and edited using PyMOL. A superimposition of the catalytic domains is shown, with the chicken catalytic domain represented in green and the human catalytic domain in blue. This comparison reveals the structural similarities and subtle differences between the catalytic domains of these orthologous proteins, providing insights into potential functional conservation and divergence.

### 3.4: Chapter Discussion

Our bioinformatics analysis has provided valuable insights into the conservation and evolution of PARP proteins in the chicken genome, offering a comparative perspective against their human counterparts. While our findings reveal significant structural conservation, the evolutionary journey of these genes appears to have involved some interesting genomic rearrangements and varying degrees of sequence divergence within the avian lineage.

One of the key observations from our analysis is the remarkable conservation of domain organization between chPARP proteins and their human homologs human PARPs (Ke, Wang, et al., 2019). The presence of similar functional domains, including the DNA-binding domains and the catalytic domain responsible for poly (ADP-ribosyl) ation, strongly suggests that the fundamental biochemical functions of these proteins are likely conserved in chicken. This structural similarity implies that chPARPs likely play comparable roles in DNA repair, genome maintenance, and cellular signaling pathways as their human counterparts.

However, our synteny analysis revealed a notable lack of conserved gene order and surrounding genomic environment for PARP genes between chicken and humans. This observation is particularly intriguing. While the core protein structures appear conserved, the differing genomic context suggests that the regulatory landscape and potentially the co-expression patterns of these genes might have diverged over evolutionary time. The surrounding genes and their regulatory elements can influence the expression levels, timing, and tissue specificity of the PARP genes. Therefore, the altered genomic environment in chicken could subtly modulate the overall function or regulation of these proteins compared to humans.

Interestingly, our synteny analysis provided further nuances within the avian lineage itself. We observed a slightly higher degree of synteny for PARP genes between chicken and duck compared to the chicken and turkey comparison. This finding hints at a closer evolutionary relationship and potentially a more conserved genomic organization of these genes between chicken and duck within the Galliformes order. Further investigation into the specific genes surrounding the PARP loci in these species could provide more detailed insights into the nature of these genomic rearrangements.

Despite the conserved domain architecture, our sequence identity analysis revealed varying degrees of sequence similarity between chPARPs and their human counterparts. This ranged from a high of approximately 85% identity for PARP8 to a lower value of around 50% for PARP14. This variation in sequence conservation across different PARP family members suggests that these individual proteins have experienced different evolutionary pressures. Some PARPs, like PARP8, appear to have maintained a higher degree of sequence conservation, potentially indicating a more critical and tightly constrained function. Conversely, PARP14, with its lower sequence identity, might have undergone more rapid evolution or might have acquired more species-specific adaptations in its function.

The phylogenetic analysis further illuminated the evolutionary history of the PARP gene family within the avian lineage. The observation that the avian clade for PARP12 split into two distinct branches and for PARP14 split into three branches suggests that gene duplication events and subsequent diversification have occurred within the avian lineage. These duplication events could have led to the emergence of paralogous genes with potentially specialized or slightly altered functions within birds. The specific

functional consequences of these avian-specific duplications warrant further investigation.

Finally, the varying degrees of conservation observed within the catalytic domains across different chPARPs further support the notion of differential evolutionary pressures acting on these proteins. The catalytic domain is the functional core responsible for the enzymatic activity of PARPs. While the overall domain structure is conserved, variations in the amino acid sequence within this critical region could lead to subtle differences in enzymatic efficiency, substrate specificity, or regulatory mechanisms. These differences could contribute to species-specific adaptations in DNA repair pathways or cellular responses involving PARP activity.

In conclusion, our bioinformatics analysis provides a comprehensive overview of the evolutionary landscape of PARP proteins in chicken. While the fundamental domain architecture and likely core functions are conserved with their human counterparts, the lack of synteny and the varying degrees of sequence conservation highlight the dynamic nature of gene evolution. The observed differences in synteny within the avian lineage and the phylogenetic branching patterns suggest that gene duplication and subsequent diversification have played a role in shaping the PARP gene family in birds. Future functional studies in chicken models are warranted to further elucidate the specific roles and potential species-specific adaptations of these PARP proteins in the context of their unique genomic environment and varying sequence identities. Understanding these nuances will not only enhance our knowledge of PARP biology but also provide valuable insights into the evolutionary adaptations of these crucial proteins across different vertebrate species.

### **3.5: Future Directions:**

The comprehensive analysis of chicken PARP genes presented in this study provides a solid foundation for future research. Further experimental studies are necessary to elucidate the precise functions of these proteins, particularly those with potential antiviral properties. Investigating the role of chicken PARPs in avian diseases could provide valuable insights into potential therapeutic targets. Expanding comparative genomic analyses to a wider range of avian species would help unravel the evolutionary dynamics of PARP genes within this lineage. Additionally, high-resolution structural studies of chicken PARPs can provide insights into their interactions with substrates and inhibitors, facilitating the development of targeted therapies. By combining bioinformatics and experimental approaches, future research can shed light on the complex roles of chicken PARPs in avian biology, potentially leading to the development of novel disease prevention and treatment strategies.

**Chapter 4: Influenza Virus  
Transcriptionally Regulates PARP  
Genes in Chicken Primary  
Fibroblasts**

## 4.1: Abstract

Total RNA was extracted from CEF cells infected with IAV or left mock-treated, for comparative RNA-sequencing and subsequent analysis. To ensure accurate downstream analysis, the dataset was normalized to remove potential bias. Normalization was achieved by transforming the data and adjusting dispersion estimates to minimize false positives. To assess data variability, dispersion box plots, estimation plots, and density plots were generated using DESeq4. Principal component analysis (PCA) revealed distinct clustering of mock-treated and IAV-treated samples, indicating significant transcriptional differences induced by viral infection. Differential gene expression analysis identified 2243 differentially expressed genes (DEGs), including several members of the Poly (ADP-ribose) polymerase (PARP) family. PARP14, PARP12, and PARP10 were significantly upregulated in IAV-infected cells, suggesting their potential involvement in antiviral responses. Further analysis using volcano plots and a lollipop chart highlighted the activation of various biological pathways, including immune response, response to stress, and extracellular region pathways. These findings provide valuable insights into the molecular mechanisms underlying IAV infection and the host's response to viral challenge.

## **4.2: Introduction**

### **4.2.1: Chicken as Influenza Virus Reservoirs**

The influenza A virus (IAV) is a formidable and highly adaptable virus that poses a significant threat to both animal and human health worldwide. This highly contagious respiratory virus can infect a remarkably broad range of host species, including humans, birds, and other mammals (Su et al., 2024). At the heart of this viral threat lie domestic poultry populations, particularly chickens, which play a pivotal role in the transmission and evolution of IAV. These ubiquitous birds serve as a crucial link between the natural reservoir of the virus in wild avian populations and the potential for devastating outbreaks in human communities (Arruda et al., 2024; Wille & Holmes, 2020). Domestic chickens are highly susceptible to influenza virus infections, making them an ideal environment for the virus to thrive and mutate (Ellis et al., 2021). The high population densities often found in industrial poultry farming operations provide many opportunities for rapid viral transmission and genetic diversification within chicken flocks. Worryingly, chickens can harbour influenza A viruses asymptotically such as H9N2, H2N3, and H7N7 LPAIV strains, acting as silent reservoirs that can then spread the pathogens to other domestic fowl and wild bird species (Hao et al., 2019; Kuchipudi et al., 2014). This silent proliferation is especially concerning, as it increases the likelihood of certain influenza strains (e.g. H9N2) eventually acquiring the ability to cross the species barrier and become transmissible to humans. Such adaptations could spark localized outbreaks or even trigger full-blown pandemics, posing a grave threat to public health. Beyond influenza, chickens have been identified as carriers of other zoonotic viruses, such as West Nile virus, which can then be transmitted to humans via direct contact or mosquito

vectors (WHO). The high population turnover and global distribution of these ubiquitous birds make them a significant factor in the epidemiology of numerous viral diseases. Consequently, the careful monitoring and understanding of the viral profiles within chicken flocks is of paramount importance in mitigating the considerable public health risks posed by these avian reservoirs. Effective strategies to control influenza virus infection in domestic poultry are crucial for safeguarding both animal and human health, as these birds serve as a critical link in the transmission and evolution of this formidable pathogen.

#### **4.2.2: Influenza-induced transcriptomics in chicken**

IAV can have dire consequences for chickens, causing significant economic losses to the poultry industry. IAV interacts with the host cell's genetic machinery, influencing gene expression and triggering a complex transcriptional response. This study aims to investigate the global changes in gene expression that occur in chicken embryonic fibroblast (CEF) cells in response to IAV infection (Figure 4.1). Transcriptomic analysis of RNA-sequencing data obtained from IAV-infected CEF cells can provide invaluable information about the cellular responses to viral infection. This powerful technique, which examines the expression patterns of thousands of genes, explains how CEF cells, a common model for studying avian influenza, react to and attempt to combat IAV. Of particular interest are the genes encoding the PARP proteins, which play crucial roles in the cellular stress response and have been implicated in the modulation of influenza virus replication. There is limited information on the roles PARPs play in IAV infection in chickens. Through transcriptomic analysis, we can identify significant changes in PARP

gene expression during IAV infection, shedding light on the complex interplay between the virus and this important class of host defence proteins.

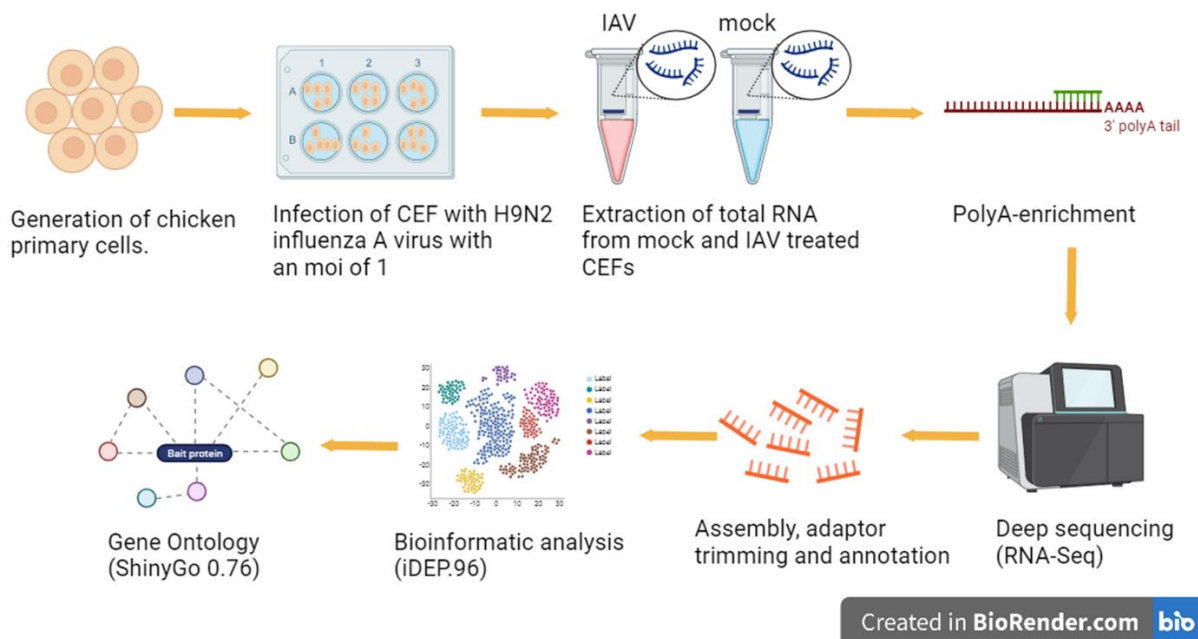


**Figure 4. 1 Overview of the experimental design used for transcriptomic study.** The experimental approach involved infecting a population of CEF cells with the IAV strain at a specified multiplicity of infection (MOI) to ensure consistent viral exposure across replicates. Mock-infected cells were maintained in parallel as a control group. The extracted RNA from both biological conditions underwent library preparation and high-throughput RNA sequencing to generate transcriptomic profiles for each condition.

The main objective of this chapter is

- (i) To elucidate the global gene expression profile of CEF cells following IAV infection-  
This will provide a broad overview of the cellular response to viral infection.
- (ii) To investigate the expression patterns of PARPs in IAV-infected CEF cells- This will explore the potential role of PARPs in the cellular response to IAV infection.
- (iii) To identify and characterize the cellular pathways activated during IAV infection in CEF cells- This will reveal the key biological processes modulated by the virus.

- (iv) To validate the transcriptomic findings through reverse transcription quantitative polymerase chain reaction (RT-qPCR)- This will ensure the accuracy and reliability of the transcriptomic data.
- (v) To determine the cellular localization of selected chPARPs in DF1 cells- This will provide insights into the functional roles of specific PARPs.

## **4.3: Results**

### **4.3.1: Pre-processing of RNA-seq data**

Total RNA was extracted from CEF cells that had been infected with the IAV or left untreated, and three biological replicates were used for comparative RNA-seq analysis. Before examining transcript expression and abundance in infected CEF cells, we normalised the dataset to remove any potential variance or bias. Normalisation methods that combine data from genes across sites are strongly recommended for identifying and eliminating site-specific effects, and they can significantly improve RNA-seq studies (Love et al., 2014). Normalisation was required for accurate downstream analysis, differential expression, and functional annotation of transcriptome data. This normalisation was accomplished by producing transformed data. To assess the level of variation in the RNA-seq data, DESeq2 was used to generate a dispersion box plot (Figure 4.2) and an estimation plot. Dispersion measures how closely the expression values for a given gene cluster around the average expression level. A high dispersion indicates significant variability in gene expression between replicates, whereas a low dispersion indicates that gene expression levels are relatively stable across replicates (Anders & Huber, 2010; Love et al., 2014).

An initial dispersion for each gene was generated using maximum likelihood estimation and plotted as an indicator of mean expression level, with each gene represented by a black dot. A curve was then fitted to these gene-wise dispersion estimates (represented by a blue line), indicating the expected dispersion value for genes with a given expression level. This is useful in demonstrating that individual genes have diverse levels of variability, but overall, there will be a distribution of acceptable dispersion estimates (Figure 4.3).

To obtain final dispersion estimates, the initial gene-wise dispersion estimates were reduced to the fitted curve. The reduction of dispersion estimates is critical in lowering the risk of false positives in subsequent differential expression analysis. Adjusting the dispersion value results in an increase for some genes, reducing the possibility of false positives caused by an underestimated dispersion. Dispersion estimates that are slightly above the plotted curve are adjusted downwards, moving them closer to the expected value. However, dispersion estimates with extremely high values must not be shrunk towards the curve here, as this may result in false positives (Love et al., 2014). Gene dispersion estimates are distributed around the curve, with dispersion decreasing as mean expression levels of normalised counts increase.

Additionally, a density plot for the transformed data was presented. Density plots were used to better understand the samples numeric continuous variables. It features the normalized likelihoods of the biological samples, and a wider and less sharp likelihood (represented by a redline) indicates higher dispersion of the treated sample (Figure 4.4).

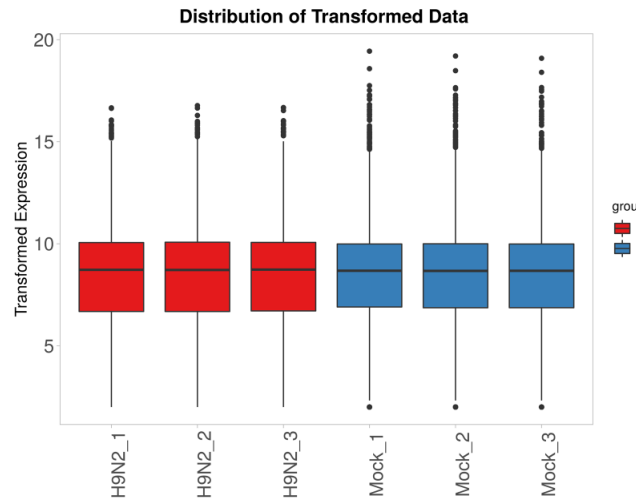


**Figure 4. 2 Dispersion box Plot of RNA-seq data.** This figure displays the dispersion box plot generated using DESeq2, demonstrating the variation in RNA-seq data from CEF cells. Dispersion measures the variability of gene expression across biological replicates. A high dispersion indicates significant variability, while a low dispersion suggests stable gene expression. The box plot provides an overview of the distribution of dispersion values across the dataset, highlighting the overall level of variability in gene expression between replicates.

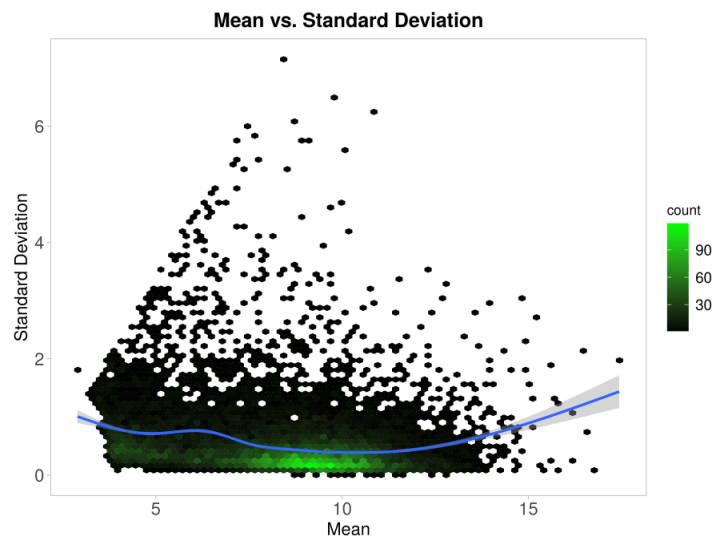


**Figure 4. 3 Gene-Wise Dispersion Estimation Plot.** This figure presents the gene-wise dispersion estimation plot, illustrating the relationship between mean gene expression levels and dispersion. Each black dot represents the initial dispersion estimate for a gene, calculated using maximum likelihood estimation. The blue line represents the fitted curve, indicating the expected dispersion value for genes with a given expression level. This plot demonstrates the diverse levels of variability across individual genes and the overall distribution of acceptable dispersion estimates. The final dispersion estimates are shrunk towards the fitted curve to minimize the risk of false positives in subsequent differential expression analysis.

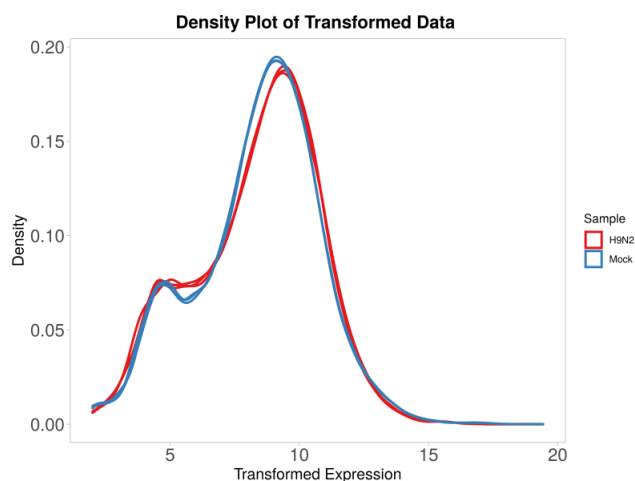


**Figure 4. 4 Density Plot of Transformed RNA-seq data.** This figure depicts the density plot of transformed RNA-seq data from CEF cells, comparing mock and IAV-infected samples. The plot illustrates the normalized likelihoods of the biological samples. A wider and less sharp likelihood curve (red line) for the IAV-treated sample indicates a higher dispersion of gene expression compared to the untreated sample. This reflects the increased variability in gene expression observed in infected cells.

Finally, to confirm the overall variability within the normalised sample counts and determine whether biological replicates clustered together, we used principal component analysis (PCA) (Figure 4.5A & B). Triplicate biological replicates of mock and IAV-treated CEF cell transcriptomes were analysed. PCA was used to capture most of the variance in the data. It determines the direction of the top principal components and transforms the data into the low-dimension space. It shows how samples are related according to their expression levels. PCA is a dimension reduction technique that identifies the most significant amounts of variation in a dataset and assigns it to principal components. The principal component 1 (PC1) accounts for the principal direction along which the samples exhibit the greatest amount of variation; the second principal component (PC2) is calculated in the same manner with the condition that is uncorrelated with the first principal component and orthogonal to the PC1 axis, accounting for the next highest variance; and the principal component (PC3) with the

least variance (Morais et al., 2019; Philip D Glaves 1, 2011). Biological replicates are expected to cluster closely together, while the various sample groups tend to cluster apart from one another within the PCA plot.

Our PCA results show that biological replicates are closely clustered in both sample groups. The PCA revealed that the transcriptomes of mock-treated samples clustered closely together, as expected for a control group. There was a variance (PC1 with 95.6%) between IAV-treated and untreated samples, as well as a variance (PC2 with 4.3%) among the treated samples, with the untreated samples exhibiting the least variance (PC3 with 1.9%). This is to be expected in this study, as untreated samples exhibit little to no variation, while variation in IAV-treated samples can be attributed to viral infection. A scree plot was used to reduce the dimensionality of multivariate data to two or three principal components, which were then graphically represented with minimal loss of information (Figure 4.5C).

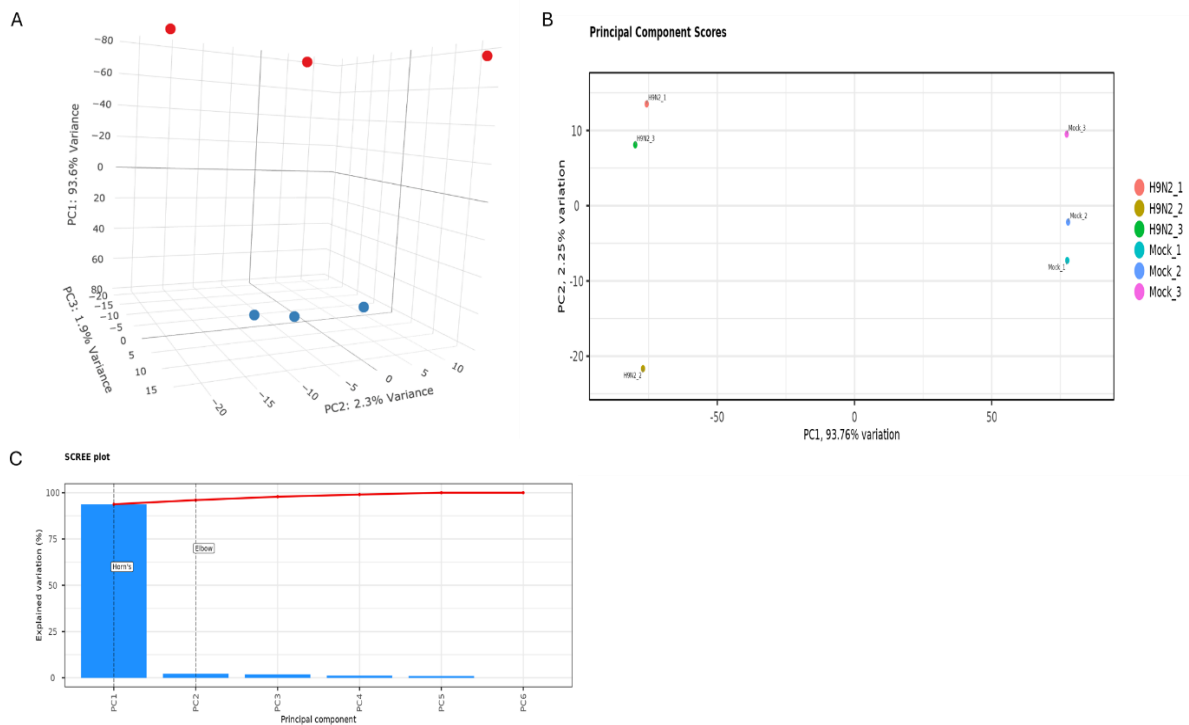


**Figure 4.5 Principal component analysis of RNA-seq data from IAV-treated and Mock CEF cells.** (A & B) PCA Scatter Plot: This figure displays the results of PCA performed on RNA-seq data from triplicate biological replicates of mock and IAV-treated CEF cells. The plot illustrates the relationship between samples based on their gene expression levels. PC1 and PC2 represent the directions of maximum variance in the data. PC1 accounts for 95.6% of the variance, distinguishing between mock and IAV-treated samples. PC2 accounts for 4.3% of the variance, showing variance within the IAV treated samples. The close clustering of biological replicates within each treatment group indicates high reproducibility. The separation of mock and IAV-treated samples demonstrates distinct gene expression profiles. (C) Scree Plot: The scree plot shows the percentage of variance explained by each principal component. This plot aids in determining the optimal number of principal components to represent the data, confirming that the majority of variance is captured by the first two principal components. This validates the use of PC1 and PC2 to visualize the data in the scatter plot. PC3 accounted for 1.9% of the variance.

#### 4.3.2: IAV-induced Differential Gene Expression Analysis.

Differential gene expression analysis quantifies the expression of genes discovered through computational analyses of raw RNA-seq data. It is critical to comprehend how gene expression levels vary across different experimental settings. It identifies which genes have a statistically significant difference and provides information on each gene's expression level (Costa-Silva et al., 2017; Monier et al., 2019). DEGs may be upregulated

or downregulated in one condition versus another. Filtering genes based on expression yielded 9672 out of the total genes identified in the RNA-seq analysis. A total of 3785 DEGs (1603 up-regulated and 2182 down-regulated) were found. Following final filtering, 2243 DEGs (910 up-regulated and 1333 down-regulated) were identified as having significantly different expression levels (Figure 4.6).

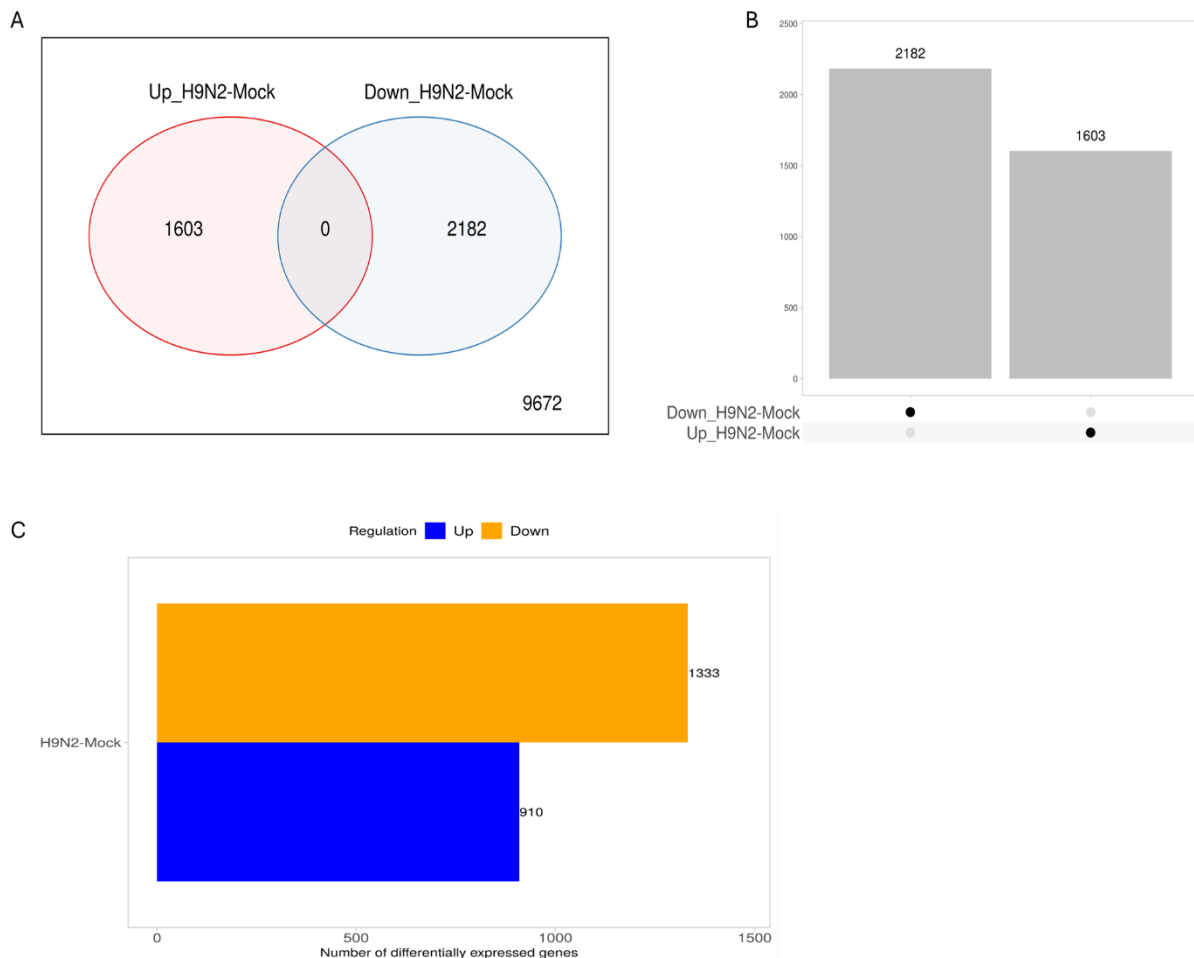


**Figure 4. 6 Differential Gene Expression Analysis of IAV-infected CEF cells.** This figure Summarizes the differential gene expression analysis comparing IAV-infected CEF cells to mock. The analysis quantified gene expression changes using RNA-seq data to identify DEGs. A-B) The RNA-seq analysis initially identified 9672 genes. After applying an initial filtering step, 3785 DEGs were obtained. The distribution of these DEGs is shown, with 1603 upregulated and 2182 downregulated in IAV-infected cells. The X-axis indicates the direction of gene expression change (upregulation or downregulation), and the Y-axis represents the corresponding number of genes. C) Following final filtering for statistical significance, 2243 DEGs were identified as having significantly different expression levels. Of these, 910 genes were upregulated, and 1333 genes were downregulated in IAV-infected CEF cells compared to mock-treated cells. This figure represents the final count of statistically significant DEGs used for further analysis.

### **4.3.3: IAV-induced Differential Gene Expression Analysis of Top 100 DEGs**

Heat map analysis for the top 100 DEGs in IAV treated CEF cells (Figure 4.7) showed that several genes including MX2, OAS1, IRF7, ISG15, CXCL10, IFIT3, MX1, IL8L2, IL1A, CSF3, TRIM22, ISG20, OASL, and CCL20, were upregulated in response to H9N2 infection. This upregulation suggests an activation of the host's antiviral response as these genes play crucial roles in antiviral defence mechanisms, such as interferon signalling, immune cell activation, and viral inhibition (Choi et al., 2015; Liu et al., 2011; Perng & Lenschow, 2018; Reddi et al., 2021; Zhang et al., 2023). For example, MX2 and MX1 are interferon-induced GTPases with antiviral activity, while IRF7 is a transcription factor that regulates the expression of interferon-stimulated genes (Moschonas et al., 2024; Ning et al., 2011).

Conversely, certain genes were downregulated in H9N2-treated samples, potentially indicating a disruption of cellular processes or a suppression of immune responses including, CXCL14, ITGBL1, ALK, COL12A1, CST6, SCEL, PCSK1, HTR1B, ACTG2, PTN, NPR3, FLBN5, TIMP3, MATN3, ENPEP, ACTC1, FAT3, DED3, COLBA1, TNFSF18, KRT18, which are involved in various cellular functions, including cell adhesion, extracellular matrix formation, signalling pathways, and cytoskeletal organisation (Ceron et al., 2024; Fan & Kassiri, 2020; Lu et al., 2016; Wang, 2020). Downregulation of these genes could impair cellular functions and compromise the host's ability to mount an effective immune response. The observed changes in gene expression patterns highlight the complexity of the host response to H9N2 infection. The upregulation of antiviral genes suggests that the host is actively attempting to combat the viral infection, while the

downregulation of certain genes may represent a trade-off between antiviral defence and cellular homeostasis.

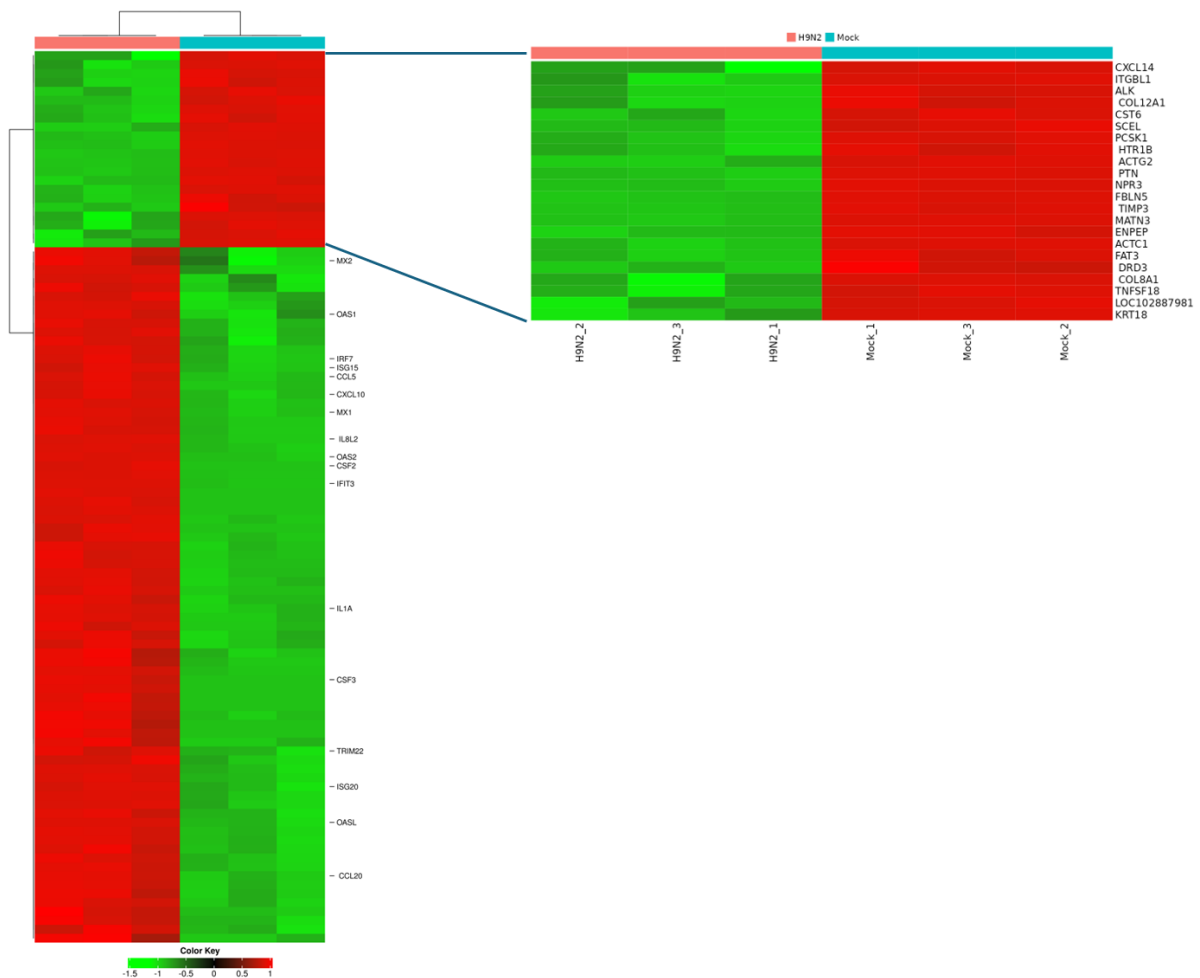


**Figure 4. 7 Comparison of Top 100 DEGs in Mock and IAV-treated CEF cells.** The heatmap visualisation of the top 100 DEGs in CEF cells following H9N2 infection. Red indicates upregulated genes, while green indicates downregulated genes, relative to mock controls. Notably, genes involved in antiviral defence, such as MX2, OAS1, and IRF7, are significantly upregulated, suggesting an activated host immune response. Conversely, downregulation of genes involved in cellular processes like cell adhesion and extracellular matrix formation may reflect a disruption of cellular functions during viral infection.

#### 4.3.4: IAV-induced Differential Gene Expression Analysis of PARP genes

Differential gene expression analyses were carried out on the RNA-seq data to better understand the changes in the expression patterns of various PARPs in the IAV-treated samples. A normalised histogram (Figure 4.8A) was used to show the difference in PARP

expression levels between the two biological samples. PARP14, PARP12, and PARP10, followed by PARP 9, showed a notable upregulation in the treated sample. However, PARP1, PARP3, and PARP4 were slightly downregulated in the treated sample and PARP 2 remained unaffected. A heat map of the top two thousand DEGs was also created (Figure 4.8B). Heat maps are used to visually represent gene expression patterns and clustering across samples. In heatmaps, data is represented by colours, with each cell representing a gene expression level. The rows represent different biological samples, while the columns represent gene expression levels. Colour intensity expresses gene expression level; for example, red indicates higher expression. The results show that five of the total PARPs are DEGs. In IAV-infected CEF cells, all five PARPs showed increased variability, with PARP14 having the highest variability among the five PARPs, followed by PARP9, PARP11, PARP12, and finally PARP10. These findings allow us to examine the expression of differentially expressed PARPs and their potential antiviral role in IAV-infected CEF cells.

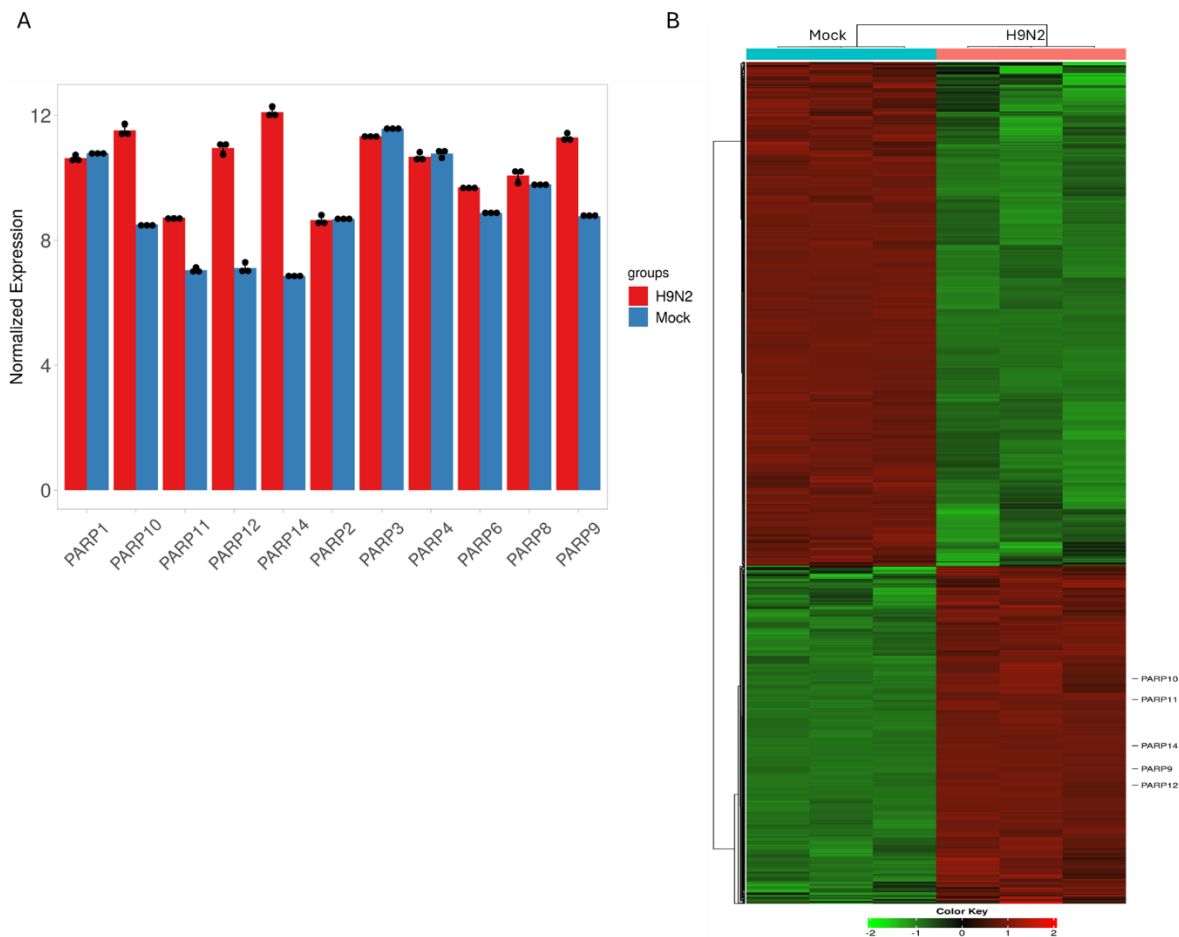


**Figure 4. 8 Comparison of differentially expressed PARP genes in mock and IAV-treated CEF cells.** A) Normalized histogram depicting the differential expression of PARP genes in IAV-infected CEF cells compared to mock controls. Notable upregulation is observed for PARP14, PARP12, and PARP10, followed by PARP9. Conversely, slight downregulation is evident for PARP1, PARP3, and PARP4, while PARP2 expression remains largely unchanged. B) Heatmap visualisation of the top two thousand DEGs in IAV-infected CEF cells. The X-axis represents the gene name, and the Y-axis represents the type of treatment administered. Notably, all five differentially expressed PARP genes (PARP1, PAR3, PARP4, PARP10, PARP14) exhibit increased variability in expression levels in the infected cells, with PARP14 demonstrating the highest level of variability.

#### 4.3.5: Volcano Plot Analysis Reveals Differential Expression of PARP Genes and Global Gene Changes in IAV-infected CEF Cells

Volcano plots are a powerful visual tool for analysing and comparing gene expression data between treatment groups. In the case presented, the volcano plots are used to examine the expression patterns of the PARP genes, which play crucial roles in various cellular processes. The y-axis of the volcano plot represents the negative base-10

logarithm of the adjusted p-value, indicating the statistical significance of the differences observed between the two treatment groups. As the data points move higher along the y-axis, the p-values decrease, signifying increasingly significant differences. The x-axis depicts the base-2 logarithm of the fold change, which reveals the magnitude of the differences in gene expression. Genes with extreme values on the x-axis, further away from the centre, exhibit more significant differences in their mean expression levels between the two groups (McDermaid et al., 2019).

The volcano plots in the description highlight several PARP genes that are differentially expressed between the treatment groups (Figure 4.9A). PARP14 stands out as the most significantly upregulated gene, with the highest  $\log_{10}$  value, indicating its strong upregulation and high statistical significance. This is followed by other PARP genes, such as PARP12, PARP10, PARP9, and PARP11, which are also shown to be upregulated and positioned on the right side of the volcano plot, represented by red data points. The upregulation of these PARP genes suggests their potential involvement in the biological processes underlying the treatment differences, potentially related to functions like DNA repair, cell signalling, transcriptional regulation, and immune responses.

The second volcano plot presented in the description broadens the analysis by revealing additional upregulated and downregulated genes outside the PARP family (Figure 4.9B). Downregulation of genes such as ACTG2, TIMP3, ACTA2, COL1A2, PTN, and ALDH1A1 has been observed, which may have an impact on various cellular processes such as cell motility, extracellular matrix remodelling, and cellular differentiation (Ceron et al., 2024; Fan & Kassiri, 2020; Sebastian et al., 2024; Wang, 2020). On the other hand, genes such as IL6, DHX58, IL8L2, and GSDME are significantly upregulated, which are involved in immune response, inflammation, and cell death pathways (Bourdon et al., 2020; Jiang et

al., 2020; Luo et al., 2018; Tanaka et al., 2014). The comprehensive analysis of these differentially expressed genes, both within and outside the PARP family, provides important insights into the underlying molecular mechanisms and cellular responses associated with the treatments under consideration.

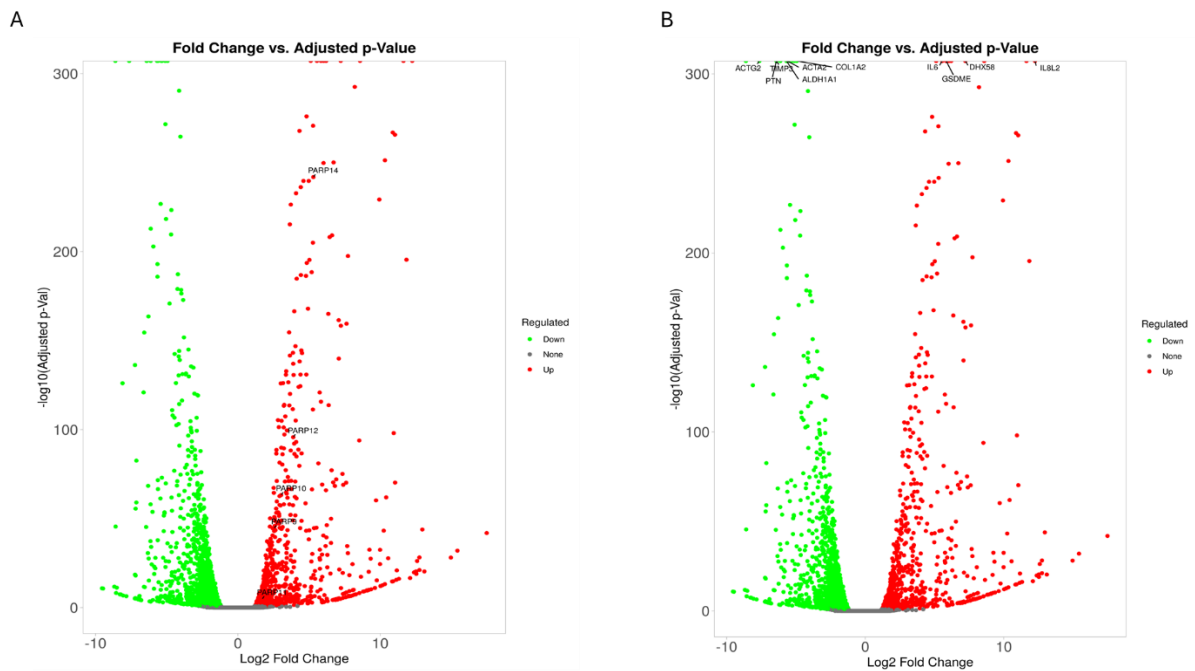


**Figure 4. 9 The volcano plot of differentially expressed genes in IAV-treated CEF cells.** A) This volcano plot displays the differential expression of PARP genes in IAV-infected CEF cells compared to mock-treated cells. The Y-axis represents the negative base-10 logarithm of the adjusted p-value ( $-\log_{10}(p\text{-value})$ ), indicating statistical significance. The X-axis represents the base-2 logarithm of the fold change ( $\log_2(\text{fold change})$ ), indicating the magnitude of gene expression change. Red data points signify upregulated PARP genes. PARP14 is the most significantly upregulated gene, followed by PARP12, PARP10, PARP9, and PARP11, suggesting their potential roles in the cellular response to IAV infection. B) This volcano plot shows the global differential gene expression between IAV-infected and mock-treated CEF cells. The axes are the same as in (A). Red data points indicate upregulated genes, and blue data points indicate downregulated genes. Upregulated genes include IL6, DHX58, IL8L2, and GSDME, associated with immune response, inflammation, and cell death. Downregulated genes include ACTG2, TIMP3, ACTA2, COL1A2, PTN, and ALDH1A1, involved in cell motility, extracellular matrix remodelling, and cellular differentiation. This plot provides a comprehensive overview of the gene expression changes induced by IAV infection.

#### 4.3.6: PARP-Related Pathways Dominate the Cellular Response to IAV infection

The lollipop chart illustrates the biological pathways significantly altered during IAV infection in CEF cells, showcasing statistical measures for each identified pathway (Figure 4.10). The dot plot reveals the number of genes, fold enrichment, and  $-\log_{10}$  False Discovery Rate (FDR) for various pathways. Notably, pathways like cellular response to chemical stimulus, extracellular region, and those related to immune system regulation and development, along with NAD<sup>+</sup> ADP-ribosyltransferase activity, exhibit the highest statistical significance ( $-\log_{10}$ (FDR) of 6). While cellular response to chemical stimulus and extracellular region involve the most genes with a fold enrichment around 2, and immune system-related pathways have 60 genes with approximately 2.5-fold enrichment, the NAD<sup>+</sup> ADP-ribosyltransferase activity pathway, despite having the fewest genes, demonstrates the highest fold enrichment of ~14. This strong enrichment of the NAD<sup>+</sup> ADP-ribosyltransferase activity pathway, linked to PARP proteins, strongly suggests a crucial role for PARPs in the cellular response to IAV infection.

In addition to these major pathways, the lollipop chart highlights a number of other biological processes that are activated in response to IAV infection, such as response to external stimuli, response to other organisms, cellular response to cytokine stimulus, inflammatory response, immune response, and stress response. These diverse pathways underscore the multifaceted and interconnected nature of the cellular response to viral infection, as the host cells mount a comprehensive defence involving various signalling molecules, immune modulators, and cellular adaptations. Overall, the lollipop chart provides a compelling visual snapshot of the complex and dynamic biological landscape within IAV-infected CEF cells, revealing the intricate web of pathways and gene expression patterns that underlie the host cell's attempt to combat

the viral threat. This detailed information can inform our understanding of the host-pathogen interactions and potentially guide the development of more effective therapeutic strategies against influenza infections.

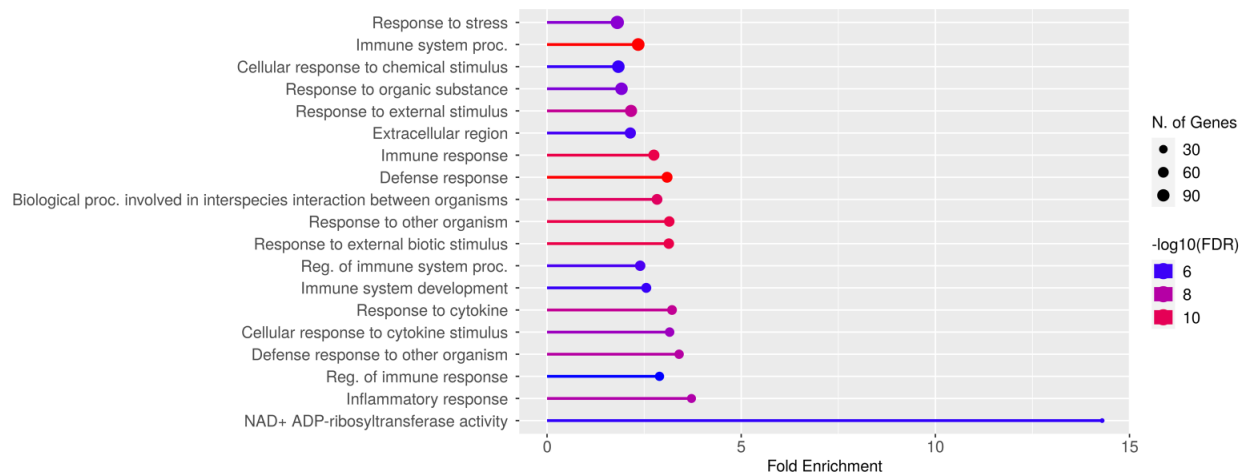


**Figure 4. 10** The lollipop chart for cells infected with IAV provides a compelling visual representation of the various biological pathways at play. It highlights the cells efforts to combat the viral infection. Each lollipop represents a significantly enriched biological pathway, with the horizontal position indicating the fold enrichment. The size of the dot corresponds to the number of genes within that pathway, and the color intensity reflects the statistical significance, represented by  $-\log_{10}(\text{FDR})$ . The NAD+ ADP-ribosyltransferase activity pathway shows the highest fold enrichment ( $\sim 14$ ), and highest statistical significance ( $-\log_{10}(\text{FDR}) = 6$ ), despite having fewer genes, strongly implicating PARP proteins in the cellular response to IAV infection. The chart also highlights other activated pathways such as response to external stimulus, Response to other organism, immune system development, and various immune and inflammatory response categories, illustrating the comprehensive and interconnected nature of the host cell's defense mechanisms against viral infection. This analysis provides insights into the key biological processes modulated during IAV infection in CEF cells, potentially informing the understanding of host-pathogen interactions and the development of therapeutic strategies.

#### 4.3.7: Confirmation of the Transcriptomics with conventional RT-PCR

To validate the transcriptomic data obtained from RNA-seq analysis, RT-qPCR was performed on cells transiently expressing various PARP family members and subsequently infected with H9N2 virus. This approach allowed for a quantitative assessment of gene expression levels at the mRNA level (Wagner, 2013).

The RT-qPCR results confirmed the upregulation of several PARP family members observed in the transcriptomic analysis (Figure 4.11) Specifically, PARP3, 5, 4, 7, 8, and 11 exhibited minimal or negligible changes in expression levels, as indicated by their low  $\Delta\Delta C_t$  values (less than 0.5). This suggests that these PARPs may not be significantly influenced by H9N2 infection in the context of transient overexpression. In contrast, PARP1, 6, 9, and 12 showed slightly higher  $\Delta\Delta C_t$  values, indicating a modest upregulation in expression. This suggests a potential role for these PARPs in the cellular response to H9N2 infection. However, the most significant upregulation was observed for PARP14, with a  $\Delta\Delta C_t$  value of 1.6. This finding strongly corroborates the transcriptomic data and further emphasizes the crucial role of PARP14 in the host response to H9N2 infection.

**Table 4. 1 Primers Used for RT-qPCR Validation of PARP Expression**

PARP	F-Primer	R-Primer
PARP1	AGCTAAACTGCAAGAGCGGT	CCCCCACAATAGAAGCGGT
PARP3	ACACCCTGATCGAAGTGACAG	GTGGTCTCATCCAAGGCACA
PARP4	AGGGCCATGCTGTCATCCAGAGAG	CTGTTTTCCAGCTGAGCAACCCCC
PARP5b	AGTTGTCAATCTCCTCTGCGGCA	GTCCGGATGGTTGTTTCAGCACC
PARP6	GGACGATGACTCCGATGGGGACAA	CGCTGTAGATCTCCTTCACGGCCT
PARP7	TGTCCCAGCTCCAGCTCCAACACTAC	CCAGGTAACGAAGCGGACCTCCTT
PARP8	ACCGTGGCTTCTTGTCAGACTA	TCACAAACGGTGGGCCTCAGCATA
PARP9	TATCAAGTCCGTGGCTATCCGGC	TGGATCTCCTTGAGGCAGCTTGGC
PARP11	TGCTGCTGTATATGAAAAGGGACC	CTGGTTTGTGCAAATGAGGCTGCA
PARP12	AGCCTCCTCTGTGACCAAACCACC	GCTTACAGTGGCAGCTGCTCGATC
PARP13	CACCTCATGGGCAGGTGCAGTCTG	TGGAGAAGCAGGATTCGCAGCTCA
PARP14	GCGCAAGAAGCTGCTGCTCTACTT	TCTCAAGGACCTGCTGCTTACAGT

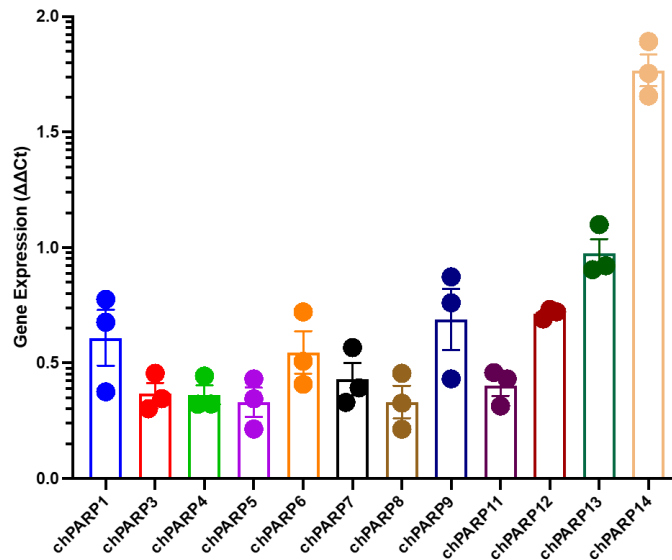


**Figure 4. 11 Validation of PARP Expression by RT-qPCR.** The analysis revealed that several PARP family members, including PARP3, 5, 4, 7, 8, and 11, exhibited minimal or negligible changes in expression levels ( $\Delta\Delta Ct < 0.5$ ) following H9N2 infection in the context of transient overexpression. PARP1, 6, 9, and 12 showed a modest upregulation with slightly higher  $\Delta\Delta Ct$  values. Notably, PARP14 demonstrated the most noticeable upregulation, with a  $\Delta\Delta Ct$  value of 1.6, strongly supporting the findings from the transcriptomic analysis and highlighting a potential crucial role for PARP14 in the host response to H9N2 infection. The  $2^{-\Delta\Delta Ct}$  method was used to calculate relative gene expression levels, which were then normalised to GAPDH. The data represents the mean  $\pm$  SEM of three independent experiments.

#### 4.3.8: Cellular Localisation of Chicken PARPs

The cellular localisation of several chPARPs transfected into the cells provides valuable insights into the subcellular distribution and potential functions of the encoded proteins.

The DF1 cells were transfected with mammalian expression plasmids encoding PARP genes followed by immunofluorescence 24 hours post-transfection. Cellular distribution of analysis of all PARP proteins showed that PARP1 was exclusively localized within the nucleus, suggesting the encoded protein likely functions in a nuclear-specific capacity, perhaps regulating gene expression or participating in nuclear processes, consistent with its DNA repair function (Figure 4.12). In contrast, PARP3 exhibited a dual localization, being present in both the nucleus and the cytoplasm, hinting at a more versatile role for its encoded protein that involves shuttling between these two cellular compartments.

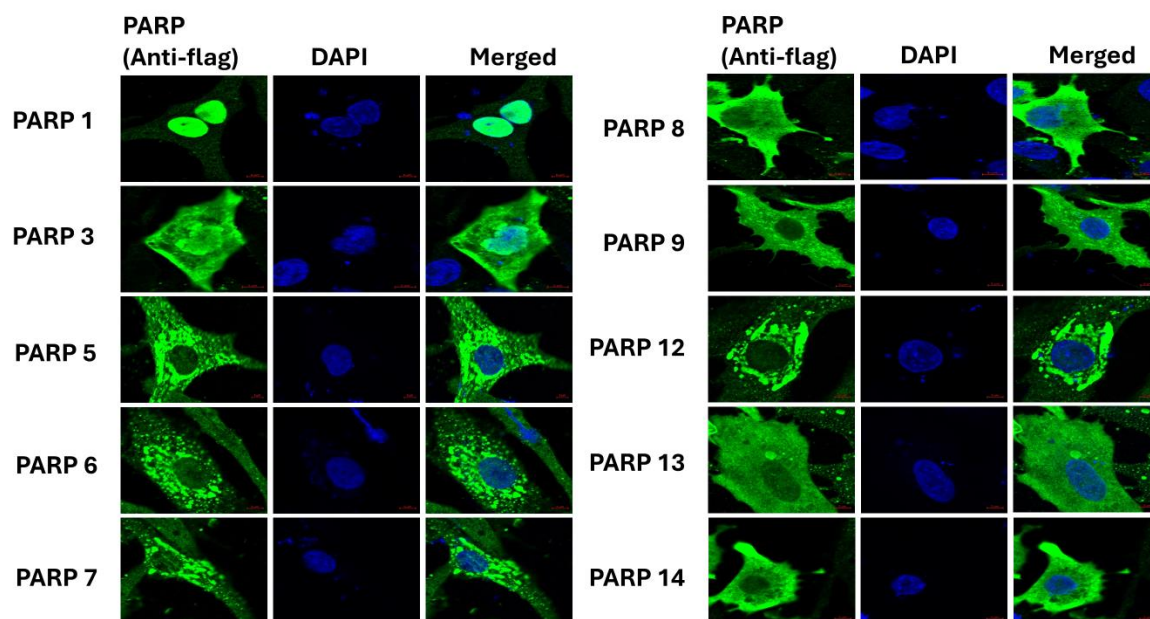


**Figure 4.12 Cellular Localisation of chPARPs in DF1 cells** depicts the subcellular localization of various chPARPs in DF1 cells. PARP1 was observed exclusively within the nucleus, suggesting a functional role in nuclear processes such as DNA repair and gene regulation. In contrast, PARP3 exhibited a dual localization, present in both the nucleus and cytoplasm, implying a more versatile role potentially involving shuttling between these compartments. PARP5, 6, 7, 8, 9, 12, 13, and 14 all demonstrated cytoplasmic localization, indicating their involvement in cytoplasmic functions such as signaling or protein trafficking.

On the other hand, PARP5, 6, 7, 8, 9, 12, 13, and 14 all showed cytoplasmic localization, implying their encoded proteins function primarily in the cytoplasm, potentially participating in signalling cascades, protein trafficking, or other cytoplasmic processes. The consistent cytoplasmic distribution of these proteins suggests a common theme or related functionality among the encoded proteins. Interestingly, PARP4 and 11 did not produce any detectable signal, indicating the encoded proteins may not have been expressed or were present at levels too low to be observed in this assay. Overall, this data provides a snapshot of the diverse subcellular localization patterns exhibited by the proteins encoded by these chPARPs, hinting at their varied functional roles within the cell.

#### **4.4: Discussion**

This study provides a comprehensive RNA-seq analysis of CEF cells infected with IAV, revealing the intricate transcriptional changes that accompany viral infection. A crucial first step was the meticulous normalization of the RNA-seq dataset, addressing potential biases and variances that can significantly impact downstream analyses (Crist et al., 2021; Mezencev & Auerbach, 2020). As highlighted by several studies, proper normalization is essential for accurate differential gene expression analysis, ensuring that observed changes reflect genuine biological effects rather than technical artifacts (Anders, 2010; Dillies, 2013). The increased dispersion observed in IAV-treated samples, evidenced by the density and dispersion estimation plots, aligns with the expected dynamic transcriptional response of infected cells, reflecting the activation of diverse cellular pathways to combat viral invasions (Love et al., 2014).

To gain a holistic understanding of the transcriptional changes induced by IAV infection, we employed PCA. The PCA results revealed a clear separation between the mock and IAV-infected samples, with the biological replicates within each group tightly clustered together. This observation confirmed the robust and reproducible nature of the transcriptional signatures associated with viral infection, as opposed to the homogeneous expression profiles observed in the uninfected control samples. Building upon the normalized data and the insights gleaned from the PCA, we proceeded to perform a comprehensive differential gene expression analysis. This computational approach identified a substantial number of DEGs, with over 3,700 genes showing significant upregulation or downregulation in response to IAV infection. Further scrutiny of the DEG list revealed that several members of the PARP family, which play crucial roles in diverse cellular processes, were among the most prominently upregulated genes. The

volcano plots were used to visually highlight the magnitude and statistical significance of these PARP gene expression changes, with PARP14 emerging as the most significantly upregulated PARP in the IAV-infected CEF cells.

Gene Ontology (GO) enrichment analysis, presented through a lollipop chart, revealed the activation of key biological pathways, including immune system-related processes, stress responses, extracellular signaling, and inflammatory pathways. These findings are consistent with the established understanding of host responses to viral infections, where the activation of immune defense mechanisms and the modulation of cellular signaling pathways are crucial for viral clearance (Medzhitov, 2008; Iwasaki & Medzhitov, 2015). The significant enrichment of NAD<sup>+</sup> ADP-ribosyltransferase activity, associated with PARP proteins, further underscores the central role of PARPs in the cellular response to IAV. To further validate the RNA-seq findings, we performed RT-qPCR analysis on a subset of PARP family members. This technique allowed us to quantitatively assess the expression levels of these genes at the mRNA level. Consistent with the RNA-seq data, RT-qPCR confirmed the upregulation of PARP14. Additionally, we observed a modest upregulation of PARP1, 6, 9, and 12, suggesting their potential involvement in the antiviral response. Interestingly, PARP3, 5, 4, 7, 8, and 11 exhibited minimal or negligible changes in expression levels, indicating that these PARPs may not play a significant role in the host response to IAV infection in the context of transient overexpression. This degree of verification is critical since RNA-seq can sometimes produce false positives. Differences in expression patterns of different PARPs may reflect context-specific roles or limitations in the temporary overexpression test.

The discovery that PARP1 localises solely in the nucleus, PARP3 has dual localisation, and PARP5, 6, 7, 8, 9, 12, 13, and 14 localise in the cytoplasm sheds light on their

probable functional roles. This is consistent with known PARP functions, such as involvement of PARP1 in DNA repair and transcriptional control within the nucleus (Lord & Ashworth, 2017). The cytoplasmic localisation of other PARPs indicates their involvement in cytoplasmic signalling pathways, presumably in response to viral infection. The absence of a detectable signal for PARP4 and 11 could imply low expression levels or a requirement for specific activation signals.

In conclusion, this study has provided a complete picture of the transcriptional landscape in IAV-infected CEF cells, emphasising the importance of PARPs, notably PARP14, in the host's antiviral response. The combination of RNA-seq, RT-qPCR, and cellular localisation data has resulted in a thorough and comprehensive understanding of the cellular responses induced by IAV infection. These discoveries not only increase our understanding of host-pathogen interactions but also open the door to investigating PARPs as possible therapeutic targets for influenza infections. The insights gleaned from this chapter, coupled with the bioinformatic analysis presented in Chapter 3, not only advance our fundamental knowledge of host-pathogen interactions but also enabled us to screen several chPARPs and identify PARP14 as a promising candidate for further investigation in the context of H9N2 infection.

#### **4.5: Conclusion**

In conclusion, this comprehensive RNA-seq analysis has provided invaluable insights into the intricate transcriptional landscape and cellular responses elicited by IAV infection in CEF cells. Through meticulous normalization and rigorous statistical

analyses, we have identified a significant number of differentially expressed genes (DEGs) and elucidated the underlying biological processes that are activated or repressed during viral infection.

The upregulation of several PARP family members, particularly PARP14, highlights their potential role in the antiviral response. Additionally, the enrichment of immune response pathways, stress response mechanisms, and inflammatory processes underscores the host's concerted effort to combat viral infection.

These findings not only deepen our understanding of host-pathogen interactions but also offer potential therapeutic targets for the development of novel antiviral strategies against influenza infections.

**Chapter 5: PARP14 Protein of  
chicken and human Display  
Antiviral Effects Against Influenza  
A viruses**

## 5.1: Abstract

This study investigates the role of chicken PARP14 (chPARP14) in antiviral responses against influenza A virus (IAV). For this purpose, we cloned and expressed full length chPARP14 and various domains of chPARP14 in DF1 cells to examine their localisation and antiviral efficacy and to compare them with their human counterparts' expression in human embryonic kidney (HEK) cells. Our results demonstrate that chPARP14 is primarily localized in the cytoplasm and exhibits antiviral activity against IAV. Structurally, the macrodomain of chuPARP14 played a crucial role in its cytoplasmic localization and antiviral function. Furthermore, we identified specific chuPARP14 constructs (full length chPARP14 and chPARP14 $\Delta$ CWC, that significantly reduced viral replication, suggesting their potential as therapeutic targets. These findings provide valuable insights into the antiviral mechanisms of chPARP14 and highlight its potential for the development of novel antiviral strategies against the IAV infections in chicken.

## 5.2: Introduction

Poly ADP-ribose polymerases (PARPs) are a group of enzymes that play important roles in various cellular processes, including DNA repair, inflammation, cell death and many more (Zhu et al., 2021). PARP14 has emerged as a protein of great interest due to its multiple functions and potential involvement in a variety of diseases (Archimede Torretta 2023). PARP14 is the largest protein (1823 a.a) amongst chPARP family members and is only active in mono-ART. PARP14 is also known as B-cell aggressive lymphoma 2 (BAL2) and CoaST-6 (Parthasarathy & Fehr, 2022). PARP14 is distinguished by its distinct domain

structure comprising RRM domains, a Macro domain, a D-domain, a WWE domain, and a catalytic domain. The Macro domain is known to bind ADP-ribose, a modification that aids in DNA repair and inflammation and the WWE domain is thought to mediate protein-protein interactions, which implies a role in regulatory pathways (Al-Rahahleh et al., 2023; Z. Li et al., 2023).

As a macro-PARP, it belongs to a unique group that includes PARP9 and PARP15, both of which have multiple macrodomains (MD) (Fehr et al., 2020). These MDs are distinguished by their ability to bind MARylates but not PARylated proteins. PARP14 macrodomains can interact with STAT6 to promote IL-4-induced gene expression and are known to enhance IL-4-induced gene expression by interacting with STAT6, functioning as a transcriptional co-activator (Dukic et al., 2023; Mentz et al., 2022). To maintain gene silencing in the absence of IL-4, the PARP14 protein binds to histone deacetylases 2 and 3 (HDAC2 and HDAC3) as well as IL-4 responsive promoters (Parthasarathy & Fehr, 2022). In response to IL-4 stimulation, STAT6 binds to its target genes, activating PARP14 catalytically (Parthasarathy & Fehr, 2022). The macrodomain1 of PARP14 is an ADP-ribosyl glycohydrolase that catalyses the removal of ADPr from the MARylated proteins and functions more efficiently when combined with the remaining macrodomains (Dukic et al., 2023; Torretta et al., 2023).

### **5.2.1: Impact of PARP14 on Viral Replication and Host Responses**

PARP14 has been shown to interact with viral proteins, influencing their replication and in some cases, PARP14 activity is required for efficient viral replication (Parthasarathy & Fehr, 2022). For example, in certain herpesviruses, PARP14 is essential for viral genome

replication and capsid assembly (Malgras et al., 2021; Zhu et al., 2021). PARP14 also plays a crucial role in the host's response to viral infection and it can be activated by viral components or cellular stress induced by infection (Parthasarathy & Fehr, 2022; Zhu et al., 2021). Activated PARP14 catalyses the addition of ADP-ribose units to target proteins, which can have an array of effects, such as gene expression regulation, DNA repair, and cell death (Malgras et al., 2021; Parthasarathy & Fehr, 2022). PARP14-mediated ADP-ribosylation can alter transcription factor activity, resulting in changes in gene expression patterns that are critical for antiviral responses (Zhu et al., 2021). PARP14 is involved in DNA repair pathways, and its activation can help to the repair DNA damage caused by viral infection or the host's immune response. In some cases, excessive PARP14 activity can cause cell death, which can be beneficial or detrimental to the host depending on the context of the infection (Dukic et al., 2023; Morone & Grimaldi, 2024).

### **5.2.2: Implications for Antiviral Therapies**

Understanding the role of PARP14 in viral infections has potential implications for the development of novel antiviral therapies. For example, inhibitors of PARP14 could be explored as potential antiviral agents, particularly for viruses that rely on PARP14 for their replication. Additionally, targeting PARP14 might be useful for modulating the host's response to viral infection, such as by enhancing antiviral gene expression or reducing inflammation.

In summary, PARP14 is a multifaceted enzyme that plays a significant role in viral infections. Its involvement in both viral replication and the host response makes it an attractive target for antiviral research. Further studies are needed to fully elucidate the

mechanisms by which PARP14 influences viral infections and to explore its potential as a therapeutic target.

The aim of this study is to investigate the antiviral role of chPARP14 against IAV infection and to elucidate the mechanisms underlying their antiviral activity.

Specifically, the study aims to:

1. Characterize the subcellular localization of different chPARP proteins to understand their potential functions within the cell.
2. Determine the antiviral efficacy of individual chPARP proteins against IAV infection.
3. Identify the specific domains or regions of chPARP14 that are responsible for their antiviral activity.
4. Investigate the molecular mechanisms by which chPARP14 exert their antiviral effects.
5. Explore the potential of chPARP14 as therapeutic targets for the treatment of IAV infection.

Understanding the role of PARP14 in IAV infection has potential therapeutic implications. For example, inhibitors of PARP14 could be explored as potential antiviral agents. By blocking PARP14 activity, it might be possible to interfere with viral replication or reduce the severity of the host's immune responses. Additionally, targeting PARP14 might be useful for modulating the inflammatory response during IAV infection, potentially reducing tissue damage, and improving patient outcomes.

## 5.3: Results

### 5.3.1: Determining the Antiviral Efficacy of Several chPARP Proteins

To determine the antiviral efficacy of various chPARP proteins, DF1 cells were transfected with plasmids expressing chPARP protein-encoding genes. After 24 hours, the transfected cells were infected with AIV H9N2 strain at a MOI of 1.0. The subsequent formation of plaque-forming units (PFUs) was measured to assess the antiviral efficacy of different chPARP proteins. Statistical analysis revealed that chPARP1, 7, 8, 9, 11, 12, 13, and 14 exhibited a higher degree of significance in their antiviral activity. In contrast, chPARP3 and chuPARP6 demonstrated the lowest significance. Interestingly, chuPARP4 and chuPARP5 were found to be statistically non-significant (Figure 5.1).

When examining the virus plaque-forming units (PFU), an intriguing pattern was observed. chPARP3 and chPARP5 produced more PFUs than the control, indicating they may have limited or even impaired the antiviral response. However, the remaining chPARPs, except for chPARP4, all demonstrated reduced PFU counts relative to the control, suggesting they were effective in restricting viral replication and spread. Among these, chPARP13 exhibited the lowest PFU count, followed by chuPARP8, 11, and 12, which had comparable PFU levels. chPARP7 and chPARP14 also showed comparable, but moderately low PFU counts.

The findings highlight the complex and nuanced nature of the host's antiviral defences, which confirm that chPARP proteins play a prominent role in conferring protection from viral infection, while others may even inadvertently facilitate viral proliferation. The observed variations in antiviral efficacy might be attributed to factors such as the specific

mechanisms of action of these proteins, their interaction with viral components, or differences in their expression levels.

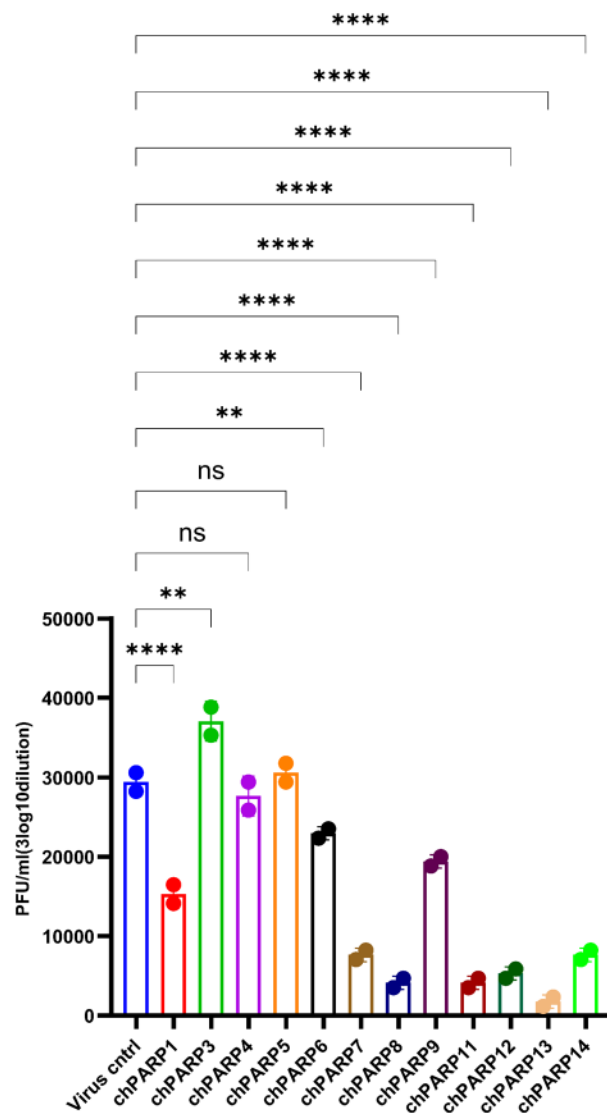


**Figure 5. 1 Antiviral Efficacy of chPARP Proteins.** This bar graph compares the antiviral activity of various chPARP proteins against IAV H9N2. The formation of plaque-forming units (PFUs) was measured to assess the antiviral efficacy. Statistical analysis revealed that chPARP1, 7, 8, 9, 11, 12, 13, and 14 exhibited significant antiviral activity, while chPARP3 demonstrated the lowest significance, coupled with increased PFU counts compared to the control, suggesting potential impairment of the antiviral response. Proteins 4 and 5 were found to be non-significant. The remaining proteins, with the exception of chPARP6, effectively restricted viral replication and spread, as evidenced by reduced PFU counts.

### 5.3.2: Summary of chPARPs Characteristics

A comprehensive overview of the various chPARP proteins and their key properties are outlined in Table 5.1. The cellular localisation of these proteins was determined using immunofluorescence assays, revealing their distribution within cells. Surprisingly, the data show that the various chPARP variants have diverse subcellular localisations, with some concentrated in the nucleus and others distributed throughout the cytoplasm. This suggests that individual chPARP proteins may play specialised roles within the cell depending on their physical location. The table also includes the subcellular localisation of human PARP proteins. While most PARPs exhibit similar localization patterns in both species, notable exceptions exist. For example, PARP5b and PARP7, which exhibit cytoplasmic localization in chicken, demonstrate both cytoplasmic and nuclear localization in humans. Furthermore, PARP8, primarily cytoplasmic in chicken, exhibits nuclear envelope localization in humans. These species-specific differences in PARP localization suggest potential variations in their functions and interactions with cellular components, highlighting the importance of considering species-specific contexts when investigating PARP biology.

The table also explores the antiviral and proviral properties of the chPARP enzymes in relation to the H9N2 influenza virus strain. Using plaque assays, we were able to determine the impact, either inhibitory or facilitative, that each chPARP has on the replication and spread of this particular viral pathogen. Certain chPARP variants appear to have a protective, antiviral effect, while others may inadvertently promote viral proliferation, underscoring the nuanced and multifaceted nature of this host-pathogen dynamic.

Finally, the table delves into the nuclear localization of the chPARP proteins, as determined by in silico tools (the <http://www.moseslab.csb.utoronto.ca/>). This computational analysis provides further insights into the sub-nuclear distribution and potential functions of these enzymes, which are known to be intimately involved in DNA repair, transcriptional regulation, and other critical nuclear processes. The varying degrees of nuclear enrichment observed across the chPARP family suggest that each member may have evolved to specialize in distinct nuclear activities, contributing to the cell's overall genomic integrity and regulatory capacity.

Taken together, this concise yet information-rich table offers a valuable snapshot of the chPARP system, illuminating its diverse cellular roles, antiviral properties, and nuclear dynamics – all of which are crucial for understanding the complex host-pathogen interactions at play within avian species.

**Table 5. 1** Localisation and Antiviral/Proviral Nature of chPARPs.

chPARP	Subcellular localisation	Virus targeted	Antiviral/proviral	NLS (moseslab)	huPARP subcellular localisation	References
Parp1	Only Nucleus	IAV	Anti	206-233	Nuclear	(Gibson and Kraus 2012)
PARP3	Nucleus & cytoplasm	IAV	Pro	none	Nuclear	(Gibson and Kraus 2012)
PARP4		IAV	Anti	1421-1427	Cytosolic	(Gibson and Kraus 2012)
PARP5b/ TNKS2	Cytoplasm	IAV	NS	None	Nuclear and cytosolic	(Gibson and Kraus 2012)
PARP6	cytoplasm	IAV	Anti	None		
PARP7/ TiPARP	cytoplasm	IAV	Anti	None	Nucleus and subnuclear foci	(Sanderson and Cohen 2020)
PARP8	cytoplasm	IAV	Anti	None	Nuclear envelope	(Vyas, Chesarone-Cataldo et al. 2013)
PARP9	Cytoplasm	IAV	Anti	None	Plasma membrane	(Vyas, Chesarone-Cataldo et al. 2013)
PARP11		IAV	Anti	None	Nuclear envelope	(Sanderson and Cohen 2020)
PARP12	Cytoplasm	IAV	Anti	31-83	cytosolic	(Gibson and Kraus 2012)
PARP13/ZC3HAV1	cytoplasm	IAV	Anti	None	cytosolic	(Gibson and Kraus 2012)
				216-224		
PARP14	Cytoplasm	IAV	Anti	1352-1364		
				1576-1587		

### 5.3.3: Rationale for Mechanistic Investigation of chPARP14.

#### 5.3.3.1: A Versatile MARYlation Protein

PARP14 is a highly versatile and multifunctional MARYlation protein with a pivotal role in various biological processes. Its unique structure, characterized by distinct domains, enables it to participate in a wide range of cellular pathways.

At its core, it possesses five distinct domains that work in concert to facilitate its diverse functions (Figure 5.2). Two RNA recognition motif (RRM) domains reside on the N-terminus, which facilitate interactions with RNA molecules, suggesting a potential role in gene regulation or RNA processing (Maris et al., 2005). Additionally, three macrodomains specialize in binding ADP-ribose, a crucial post-translational modification associated with MARYlation that influences numerous cellular activities. Macrodomains are crucial

for recognizing and interacting with ADP-ribosylated proteins, playing a role in both MARYlation and de-MARYlation processes (Challa et al., 2021; Fehr et al., 2018). Moving down the protein structure, chPARP14 also contains a WWE domain responsible for mediating protein-protein interactions, allowing it to form complexes with other proteins, expanding its functional repertoire and enabling it to participate in diverse cellular pathways (Munzker et al., 2024). Importantly, it also houses a catalytic domain that confers its MARYlation capabilities, allowing it to covalently attach single ADP-ribose moieties onto target proteins, thereby modulating their behaviour (Hoch & Polo, 2019; van Beek et al., 2021). Lastly, it features a D-domain with an as-yet-unknown function, hinting at even more undiscovered regulatory roles for this remarkable protein.

The PARP14 serves an array of functions, emphasising its importance in a number of biological pathways. It aids the host immune system in fighting SARS-CoV and HSV-1 infections and is likely involved in antiviral mechanisms by targeting viral proteins for MARYlation, resulting in their inactivation or degradation (Parthasarathy et al., 2024). It functions as a molecular switch, controlling IL-4-dependent gene transcription, implying that it can affect the expression of genes involved in immune responses and inflammation. PARP14 controls STAT6-dependent gene expression in B cells, a transcription factor involved in B cell differentiation and antibody production, modulating STAT6 activity and influencing B cell function and immune responses (Riley et al., 2013).

PARP14 has also been implicated in the survival of multiple myeloma cells, prostate cancer cells, and hepatocellular carcinoma cells, suggesting its potential contribution to tumorigenesis or cancer progression by promoting cell survival and proliferation (Barbarulo et al., 2013; Parthasarathy & Fehr, 2022).

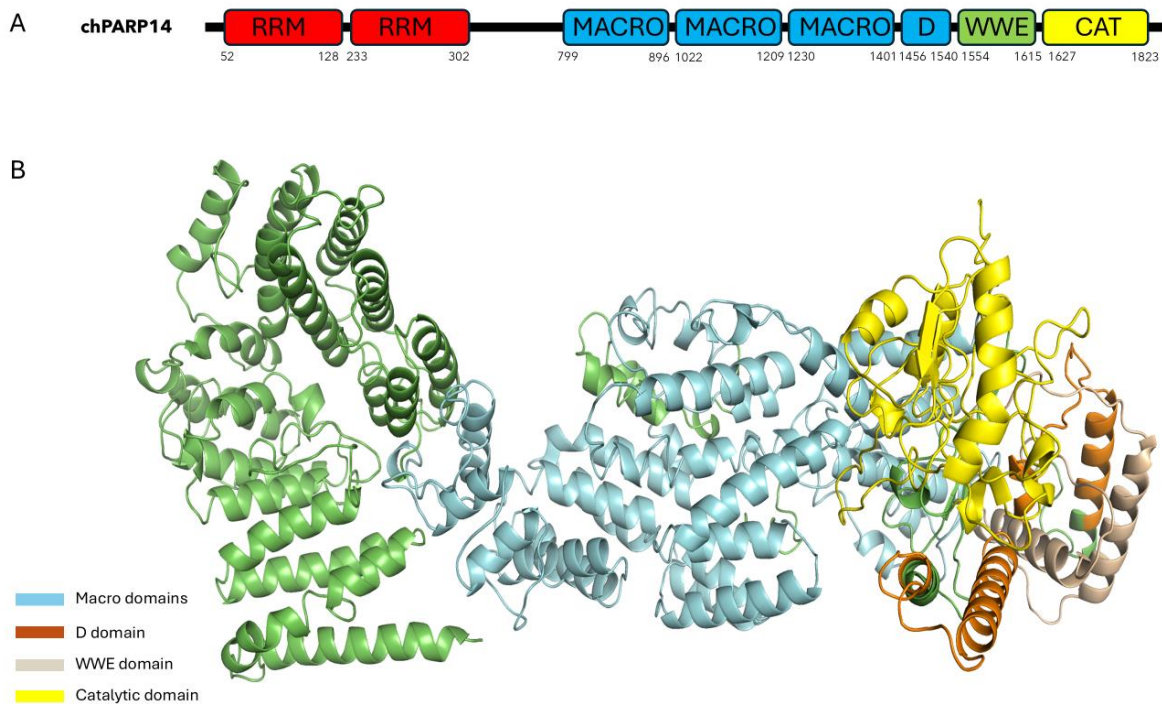


**Figure 5. 2 Structural Prediction of chPARP14.** A) Domain organisation of chPARP14. B) predicted 3D structure of the chPARP14.

### 5.3.3.2: PARP14: A Promising Candidate for Antiviral Studies against Influenza A Virus

The decision to prioritize PARP14 over other PARPs in IAV infection studies is influenced by several factors: The PARP14 showed the highest evolutionary divergence. It exhibits only around 50% sequence identity with its human counterpart, making it one of the PARPs with the least percentage identity across the entire group under investigation. This high level of evolutionary divergence is particularly pronounced within the avian species. Lower sequence identity of chPARP14 with its human counterpart suggests a greater degree of functional specialization. This divergence could have led to the acquisition of unique antiviral mechanisms that are not observed in other PARP proteins. Notably, it

displays remarkably upregulated mRNA levels, with the highest fold changes observed among all the PARPs when CEF cells were treated with IAV. The significant transcriptional response suggests its involvement in the host's antiviral defence against IAV infection. Indeed, previous studies have demonstrated antiviral activities of PARP14 (Parthasarathy et al., 2024; Tauber et al., 2021). Finally, while previous studies have explored PARP14 antiviral properties in other contexts, its specific role in IAV infection remains uncharted territory. This presents a unique opportunity to uncover novel antiviral mechanisms. This makes it a prime candidate for further investigation.

#### **5.3.4: The Importance of Cloning Gene Fragments to Understand Antiviral Responses**

To study and understand the impact of PARP14 and its domains on IAV replication, we cloned PARP14 and its various domains into the EGFP-Flag-C1-ku70 mammalian expression vector.

Cloning gene fragments is a powerful technique for understanding antiviral proteins. By isolating specific regions of these complex proteins, we can pinpoint functional domains responsible for protein interactions, enzymatic activity, and cellular localization. This approach allows analysing the specific roles of individual domains in antiviral pathways, such as viral recognition, signalling, and effector functions. Additionally, introducing mutations into specific domains enables the study of their effects on protein function and antiviral activity, revealing critical residues or regions involved in antiviral responses and potential therapeutic targets. This knowledge is essential for understanding the intricate mechanisms of antiviral defence and developing innovative strategies to combat viral infections (Gack et al., 2007; Gurevich, 2019). If a specific domain is

discovered to be required for viral replication or pathogenesis, it can be targeted in the development of antiviral drugs or therapeutic interventions. Comparing the sequences and structures of gene fragments from different species can reveal information about a gene's evolutionary history and how its function has changed over time. This information can aid in identifying conserved regions that are required for antiviral responses.

### 5.3.5: Cloning of chPARP14 Constructs into pEGFP-C1-FLAG-ku70 Expression Vector

The cloning of PARP14 constructs into the pEGFP-C1-FLAG-ku70 expression vector was designed to study the specific functions of PARP14 domains (Figure 5.3).

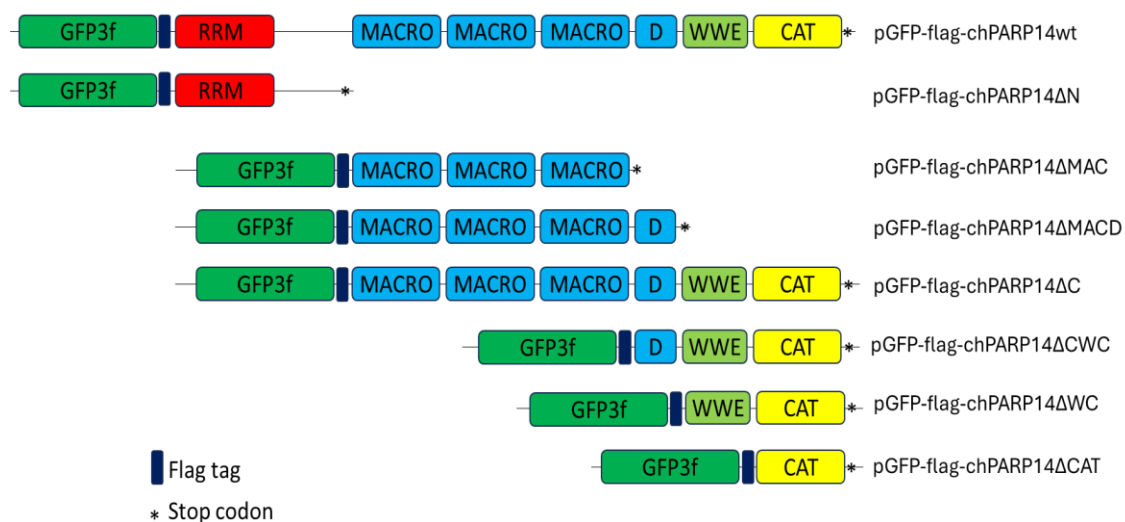


**Figure 5. 3 Structure basis for Primer Designing.** Design of primers based on the domain structure for cloning chPARP14 into EGFP-FLAG-C1-ku70 mammalian expression vector.

The pEGFP-C1-FLAG-ku70 vector is a versatile expression vector that allows for the expression of proteins with an N-terminal EGFP tag and a C-terminal FLAG tag. The EGFP tag can be used to visualize protein expression and localization, while the FLAG tag can be used for protein purification and detection. The pEGFP-C1-FLAG-ku70 backbone is a

valuable tool for the study of protein function. The EGFP tag allows for the visualization of protein expression and localization, which is important for understanding the role of a protein in cellular processes. The FLAG tag can be used for protein purification and detection, which is important for biochemical and structural studies.

In addition, the pEGFP-C1-FLAG-ku70 backbone contains a multiple cloning site (MCS) that allows for the insertion of genes of interest. The MCS is flanked by restriction enzyme sites, which can be used to clone genes into the vector. The pEGFP-C1-FLAG-ku70 backbone also contains a CMV promoter, which is a strong promoter that drives the expression of genes in mammalian cells. This promoter is often used for the overexpression of genes in cell culture studies (Figure 5.4).

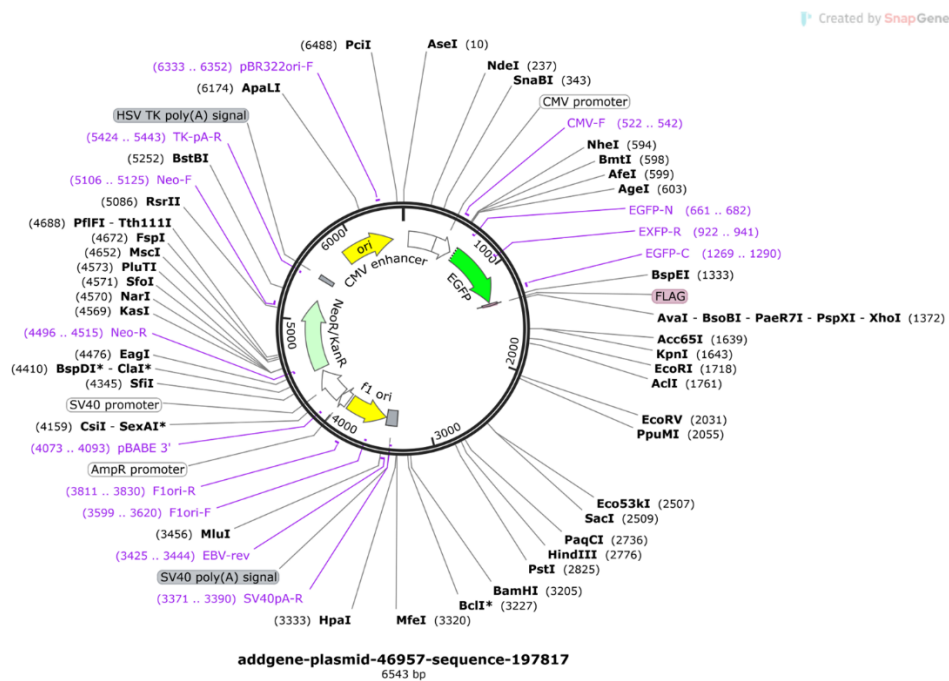


**Figure 5. 4 Map of EGFP-FLAG-C1-ku 70 mammalian expression vector (addgene).** The plasmid contains the enhanced green fluorescent protein (EGFP) gene fused in-frame with a FLAG-tagged Ku70 gene. Key features of the plasmid are indicated, including the CMV promoter, EGFP coding sequence, FLAG tag, Ku70 coding sequence, and the selection marker.

### 5.3.6: Cloning of chPARP14 Constructs

The cloning of these constructs was designed to allow for the study of the individual functions of each PARP14 domain (Table 5.2). For example, the chPARP14 $\Delta$ N construct can be used to study the role of the N-terminal domain in DNA damage repair, while the chPARP14 $\Delta$ MAC construct can be used to study the role of the macrodomain in protein-protein interactions.

**Table 5. 2 Primers used for cloning chPARP14 constructs.**

Primer	Sequence
pGFP-chPARP14 Wt-F	AAGCTCGAGATGGCCGGACCTAGGCCTGGCAG
pGFP-chPARP14 Wt-R	CTGGATCCCTAGCGTCTAAAGTTATCAGGTACTIONCAGGGTAC
pGFP-chPARP14 N-R	CTGGATCCCTACTTATCCACGTTCTACTCTTTTGCTGCTC
pGFP-chPARP14 MAC-F	AAGCTCGAGGTGGAACGTAACGTATTACAAGTTGAC
pGFP-chPARP14 MAC-R	CTGGATCCCTAGTCGACATTCTCTGGCTCTCGCCACAAATC
pGFP-chPARP14 MACD-R	CTGGATCCCTATTCCTGAGCAGCTTCTCTTCTGGATCATCTTCTG
pGFP-chPARP14 CWC-F	AAGCTCGAGGCCACGGAGTCTGGATAATTGACGTGATC
pGFP-chPARP14 WC-F	AAGCTCGAGGAGCAGAACAAAGCTGAAGTATATATAAACTGG
pGFP-chPARP14 CAT-F	AAGCTCGAGCAGAACCCATTCTGTGGCAGTCTCATCAG

### 5.3.7: Cellular Localisation of chPARP14 Constructs in DF1

The DF1 cells were transfected with plasmids expressing chPARP14 constructs for 24 hours before imaging. Protein localisation was then determined, revealing some intriguing patterns. The full-length construct was found to be primarily cytoplasmic in its distribution, suggesting it functions in the cellular cytoplasm rather than the nucleus. In

contrast, the chP14 $\Delta$ N construct containing RRM domains was observed to be localized within the nucleus. Interestingly, the chP14 $\Delta$ MAC construct, which contains macrodomains, exhibited a dual localization - it was present in both the cytoplasm and the nucleus, indicating this construct may have functions in multiple cellular compartments. Similarly, the chP14 $\Delta$ MACD construct, which includes macrodomains as well as a D domain, was also found to be concentrated in the nuclear region. On the other hand, the chP14 $\Delta$ CWC construct, comprising a D domain, WWE domain, and catalytic domain, was observed exclusively in the cytoplasm, suggesting this arrangement of domains is responsible for its cytoplasmic localization. Likewise, the chP14 $\Delta$ WC construct, containing only the WWE and catalytic domains, was also confined to the cytoplasmic space. Finally, the CAT construct, which solely contains the catalytic domain, was likewise determined to be cytoplasmic in its distribution (Figure 5.5).

These results suggest that the different domains of the protein play a role in determining its localization. The RRM domain may be involved in nuclear localization, while the MAC domain may be involved in both nuclear and cytoplasmic localization. The D domain may also play a role in nuclear localization, as it is found in both the MACD and CWC constructs. The WWE and catalytic domains may be involved in cytoplasmic localization. Overall, this detailed analysis of the localization patterns of the various constructs provides valuable insights into the functional roles and domain-specific behaviours of these molecular components. The observed compartmentalization within the cell likely reflects the distinct activities and interactions associated with each construct, highlighting the importance of understanding the spatial organization of cellular processes.

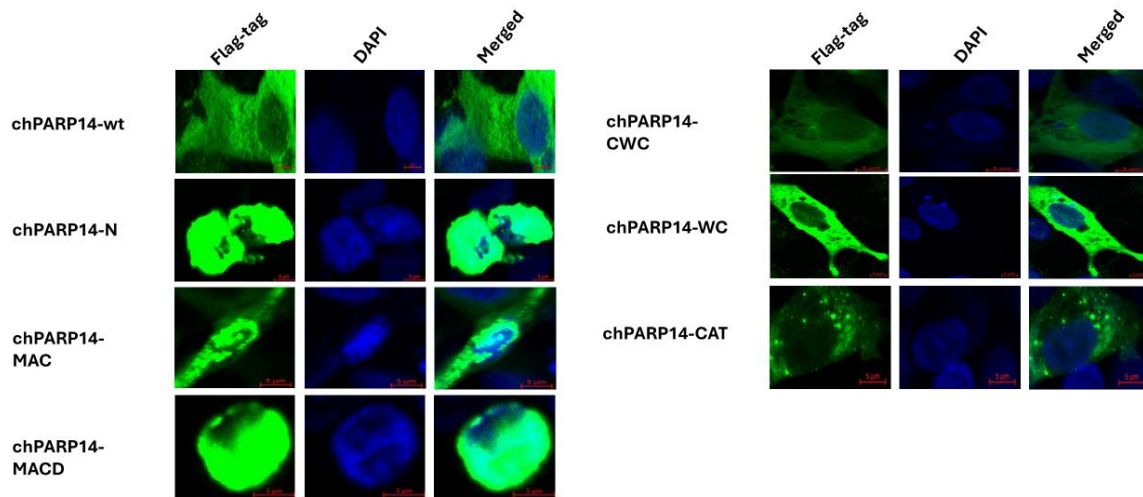


**Figure 5.5 Labelling of chPARP14 constructs Cellular Localisation.** DF1 cells were transfected with plasmids encoding different chPARP14 constructs: full-length (FL), chP14 $\Delta$ N, chP14 $\Delta$ MAC, chP14 $\Delta$ MACD, chP14 $\Delta$ CWC, chP14 $\Delta$ WC, and CAT. After 24 hours, cells were fixed and stained with an antibody against FLAG, followed by a secondary antibody. Nuclei were stained with DAPI. Scale bar: 5  $\mu$ m.

### 5.3.8: Expression of chPARP14 using Western Blot

The Western blot analysis of the various constructs of the chPARP14 protein cloned into a mammalian expression vector was conducted. The full-length protein expression was lower compared to truncated domains, indicating that the overall yield and stability of the complete protein was suboptimal under the experimental conditions. This could suggest potential challenges in the expression or stability of the full-length construct within the mammalian cell system utilized. Interestingly, the shortest construct, chPARP14 $\Delta$ CAT, was not observed to be expressed at all. This lack of detectable expression for the shortest variant points to potential issues with the proper folding, trafficking, or overall viability of this particular construct in the mammalian cell environment. In contrast, chPARP14 $\Delta$ MACD exhibited a slightly lower expressing, hinting that this particular construct may have been moderately expressed, albeit at lower levels compared to the optimal variants. Interestingly, the Western blot analysis showed the presence of faint secondary bands for constructs chPARP14 $\Delta$ N, chPARP14 $\Delta$ MAC, and chPARP14 $\Delta$ CWC.

The appearance of these additional bands could indicate the existence of alternative isoforms, proteolytic cleavage products, or even non-specific interactions occurring with the target protein (Figure 5.6).

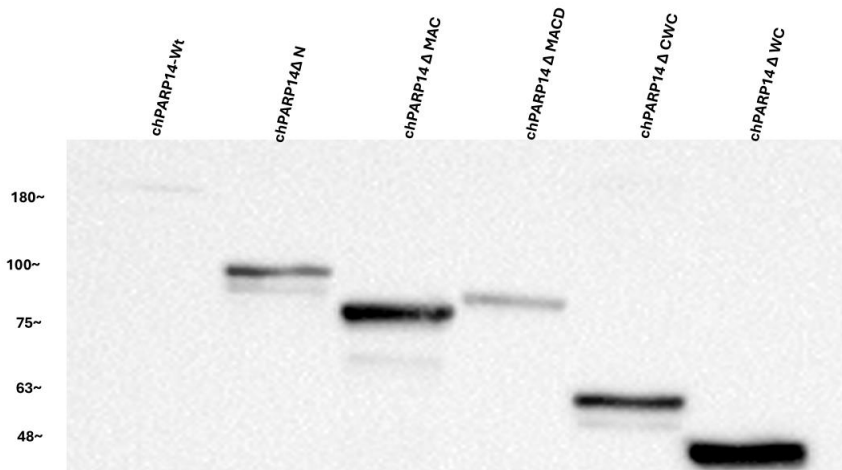


**Figure 5. 6 Confirming the expression of chPARP14 constructs in the protein extract.** DF1 cells were transfected with plasmids encoding different chPARP14 constructs: full-length (FL), chP14ΔN, chP14ΔMAC, chP14ΔMACD, chP14ΔCWC, chP14ΔWC, and chP14ΔCAT. Whole-cell lysates were subjected to SDS-PAGE and Western blot analysis using an antibody against FLAG.

### 5.3.9: RT-qPCR Analysis for Quantification of Viral Gene Expression in DF1 cells treated with chPARP14 constructs.

Next, to assess the effect of various chPARP14 constructs (both full-length and truncated) on IAV viral replication in DF1 cells, truncated chPARP14 constructs were transfected into DF1 cells and were subsequently 24 hours later with the H9N2 at MOI of 1.0. The goal was to use RT-qPCR to see how overexpression of chPARP14 constructs influenced viral replication.

Statistical analysis revealed that none of the chPARP14 constructs significantly altered the viral replication compared to the control group (treated with virus only). However, truncated constructs chPARP14ΔN, chPARP14ΔMAC, chPARP14ΔMACD and

chPARP14 $\Delta$ WC showed a trend towards lower viral replication levels, suggesting that these truncated versions of the protein may have some inherent antiviral properties, even if the differences did not reach the threshold of statistical significance (Figure 5.7). The fact that the full-length protein did not demonstrate a significantly stronger antiviral effect than the truncated forms was somewhat unexpected, as one might have hypothesized that the complete protein would have a more pronounced impact. However, the data indicates that certain regions or domains within the protein structure may be responsible for its antiviral capabilities, which are maintained even when the protein is truncated.

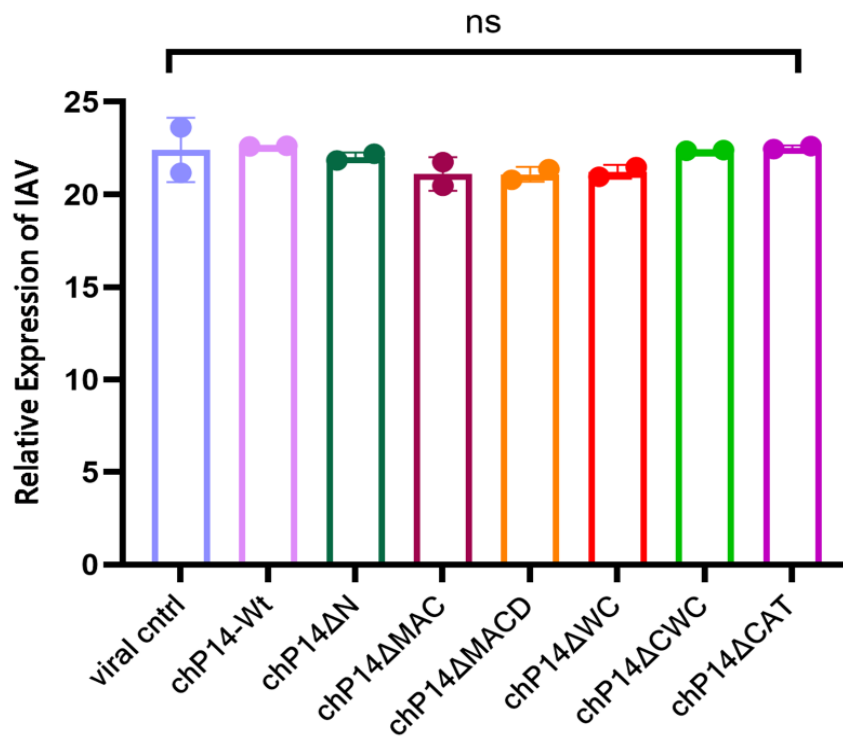


**Figure 5. 7 RT-qPCR analysis of viral replication in cells treated with various protein constructs.** Viral RNA levels were measured in cells treated with full-length protein, truncated constructs, or a control group (virus only). Relative viral replication fold change was calculated compared to the control group.

### **5.3.10: Plaque Assay Analysis to determine the Antiviral Efficacy of chPARP14 constructs in DF1 cells.**

To further verify the results obtained from RT-qPCR, we performed a plaque assay to evaluate the antiviral efficacy of several chPARP14 constructs against the H9N2. DF1 cells were treated with chPARP14 expression plasmids for 24 hours before cells were then infected with the H9N2 at MOI 1.0, and the resulting viral supernatant was used to infect MDCK cells for plaque assay-based quantification. Plaque formation was counted at a dilution of 3 (1:1000) to assess the antiviral activity of the constructs.

The observation that all constructs exhibited reduced plaque formation compared to the viral control suggests that the full-length chPARP14 and its constructs have antiviral activity against IAV (Figure 5.8). Plaque formation is a measure of viral replication, so a decrease in plaque formation indicates inhibition of viral growth.

However, not all of these differences were statistically significant. The statistical significance of the antiviral effect varied among the constructs. Full-length and chPARP14 $\Delta$ CWC showed statistically significant reductions in plaque formation, indicating a more robust antiviral activity. The remaining constructs, while exhibiting reduced plaque formation, did not reach statistical significance. This could be due to mechanisms such as inhibition of viral entry, replication, or assembly.

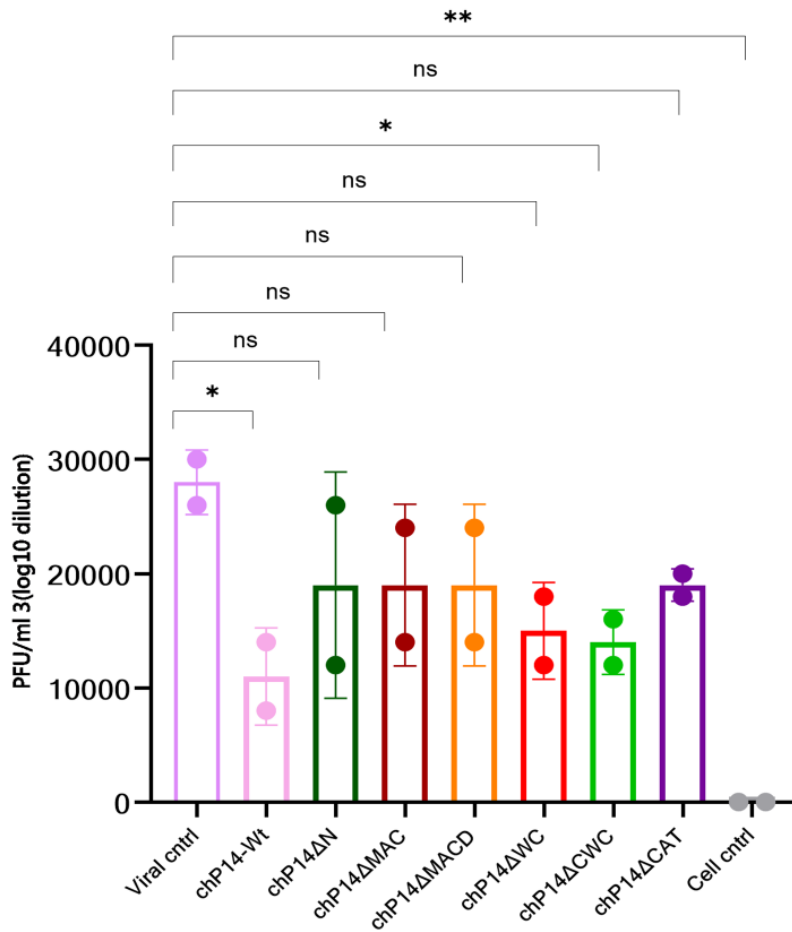


**Figure 5. 8** Plaque assay to determine the antiviral efficacy of chPARP14 and its constructs against IAV in DF1 cells. All the constructs show a reduction in plaque formation, although not all of them being statistically significant implies the antiviral nature of the protein. Plaques were counted at  $10^{-3}$  dilution and the significance between groups was assessed using One-Way ANOVA with GraphPad Prism 10 software.

### 5.3.11: Cellular Localisation of huPARP14 Constructs

We further wanted to understand and compare the antiviral efficacy of chPARP14 to that of huPARP14. We used the constructs designed based on the domain structure (a gift from Gabrielle Grundy, North West Cancer Research Fellow, University of Liverpool) to investigate the localisation of specific domains of huPARP14 within a HEK cells (Figure 5.9). Our results showed that the full-length protein is found to be localized within the

nucleus, suggesting it likely plays a role in nuclear processes and regulation. On the other hand, the construct containing the macrodomains, such as huPARP14 $\Delta$ MAC, are observed to be cytoplasmic in their localization. This indicates these macrodomain-containing proteins may be involved in cytoplasmic functions, potentially interacting with other cytoplasmic factors or organelles. huPARP14 $\Delta$ C, which contains macrodomains as well as a D domain and WW and CAT domains, is also seen to be cytoplasmic in its localization. This aligns with the cytoplasmic distribution of the huPARP14 $\Delta$ MAC construct, further supporting the notion that the macrodomain regions direct these proteins to the cytoplasm. Similarly, the huPARP14 $\Delta$ CW construct, which has the D domain and WWE and CAT domains, is likewise found to be cytoplasmic. Interestingly, the huPARP14 $\Delta$ WC construct, containing only the WWE and CAT domains, exhibits both cytoplasmic and nuclear localization (Figure 5.10). This dual localization implies the WWE and CAT domains may facilitate shuttling of this protein between the cytoplasm and nucleus, potentially allowing it to participate in processes in both cellular compartments. The results indicate that the macrodomain and a combination of the D, WWE, and CAT domains are determinants for cytoplasmic localization. The presence of the D, WWE, and CAT domains alone, without the macrodomain, is also sufficient for cytoplasmic localization. However, the WWE and CAT domains without the D domain can be found in both the cytoplasm and the nucleus. In contrast, the huPARP14 $\Delta$ MACD and huPARP14 $\Delta$ CAT containing constructs were not expressed at high enough levels to detect a clear signal, suggesting potential challenges in their expression or stability. Overall, this data provides a nuanced picture of how the different structural domains within these proteins influence their subcellular distribution and likely functions within the cell.

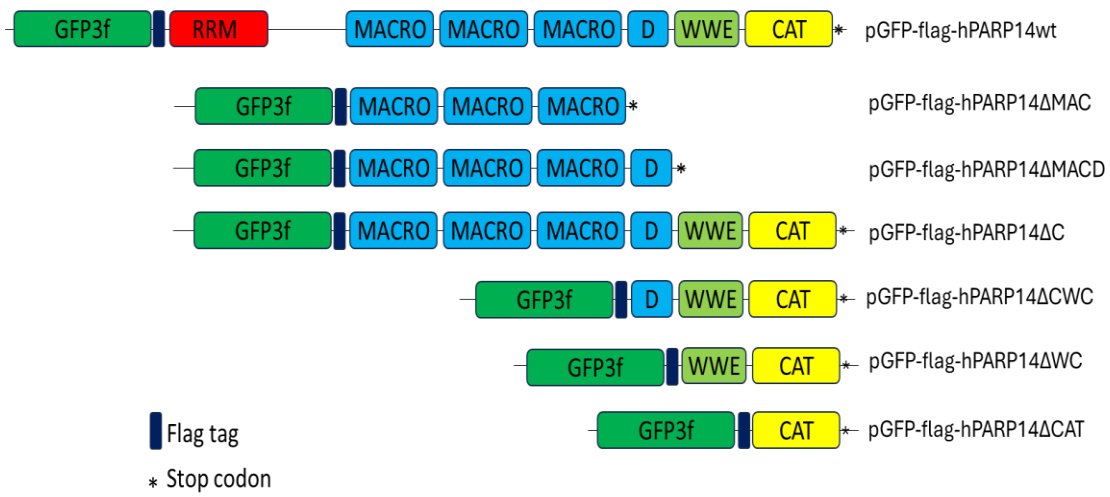


**Figure 5. 9 Domain structure framework for the design of huPARP14 construct cloning into EGFP-Flag-C1-ku70 mammalian expression vector.**

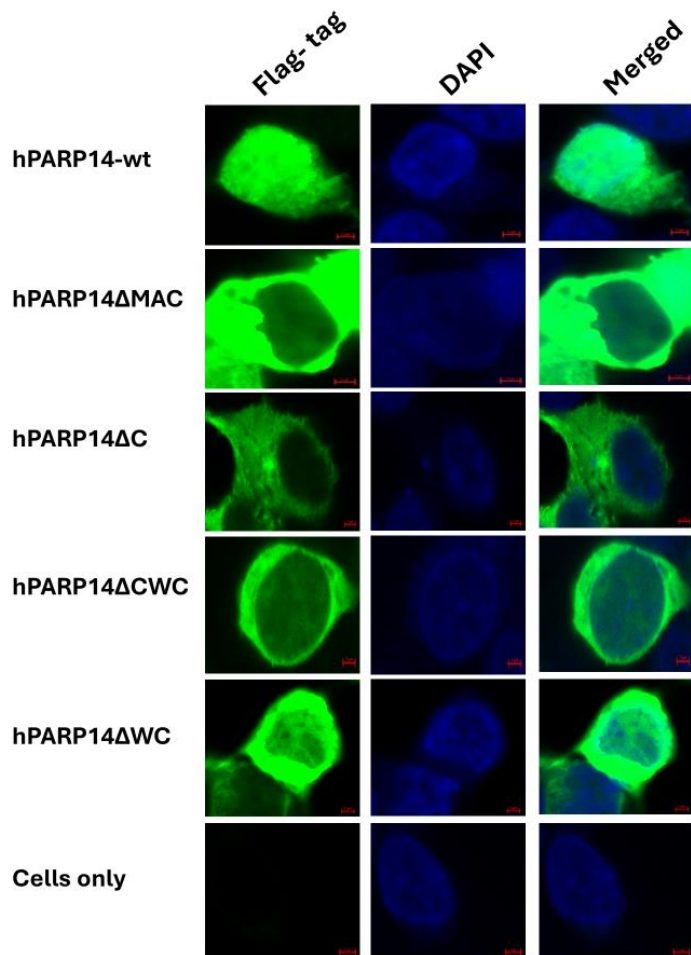


**Figure 5. 10 Cellular Localisation of huPARP14 Constructs in HEK cells.** Immunofluorescence images showing the localization of huPARP14 constructs. Full-length huPARP14 was nuclear. Macrodomain-containing constructs (huPARP14ΔMAC, huPARP14ΔC) and huPARP14ΔCW were cytoplasmic. huPARP14ΔWC was both cytoplasmic and nuclear. huPARP14ΔMACD and huPARP14ΔCAT were not detected. Macrod domains and D/WWE/CAT domains dictate cytoplasmic localization; WWE/CAT alone allows dual localization.

### 5.3.12: Western Blot Confirmation of huPARP14 constructs in the HEK cell protein extract.

Western blot was used to confirm the presence of huPARP14 constructs in HEK cell extract. Figure 5.11 shows that certain proteins of interest, namely huPARP14ΔMAC, huPARP14ΔWC, and huPARP14ΔCAT, were successfully expressed at high enough levels

to be detected. The clear bands observed for these target proteins on the western blot membrane confirm their presence and relative abundance in the cell extract sample.

However, the findings also reveal that other proteins, chPARP14 $\Delta$ MACD exhibited a faint band, hinting that this particular construct may have been moderately expressed, albeit at lower levels compared to the optimal variants. The full-length, huPARP14 $\Delta$ CWC, and huPARP14 $\Delta$ C variants were not expressed at all, or at least not to a detectable degree. This could be due to a variety of factors, such as issues with the expression construct, problems with the induction conditions, or inherent difficulties in producing those specific protein truncations.

Nonetheless, the successful confirmation of huPARP14 $\Delta$ MAC, huPARP14 $\Delta$ WC, and huPARP14 $\Delta$ CAT expression provides an important foundation for subsequent experiments and analyses.

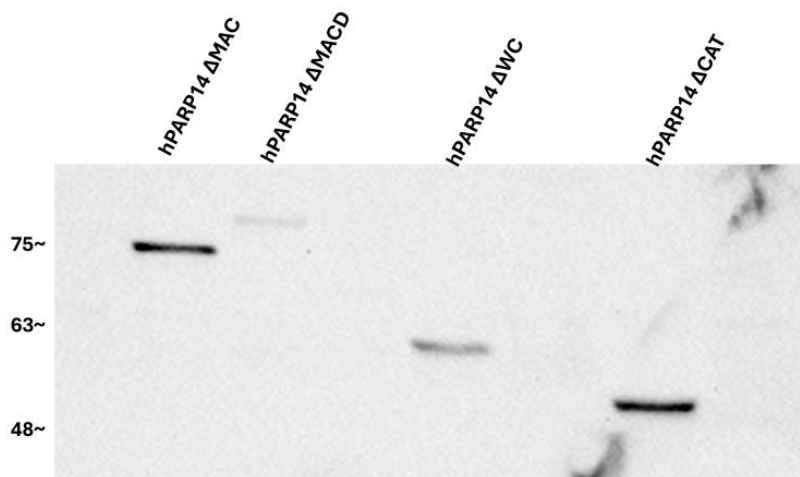


**Figure 5. 11 Confirming the expression of huPARP14 constructs in the protein extract.** HEK cells were transfected with full-length huPARP14, huPARP14 $\Delta$ MAC, huPARP14 $\Delta$ MACD, huPARP14 $\Delta$ C, huPARP14 $\Delta$ CWC, huPARP14 $\Delta$ WC, and huPARP14 $\Delta$ CAT. Anti-FLAG antibodies were used to analyse whole-cell lysates via SDS-PAGE and Western blot.

### **5.3.13: Plaque Assay Analysis to determine the Antiviral Efficacy of huPARP14 constructs in HEK cells.**

To evaluate the antiviral efficacy of several huPARP14 constructs against the H1N1, cells were transfected with huPARP14 WT and truncates and after 24 hours, the cells were then infected with the H1N1 at a MOI of 1.0. Following another 24-hour incubation period, the resulting supernatant was used to infect MDCK cells. This secondary infection helps to quantify the antiviral potency of the original constructs by counting the number of viral plaques formed in the MDCK monolayer. Plaque assay is a technique used to quantify the number of infectious virus particles. A reduction in plaque formation in MDCK cells treated with the supernatant from construct-treated cells indicates that the constructs might have antiviral activity, while an increase suggests the opposite.

The findings show that the antiviral effects of the constructs varied, with several exhibiting significant antiviral activity. huPARP14-Wt, huPARP14 $\Delta$ MAC, huPARP14 $\Delta$ MACD, and huPARP14 $\Delta$ WC showed reduced plaque formation compared to the viral control, suggesting they can suppress viral replication to some extent. In contrast, huPARP14 $\Delta$ C, huPARP14 $\Delta$ CWC, and huPARP14 $\Delta$ CAT showed increased plaque counts relative to the control, implying they lacked significant antiviral properties or may have enhanced viral infectivity. However, it is worth noting that some differences were statistically significant (Figure 5.12).

Only huPARP14-Wt, huPARP14 $\Delta$ MAC, huPARP14 $\Delta$ MACD, huPARP14 $\Delta$ C, and huPARP14 $\Delta$ CAT displayed antiviral effects that reached the threshold of statistical significance. The huPARP14 $\Delta$ CWC and huPARP14 $\Delta$ WC did not show statistically meaningful antiviral activity. Interestingly, the data revealed that huPARP14 $\Delta$ MACD

appeared to be the most potent antiviral, with high reduction in plaque formation. Conversely, huPARP14 $\Delta$ C demonstrated the strongest enhancement of viral replication, with a statistically significant increase in plaque counts compared to the control. These findings suggest that the various constructs likely have differing mechanisms of action when it comes to modulating the host-virus interaction and warrants further investigation to elucidate their precise modes of antiviral or proviral activity.

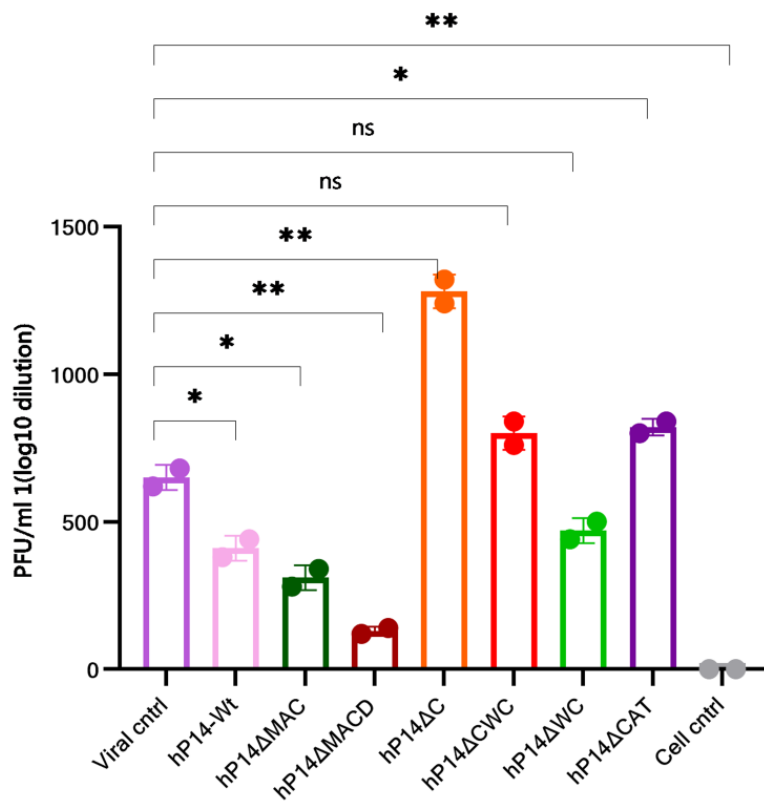


**Figure 5. 12 Statistical analysis of plaque assay for huPARP14 constructs in HEK cells.** Plaques were counted at 10<sup>-1</sup> dilution and the significance between groups was assessed using One-Way ANOVA with GraphPad Prism 10 software.

## 5.4: Discussion

This chapter sought to understand the diverse role of chicken chPARP14 during IAV infection, with an emphasis on its subcellular localisation, antiviral efficacy, and domain-specific functions. PARP14, a member of the PARP family, has been linked to a variety of cellular activities, including transcriptional control and immunological responses (Ame et al., 2004; Gibson and Kraus, 2012). Beyond IAV, PARP14 has been linked to the cellular response to various viral infections. PARP14, for example, has been demonstrated to modulate interferon signalling and antiviral gene expression in the innate immune response against RNA viruses such as dengue virus and hepatitis C virus (Li et al., 2017; Zhang et al., 2018). These studies suggest that PARP14 can act as a broad-spectrum antiviral factor. Our findings, which demonstrate antiviral activity of chPARP14 against IAV, support this notion, indicating that PARP14's antiviral function is not limited to a specific virus type. Our findings of chPARP14 contributing to antiviral responses in avian cells expand the known antiviral role of PARP14. However, the precise mechanisms through which PARP14 exerts its antiviral effects can vary depending on the virus and cellular context. Some studies suggest that PARP14 can directly interact with viral components, while others highlight its role in modulating host cell signaling pathways (Li et al., 2017; Zhang et al., 2018). Our findings reveal diverse subcellular localizations of chPARP14 variants, suggesting its involvement in a broad spectrum of cellular activities, ranging from nuclear functions to cytoplasmic interactions. This versatility underscores its potential significance in modulating viral replication at multiple stages of the IAV life cycle within the host cell.

A key finding of this study is the observed antiviral activity of chPARP14 constructs, highlighting its potential as a therapeutic target not only for IAV but also potentially for

other viral infections. The identification of specific domains within chPARP14 that contribute to its localization and antiviral capabilities provides a foundation for future studies aimed at exploiting these features. By selectively modulating these domains, it may be possible to develop novel antiviral strategies that enhance chPARP14 activity, thereby disrupting viral replication and spread.

While RT-qPCR analysis of chPARP14 construct overexpression in DF1 cells showed a trend towards reduced IAV replication with truncates such as chPARP14 $\Delta$ N, chPARP14 $\Delta$ MAC, chPARP14 $\Delta$ MACD, and chPARP14 $\Delta$ WC, statistical significance was not achieved compared to the control group. However, plaque assays demonstrated that all chPARP14 constructs exhibited reduced plaque formation, indicating antiviral activity. Notably, full-length chPARP14 and chPARP14 $\Delta$ CWC showed statistically significant reductions, suggesting more robust antiviral activity. These results suggest that chPARP14 may exert its antiviral effects through mechanisms that are not fully captured by RT-qPCR alone, potentially involving post-transcriptional regulation or direct interference with viral assembly or release.

In contrast, the antiviral activity of the huPARP14 exhibited more variability. Among the huPARP14 constructs tested, only huPARP14Wt, huPARP14 $\Delta$ MAC, huPARP14 $\Delta$ MACD, and huPARP14 $\Delta$ CAT showed statistically significant antiviral effects. Notably, huPARP14 $\Delta$ MACD displayed the most potent antiviral activity, while huPARP14 $\Delta$ C exhibited a proviral effect (Table 5.3).

**Table 5. 3 Antiviral efficacy of chPARP14 and huPARP14 constructs.**

Construct	Virus Tested	Observation	Statistical Significance
chPARP14Wt	H9N2	Reduced plaque formation.	Statistically significant
chPARP14ΔN	H9N2	Reduced plaque formation, but did not reach statistical significance.	Not statistically significant
chPARP14ΔMAC	H9N2	Reduced plaque formation, but did not reach statistical significance.	Not statistically significant
chPARP14ΔMACD	H9N2	Reduced plaque formation, but did not reach statistical significance.	Not statistically significant
chPARP14ΔWC	H9N2	Reduced plaque formation, but did not reach statistical significance.	Not statistically significant
chPARP14ΔCWC	H9N2	Reduced plaque formation.	Statistically significant
chPARP14ΔCAT	H9N2	Reduced plaque formation, but did not reach statistical significance.	Not statistically significant
huPARP14Wt	H1N1	Reduced plaque formation.	Statistically significant
huPARP14ΔMAC	H1N1	Reduced plaque formation.	Statistically significant
huPARP14ΔMACD	H1N1	Reduced plaque formation (appeared most potent antiviral).	Statistically significant
huPARP14ΔWC	H1N1	Reduced plaque formation.	Not statistically significant
huPARP14ΔC	H1N1	Increased plaque counts relative to the control (suggesting lack of or enhanced viral infectivity).	Statistically significant
huPARP14ΔCWC	H1N1	Increased plaque counts relative to the control.	Not statistically significant
huPARP14ΔCAT	H1N1	Increased plaque counts relative to the control.	Statistically significant

The observed differences in antiviral and expression properties between chicken and human PARP14 likely stem from species-specific evolutionary divergence. Over time, the amino acid sequences of these proteins have diverged, leading to variations in their structure, function, and interactions with other cellular components. These variations ultimately translate into differences in their antiviral capabilities, subcellular localization, and levels of expression within the cell (Lynch & Conery, 2003).

However, only two biological samples of each construct were used in this study. This small sample size has several implications. Firstly, it limits the statistical power of the experiments, making it more difficult to detect true differences between groups and increasing the likelihood of false positives or false negatives. Secondly small sample sizes are susceptible to random variability and experimental noise, which can obscure true biological effects. Thirdly, with only two replicates, it becomes difficult to assess whether the assumptions of statistical tests are met, making the interpretation of

statistical significance more uncertain. To address these limitations, increasing the number of biological replicates is crucial. A larger sample size would increase statistical power, reduce the impact of random variability, and allow for more robust statistical analysis. This would provide a more accurate assessment of the observed differences and strengthen the conclusions drawn from the study. In addition to increasing the sample size, other methods could be employed to investigate the role of chPARP14 in antiviral defence and to further elucidate its mechanisms of action including, chemical inhibition which could be employed to block chPARP14 activity and assess its impact on viral replication. RNA interference, such as siRNA or shRNA, to specifically knockdown the expression of chPARP14 mRNA, thus reducing the levels of the protein and its antiviral activity. Gene Editing to precisely edit the chPARP14 gene, introducing mutations that disrupt its function or expression. These approaches would provide valuable insights into the role of chPARP14 in antiviral defence and help to validate the findings obtained in this study.

## **5.5: Limitations and Future Directions**

While the study provides valuable insights, it also has certain limitations. The lack of statistical significance of some antiviral effects suggests that the observed differences may not be robust. Further studies with larger sample sizes and more stringent statistical analyses are needed to confirm these findings. Additionally, the study focused on IAV infection; investigating the role of chPARP14 in other viral infections in chicken would broaden our understanding of its antiviral potential.

Future research should also explore the molecular mechanisms underlying the antiviral activity of chPARP14. Identifying the specific viral and host factors that interact with

chPARP14 could provide insights into its mode of action and potential therapeutic targets. Furthermore, investigating the potential off-target effects of targeting chPARP14 is crucial to assess its safety and efficacy as a therapeutic agent.

## **5.6: Conclusion**

This chapter provides useful information about the role of chPARP14 in IAV infection. The study focusses on the various subcellular localisations of chPARP14 variants, their antiviral efficacy, and the possibility of targeting specific domains to develop novel antiviral strategies. More research is needed to fully understand the mechanisms underlying chPARP14's antiviral effects and to investigate its potential as a therapeutic target for IAV and other viral infections.

## Chapter 6: Discussion

The purpose of this study was to identify and characterise a chPARP with potential antiviral activity against IAV. To accomplish this, we used a multifaceted approach that included bioinformatics, transcriptomic analysis, and functional assays. Initially, we performed a thorough bioinformatic analysis of chPARPs, which included percentage identity, phylogenetic analysis, and multiple sequence alignment with human counterparts. We hoped to identify any unique characteristics or differences in the structural features of these proteins that could contribute to antiviral activity. Furthermore, we generated 3D structural predictions for the chPARP proteins, which revealed important information about their potential functional domains and interactions.

Moving to the next phase of the study, we performed transcriptomic analysis on CEF cells that had been infected with IAV. This allowed us to observe the transcriptional changes occurring in the host cells in response to viral infection, particularly focusing on the expression patterns of the various chPARP genes. By analysing this data, we hoped to uncover any chPARPs that demonstrated significant upregulation or differential expression, as these could be promising candidates for further investigation.

Ultimately, based on the findings from the structural and transcriptomic analyses, we selected the chPARP14 protein as the focus of our antiviral studies. To assess its direct impact on IAV infection, we conducted plaque assays and viral quantification using RT-qPCR. These experiments provided valuable insights into the ability of chPARP14 to inhibit or reduce viral replication, shedding light on its potential as an antiviral therapeutic target.

Our initial bioinformatics analysis revealed the evolutionary landscape of PARP proteins in the chicken genome, highlighting both conservation and divergence compared to human PARPs. While domain organization, essential for core functions like DNA repair and ADP-ribosylation, is largely conserved (Ke, Wang, et al., 2019), synteny analysis indicated significant differences in

the genomic context of PARP genes between chicken and humans. This suggests potential variations in regulatory mechanisms and co-expression patterns, which could subtly modulate PARP functions.(Dong et al., 2009; Steenwyk & King, 2024). Furthermore, observed differences in synteny within the avian lineage, particularly between chicken-duck and chicken-turkey, point to ongoing evolutionary refinement within the Galliformes order. Sequence identity analysis revealed varying degrees of conservation, with PARP14 showing lower similarity, suggesting species-specific adaptations. Phylogenetic analysis further supported this, indicating gene duplication and diversification events within the avian lineage, notably for PARP14.

Building upon these evolutionary insights, we conducted an RNA-seq analysis of IAV-infected CEF cells, revealing significant transcriptional changes. Proper normalization of the RNA-seq data was crucial to ensure accurate differential gene expression analysis (Anders, 2010; Crist et al., 2021; Dillies, 2013; Love et al., 2014; Mezencev & Auerbach, 2020; Schafer et al., 2024). PCA confirmed robust transcriptional signatures associated with IAV infection. Differential gene expression analysis identified a substantial number of DEGs, with PARP14 emerging as the most significantly upregulated PARP. GO enrichment analysis highlighted the activation of immune-related pathways and NAD<sup>+</sup> ADP-ribosyltransferase activity, consistent with PARP involvement in antiviral responses (Iwasaki & Medzhitov, 2015; Medzhitov, 2008). RT-qPCR validation confirmed the upregulation of PARP14 and other PARP family members, reinforcing the RNA-seq findings. Cellular localization studies provided further context, revealing distinct localization patterns for different PARPs, suggesting diverse functional roles in response to viral infection.

The focus then shifted to the functional characterization of chPARP14 during IAV infection. We observed antiviral activity of chPARP14 constructs, supporting its potential as a therapeutic target. This aligns with previous studies demonstrating PARP14's role in antiviral responses against other RNA viruses, such as dengue and hepatitis C (Li et al., 2017; Zhang et al., 2018). Our findings in avian cells expand the known antiviral role of PARP14, suggesting a broad-spectrum

antiviral function. Diverse subcellular localizations of chPARP14 variants indicate its involvement in multiple stages of the viral life cycle.

While RT-qPCR showed a trend towards reduced viral replication with chPARP14 truncates, plaque assays demonstrated significant antiviral activity, particularly with full-length chPARP14 and chPARP14 $\Delta$ CWC. Conversely, huPARP14 constructs exhibited more variable antiviral activity, highlighting species-specific differences. These variations likely stem from evolutionary divergence, leading to differences in protein structure and function (Lynch & Conery, 2003).

This study significantly contributes to the growing body of knowledge on the antiviral mechanisms of PARP proteins. While PARPs are well-known for their roles in DNA repair and other cellular processes, their antiviral properties have been increasingly recognized in recent years (Zhu & Zheng, 2021). This study adds to this growing body of evidence by identifying a specific chPARP14, with potent antiviral activity against IAV. The bioinformatic analysis provides valuable insights into the structural and functional diversity of chPARPs, particularly in relation to their human counterparts. The identification of unique structural features and potential functional domains in chPARP14 may offer new avenues for drug discovery and therapeutic interventions. The transcriptomic analysis of IAV-infected CEF cells provides a comprehensive overview of the host response to viral infection, including the upregulation of various PARP genes. This data aligns with previous studies that have implicated PARPs in antiviral responses, such as those involving interferon signaling and innate immunity (Malgras et al., 2021; Zhu et al., 2021). The functional assays demonstrate the direct antiviral activity of chPARP14 against IAV. While the precise mechanism of action remains to be fully elucidated, the study provides valuable clues, such as the potential involvement of subcellular localization and interactions with viral proteins. The comparison of chPARP14 and huPARP14 highlights potential species-specific differences in their antiviral properties. This finding underscores the importance of studying host-specific factors in antiviral research.

While this study contributes significantly to our understanding of chPARP14's role in antiviral defence against IAV, it also raises several intriguing questions that may guide future research in this area. Moving forward, one of the top priorities will be to identify the specific viral targets that interact with chPARP14 to inhibit viral replication. Further investigation into the precise molecular interactions between chPARP14 and viral proteins could reveal the exact mechanisms underlying its potent antiviral activity. Furthermore, investigating the potential role of post-translational modifications, such as phosphorylation or acetylation, in regulating chPARP14 function and antiviral properties could provide useful insights. Questions around the involvement of specific cellular signaling pathways, like the interferon response pathway, in mediating chPARP14's antiviral effects, and the subcellular localization of chPARP14 and how this impacts its antiviral role are also ripe for exploration. Broadening the investigation to examine chPARP14's antiviral activity against a wider range of viruses, including emerging and re-emerging pathogens, could uncover how conserved and versatile this defence mechanism is across different viral threats. Finally, understanding the specific mechanistic differences in antiviral function between chPARP14 and huPARP14, may reveal unique targetable vulnerabilities. By addressing these multifaceted future research directions, we can gain an even deeper, more comprehensive understanding of chPARP14's role in antiviral immunity, paving the way for the development of groundbreaking new treatment strategies to combat IAV infection.

# Chapter 7: Conclusions

In conclusion, this study successfully identified and characterised chPARP14 as a novel antiviral factor against IAV. Through a combined approach of bioinformatics, transcriptomic analysis, and functional assays, we demonstrated the significant upregulation of chPARP14 in response to IAV infection and its direct antiviral activity, evidenced by reduced viral replication. Bioinformatic analysis revealed unique structural features of chPARP14 compared to its human counterpart, hPARP14, suggesting potential species-specific mechanisms of action.

Transcriptomic analysis revealed a robust host response to IAV infection, with significant upregulation of several PARP genes, including chPARP14. Functional assays confirmed chPARP14's antiviral activity, though the precise mechanism has yet to be determined. The observed differences in antiviral activity between chPARP14 and huPARP14 highlight the importance of investigating host-specific factors in antiviral research. This study contributes significantly to our understanding of the antiviral roles of PARPs and identifies chPARP14 as a promising therapeutic target against IAV and possibly other viral infections. Future research focusing on the specific molecular interactions between chPARP14 and viral proteins, the role of post-translational modifications, the involvement of cellular signalling pathways, the impact of subcellular localization, and the breadth of its antiviral activity against other viruses will be crucial for fully realizing the therapeutic potential of this novel antiviral factor.

## Chapter 8: Future Directions

Future research should prioritize elucidating the precise mechanism by which chPARP14 exerts its antiviral effects against IAV. This involves identifying the specific viral target(s) of chPARP14 interaction, characterizing the molecular details of these interactions through structural and biophysical studies, and determining how chPARP14 disrupts the viral life cycle. Further investigation into the regulation of chPARP14 activity is crucial, including exploring the role of post-translational modifications, the involvement of cellular signaling pathways like the interferon response, and the impact of subcellular localization on function. Expanding the scope of investigation to test chPARP14's antiviral activity against a broader range of viruses and comparing it more thoroughly with hPARP14 will provide insights into its specificity and breadth. Moving towards *in vivo* studies in animal models is essential for evaluating therapeutic potential, along with exploring the development of chPARP14-based therapies and investigating synergistic effects with existing antivirals. Finally, conducting more extensive comparative genomics of PARP families across avian species and further investigating the lack of synteny between avian and mammalian PARP gene clusters will enhance our understanding of their evolutionary history and functional diversification.

# Chapter 9: References

- Al-Rahahleh, R. Q., Saville, K. M., Andrews, J. F., Wu, Z., Koczor, C. A., & Sobol, R. W. (2023). Overexpression of the WWE domain of RNF146 modulates poly-(ADP)-ribose dynamics at sites of DNA damage. *bioRxiv*. <https://doi.org/10.1101/2023.12.29.573650>
- Alemasova, E. E., & Lavrik, O. I. (2019). Poly(ADP-ribosyl)ation by PARP1: reaction mechanism and regulatory proteins. *Nucleic Acids Res*, 47(8), 3811-3827. <https://doi.org/10.1093/nar/gkz120>
- Alexander, D. J. (2000). A review of avian influenza in different bird species. *Vet Microbiol*, 74(1-2), 3-13. [https://doi.org/10.1016/s0378-1135\(00\)00160-7](https://doi.org/10.1016/s0378-1135(00)00160-7)
- Allen, I. C., Scull, M. A., Moore, C. B., Holl, E. K., McElvania-TeKippe, E., Taxman, D. J., Guthrie, E. H., Pickles, R. J., & Ting, J. P. (2009). The NLRP3 inflammasome mediates in vivo innate immunity to influenza A virus through recognition of viral RNA. *Immunity*, 30(4), 556-565. <https://doi.org/10.1016/j.immuni.2009.02.005>
- Anders, S., & Huber, W. (2010). Differential expression analysis for sequence count data. *Genome Biol*, 11(10), R106. <https://doi.org/10.1186/gb-2010-11-10-r106>
- Archimede Torretta, C. C., Carmen Ebenwaldner, and Herwig Schüler. (2023). PARP14 is a writer, reader, and eraser of mono-ADP-ribosylation. *Journal of Biological Chemistry*, 299(9) 105096 <https://doi.org/10.1016/j.jbc.2023.105096>
- Arruda, B., Baker, A. L. V., Buckley, A., Anderson, T. K., Torchetti, M., Bergeson, N. H., Killian, M. L., & Lantz, K. (2024). Divergent Pathogenesis and Transmission of Highly Pathogenic Avian Influenza A(H5N1) in Swine. *Emerg Infect Dis*, 30(4), 738-751. <https://doi.org/10.3201/eid3004.231141>
- Barbarulo, A., Iansante, V., Chaidos, A., Naresh, K., Rahemtulla, A., Franzoso, G., Karadimitris, A., Haskard, D. O., Papa, S., & Bubici, C. (2013). Poly(ADP-ribose) polymerase family member 14 (PARP14) is a novel effector of the JNK2-dependent pro-survival signal in multiple myeloma. *Oncogene*, 32(36), 4231-4242. <https://doi.org/10.1038/onc.2012.448>
- Baudin, F., Petit, I., Weissenhorn, W., & Ruigrok, R. W. (2001). In vitro dissection of the membrane and RNP binding activities of influenza virus M1 protein. *Virology*, 281(1), 102-108. <https://doi.org/10.1006/viro.2000.0804>
- Beck, C., Rodriguez-Vargas, J. M., Boehler, C., Robert, I., Heyer, V., Hanini, N., Gauthier, L. R., Tissier, A., Schreiber, V., Elofsson, M., Reina San Martin, B., & Dantzer, F. (2019). PARP3, a new therapeutic target to alter Rictor/mTORC2 signaling and tumor progression in BRCA1-associated cancers. *Cell Death Differ*, 26(9), 1615-1630. <https://doi.org/10.1038/s41418-018-0233-1>
- Berche, P. (2022). The enigma of the 1889 Russian flu pandemic: A coronavirus? *Presse Med*, 51(3), 104111. <https://doi.org/10.1016/j.lpm.2022.104111>
- Biswas, S. K., & Nayak, D. P. (1996). Influenza virus polymerase basic protein 1 interacts with influenza virus polymerase basic protein 2 at multiple sites. *J Virol*, 70(10), 6716-6722. <https://doi.org/10.1128/JVI.70.10.6716-6722.1996>
- Bourdon, M., Manet, C., & Montagnetelli, X. (2020). Host genetic susceptibility to viral infections: the role of type I interferon induction. *Genes Immun*, 21(6-8), 365-379. <https://doi.org/10.1038/s41435-020-00116-2>
- Bouvier, N. M., & Palese, P. (2008). The biology of influenza viruses. *Vaccine*, 26 Suppl 4(Suppl 4), D49-53. <https://doi.org/10.1016/j.vaccine.2008.07.039>
- Bui, M., Whittaker, G., & Helenius, A. (1996). Effect of M1 protein and low pH on nuclear transport of influenza virus ribonucleoproteins. *J Virol*, 70(12), 8391-8401. <https://doi.org/10.1128/JVI.70.12.8391-8401.1996>

- Cady, S. D., Luo, W., Hu, F., & Hong, M. (2009). Structure and function of the influenza A M2 proton channel. *Biochemistry*, 48(31), 7356-7364. <https://doi.org/10.1021/bi9008837>
- Carroll, S. M., & Paulson, J. C. (1985). Differential infection of receptor-modified host cells by receptor-specific influenza viruses. *Virus Res*, 3(2), 165-179. [https://doi.org/10.1016/0168-1702\(85\)90006-1](https://doi.org/10.1016/0168-1702(85)90006-1)
- Ceron, R. H., Baez-Cruz, F. A., Palmer, N. J., Carman, P. J., Boczkowska, M., Heuckeroth, R. O., Ostap, E. M., & Dominguez, R. (2024). Molecular mechanisms linking missense ACTG2 mutations to visceral myopathy. *Sci Adv*, 10(22), eadn6615. <https://doi.org/10.1126/sciadv.adn6615>
- Challa, S., Stokes, M. S., & Kraus, W. L. (2021). MARTs and MARYlation in the Cytosol: Biological Functions, Mechanisms of Action, and Therapeutic Potential. *Cells*, 10(2). <https://doi.org/10.3390/cells10020313>
- Chauhan, R. P., & Gordon, M. L. (2022). An overview of influenza A virus genes, protein functions, and replication cycle highlighting important updates. *Virus Genes*, 58(4), 255-269. <https://doi.org/10.1007/s11262-022-01904-w>
- Chen, A. (2011). PARP inhibitors: its role in treatment of cancer. *Chin J Cancer*, 30(7), 463-471. <https://doi.org/10.5732/cjc.011.10111>
- Chen, L. M., Davis, C. T., Zhou, H., Cox, N. J., & Donis, R. O. (2008). Genetic compatibility and virulence of reassortants derived from contemporary avian H5N1 and human H3N2 influenza A viruses. *PLoS Pathog*, 4(5), e1000072. <https://doi.org/10.1371/journal.ppat.1000072>
- Choi, U. Y., Kang, J. S., Hwang, Y. S., & Kim, Y. J. (2015). Oligoadenylate synthase-like (OASL) proteins: dual functions and associations with diseases. *Exp Mol Med*, 47(3), e144. <https://doi.org/10.1038/emm.2014.110>
- Cohen, M., Zhang, X. Q., Senaati, H. P., Chen, H. W., Varki, N. M., Schooley, R. T., & Gagneux, P. (2013). Influenza A penetrates host mucus by cleaving sialic acids with neuraminidase. *Virology*, 45, 321. <https://doi.org/10.1016/j.virus.2013.05.011>
- Costa-Silva, J., Domingues, D., & Lopes, F. M. (2017). RNA-Seq differential expression analysis: An extended review and a software tool. *PLoS One*, 12(12), e0190152. <https://doi.org/10.1371/journal.pone.0190152>
- Crist, A. M., Hinkle, K. M., Wang, X., Moloney, C. M., Matchett, B. J., Labuzan, S. A., Frankenhauser, I., Azu, N. O., Liesinger, A. M., Lesser, E. R., Serie, D. J., Quicksall, Z. S., Patel, T. A., Carnwath, T. P., DeTure, M., Tang, X., Petersen, R. C., Duara, R., Graff-Radford, N. R.,...Murray, M. E. (2021). Transcriptomic analysis to identify genes associated with selective hippocampal vulnerability in Alzheimer's disease. *Nat Commun*, 12(1), 2311. <https://doi.org/10.1038/s41467-021-22399-3>
- D'Amours, D., Desnoyers, S., D'Silva, I., & Poirier, G. G. (1999). Poly(ADP-ribosyl)ation reactions in the regulation of nuclear functions. *Biochem J*, 342 ( Pt 2)(Pt 2), 249-268. <https://www.ncbi.nlm.nih.gov/pubmed/10455009>
- Daugherty, M. D., Young, J. M., Kerns, J. A., & Malik, H. S. (2014). Rapid evolution of PARP genes suggests a broad role for ADP-ribosylation in host-virus conflicts. *PLoS Genet*, 10(5), e1004403. <https://doi.org/10.1371/journal.pgen.1004403>
- Dong, X., Fredman, D., & Lenhard, B. (2009). Synorth: exploring the evolution of synteny and long-range regulatory interactions in vertebrate genomes. *Genome Biol*, 10(8), R86. <https://doi.org/10.1186/gb-2009-10-8-r86>
- Dou, D., Revol, R., Ostbye, H., Wang, H., & Daniels, R. (2018). Influenza A Virus Cell Entry, Replication, Virion Assembly and Movement. *Front Immunol*, 9, 1581. <https://doi.org/10.3389/fimmu.2018.01581>
- Du, Q., Miao, Y., He, W., & Zheng, H. (2023). ADP-Ribosylation in Antiviral Innate Immune Response. *Pathogens*, 12(2). <https://doi.org/10.3390/pathogens12020303>

- Duan, M., Gao, J., Li, J. et al. (2024). Targeting Selective Inhibitors of PARPs in drug discovery and development. *Med Chem Res* <https://doi.org/https://doi.org/10.1007/s00044-024-03282-4>
- DuBois, R. M., Aguilar-Yanez, J. M., Mendoza-Ochoa, G. I., Oropeza-Almazan, Y., Schultz-Cherry, S., Alvarez, M. M., White, S. W., & Russell, C. J. (2011). The receptor-binding domain of influenza virus hemagglutinin produced in *Escherichia coli* folds into its native, immunogenic structure. *J Virol*, 85(2), 865-872. <https://doi.org/10.1128/JVI.01412-10>
- Dukic, N., Stromland, O., Elsborg, J. D., Munnur, D., Zhu, K., Schuller, M., Chatrin, C., Kar, P., Duma, L., Suyari, O., Rack, J. G. M., Baretic, D., Crudgington, D. R. K., Gros Lambert, J., Fowler, G., Wijngaarden, S., Prokhorova, E., Rehwinkel, J., Schuler, H.,...Ahel, I. (2023). PARP14 is a PARP with both ADP-ribosyl transferase and hydrolase activities. *Sci Adv*, 9(37), eadi2687. <https://doi.org/10.1126/sciadv.adi2687>
- Ellis, J. W., Root, J. J., McCurdy, L. M., Bentler, K. T., Barrett, N. L., VanDalen, K. K., Dirsmith, K. L., & Shriner, S. A. (2021). Avian influenza A virus susceptibility, infection, transmission, and antibody kinetics in European starlings. *PLoS Pathog*, 17(8), e1009879. <https://doi.org/10.1371/journal.ppat.1009879>
- Fan, D., & Kassiri, Z. (2020). Biology of Tissue Inhibitor of Metalloproteinase 3 (TIMP3), and Its Therapeutic Implications in Cardiovascular Pathology. *Front Physiol*, 11, 661. <https://doi.org/10.3389/fphys.2020.00661>
- Fehr, A. R., Jankevicius, G., Ahel, I., & Perlman, S. (2018). Viral Macrod domains: Unique Mediators of Viral Replication and Pathogenesis. *Trends Microbiol*, 26(7), 598-610. <https://doi.org/10.1016/j.tim.2017.11.011>
- Fehr, A. R., Singh, S. A., Kerr, C. M., Mukai, S., Higashi, H., & Aikawa, M. (2020). The impact of PARPs and ADP-ribosylation on inflammation and host-pathogen interactions. *Genes Dev*, 34(5-6), 341-359. <https://doi.org/10.1101/gad.334425.119>
- Feltes, B. C., & Alvares, L. O. (2024). PARP1 in the intersection of different DNA repair pathways, memory formation, and sleep pressure in neurons. *J Neurochem*, 168(9), 2351-2362. <https://doi.org/10.1111/jnc.16131>
- Fereidouni, S., Starick, E., Karamendin, K., Genova, C. D., Scott, S. D., Khan, Y., Harder, T., & Kydyrmanov, A. (2023). Genetic characterization of a new candidate hemagglutinin subtype of influenza A viruses. *Emerg Microbes Infect*, 12(2), 2225645. <https://doi.org/10.1080/22221751.2023.2225645>
- Gack, M. U., Shin, Y. C., Joo, C. H., Urano, T., Liang, C., Sun, L., Takeuchi, O., Akira, S., Chen, Z., Inoue, S., & Jung, J. U. (2007). TRIM25 RING-finger E3 ubiquitin ligase is essential for RIG-I-mediated antiviral activity. *Nature*, 446(7138), 916-920. <https://doi.org/10.1038/nature05732>
- Galloway, S. E., Reed, M. L., Russell, C. J., & Steinhauer, D. A. (2013). Influenza HA subtypes demonstrate divergent phenotypes for cleavage activation and pH of fusion: implications for host range and adaptation. *PLoS Pathog*, 9(2), e1003151. <https://doi.org/10.1371/journal.ppat.1003151>
- Gibson, B. A., & Kraus, W. L. (2012). New insights into the molecular and cellular functions of poly(ADP-ribose) and PARPs. *Nat Rev Mol Cell Biol*, 13(7), 411-424. <https://doi.org/10.1038/nrm3376>
- Goncalves-Carneiro, D., Takata, M. A., Ong, H., Shilton, A., & Bieniasz, P. D. (2021). Origin and evolution of the zinc finger antiviral protein. *PLoS Pathog*, 17(4), e1009545. <https://doi.org/10.1371/journal.ppat.1009545>
- Grundy, G. J., Polo, L. M., Zeng, Z., Rulten, S. L., Hoch, N. C., Paomephan, P., Xu, Y., Sweet, S. M., Thorne, A. W., Oliver, A. W., Matthews, S. J., Pearl, L. H., & Caldecott, K. W. (2016). PARP3 is a sensor of nicked nucleosomes and monoribosylates histone H2B(Glu2). *Nat Commun*, 7, 12404. <https://doi.org/10.1038/ncomms12404>
- Guo, T., Zuo, Y., Qian, L., Liu, J., Yuan, Y., Xu, K., Miao, Y., Feng, Q., Chen, X., Jin, L., Zhang, L., Dong, C., Xiong, S., & Zheng, H. (2019). ADP-ribosyltransferase PARP11 modulates the

- interferon antiviral response by mono-ADP-ribosylating the ubiquitin E3 ligase beta-TrCP. *Nat Microbiol*, 4(11), 1872-1884. <https://doi.org/10.1038/s41564-019-0428-3>
- Gupte, R., Liu, Z., & Kraus, W. L. (2017). PARPs and ADP-ribosylation: recent advances linking molecular functions to biological outcomes. *Genes Dev*, 31(2), 101-126. <https://doi.org/10.1101/gad.291518.116>
- Gurevich, V. V. (2019). Protein multi-functionality: introduction. *Cell Mol Life Sci*, 76(22), 4405-4406. <https://doi.org/10.1007/s00018-019-03271-6>
- Hao, M., Han, S., Meng, D., Li, R., Lin, J., Wang, M., Zhou, T., & Chai, T. (2019). The PA Subunit of the Influenza Virus Polymerase Complex Affects Replication and Airborne Transmission of the H9N2 Subtype Avian Influenza Virus. *Viruses*, 11(1). <https://doi.org/10.3390/v11010040>
- Hao, W., Wang, L., & Li, S. (2020). Roles of the Non-Structural Proteins of Influenza A Virus. *Pathogens*, 9(10). <https://doi.org/10.3390/pathogens9100812>
- Hayakawa, S., Shiratori, S., Yamato, H., Kameyama, T., Kitatsuji, C., Kashigi, F., Goto, S., Kameoka, S., Fujikura, D., Yamada, T., Mizutani, T., Kazumata, M., Sato, M., Tanaka, J., Asaka, M., Ohba, Y., Miyazaki, T., Imamura, M., & Takaoka, A. (2011). ZAPS is a potent stimulator of signaling mediated by the RNA helicase RIG-I during antiviral responses. *Nat Immunol*, 12(1), 37-44. <https://doi.org/10.1038/ni.1963>
- Hoch, N. C., & Polo, L. M. (2019). ADP-ribosylation: from molecular mechanisms to human disease. *Genet Mol Biol*, 43(1 suppl 1), e20190075. <https://doi.org/10.1590/1678-4685-GMB-2019-0075>
- Hurtado-Bages, S., Knobloch, G., Ladurner, A. G., & Buschbeck, M. (2020). The taming of PARP1 and its impact on NAD(+) metabolism. *Mol Metab*, 38, 100950. <https://doi.org/10.1016/j.molmet.2020.01.014>
- Iqbal, M. B., Johns, M., Cao, J., Liu, Y., Yu, S. C., Hyde, G. D., Laffan, M. A., Marchese, F. P., Cho, S. H., Clark, A. R., Gavins, F. N., Woollard, K. J., Blackshear, P. J., Mackman, N., Dean, J. L., Boothby, M., & Haskard, D. O. (2014). PARP-14 combines with tristetraproline in the selective posttranscriptional control of macrophage tissue factor expression. *Blood*, 124(24), 3646-3655. <https://doi.org/10.1182/blood-2014-07-588046>
- Iwata, H., Goettsch, C., Sharma, A., Ricchiuto, P., Goh, W. W., Halu, A., Yamada, I., Yoshida, H., Hara, T., Wei, M., Inoue, N., Fukuda, D., Mojcher, A., Mattson, P. C., Barabasi, A. L., Boothby, M., Aikawa, E., Singh, S. A., & Aikawa, M. (2016). PARP9 and PARP14 cross-regulate macrophage activation via STAT1 ADP-ribosylation. *Nat Commun*, 7, 12849. <https://doi.org/10.1038/ncomms12849>
- Javanian, M., Barary, M., Ghebrehewet, S., Koppolu, V., Vasigala, V., & Ebrahimpour, S. (2021). A brief review of influenza virus infection. *J Med Virol*, 93(8), 4638-4646. <https://doi.org/10.1002/jmv.26990>
- Jiang, M., Qi, L., Li, L., & Li, Y. (2020). The caspase-3/GSDME signal pathway as a switch between apoptosis and pyroptosis in cancer. *Cell Death Discov*, 6, 112. <https://doi.org/10.1038/s41420-020-00349-0>
- Kalthoff, D., Globig, A., & Beer, M. (2010). (Highly pathogenic) avian influenza as a zoonotic agent. *Vet Microbiol*, 140(3-4), 237-245. <https://doi.org/10.1016/j.vetmic.2009.08.022>
- Karakus, U., Mena, I., Kottur, J., El Zahed, S. S., Seoane, R., Yildiz, S., Chen, L., Plancarte, M., Lindsay, L., Halpin, R., Stockwell, T. B., Wentworth, D. E., Boons, G. J., Krammer, F., Stertz, S., Boyce, W., de Vries, R. P., Aggarwal, A. K., & Garcia-Sastre, A. (2024). H19 influenza A virus exhibits species-specific MHC class II receptor usage. *Cell Host Microbe*, 32(7), 1089-1102 e1010. <https://doi.org/10.1016/j.chom.2024.05.018>
- Karakus, U., Thamamongood, T., Ciminski, K., Ran, W., Gunther, S. C., Pohl, M. O., Eletto, D., Jeney, C., Hoffmann, D., Reiche, S., Schinkothe, J., Ulrich, R., Wiener, J., Hayes, M. G. B., Chang, M. W., Hunziker, A., Yanguez, E., Aydilillo, T., Krammer, F.,...Stertz, S. (2019). MHC class II proteins mediate cross-species entry of bat influenza viruses. *Nature*, 567(7746), 109-112. <https://doi.org/10.1038/s41586-019-0955-3>

- Kawaguchi, A., Naito, T., & Nagata, K. (2005). Involvement of influenza virus PA subunit in assembly of functional RNA polymerase complexes. *J Virol*, 79(2), 732-744. <https://doi.org/10.1128/JVI.79.2.732-744.2005>
- Kawaoka, Y., & Neumann, G. (2012). Influenza viruses: an introduction. *Methods Mol Biol*, 865, 1-9. [https://doi.org/10.1007/978-1-61779-621-0\\_1](https://doi.org/10.1007/978-1-61779-621-0_1)
- Ke, Y., Wang, C., Zhang, J., Zhong, X., Wang, R., Zeng, X., & Ba, X. (2019). The Role of PARPs in Inflammation-and Metabolic-Related Diseases: Molecular Mechanisms and Beyond. *Cells*, 8(9). <https://doi.org/10.3390/cells8091047>
- Ke, Y., Zhang, J., Lv, X., Zeng, X., & Ba, X. (2019). Novel insights into PARPs in gene expression: regulation of RNA metabolism. *Cell Mol Life Sci*, 76(17), 3283-3299. <https://doi.org/10.1007/s00018-019-03120-6>
- Kerr, C. M., Parthasarathy, S., Schwarting, N., O'Connor, J. J., Pfannenstiel, J. J., Giri, E., More, S., Orozco, R. C., & Fehr, A. R. (2023). PARP12 is required to repress the replication of a Mac1 mutant coronavirus in a cell- and tissue-specific manner. *J Virol*, 97(9), e0088523. <https://doi.org/10.1128/jvi.00885-23>
- Kerviel, A., Thomas, A., Chaloin, L., Favard, C., & Muriaux, D. (2013). Virus assembly and plasma membrane domains: which came first? *Virus Res*, 171(2), 332-340. <https://doi.org/10.1016/j.virusres.2012.08.014>
- Kickhoefer, V. A., Siva, A. C., Kedersha, N. L., Inman, E. M., Ruland, C., Streuli, M., & Rome, L. H. (1999). The 193-kD vault protein, VPARP, is a novel poly(ADP-ribose) polymerase. *J Cell Biol*, 146(5), 917-928. <https://doi.org/10.1083/jcb.146.5.917>
- Kida, H., Yanagawa, R., & Matsuoka, Y. (1980). Duck influenza lacking evidence of disease signs and immune response. *Infect Immun*, 30(2), 547-553. <https://doi.org/10.1128/jai.30.2.547-553.1980>
- Kuchipudi, S. V., Tellabati, M., Sebastian, S., Londt, B. Z., Jansen, C., Vervelde, L., Brookes, S. M., Brown, I. H., Dunham, S. P., & Chang, K. C. (2014). Highly pathogenic avian influenza virus infection in chickens but not ducks is associated with elevated host immune and pro-inflammatory responses. *Vet Res*, 45(1), 118. <https://doi.org/10.1186/s13567-014-0118-3>
- Kumar, V., Kumar, A., Mir, K. U. I., Yadav, V., & Chauhan, S. S. (2022). Pleiotropic role of PARP1: an overview. *3 Biotech*, 12(1), 3. <https://doi.org/10.1007/s13205-021-03038-6>
- Kuriakose, T., & Kanneganti, T. D. (2017). Regulation and functions of NLRP3 inflammasome during influenza virus infection. *Mol Immunol*, 86, 56-64. <https://doi.org/10.1016/j.molimm.2017.01.023>
- Laghlali, G., Lawlor, K. E., & Tate, M. D. (2020). Die Another Way: Interplay between Influenza A Virus, Inflammation and Cell Death. *Viruses*, 12(4). <https://doi.org/10.3390/v12040401>
- Li, W. H., Wang, F., Song, G. Y., Yu, Q. H., Du, R. P., & Xu, P. (2023). PARP-1: a critical regulator in radioprotection and radiotherapy-mechanisms, challenges, and therapeutic opportunities. *Front Pharmacol*, 14, 1198948. <https://doi.org/10.3389/fphar.2023.1198948>
- Li, Y., Arcos, S., Sabsay, K. R., Te Velthuis, A. J. W., & Luring, A. S. (2023). Deep mutational scanning reveals the functional constraints and evolutionary potential of the influenza A virus PB1 protein. *J Virol*, 97(11), e0132923. <https://doi.org/10.1128/jvi.01329-23>
- Li, Z., Luo, A., & Xie, B. (2023). The Complex Network of ADP-Ribosylation and DNA Repair: Emerging Insights and Implications for Cancer Therapy. *Int J Mol Sci*, 24(19). <https://doi.org/10.3390/ijms241915028>
- Liu, M., Guo, S., Hibbert, J. M., Jain, V., Singh, N., Wilson, N. O., & Stiles, J. K. (2011). CXCL10/IP-10 in infectious diseases pathogenesis and potential therapeutic implications. *Cytokine Growth Factor Rev*, 22(3), 121-130. <https://doi.org/10.1016/j.cytogfr.2011.06.001>
- Liu, Y., Snow, B. E., Kickhoefer, V. A., Erdmann, N., Zhou, W., Wakeham, A., Gomez, M., Rome, L. H., & Harrington, L. (2004). Vault poly(ADP-ribose) polymerase is associated with mammalian telomerase and is dispensable for telomerase function and vault structure

- in vivo. *Mol Cell Biol*, 24(12), 5314-5323. <https://doi.org/10.1128/MCB.24.12.5314-5323.2004>
- Long, J. C., & Fodor, E. (2016). The PB2 Subunit of the Influenza A Virus RNA Polymerase Is Imported into the Mitochondrial Matrix. *J Virol*, 90(19), 8729-8738. <https://doi.org/10.1128/JVI.01384-16>
- Love, M. I., Huber, W., & Anders, S. (2014). Moderated estimation of fold change and dispersion for RNA-seq data with DESeq2. *Genome Biol*, 15(12), 550. <https://doi.org/10.1186/s13059-014-0550-8>
- Lu, J., Chatterjee, M., Schmid, H., Beck, S., & Gawaz, M. (2016). CXCL14 as an emerging immune and inflammatory modulator. *J Inflamm (Lond)*, 13, 1. <https://doi.org/10.1186/s12950-015-0109-9>
- Luo, C., Liu, J., Qi, W., Ren, X., Lu, R., Liao, M., & Ning, Z. (2018). Dynamic analysis of expression of chemokine and cytokine gene responses to H5N1 and H9N2 avian influenza viruses in DF-1 cells. *Microbiol Immunol*, 62(5), 327-340. <https://doi.org/10.1111/1348-0421.12588>
- Luo, S., Xie, Z., Xie, Z., Xie, L., Huang, L., Huang, J., Deng, X., Zeng, T., Wang, S., Zhang, Y., & Liu, J. (2017). Surveillance of Live Poultry Markets for Low Pathogenic Avian Influenza Viruses in Guangxi Province, Southern China, from 2012-2015. *Sci Rep*, 7(1), 17577. <https://doi.org/10.1038/s41598-017-17740-0>
- MacPherson, L., Tamblyn, L., Rajendra, S., Bralha, F., McPherson, J. P., & Matthews, J. (2013). 2,3,7,8-Tetrachlorodibenzo-p-dioxin poly(ADP-ribose) polymerase (TiPARP, ARTD14) is a mono-ADP-ribosyltransferase and repressor of aryl hydrocarbon receptor transactivation. *Nucleic Acids Res*, 41(3), 1604-1621. <https://doi.org/10.1093/nar/gks1337>
- Malgras, M., Garcia, M., Jousset, C., Bodet, C., & Leveque, N. (2021). The Antiviral Activities of Poly-ADP-Ribose Polymerases. *Viruses*, 13(4). <https://doi.org/10.3390/v13040582>
- Mao, K., & Zhang, G. (2022). The role of PARP1 in neurodegenerative diseases and aging. *FEBS J*, 289(8), 2013-2024. <https://doi.org/10.1111/febs.15716>
- Maris, C., Dominguez, C., & Allain, F. H. (2005). The RNA recognition motif, a plastic RNA-binding platform to regulate post-transcriptional gene expression. *FEBS J*, 272(9), 2118-2131. <https://doi.org/10.1111/j.1742-4658.2005.04653.x>
- Massari, S., Goracci, L., Desantis, J., & Tabarrini, O. (2016). Polymerase Acidic Protein-Basic Protein 1 (PA-PB1) Protein-Protein Interaction as a Target for Next-Generation Anti-influenza Therapeutics. *J Med Chem*, 59(17), 7699-7718. <https://doi.org/10.1021/acs.jmedchem.5b01474>
- Matrosovich, M. N., Gambaryan, A. S., Teneberg, S., Piskarev, V. E., Yamnikova, S. S., Lvov, D. K., Robertson, J. S., & Karlsson, K. A. (1997). Avian influenza A viruses differ from human viruses by recognition of sialyloligosaccharides and gangliosides and by a higher conservation of the HA receptor-binding site. *Virology*, 233(1), 224-234. <https://doi.org/10.1006/viro.1997.8580>
- Matrosovich, M. N., Matrosovich, T. Y., Gray, T., Roberts, N. A., & Klenk, H. D. (2004). Neuraminidase is important for the initiation of influenza virus infection in human airway epithelium. *J Virol*, 78(22), 12665-12667. <https://doi.org/10.1128/JVI.78.22.12665-12667.2004>
- McAuley, J. L., Gilbertson, B. P., Trifkovic, S., Brown, L. E., & McKimm-Breschkin, J. L. (2019). Influenza Virus Neuraminidase Structure and Functions. *Front Microbiol*, 10, 39. <https://doi.org/10.3389/fmicb.2019.00039>
- McDermaid, A., Monier, B., Zhao, J., Liu, B., & Ma, Q. (2019). Interpretation of differential gene expression results of RNA-seq data: review and integration. *Brief Bioinform*, 20(6), 2044-2054. <https://doi.org/10.1093/bib/bby067>
- McLachlan, J., George, A., & Banerjee, S. (2016). The current status of PARP inhibitors in ovarian cancer. *Tumori*, 102(5), 433-440. <https://doi.org/10.5301/tj.5000558>

- Mentz, M., Keay, W., Strobl, C. D., Antonioli, M., Adolph, L., Heide, M., Lechner, A., Haebe, S., Osterode, E., Kridel, R., Ziegenhain, C., Wange, L. E., Hildebrand, J. A., Shree, T., Silkenstedt, E., Staiger, A. M., Ott, G., Horn, H., Szczepanowski, M.,...Weigert, O. (2022). PARP14 is a novel target in STAT6 mutant follicular lymphoma. *Leukemia*, 36(9), 2281-2292. <https://doi.org/10.1038/s41375-022-01641-x>
- Meyer-Ficca, M. L., Ihara, M., Bader, J. J., Leu, N. A., Beneke, S., & Meyer, R. G. (2015). Spermatid head elongation with normal nuclear shaping requires ADP-ribosyltransferase PARP11 (ARTD11) in mice. *Biol Reprod*, 92(3), 80. <https://doi.org/10.1095/biolreprod.114.123661>
- Mezencev, R., & Auerbach, S. S. (2020). The sensitivity of transcriptomics BMD modeling to the methods used for microarray data normalization. *PLoS One*, 15(5), e0232955. <https://doi.org/10.1371/journal.pone.0232955>
- Monier, B., McDermaid, A., Wang, C., Zhao, J., Miller, A., Fennell, A., & Ma, Q. (2019). IRIS-EDA: An integrated RNA-Seq interpretation system for gene expression data analysis. *PLoS Comput Biol*, 15(2), e1006792. <https://doi.org/10.1371/journal.pcbi.1006792>
- Morais, C. L. M., Martin-Hirsch, P. L., & Martin, F. L. (2019). A three-dimensional principal component analysis approach for exploratory analysis of hyperspectral data: identification of ovarian cancer samples based on Raman microspectroscopy imaging of blood plasma. *Analyst*, 144(7), 2312-2319. <https://doi.org/10.1039/c8an02031k>
- Morone, B., & Grimaldi, G. (2024). PARP enzymes and mono-ADP-ribosylation: advancing the connection from interferon-signalling to cancer biology. *Expert Rev Mol Med*, 26, e17. <https://doi.org/10.1017/erm.2024.13>
- Moschonas, G. D., Delhaye, L., Cooreman, R., Husers, F., Bhat, A., Stylianidou, Z., De Bousser, E., De Pryck, L., Grzesik, H., De Sutter, D., Parthoens, E., De Smet, A. S., Maciejczuk, A., Lippens, S., Callewaert, N., Vandekerckhove, L., Debyser, Z., Sodeik, B., Eyckerman, S., & Saelens, X. (2024). MX2 forms nucleoporin-comprising cytoplasmic biomolecular condensates that lure viral capsids. *Cell Host Microbe*, 32(10), 1705-1724 e1714. <https://doi.org/10.1016/j.chom.2024.09.002>
- Mostafa, A., Abdelwhab, E. M., Mettenleiter, T. C., & Pleschka, S. (2018). Zoonotic Potential of Influenza A Viruses: A Comprehensive Overview. *Viruses*, 10(9). <https://doi.org/10.3390/v10090497>
- Munzker, L., Kimani, S. W., Fowkes, M. M., Dong, A., Zheng, H., Li, Y., Dasovich, M., Zak, K. M., Leung, A. K. L., Elkins, J. M., Kessler, D., Arrowsmith, C. H., Halabelian, L., & Bottcher, J. (2024). A ligand discovery toolbox for the WWE domain family of human E3 ligases. *Commun Biol*, 7(1), 901. <https://doi.org/10.1038/s42003-024-06584-w>
- Neumann, G., Noda, T., Kawaoka, Y. (2009). Emergence and pandemic potential of swine-origin H1N1 influenza virus. *Nature*, 459(7249), 931-939. <https://doi.org/10.1038/nature08157>
- Nilsson, B. E., Te Velthuis, A. J. W., & Fodor, E. (2017). Role of the PB2 627 Domain in Influenza A Virus Polymerase Function. *J Virol*, 91(7). <https://doi.org/10.1128/JVI.02467-16>
- Ning, S., Pagano, J. S., & Barber, G. N. (2011). IRF7: activation, regulation, modification and function. *Genes Immun*, 12(6), 399-414. <https://doi.org/10.1038/gene.2011.21>
- Nogales, A., Martinez-Sobrido, L., Topham, D. J., & DeDiego, M. L. (2018). Modulation of Innate Immune Responses by the Influenza A NS1 and PA-X Proteins. *Viruses*, 10(12). <https://doi.org/10.3390/v10120708>
- Ong, J. D., Mansell, A., & Tate, M. D. (2017). Hero turned villain: NLRP3 inflammasome-induced inflammation during influenza A virus infection. *J Leukoc Biol*, 101(4), 863-874. <https://doi.org/10.1189/jlb.4MR0616-288R>
- Parthasarathy, S., & Fehr, A. R. (2022). PARP14: A key ADP-ribosylating protein in host-virus interactions? *PLoS Pathog*, 18(6), e1010535. <https://doi.org/10.1371/journal.ppat.1010535>
- Parthasarathy, S., Saenjamsai, P., Hao, H., Ferkul, A., Pfannenstiel, J. J., Suder, E. L., Bejan, D. S., Chen, Y., Schwarting, N., Aikawa, M., Muhlberger, E., Orozco, R. C., Sullivan, C. S.,

- Cohen, M. S., Davido, D. J., Hume, A. J., & Fehr, A. R. (2024). PARP14 is pro- and anti-viral host factor that promotes IFN production and affects the replication of multiple viruses. *bioRxiv*. <https://doi.org/10.1101/2024.04.26.591186>
- Perng, Y. C., & Lenschow, D. J. (2018). ISG15 in antiviral immunity and beyond. *Nat Rev Microbiol*, 16(7), 423-439. <https://doi.org/10.1038/s41579-018-0020-5>
- Philip D Glaves 1, J. D. T. (2011). Generation and analysis of transcriptomics data *Methods Mol Biol* 2011:691:167-85. . [https://doi.org/doi:10.1007/978-1-60761-849-2\\_10](https://doi.org/doi:10.1007/978-1-60761-849-2_10).
- Qi, W., Zhou, X., Shi, W., Huang, L., Xia, W., Liu, D., Li, H., Chen, S., Lei, F., Cao, L., Wu, J., He, F., Song, W., Li, Q., Li, H., Liao, M., & Liu, M. (2014). Genesis of the novel human-infecting influenza A(H10N8) virus and potential genetic diversity of the virus in poultry, China. *Euro Surveill*, 19(25). <https://doi.org/10.2807/1560-7917.es2014.19.25.20841>
- Qin, W., Wu, H. J., Cao, L. Q., Li, H. J., He, C. X., Zhao, D., Xing, L., Li, P. Q., Jin, X., & Cao, H. L. (2019). Research Progress on PARP14 as a Drug Target. *Front Pharmacol*, 10, 172. <https://doi.org/10.3389/fphar.2019.00172>
- Reddi, T. S., Merkl, P. E., Lim, S. Y., Letvin, N. L., & Knipe, D. M. (2021). Tripartite Motif 22 (TRIM22) protein restricts herpes simplex virus 1 by epigenetic silencing of viral immediate-early genes. *PLoS Pathog*, 17(2), e1009281. <https://doi.org/10.1371/journal.ppat.1009281>
- Richard, I. A., Burgess, J. T., O'Byrne, K. J., & Bolderson, E. (2021). Beyond PARP1: The Potential of Other Members of the Poly (ADP-Ribose) Polymerase Family in DNA Repair and Cancer Therapeutics. *Front Cell Dev Biol*, 9, 801200. <https://doi.org/10.3389/fcell.2021.801200>
- Riley, J. P., Kulkarni, A., Mehrotra, P., Koh, B., Perumal, N. B., Kaplan, M. H., & Goenka, S. (2013). PARP-14 binds specific DNA sequences to promote Th2 cell gene expression. *PLoS One*, 8(12), e83127. <https://doi.org/10.1371/journal.pone.0083127>
- Rose, M., Burgess, J. T., O'Byrne, K., Richard, D. J., & Bolderson, E. (2020). PARP Inhibitors: Clinical Relevance, Mechanisms of Action and Tumor Resistance. *Front Cell Dev Biol*, 8, 564601. <https://doi.org/10.3389/fcell.2020.564601>
- Rossman, J. S., Jing, X., Leser, G. P., & Lamb, R. A. (2010). Influenza virus M2 protein mediates ESCRT-independent membrane scission. *Cell*, 142(6), 902-913. <https://doi.org/10.1016/j.cell.2010.08.029>
- Schafer, M., Di Maria, M. V., Stone, M. L., Barker, A. J., Carmody, K. K., Reece, T. B., Ivy, D. D., Jagers, J., & Mitchell, M. B. (2024). Principal component analysis identified neo-aortic diameter variations post Norwood surgery associated with the single ventricle performance and flow quality. *Int J Cardiovasc Imaging*. <https://doi.org/10.1007/s10554-024-03282-w>
- Schnell, J. R., & Chou, J. J. (2008). Structure and mechanism of the M2 proton channel of influenza A virus. *Nature*, 451(7178), 591-595. <https://doi.org/10.1038/nature06531>
- Schuller, M., & Ahel, I. (2022). Beyond protein modification: the rise of non-canonical ADP-ribosylation. *Biochem J*, 479(4), 463-477. <https://doi.org/10.1042/BCJ20210280>
- Sebastian, W. A., Inoue, M., Shimizu, N., Sato, R., Oguri, S., Itonaga, T., Kishimoto, S., Shiraishi, H., Hanada, T., & Ihara, K. (2024). Cardiac manifestations of human ACTA2 variants recapitulated in a zebrafish model. *J Hum Genet*, 69(3-4), 133-138. <https://doi.org/10.1038/s10038-024-01221-0>
- Selzer, L., Su, Z., Pintilie, G. D., Chiu, W., & Kirkegaard, K. (2020). Full-length three-dimensional structure of the influenza A virus M1 protein and its organization into a matrix layer. *PLoS Biol*, 18(9), e3000827. <https://doi.org/10.1371/journal.pbio.3000827>

- Shao, C., Qiu, Y., Liu, J., Feng, H., Shen, S., Saiyin, H., Yu, W., Wei, Y., Yu, L., Su, W., & Wu, J. (2018). PARP12 (ARTD12) suppresses hepatocellular carcinoma metastasis through interacting with FHL2 and regulating its stability. *Cell Death Dis*, 9(9), 856. <https://doi.org/10.1038/s41419-018-0906-1>
- Shao, W., Li, X., Goraya, M. U., Wang, S., & Chen, J. L. (2017). Evolution of Influenza A Virus by Mutation and Re-Assortment. *Int J Mol Sci*, 18(8). <https://doi.org/10.3390/ijms18081650>
- Sharif-Askari, B., Amrein, L., Aloyz, R., & Panasci, L. (2018). PARP3 inhibitors ME0328 and olaparib potentiate vinorelbine sensitization in breast cancer cell lines. *Breast Cancer Res Treat*, 172(1), 23-32. <https://doi.org/10.1007/s10549-018-4888-6>
- Shreevrat Goenka†1, S. H., and Mark Boothby†§. (2007). Collaborator of Stat6 (CoaSt6)-associated Poly(ADP-ribose)
- Polymerase Activity Modulates Stat6-dependent  
Gene Transcription. *THE JOURNAL OF BIOLOGICAL CHEMISTRY VOL. 282, NO. 26, pp. 18732–18739*, . <https://doi.org/10.1074/jbc.M611283200>
- Sid, H., Hartmann, S., Winter, C., & Rautenschlein, S. (2017). Interaction of Influenza A Viruses with Oviduct Explants of Different Avian Species. *Front Microbiol*, 8, 1338. <https://doi.org/10.3389/fmicb.2017.01338>
- Sousa, F. G., Matuo, R., Soares, D. G., Escargueil, A. E., Henriques, J. A., Larsen, A. K., & Saffi, J. (2012). PARPs and the DNA damage response. *Carcinogenesis*, 33(8), 1433-1440. <https://doi.org/10.1093/carcin/bgs132>
- Spiegel, J. O., Van Houten, B., & Durrant, J. D. (2021). PARP1: Structural insights and pharmacological targets for inhibition. *DNA Repair (Amst)*, 103, 103125. <https://doi.org/10.1016/j.dnarep.2021.103125>
- Sriwilaijaroen, N., & Suzuki, Y. (2012). Molecular basis of the structure and function of H1 hemagglutinin of influenza virus. *Proc Jpn Acad Ser B Phys Biol Sci*, 88(6), 226-249. <https://doi.org/10.2183/pjab.88.226>
- Steenwyk, J. L., & King, N. (2024). The promise and pitfalls of synteny in phylogenomics. *PLoS Biol*, 22(5), e3002632. <https://doi.org/10.1371/journal.pbio.3002632>
- Steffen, J. D., Brody, J. R., Armen, R. S., & Pascal, J. M. (2013). Structural Implications for Selective Targeting of PARPs. *Front Oncol*, 3, 301. <https://doi.org/10.3389/fonc.2013.00301>
- Su, G., Chen, Y., Li, X., & Shao, J. W. (2024). Virus versus host: influenza A virus circumvents the immune responses. *Front Microbiol*, 15, 1394510. <https://doi.org/10.3389/fmicb.2024.1394510>
- Sun, X., Shi, Y., Lu, X., He, J., Gao, F., Yan, J., Qi, J., & Gao, G. F. (2013). Bat-derived influenza hemagglutinin H17 does not bind canonical avian or human receptors and most likely uses a unique entry mechanism. *Cell Rep*, 3(3), 769-778. <https://doi.org/10.1016/j.celrep.2013.01.025>
- Szeto, W. C., Hsia, H. P., Tang, Y. S., & Shaw, P. C. (2020). Interaction between influenza A virus nucleoprotein and PB2 cap-binding domain is mediated by RNA. *PLoS One*, 15(9), e0239899. <https://doi.org/10.1371/journal.pone.0239899>
- Takahashi, T., Suzuki, Y., Nishinaka, D., Kawase, N., Kobayashi, Y., Hidari, K. I., Miyamoto, D., Guo, C. T., Shortridge, K. F., & Suzuki, T. (2001). Duck and human pandemic influenza A viruses retain sialidase activity under low pH conditions. *J Biochem*, 130(2), 279-283. <https://doi.org/10.1093/oxfordjournals.jbchem.a002983>
- Tanaka, T., Narazaki, M., & Kishimoto, T. (2014). IL-6 in inflammation, immunity, and disease. *Cold Spring Harb Perspect Biol*, 6(10), a016295. <https://doi.org/10.1101/cshperspect.a016295>
- Tang, X., Zhang, H., Long, Y., Hua, H., Jiang, Y., & Jing, J. (2018). PARP9 is overexpressed in human breast cancer and promotes cancer cell migration. *Oncol Lett*, 16(3), 4073-4077. <https://doi.org/10.3892/ol.2018.9124>

- Tate, M. D., & Mansell, A. (2018). An update on the NLRP3 inflammasome and influenza: the road to redemption or perdition? *Curr Opin Immunol*, 54, 80-85. <https://doi.org/10.1016/j.coi.2018.06.005>
- Taubenberger, J. K., & Kash, J. C. (2010). Influenza virus evolution, host adaptation, and pandemic formation. *Cell Host Microbe*, 7(6), 440-451. <https://doi.org/10.1016/j.chom.2010.05.009>
- Taubenberger, J. K., & Morens, D. M. (2010). Influenza: the once and future pandemic. *Public Health Rep*, 125 Suppl 3(Suppl 3), 16-26. <https://www.ncbi.nlm.nih.gov/pubmed/20568566>
- Tauber, A. L., Schweiker, S. S., & Levonis, S. M. (2021). The potential association between PARP14 and SARS-CoV-2 infection (COVID-19). *Future Med Chem*, 13(6), 587-592. <https://doi.org/10.4155/fmc-2020-0226>
- Torretta, A., Chatzicharalampous, C., Ebenwaldner, C., & Schuler, H. (2023). PARP14 is a writer, reader, and eraser of mono-ADP-ribosylation. *J Biol Chem*, 299(9), 105096. <https://doi.org/10.1016/j.jbc.2023.105096>
- Tuncel, H., Tanaka, S., Oka, S., Nakai, S., Fukutomi, R., Okamoto, M., Ota, T., Kaneko, H., Tatsuka, M., & Shimamoto, F. (2012). PARP6, a mono(ADP-ribosyl) transferase and a negative regulator of cell proliferation, is involved in colorectal cancer development. *Int J Oncol*, 41(6), 2079-2086. <https://doi.org/10.3892/ijo.2012.1652>
- Turrell, L., Lyall, J. W., Tiley, L. S., Fodor, E., & Vreede, F. T. (2013). The role and assembly mechanism of nucleoprotein in influenza A virus ribonucleoprotein complexes. *Nat Commun*, 4, 1591. <https://doi.org/10.1038/ncomms2589>
- Urbaniak, K., & Markowska-Daniel, I. (2014). In vivo reassortment of influenza viruses. *Acta Biochim Pol*, 61(3), 427-431. <https://www.ncbi.nlm.nih.gov/pubmed/25180223>
- van Beek, L., McClay, E., Patel, S., Schimpl, M., Spagnolo, L., & Maia de Oliveira, T. (2021). PARP Power: A Structural Perspective on PARP1, PARP2, and PARP3 in DNA Damage Repair and Nucleosome Remodelling. *Int J Mol Sci*, 22(10). <https://doi.org/10.3390/ijms22105112>
- Vermehren-Schmaedick, A., Huang, J. Y., Levinson, M., Pomaville, M. B., Reed, S., Bellus, G. A., Gilbert, F., Keren, B., Heron, D., Haye, D., Janello, C., Makowski, C., Danhauser, K., Fedorov, L. M., Haack, T. B., Wright, K. M., & Cohen, M. S. (2021). Characterization of PARP6 Function in Knockout Mice and Patients with Developmental Delay. *Cells*, 10(6). <https://doi.org/10.3390/cells10061289>
- Virag, L., & Szabo, C. (2002). The therapeutic potential of poly(ADP-ribose) polymerase inhibitors. *Pharmacol Rev*, 54(3), 375-429. <https://doi.org/10.1124/pr.54.3.375>
- Vyas, S., Chesaroni-Cataldo, M., Todorova, T., Huang, Y. H., & Chang, P. (2013). A systematic analysis of the PARP protein family identifies new functions critical for cell physiology. *Nat Commun*, 4, 2240. <https://doi.org/10.1038/ncomms3240>
- Vyas, S., Matic, I., Uchima, L., Rood, J., Zaja, R., Hay, R. T., Ahel, I., & Chang, P. (2014). Family-wide analysis of poly(ADP-ribose) polymerase activity. *Nat Commun*, 5, 4426. <https://doi.org/10.1038/ncomms5426>
- W. Lee Kraus, P. D. (2015). PARPs and ADP-Ribosylation: Fifty Years... and Counting. *Mol Cell*, 58(6): 902-910. <https://doi.org/doi:10.1016/j.molcel.2015.06.006>.
- Wagner, E. M. (2013). Monitoring gene expression: quantitative real-time rt-PCR. *Methods Mol Biol*, 1027, 19-45. [https://doi.org/10.1007/978-1-60327-369-5\\_2](https://doi.org/10.1007/978-1-60327-369-5_2)
- Wang, X. (2020). Pleiotrophin: Activity and mechanism. *Adv Clin Chem*, 98, 51-89. <https://doi.org/10.1016/bs.acc.2020.02.003>
- Wei, H., & Yu, X. (2016). Functions of PARylation in DNA Damage Repair Pathways. *Genomics Proteomics Bioinformatics*, 14(3), 131-139. <https://doi.org/10.1016/j.gpb.2016.05.001>
- Weis, W., Brown, J. H., Cusack, S., Paulson, J. C., Skehel, J. J., & Wiley, D. C. (1988). Structure of the influenza virus haemagglutinin complexed with its receptor, sialic acid. *Nature*, 333(6172), 426-431. <https://doi.org/10.1038/333426a0>

- Welsby, I., Hutin, D., Gueydan, C., Kruys, V., Rongvaux, A., & Leo, O. (2014). PARP12, an interferon-stimulated gene involved in the control of protein translation and inflammation. *J Biol Chem*, 289(38), 26642-26657. <https://doi.org/10.1074/jbc.M114.589515>
- Wille, M., & Holmes, E. C. (2020). Wild birds as reservoirs for diverse and abundant gamma- and deltacoronaviruses. *FEMS Microbiol Rev*, 44(5), 631-644. <https://doi.org/10.1093/femsre/fuaa026>
- Wu, Y., Xu, S., Cheng, S., Yang, J., & Wang, Y. (2023). Clinical application of PARP inhibitors in ovarian cancer: from molecular mechanisms to the current status. *J Ovarian Res*, 16(1), 6. <https://doi.org/10.1186/s13048-023-01094-5>
- Xing, J., Zhang, A., Du, Y., Fang, M., Minze, L. J., Liu, Y. J., Li, X. C., & Zhang, Z. (2021). Identification of poly(ADP-ribose) polymerase 9 (PARP9) as a noncanonical sensor for RNA virus in dendritic cells. *Nat Commun*, 12(1), 2681. <https://doi.org/10.1038/s41467-021-23003-4>
- Yang, C. S., Jividen, K., Spencer, A., Dworak, N., Ni, L., Oostdyk, L. T., Chatterjee, M., Kusmider, B., Reon, B., Parlak, M., Gorbunova, V., Abbas, T., Jeffery, E., Sherman, N. E., & Paschal, B. M. (2017). Ubiquitin Modification by the E3 Ligase/ADP-Ribosyltransferase Dtx3L/Parp9. *Mol Cell*, 66(4), 503-516 e505. <https://doi.org/10.1016/j.molcel.2017.04.028>
- Ye, J., Sorrell, E. M., Cai, Y., Shao, H., Xu, K., Pena, L., Hickman, D., Song, H., Angel, M., Medina, R. A., Manicassamy, B., Garcia-Sastre, A., & Perez, D. R. (2010). Variations in the hemagglutinin of the 2009 H1N1 pandemic virus: potential for strains with altered virulence phenotype? *PLoS Pathog*, 6(10), e1001145. <https://doi.org/10.1371/journal.ppat.1001145>
- Zhang, W., Li, Y., Xin, S., Yang, L., Jiang, M., Xin, Y., Wang, Y., Cao, P., Zhang, S., Yang, Y., & Lu, J. (2023). The emerging roles of IFIT3 in antiviral innate immunity and cellular biology. *J Med Virol*, 95(1), e28259. <https://doi.org/10.1002/jmv.28259>
- Zhang, Y., Mao, D., Roswit, W. T., Jin, X., Patel, A. C., Patel, D. A., Agapov, E., Wang, Z., Tidwell, R. M., Atkinson, J. J., Huang, G., McCarthy, R., Yu, J., Yun, N. E., Paessler, S., Lawson, T. G., Omattage, N. S., Brett, T. J., & Holtzman, M. J. (2015). PARP9-DTX3L ubiquitin ligase targets host histone H2BJ and viral 3C protease to enhance interferon signaling and control viral infection. *Nat Immunol*, 16(12), 1215-1227. <https://doi.org/10.1038/ni.3279>
- Zhu, H., Tang, Y. D., Zhan, G., Su, C., & Zheng, C. (2021). The Critical Role of PARPs in Regulating Innate Immune Responses. *Front Immunol*, 12, 712556. <https://doi.org/10.3389/fimmu.2021.712556>
- Zhu, H., & Zheng, C. (2021). When PARPs Meet Antiviral Innate Immunity. *Trends Microbiol*, 29(9), 776-778. <https://doi.org/10.1016/j.tim.2021.01.002>
- Zhu, X., Yu, W., McBride, R., Li, Y., Chen, L. M., Donis, R. O., Tong, S., Paulson, J. C., & Wilson, I. A. (2013). Hemagglutinin homologue from H17N10 bat influenza virus exhibits divergent receptor-binding and pH-dependent fusion activities. *Proc Natl Acad Sci U S A*, 110(4), 1458-1463. <https://doi.org/10.1073/pnas.1218509110>